Doctoral Thesis

COUPLING OF MULTIFOCAL CONTACT LENS DESIGNS WITH THE EYE'S OPTICS: IMPACT ON VISION

SHRILEKHA VEDHAKRISHNAN

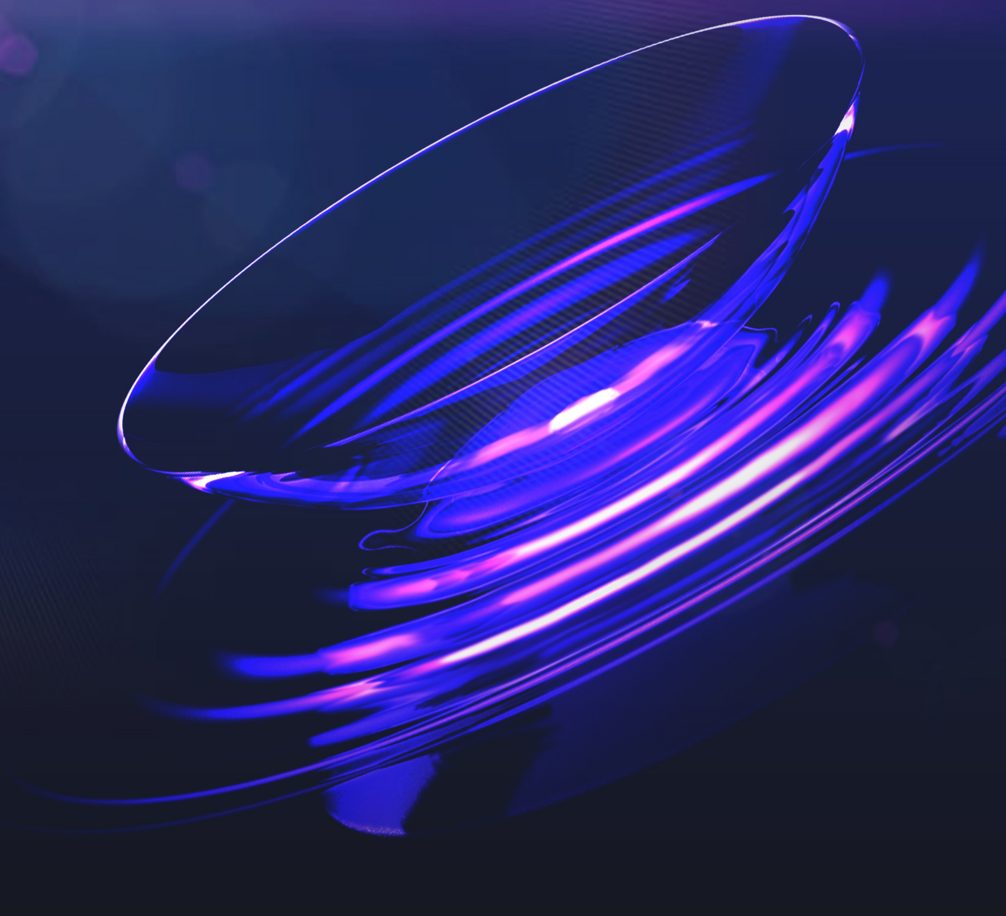

SUPERVISORS
SUSANA MARCOS CELESTINO
MARIA VIÑAS PEÑA

UNIVERSIDAD COMPLUTENSE DE MADRID

FACULTAD DE ÓPTICA Y OPTOMETRÍA

TESIS DOCTORAL

ACOPLAMIENTO DE DISEÑOS DE LENTES DE CONTACTO MULTIFOCALES CON LAOPTICA DEL OJO: IMPACTO EN LA VISION

COUPLING OF MULTIFOCAL CONTACT LENS DESIGNS WITH THE EYE'S OPTICS:IMPACT ON VISION

MEMORIA PARA OPTAR AL GRADO DE DOCTORA

PRESENTADA POR

SHRILEKHA VEDHAKRISHNAN

DIRECTORAS

SUSANA MARCOS CELESTINO

MARIA VIÑAS PEÑA

UNIVERSIDAD COMPLUTENSE DE MADRID

FACULTAD DE ÓPTICA Y OPTOMETRÍA

TESIS DOCTORAL

ACOPLAMIENTO DE DISEÑOS DE LENTES DE CONTACTO MULTIFOCALES CON LAOPTICA DEL OJO: IMPACTO EN LA VISION

COUPLING OF MULTIFOCAL CONTACT LENS DESIGNS WITH THE EYE'S OPTICS:IMPACT ON VISION

MEMORIA PARA OPTAR AL GRADO DE DOCTORA

PRESENTADA POR

SHRILEKHA VEDHAKRISHNAN

DIRECTORAS

SUSANA MARCOS CELESTINO

MARIA VIÑAS PEÑA

Laboratorio de Optica Visual y
Biofotonica
Instituto de ’Daza de Valdes’
Consejo Superior de Investigaciones
Cientificas

Facultad de Optica y Optometria
Universidad Complutense de Madrid

UNIVERSIDAD
COMPLUTENSE
MADRID

DECLARACIÓN DE AUTORÍA Y ORIGINALIDAD DE LA TESIS PRESENTADA PARA OBTENER EL TÍTULO DE DOCTOR

D./Dña. SHRILEKHA VEDHAKRISHNAN, estudiante en el Programa de Doctorado OPTICA OPTOMETRIA Y VISION,de la Facultad de OPTICA Y OPTOMETRIA de la Universidad Complutense deMadrid, como autor/a de la tesis presentada para la obtención del título de Doctor y titulada:

COUPLING OF MULTIFOCAL CONTACT LENS DESIGNS WITH THE EYE'S OPTICS: IMPACT ON VISION

ACOPLAMIENTO DE DISEÑOS DE LENTES DE CONTACTO MULTIFOCALES CON LA ÓPTICA DEL OJO: IMPACTO EN LA VISIÓN

y dirigida por: **Prof. Susana Marcos Celestino** y **Dra. Maria Viñas Peña**

DECLARO QUE:

La tesis es una obra original que no infringe los derechos de propiedad intelectual nilos derechos de propiedad industrial u otros, de acuerdo con el ordenamiento jurídico vigente, en particular, la Ley de Propiedad Intelectual (R.D. legislativo 1/1996, de 12 deabril, por el que se aprueba el texto refundido de la Ley de Propiedad Intelectual, modificado por la Ley 2/2019, de 1 de marzo, regularizando, aclarando y armonizando las disposiciones legales vigentes sobre la materia), en particular, las disposiciones referidas al derecho de cita.

Del mismo modo, asumo frente a la Universidad cualquier responsabilidad que pudiera derivarse de la autoría o falta de originalidad del contenido de la tesis presentada de conformidad con el ordenamiento jurídico vigente.

En Madrid, a 16 de diciembre de 2022

V. Shrilekha

Fdo.: SHRILEKHA VEDHAKRISHNAN

Esta DECLARACIÓN DE AUTORÍA Y ORIGINALIDAD debe ser insertada enla primera página de la tesis presentada para la obtención del título de Doctor.

Dedicated to my parents Vedhakrishnan and Devika, to my sister Pooja and my husband Ragav

ACKNOWLEDGEMENTS

My PhD was a journey that filled me with knowledge, memories and unique experiences. This journey could not have been possible without the wonderful people that were around, supporting and motivating me throughout. And it is important to thank all the people with whom I have shared this journey.

I express my sincere gratitude to my Supervisor, **Prof. Susana Marcos** for her professional guidance and her insights. I thank you for giving me the opportunity to work in this multidisciplinary research group. It has helped me grow both as a researcher and as a person. I will always be grateful to you for trusting in my abilities and always encouraging me to do my best. Your dedication, and immense knowledge has always been a great source of inspiration.

I am very thankful to my co-supervisor, **Dr. Maria Vinas** for all your support both in research and otherwise. I still remember the first day you welcomed me into our office with so much enthusiasm and positivity. Thank you for all the informal discussions and constructive criticisms which kept me going. Thank you for always finding time to help and discuss. I have never stopped learning from you both inside and outside the office.

Thanks **Alberto**, for all the support you have given me personally and professionally. I got to work with you closely during the last year of my thesis I have always felt that you're a genius, always with your doors open and saying "Talk to me if you need anything" these are the phrases which gave me so much hope. The way you explain even complex things so simplified. Thanks a lot Alberto for everything!

Rocio, thanks a lot for being an essential part in my PhD journey! You're always someone I look up to when I am in a really confused state and I have the liberty to talk about any topic to you. I still remember our mehendi day, and million discussions on Indian traditions and customs. Thanks for always supporting me Rocio.

Sara, I am extremely grateful to you for everything you have done for me. I remember our 5min conversations ending up in hours about various topics. You're such an amazing person and I am glad that I had you to back me up in all my ups and downs of my journey. We have so much in common, I will always cherish all the memories that we have. Always remember I am just a phone call away hehe! You will always have my support (I am sure you know that!).

Thanks to **Carmen, Clara, Xoana, Pilar** for all those informal gatherings and conversations that made me energetic again. Thanks Clara for including me in your Christmas celebration with the delicious food that you had made! Thanks to **Geethika**, my travel partner, we have travelled to many places as part of our MYFUN and we have had so many good memories. Thanks to **Judith**, for so many pep talks and passing your energy.

I am grateful to the then and now members of the Adaptive Optics team. Thanks to Clara, Sara, **Merche** for introducing me to the AO system for many hours of patient teaching in lab, **Ana** for being my subject so many times. Thanks to **Dani Pascual** for always being ready to fix anything, I don't think there is anything in the lab that could not be resolved when you're there. **Elena and Nohelia**, thanks a lot for all the help regarding my visa extensions, travel documents etc. My thanks to all members of VIOBIO - **Victor, James, Andres, Lupe, Edu senior, Edu junior, Alejandra, Fernando, Amal**.

Thanks again to all the VIOBIO members who volunteered in my never ending measurement sessions as part of the experiments for the doctoral research.

I am thankful to the IOSA student chapter members. The monthly meetings, last minute preparations for the week of science were fun.

I would like to express my thanks to **Prof. Pablo Artal** for giving me an opportunity to work in the LOUM lab, University of Murcia during my secondment program. I am equally grateful to **Dr.Linda Lundstrom** for a secondment at the BiOX laboratory at KTH Royal Institute, Stockholm, Sweden. Thank you Linda for all the brain storming sessions about the project and making me feel comfortable during the whole stay. Special thanks to **Abinaya Priya** for hosting me during the visit , also for the city tour and delicious home food. I am glad to have had these secondments with the group of common interest.

My sincere thanks to **Prof. Frank Schaeffel** and **Prof. Donald Mutti** for their valuable comments after every annual meeting and mid-term meeting. My extended gratitude to all MYFUN fellows for the pleasant time during the annual meetings, summer schools, complementary training events and international conferences.

I would like to acknowledge the funding supports behind this doctoral research. This work was supported by MYFUN: European Union's Horizon 2020 research and innovation programme under the Maria Sklodowska-Curie grant that supported my PhD years and the travel to the annual meetings and conferences. Thanks to Instituto de Optica, CSIC for providing an extension of funding and assistance for the added years.

I am very thankful to **Aishwarya Radhakrishnan**, for exposing me about this fellowship and this specific opportunity. I express my thanks to my institution, Elite School of Optometry and Medical Research Foundation. My heartfelt thanks to **Prof.Seshasayee**, for his continual encouragement and blessings.

I would like to thank my Indian friends who gave me the feeling of home here in Madrid. *Shreya, Jagadish* my travel buddies for all the fun and stressbusters. *Jagan,* for being there for me always with a smile as a good advisor. *Arun G* for trusting in me always. *Mani* and *Aishwarya* who opened their kitchens for my food cravings. *Pavithra, Sangamithra, Somsundar anna* for making me smile and being there for me during my down times. *Sumathi akka, Balaji* anna thanks for opening the doors of your homes for making me feel that I have a home always here in Madrid. *Vignesh Anna* thank you for all the care. *Vignesh, Vamsi, Raji, Arun* you never forget to cheer me up! *Paul* sir for all the fun and entertainment! The list goes on, but I would like to thank each one of them who have contributed in their own way.

Finally and most importantly, my sincerest thanks to my family. *Amma* and *Appa* my first mentors, words do not suffice my gratitude for their unconditional love, support and sacrifices behind building my academic career. *Pooja* my little sister, thanks for trusting in my abilities and always motivating me to excel in every field. *Ragav*, my husband thanks for being my pillar of strength for understanding me as I am, for constantly saying "you can", you have been with me throughout this journey tolerating me. I thank them all for standing on my side when needed, for supporting my decisions. Thanks to *Shyamala mami, Seshadri mama, Tulsi akka* for understanding my position and providing me the moral support in times of need. Thanks to my grandmother *Kalavathy* for being proud of me, she always keeps asking me when I will finish and I think now I have the answer for that finally.

Thank you all! Without you all this would not have been possible!.

“The important thing is not to stop questioning. Curiosity has its own reason for existence. One cannot help but be in awe when he contemplates the mysteries of eternity, of life, of the marvelous structure of reality. It is enough if one tries merely to comprehend a little of this mystery each day.” – Albert Einstein

FUNDING

The research developed during this thesis would not have been possible without the funding received from the following public and private institutions:

- European Union's Horizon 2020 Research and Innovation Program, MyFun under the Marie Sklodowska-Curie grant agreement to Shrilekha Vedhakrishnan

- European Research Council ERC-2019-AdG-833106 . PI: Susana Marcos

- Spanish Government Grant FIS2017-84753-R. PI: Susana Marcos

- European Research Council ERC-2019 SILK-EYE & Spanish Government: FIS2017-84753-R. PI: Susana Marcos

- NIH P35 grant to Susana Marcos

- Unrestricted funds Research to Prevent Blindness, NY to Susana Marcos

- EU Marie Sklodowska-Curie Individual Fellowship MSCA-IF-GF-2019-MYOMICRO- 893557 to Maria Vinas.

KEYWORDS

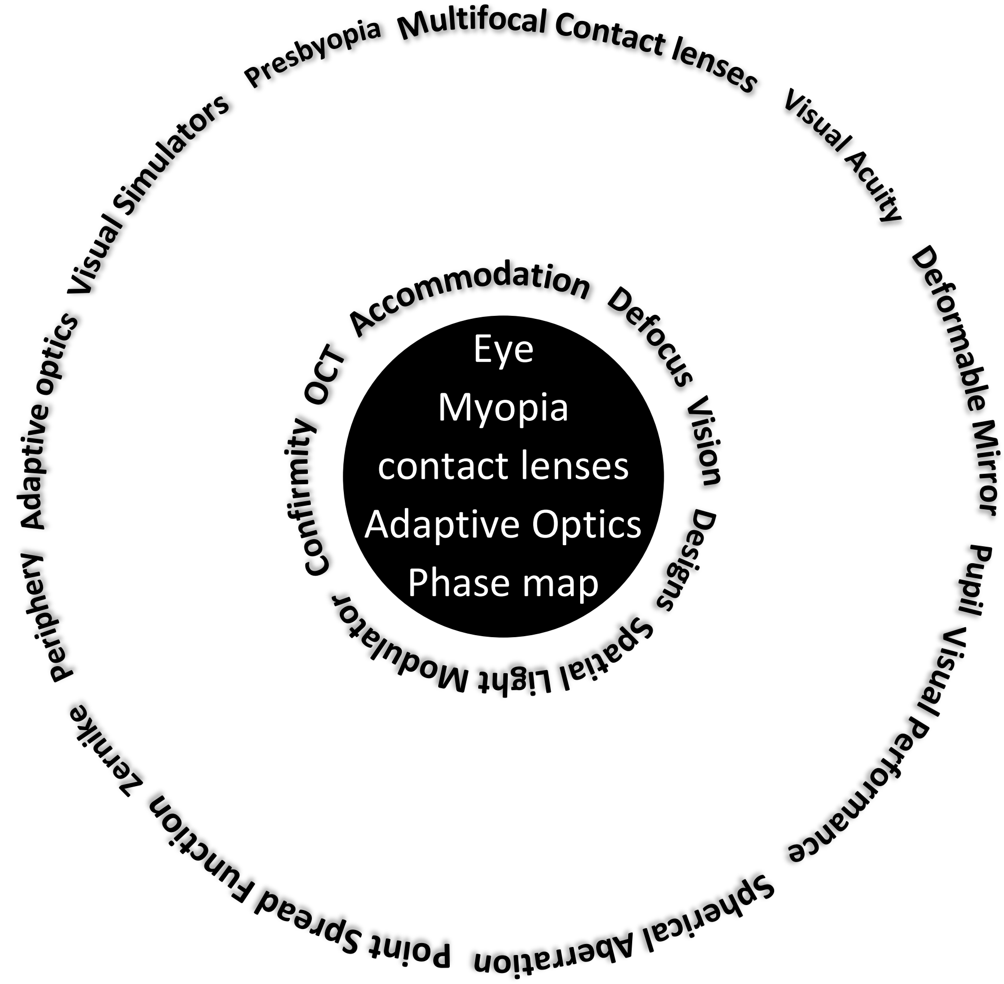
Presbyopia
Multifocal Contact lenses
Visual Acuity
Deformable Mirror
Pupil
Visual Performance
Spherical Aberration
Point Spread Function
Zernike
Periphery
Adaptive optics
Visual Simulators
Accommodation
Defocus
Vision
Designs
Spatial Light Modulator
Confirmity
OCT
Eye
Myopia
contact lenses
Adaptive Optics
Phase map

TABLE OF CONTENTS

SUMMARY OF THE THESIS

Purpose

Multifocal contact lenses are a common treatment for presbyopia (age-related loss of accommodation with age), and they are an emerging method for myopia control (aiming at stopping the progression of excessive axial elongation in near-sightedness). Multifocal contact lenses operate under the principle of simultaneous vision. Multifocal designs are very complex, it is difficult to understand how they impact vision neither in normal nor presbyopic subjects. Multifocal contact lenses do not restore accommodation in the presbyope. Also, it is not clear how accommodation may be compromised in young myopes fitted with contact lenses, not even the mechanism of operation of multifocal contact lenses in slowing down myopia progression, and how the pupil size impacts certain designs of multifocal lenses. Besides, multifocal contact lenses, while expanding the range of focus, degrade image quality at different distances. The impact on perceived and functional vision of these lenses should largely depend on their optical design. Myopia depends on a precise understanding of the interactions between optical blur, multifocal design, visual function, and accommodation. Adaptive Optics (AO) visual simulators are complex systems that combine different active optical elements allow to control and manipulate the eye optics. In particular, they allow the simulation of complex multifocal designs and study systematically the impact on vision non-invasively. This is particularly useful to study the impact of multifocal designs on the eye optics and in the visual function (foveal and periphery) and is very promising to investigate their limits for Presbyopia and Myopia applications. Moreover, changes in the real MCLs in the eye can be quantified using anterior segment optical coherent tomography (OCT) systems, allowing differentiation between the design and MCLs on eye effects. In this thesis we used AO visual simulators to study the impact of the multifocal contact lenses on the eye (foveally and periphery), in terms of visual acuity for far and near, the role of accommodation in vision, accommodative response for different induced accommodative demand, interactions with native aberrations of the eye and effective optical properties of multifocal contact lenses for myopia control. Additionally, anterior segment OCT allowed us to quantify changes in the structural properties of these lenses on the eye, as the functioning of the multifocal contact lenses depends on the proper deployment of the multifocal power profile on the cornea and optical interactions between the lenses and eye.

Methods

In this thesis, we have used two different custom-developed AO visual simulators (ViobioLab, CSIC, Madrid) were used. First, a monochromatic AO system provided with a Deformable mirror allowed evaluation of the through-focus visual performance (Visual Acuity), with real multifocal contact lenses on the eye of center near design with three different additions (Low,Medium,High) in two different age groups (young adults, presbyopes) in the presence and absence of accommodation. Second, a polychromatic AO system allowed the simulation of the multifocal lenses in a Spatial Light Modulator as phase maps, and through-focus visual acuity was measured and compared with the real contact lenses. The SLM channel was also used to simulate multiple designs of multifocal/bifocal patterns. The objective

accommodative response was evaluated for different accommodative demands induced by Hartmann-Shack aberrometry measurements. In the third monocular AO system (KTH University, Stockholm, Sweden), consisting of Hartmann-Shack, a deformable mirror, and a monitor for stimulus presentation, we measured the peripheral acuity threshold and wavefront aberrations to evaluate the foveal and peripheral visual quality and accommodation with multifocal contact lens designs. Finally, a custom-developed Anterior Segment Optical Coherence Tomography (AS-OCT) to evaluate the contact lens profile on the eye, and potential conformity to the cornea.

Results

Multifocal contact lenses on eye of center-near design with different additions (Low,Medium,High) were evaluated, the multifocal contact lenses produced a small but consistent degradation at far while consistent benefit at near in the absence of accommodation and this degradation increases with increasing addition of the lenses. These lenses did not degrade the near vision significantly, in fact improving the near vision in the absence of accommodation (paralyzed accommodative state). The through-focus visual acuity was captured through multifocal designs simulated in the spatial light modulator which was very similar to the results with the real contact lenses on the eye. The effective optical properties of the MiSight lenses are the large peripheral blur and the more asymmetric point spread function due to additional astigmatism and coma, and this leads to the larger accommodative response. The center-distance, positive spherical aberration-inducing lenses produced a reduced/lower lag of accommodation in all subjects. The AS-OCT showed that the soft multifocal contact lenses conform to the underlying cornea, both in the central area and in the periphery. However, the near central add is provided as expected.

Conclusions

The AO visual simulation has allowed the simulation of multiple multifocal lens designs on the optical elements and allowed us to test multiple designs at the same time. It also allowed testing these lenses before physically fitting them on the eye in the clinic and also making lenses specific to the individual requirements. The center-near multifocal design lenses decreased the accommodative lag hence providing a consistent vision from far to near in terms of through-focus visual acuity, although at the expense of a certain amount of degradation at far. The accommodative response was measured for the first time in this system, with the lens designs simulated in the SLM and capturing the aberrations of the eye while inducing defocus (accommodative demand) with the badal. The performance and interaction of these lenses are driven by the individual presence or absence of native high-order aberrations which alters the accommodative response. Factors such as pupil size, multifocal lens design, native aberrations of the eye, amount of spherical aberration induced should be considered in the management of myopia with MCLs and to gain insights into the mechanism of operation of these lenses.

RESUMEN DE LA TESIS EN CASTELLANO

Objectivo

Los lentes de contacto multifocales son un tratamiento común para la presbicia (pérdida de acomodación relacionada con la edad con la edad) y son un método emergente para el control de la miopía (con el objetivo de detener la progresión del alargamiento axial excesivo en la miopía). Las lentes de contacto multifocales funcionan bajo el principio de visión simultánea. Los diseños multifocales son muy complejos, es difícil entender cómo impactan en la visión ni en sujetos normales ni con presbicia. Las lentes de contacto multifocales no restauran la acomodación en el présbita. Además, no está claro cómo puede verse comprometida la acomodación en miopes jóvenes equipados con lentes de contacto, ni siquiera cuál es el mecanismo de operación de los lentes de contacto multifocales para ralentizar la progresión de la miopía, ni tampoco cómo afecta el tamaño de la pupila a ciertos diseños de lentes multifocales. Además, las lentes de contacto multifocales, al expandir el rango de enfoque, degradan la calidad de la imagen a diferentes distancias. El impacto en la visión percibida y funcional de estas lentes debería depender en gran medida de su diseño óptico. La miopía depende de una comprensión precisa de las interacciones entre la borrosidad óptica, el diseño multifocal, la función visual y la acomodación. Los simuladores visuales de Óptica Adaptativa (AO) son sistemas complejos que combinando diferentes elementos ópticos activos permiten controlar y manipular la óptica del ojo. En particular, permiten la simulación de diseños multifocales complejos y estudian sistemáticamente el impacto en la visión de forma no invasiva. Esto es particularmente útil para estudiar el impacto de los diseños multifocales en la óptica del ojo y en la función visual (foveal y periferia), y es muy prometedor para investigar sus límites para aplicaciones de Presbicia y Miopía. Además, los cambios en los MCL reales en el ojo se pueden cuantificar utilizando sistemas de tomografía coherente óptica (OCT) del segmento anterior, lo que permite diferenciar entre el diseño y los MCL en los efectos oculares. En esta tesis utilizamos simuladores visuales de la AO para estudiar el impacto de las lentes de contacto multifocales en el ojo (foveal y periférico), en términos de agudeza visual de lejos y de cerca, papel de la acomodación en la visión, respuesta acomodativa para diferentes demandas acomodativas inducidas, interacciones con aberraciones nativas del ojo y propiedades ópticas efectivas de lentes de contacto multifocales para el control de la miopía. Además, la OCT de segmento anterior permitió cuantificar los cambios en las propiedades estructurales de estos lentes en el ojo, ya que el funcionamiento de los lentes de contacto multifocales depende del despliegue adecuado del perfil de potencia multifocal en la córnea y de las interacciones ópticas entre los lentes y el ojo.

Metodologia

En esta tesis hemos utilizado dos simuladores visuales de AO diferentes desarrollados a medida (ViobioLab, CSIC, Madrid). En primer lugar, un sistema AO monocromático provisto de un espejo Deformable, permitió evaluar el rendimiento visual a través del foco (Agudeza Visual), con lentes de contacto multifocales reales en el ojo de diseño de centro cercano con tres adiciones diferentes (Bajo, Medio, Alto) en dos edades diferentes. grupos (jóvenes adultos, présbitas) en presencia y ausencia de alojamiento. En segundo lugar, un sistema AO policromático permitió simular las lentes multifocales en un Modulador de Luz Espacial como mapas de fase, ya través del enfoque se midió la agudeza visual y se comparó con las lentes de contacto reales. El canal SLM también se usó para simular múltiples diseños de patrones multifocales/bifocales. La respuesta acomodativa objetiva se evaluó para diferentes demandas acomodativas inducidas a partir de mediciones de aberrometría de Hartmann-Shack. En el tercer sistema monocular AO (Universidad KTH, Estocolmo, Suecia), que consta de Hartmann-Shack, un espejo deformable y un monitor para la presentación de estímulos, medimos el umbral de agudeza periférica y las aberraciones del frente de onda para evaluar la calidad visual foveal y periférica y la acomodación con Diseños de lentes de contacto multifocales. Por último, una tomografía de coherencia óptica del segmento anterior (AS-OCT) desarrollada a medida para evaluar el perfil de la lente de contacto en el ojo y la conformidad potencial con la córnea.

Resultados

Se evaluaron lentes de contacto multifocales en el ojo de diseño centro-cerca con diferentes adiciones (Baja, Media, Alta), las lentes de contacto multifocales produjeron una degradación pequeña pero consistente en lejos mientras que un beneficio consistente en cerca en ausencia de acomodación y esta degradación aumenta con aumento de la adición de las lentes. Estas lentes no degradaron significativamente la visión de cerca, de hecho, mejoraron la visión de cerca en ausencia de acomodación (estado acomodativo paralizado). La agudeza visual a través del foco se capturó a través de diseños multifocales simulados en el modulador de luz espacial que fue muy similar a los resultados con los lentes de contacto reales en el ojo. Las propiedades ópticas efectivas de las lentes MiSight son la gran borrosidad periférica y la función de dispersión de puntos más asimétrica debido al astigmatismo y coma adicionales, y que esto conduce a una mayor respuesta acomodativa. Las lentes inductoras de aberración esférica positiva de distancia central produjeron un retraso de acomodación reducido/menor en todos los sujetos. El AS-OCT mostró que las lentes de contacto blandas multifocales conforman la córnea subyacente, tanto en la zona central como en la periferia. Sin embargo, el complemento central cercano se proporciona como se esperaba.

Conclusiones

La simulación visual de AO ha permitido la simulación de múltiples diseños de lentes multifocales en los elementos ópticos y nos ha permitido probar múltiples diseños al mismo tiempo. También permitió probar estos lentes antes de colocarlos físicamente en el ojo en la clínica y también fabricar lentes específicos para los requisitos individuales. Los lentes de diseño multifocal centro-cerca disminuyeron el retraso acomodativo, por lo que proporcionaron una visión consistente de lejos a cerca en términos de agudeza visual de enfoque, aunque a expensas de una cierta degradación de lejos. La respuesta acomodativa se midió por primera vez en este sistema, con los diseños de lentes simulados en el SLM y capturando las aberraciones del ojo mientras se inducía el desenfoque (demanda acomodativa) con el badal. El rendimiento y la interacción de estos lentes están impulsados por la presencia o ausencia individual de aberraciones nativas de alto orden que alteran la respuesta acomodativa. Factores como el tamaño de la pupila, el diseño de la lente multifocal, las aberraciones nativas del ojo, la cantidad de aberración esférica inducida deben tenerse en cuenta en el tratamiento de la miopía con MCL y para obtener información sobre el mecanismo de funcionamiento de estas lentes.

LIST OF COMMONLY USED ABBREVIATIONS

A

Add = Addition

AO = Adaptive Optics

AOTF = Acousto-optic Tunable Filter

AOVS = Adaptive Optics visual simulators

AS-SOCT = Anterior Segment Optical Coherence Tomography

AF = Accommodative Facility

AR = Accommodative Response

AFC = Alternative Forced Choice

B

BF=Best Focus

BCVA=Best Corrected Visual Acuity

C

Cyl = Cylinder

CI = Confidence Interval

CRT = Cathode Ray Tube

CLs = Contact Lens

CSF = Contrast Sensitivity Function

CM = Command Matrix

CLT = Contact Lens Thickness

CL = Closed Loop

CN = Center Near

CD = Center Distance

CSF = Contrast Sensitivity Function

D

D = Diopter

DM = Deformable Mirror

DMD = Digital Micro Mirror

DOF = Depth of Focus

DLP = Digital Light Processing

DL = Diffraction Limit

E

EDTRS = Early Treatment Diabetic Retinopathy Study

Eq = Equation

F

FdOCT = Fourier Domain OCT

FT = Fourier Transform

H

HS = Hartmann-Shack

HD = Holographic Diffuser
HOAs = High Order Aberrations
HA = High Add
H = Habitual

I

IOL = Intraocular Lens
IM = Interaction Matrix

L

LA = Low Add
LCoS = Liquid Crystal on Silicon
LCD = Liquid Crystal Display
LRT = Laser Ray Tracing
LOAs = Low Order Aberrations
LCA = Longitudinal Chromatic Aberration

M

MCLs = Multifocal Contact Lenses
MTF = Modulation Transfer Function
MA = Medium Add
MIOLs = Multifocal Intraocular Lenses

N

NSA = Negative Spherical Aberration
NL = NoLens
NPA = Near Point of Accommodation

O

OCT = Optical Coherence Tomography
Ortho-K = Orthokeratology
O = Occasional
OTF = Optical Transfer Function

P

PSA = Positive Spherical Aberration
PSF = Point Spread Function
PP = Pupil Plane

Q

QUEST = Quick Estimate by Sequential Testing

R

RAC = Corneal radius of curvature
RMS = Root Mean Square wavefront error
RCLp = Contact lens Posterior Radius of Curvature
RCLa = Contact lens Anterior Radius of Curvature
RAF ruler = Royal Air Force ruler
RPR = Relative Peripheral Refraction

S

SD-OCT = Spectral Domain Optical Coherence Tomography
SS-OCT = Swept-Source Optical Coherence Tomography
SLM = Spatial Light Modulator
SLD = Superluminescent Diode
SimVis = Simultaneous Vision Simulator
SV = Simultaneous Vision
SCLs = Supercontinuum Laser Source
SA = Spherical Aberration
SD = Standard Deviation
SE = Spherical error
SFs = Spatial frequencies
SR = Strehl Ratio

T

THC = Corneal Thickness
TdOCT = Time Domain OCT
TF = Through-focus
TFVA = Through-focus Visual Acuity
TCA = Transverse Chromatic Aberration

U

UV = Ultraviolet
UCVA = Uncorrected Visual Acuity

V

VA = Visual Acuity
VS = Visual Strehl
VSOTF = Visual Strehl Ratio

W

W(x,y) = Wave aberration in Cartesian coordinate
WTR = With the rule Astigmatism
W(ρ,θ) = Wave aberration in the normalized radial coordinate

Z

Z = Zernike

CHAPTER-1 INTRODUCTION

Multifocal designs have different applications in Presbyopia treatment and Myopia control but are challenging in terms of simulation and understanding their interactions with the subject's optics and implications on vision. Multifocal contact lenses working under the principle of simultaneous vision are known treatments for presbyopia, the age-related loss of crystalline lens accommodation affecting almost all the population over the age of 45 yrs, but they are also proposed solutions for myopia progression control, a lifelong condition characterized by high prevalence, a significant risk in terms of associated ocular pathology. They are challenging in terms of simulation and understanding their interactions with the subject's optics and implications on vision. This thesis is aimed to understand the coupling of the optics of the eye with different multifocal lens designs, and how those impact visual function at different distances, in emmetropes and myopes. We validated the use of Adaptive Optics visual simulators, by comparison of the through-focus visual performance and aberrations through real contact lenses on the eye, and simulations in a spatial light modulator/Deformable Mirror. AO simulations allowed measurements of visual acuity, aberrations, accommodation, and pupil diameter. This work allows assessing the effects of different multifocal lens design on vision, shedding light on the mechanisms of a range of focus expansion (under paralyzed accommodation and in presbyopes), and on the mechanisms of myopia development and myopia control in myopes (contribution of the peripheral optics, and accommodation). This research work is part of the MYFUN (Myopia Fundamental Understanding needed) European research network.

The current chapter presents an overview of the optics of the eye and the major elements involved in the development of presbyopia and myopia. It presents refractive errors and higher-order aberrations, and visual simulation techniques through adaptive optics. It finally discusses solutions for controlling myopia progression and, in particular, (current and prospective) designs for multifocal contact lenses.

1.1 MOTIVATION FOR THIS THESIS

The interaction between the human eye and multifocal contact lenses is very crucial to understand, how the native aberrations of the eye play a role in the effectiveness of the multifocal contact lenses to expand the range of focus in presbyopia, and as supposedly proposed solutions for myopia control. In presbyopia, the presence of a center-near region in the lens, or induction of spherical aberration improves near vision, and the expense of degrading visual quality at far. In myopes, soft contact lenses of different designs are proposed for the control of myopia progression, either by preventing hyperopic defocus in the periphery, or improving the accommodating response (and decreasing supposedly myopic accommodative lag).

Adaptive Optics (AO) visual simulators allow the possibility to simulate and have a subject experience different optical designs before lens fitting. The subjects can see through the designs mapped as phase maps onto the active components of the adaptive optics visual simulator (Spatial Light Modulator) and this gives an opportunity to test multiple designs, without any discomfort. It also allows evaluating the interaction of the contact lens designs with the eye's optics.

The motivation for this thesis is then to bridge the gap in the understanding of the coupling of the lens design to the optics of the eye, and its impact on visual performance and accommodating response. Ultimately, this will allow the most effective designs for presbyopia correction and myopia control and a customization

1.2 THE HUMAN VISUAL SYSTEM

The human visual system comprises the eye and visual cortex. It is the most sophisticated and durable image processing system, using a well-balanced combination of optical, biological, and psychological processes. The vision process can be divided into 3 stages: the first involves ocular optics and describes how the optical system of the eye creates images on the retina; the second is known as the retinal stage and describes how photoreceptors sample the retinal image and transform the light energy into nerve impulses that travel to subsequent steps in the visual process; and the third is known as neural/cortical stage where the image is processed in the brain to enable perception of the final image.

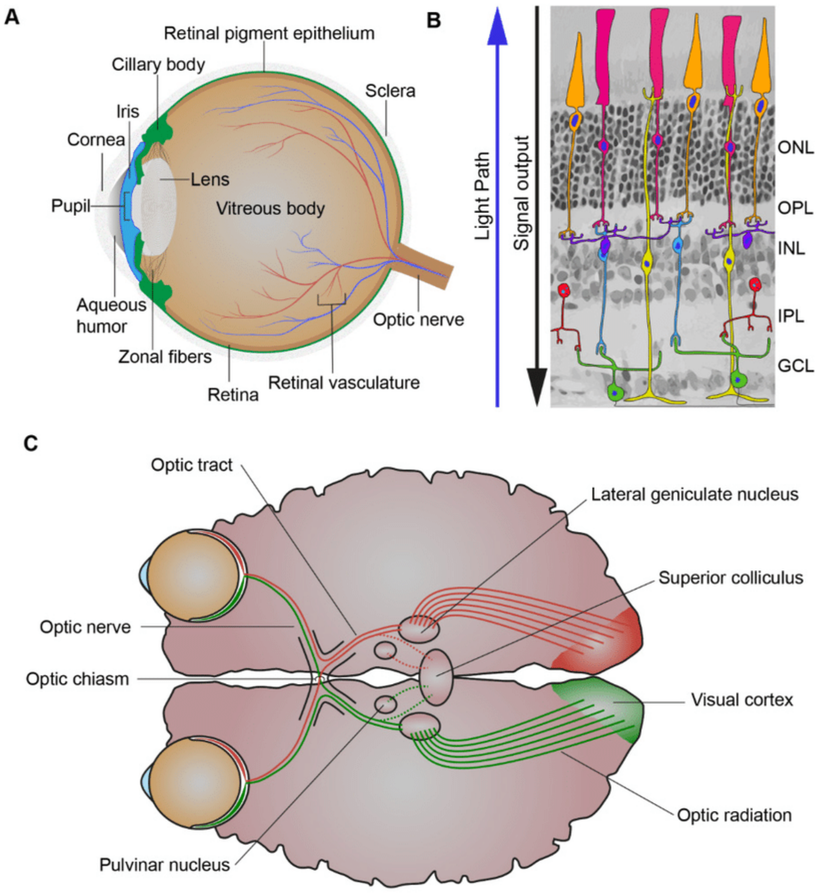

Figure 1.1. Schematic representation of the 3 stages of visual process. (A) The human eye (optical stage), (B) layers of the Retina (retinal stage), and the (C) Visual pathway from the retina through the optic nerve to the primary visual cortex (neural/cortical stage)(1).

1.2.1 Overview: The Ocular optics

In terms of anatomy, the human eye is made up of three layers: an outer layer made of fibrous tissue that acts as a thick wall to protect the eye's interior structures. The anterior region of the eye is composed of opaque sclera for the remaining three-quarters, with the last one-sixth being made up of a clear cornea. To protect the exposed sclera, the conjunctiva is tightly connected at the sclera-cornea junction or limbus. Iris, ciliary body, and choroid comprise the three components of the intermediate vascular layer (anterior to posterior respectively). All of the eye's interior structures receive nutrients from it. Rods and cones, as well as other nerve cells, are found in the retina, a photosensitive layer that makes up the inner neural coat. These photo-reactive cells convert light into electric signals when exposed to it, which travel down the visual pathway to the visual cortex and enable vision.

The eye has an approximately spherical shape of about 24mm in diameter in an adult. The optical system of the eye is made up of two lenses, the cornea ,and the crystalline lens, and by a transparent media the aqueous and the vitreous humor (Figure 1.2). The light first enters the eye through the cornea which is a transparent avascular tissue with a large number of nerve endings.

The cornea is about 12mm in diameter, about 0.6mm thick, and has a refractive index of 1.366. Most of the eye power is generated in this step (73%). Next, is the iris, a colored muscle that acts as a diaphragm controlling the amount of light that enters the eye, this diaphragm where the light enters is the pupil, with a diameter of 2mm to 8mm in a young adult. This variation, depending on the level of illumination, controls the quantity of light that reaches the retina and plays a vital role in the retinal image quality. The pupil is followed by the crystalline lens, a transparent structure controlled by a ciliary muscle, which is capable of modifying its shape to keep the image clear at the retina. Its refractive index varies from one zone to another from 1.42 in the center to 1.39 in the periphery. Then the light eventually reaches the back of the eye where the retina is located.

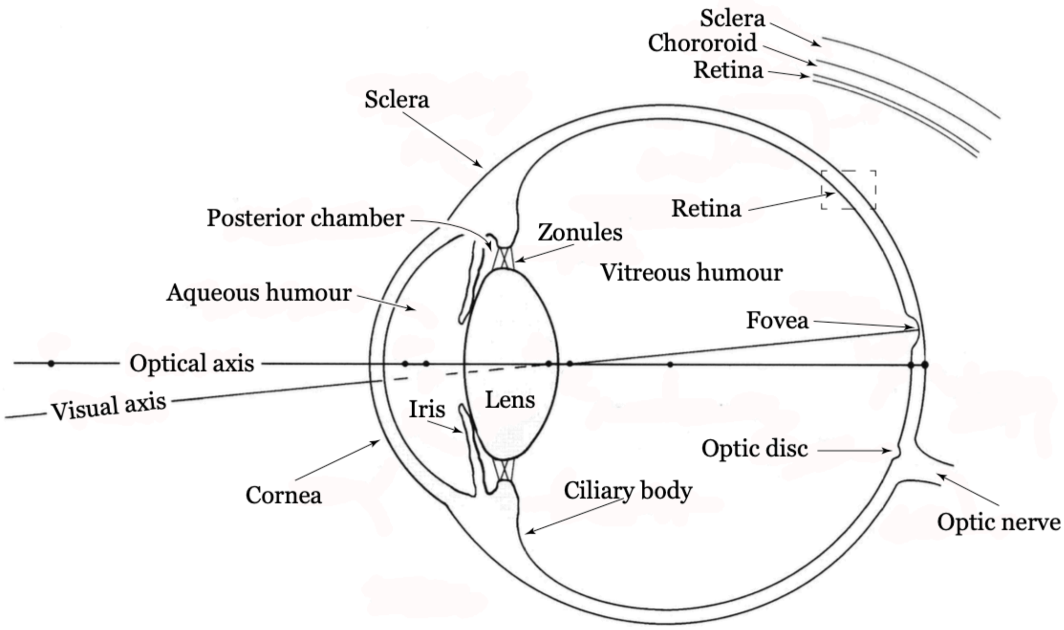

Figure 1.2. Horizontal cross section of the human eye showing the structures of the eye, the visual axis (the central point of the image focusing in the retina), and the optical axis(2).

The human crystalline lens, which is located between the iris and the vitreous humor, is a clear, biconvex lens with aspheric surfaces. The crystalline lens is a densely packed structure with concentric fibers in an elastic capsule. The ciliary body and lens equator are linked by bundles of zonular fibers that are organized radially. The lens has an equatorial diameter of 10mm and an anteroposterior thickness of roughly 4mm when it is unaccommodated. The average curvature of the front surface is 10mm, whereas the curvature of the posterior surface is 6mm. The thicker nucleus at the center and the rather loosely packed cortex are formed by lens fibers that the capsular epithelium regenerates throughout its lifespan. It adds around 16D to the eye's overall power.

With varying object vergence, the crystalline lens can change its size and shape. Accommodation is the term used to describe the process of a lens's optical power increasing while its shape changes. When the ciliary muscle contracts during accommodation, there is less zonular tension at the lens equator, which causes the lens capsule to relax. In turn, this causes the lens' anterior curvature and center thickness to rise. In actuality, the traditional near triad, also known as the accommodative reflex, is accompanied by the two eyes converging and the pupil constricting (miosis). The mechanical properties of the lens change with age, leading to the loss of accommodation ie presbyopia. For younger people, the aberrations between the cornea and lens compensate each other (spherical aberration), but this balance gets disturbed with age or different pathologies.

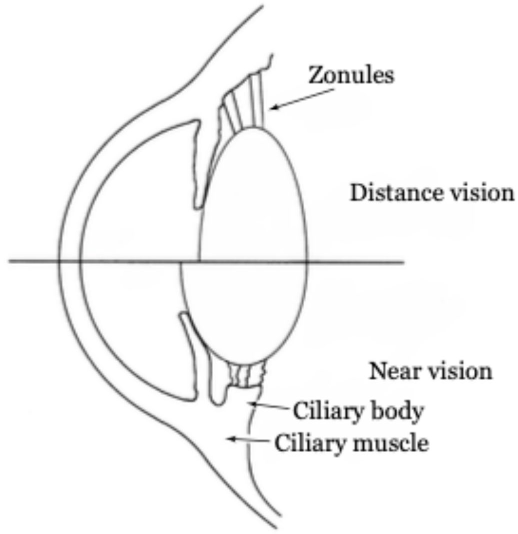

Figure 1.3. Structure of the crystalline lens showing the change of shape during accommodation for near vision and relaxing for distance vision.

1.2.2 The Neurosensory Retina

The Retina is a light-sensitive tissue that allows gathering of the information contained in the images formed by the eye's optics. The human retina is formed by a large variety of cells organized in a very stratified manner. A radial section of a portion of the retina reveals the organization of the different retinal layers. Figure 1.4 shows a section of the retina with the cells that form it and how they are connected, in layers from the outside to the inside of the eye. The neural retina consists of three main groups of neurons: the photoreceptors, the bipolar cells , and the ganglion cells. The rods and cones together comprise the photoreceptors. Rod photoreceptors are responsible for scotopic vision (dim light conditions), while cones are responsible for photopic vision, the intermediate vision where the two types of photoreceptors intervene is mesopic vision(2). These cells when they receive suitable light stimulus are excited and transduce electromagnetic energy into electrochemical signals, which are transmitted through successive neurons in the retina itself and then to the brain. The first-order neurons bridging photoreceptors and ganglion cells are known as bipolar cells. The retina's innermost ganglion cells, which are relay neurons, are located near the lens and the front of the eye. Between the ganglion cells and photoreceptors, there are two other types of cells: horizontal and amacrine so that the transmission of information can follow different paths within the connection of the different retinal cells and it will depend on their location on the retina. Thus, in the fovea, each photoreceptor cone connects with a bipolar cell, and this in turn with a ganglion following the most direct path(3,4).

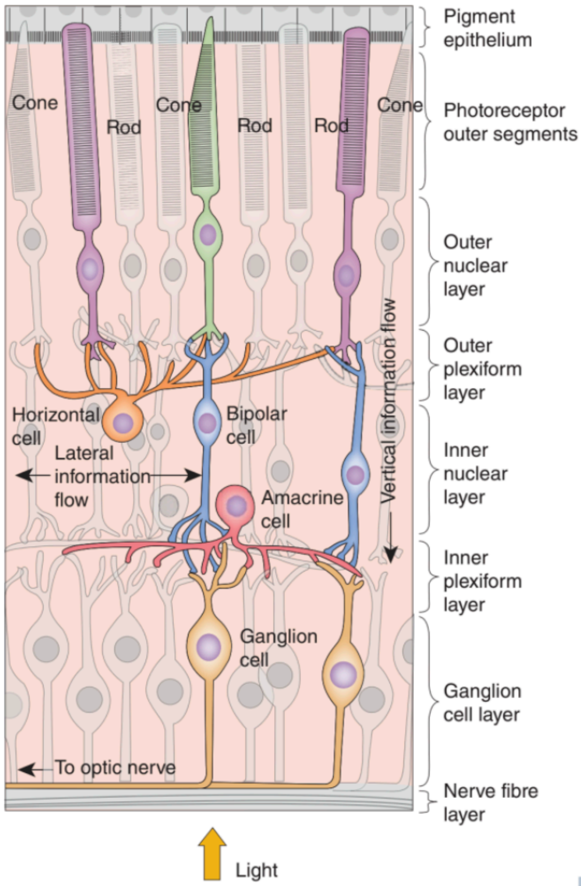

Figure 1.4. Schematic of the retina and their major synaptic connections. Rods, Cones, Horizontal, Amacrine, Bipolar and Ganglion cells(5).

The central area of the retina, called the macula, has an approximate area of 5.5mm in diameter and is rich in cones surrounded by a non-photosensitive pre-retinal pigment. The macula provides sharp and detailed vision and prevents short-wavelength radiation from reaching that area of the retina. The center of the macula has a depression that occupies approximately 1.5mm in diameter and subtends an angle of 5 deg, it is called the fovea. The central portion of the fovea is the foveola where the image of the fixation object is formed. The foveola or central fovea is composed entirely of cones. The total count of cones is about 6.4 million and roughly 125 million rods in the retina(5,6). The spatial distribution and density of the photoreceptors limit the resolution of the eye. There are three types of cone photoreceptors: red, green , and blue cones (long, medium , and short wavelength sensitive cones or L, M and S cones depending on which portion of the spectrum, their photopigment absorbs the most)(7). Normal trichromatic color vision utilizes all three cone photopigments (Figure 1.4). Cones exhibit three different types of photopsins, corresponding to short, medium , and long wavelengths with absorption peaks at 419nm, 531nm , and 559nm. Rods present the same spectral sensitivity, preventing the sensation of color to appear under low light conditions. The absorption of light within the rod photoreceptors is done by a special protein molecule known as rhodopsin, belonging to the wider type of photopsin molecules. The absorption peak of rhodopsin is around the 496nm wavelength.

An effect of the directionality of the photoreceptors is described as the Stiles-Crawford effect. When the intensity of the light coming through an off-axis pupil point is adjusted to balance the brightness drop, there is an associated change in the perceived hue(8–10).

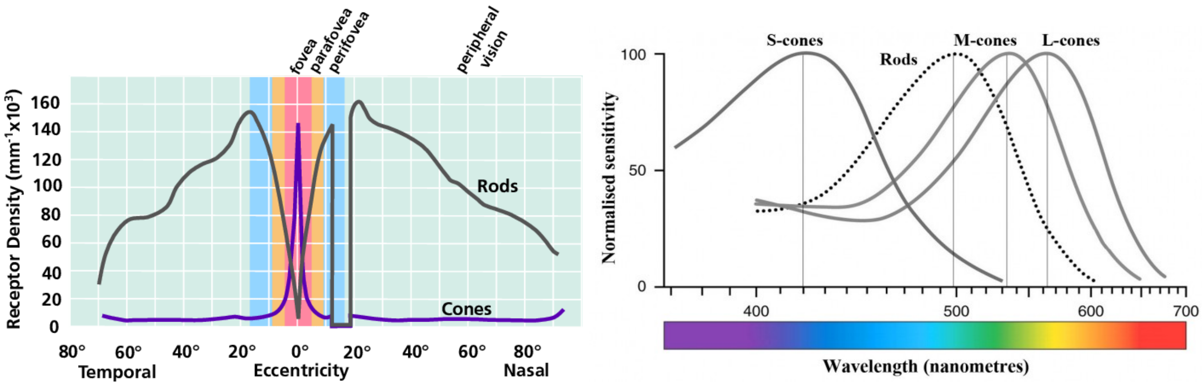

Figure 1.5. (Left) Linear density of cones, rods and ganglion cells as a function of eccentricity in the fovea. (Right) Spectral sensitivities of the L, M and S cones in the human eye(11).

1.2.3 The Visual Cortex

The primary visual cortex is where the information from the eye finally arrives after traveling further down the visual pathway (Figure 1.6). The optic chiasm is the point at which the fibers that make up the optic nerve exit the eye and continue uninterruptedly to various parts of the brain. The majority of them (about 80%) carry information to the lateral geniculate nucleus via the optic tract; the remaining information is used to control eye movements, the pupillary reflex to light, as well as mechanisms for synchronizing biological cycles (hypothalamus). The left visual field's information travels to the right lateral geniculate nucleus through the optic chiasm, while the left visual field's information travels to the left lateral geniculate nucleus, and so on.

They continue from there to the lateral geniculate nucleus of the thalamus before ending at the main visual cortex, a large region in the occipital brain (area V1- primary visual cortex). Here, for the first time in the entire perception process, the primary visual cortex received input from both eyes, that is there is binocular convergence that allows the construction of a single image of the visual scene. The visual cortex is where the information is processed, and it influences how shapes, orientations, colors, movement, size, noise reduction, edge filtering, color separation, image compression, motion analysis, pattern recognition, and other brain processing activities are handled.(12).

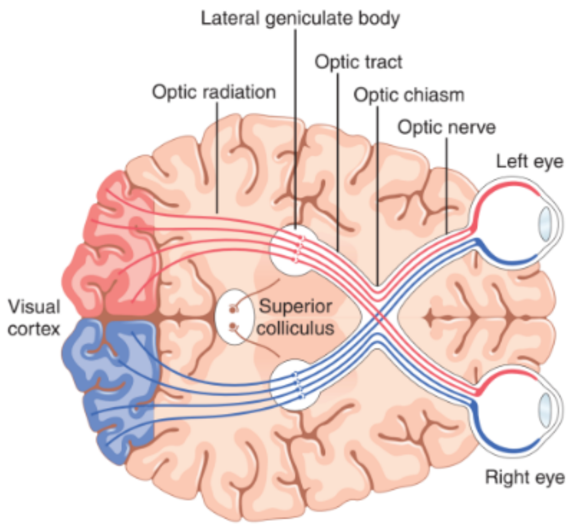

Figure 1.6. The primary visual pathway from the eye to the visual cortex, showing the optic nerve, optic tract, optic chiasm, the lateral geniculate nucleus and the optic radiation(13).

In conclusion, the human visual system process visual information in 3 stages: optics (focussing on the image), retinal (signal transduction light in electrical impulses) and finally the brain processing (cortical stage at the visual cortex).

1.3 THE OPTICAL QUALITY OF THE EYE

The human eye is an imperfect optical system. The optical quality of the images projected on the retina depends on several factors: scattering, diffraction, aberrations , and misalignment of the ocular components. All these phenomena contribute to the degradation of the retinal image. Scattering occurs at the cornea(14), but much more prominently in the lens, increasing with age (due to increased opacity in the crystalline lens). Diffraction is produced by the edges of the pupil and affects the maximum resolving power of the eye, acting as a low pass filter for spatial frequencies of the image(15). The effect of diffraction depends on pupil size, which is affected by the luminance conditions, alongside other factors.

Aberrations vary across eyes, both in magnitude and distribution, and their patterns are unique to an eye and it changes with age(16–18), with a pupillary diameter(19,20), with refraction(21–23), with accommodation(24,25) and with eccentricity(26–28) , etc. Those aberrations can be divided into two main groups: monochromatic and chromatic aberrations (Figure 1.7). The following section will describe them in more detail.

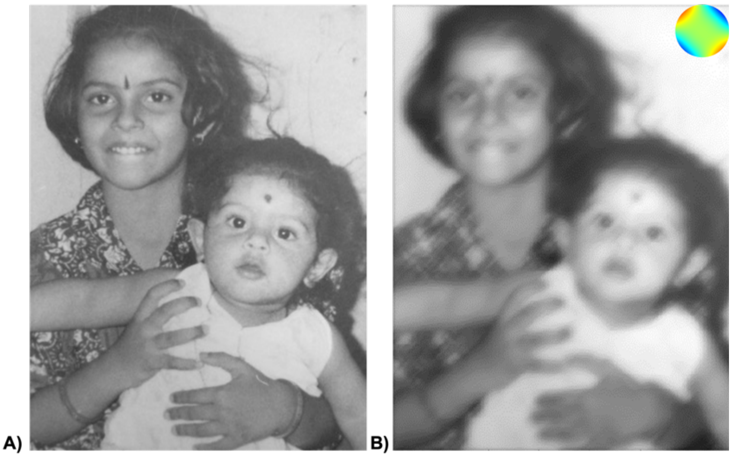

Figure 1.7. Simulated image A) Diffraction limit B) Monochromatic aberration defocus + astigmatism, using Matlab (Model thesis author).

1.3.1 Monochromatic aberrations

When only one wavelength is taken into consideration, monochromatic aberrations arise because of irregular shapes, misalignments of the optical surfaces relative to the optical axis, and inhomogeneities in the refractive indexes of the media. In a Zernike polynomial representation, the low-order aberrations (defocus and astigmatism) generally exhibit the largest magnitude in normal eyes. Defocus in the eye is referred to as ametropia, with myopia for the negative sign of defocus (an excess of power, shifting the image plane in front of the retina), and hyperopia for the positive sign (a lack of power, shifting the image plane behind the retina). The eyes with no significant defocus and astigmatism are referred to as emmetropic. Optometric refraction, i.e defocus and astigmatism in diopters can be calculated from Zernike polynomials using the following formulas.

$$M=\frac{-c_2^0\,4\sqrt{3}}{r^2}\;;\;J_0=\frac{-c_2^2\,2\sqrt{6}}{r^2}\;;\;J_{45}=\frac{-c_2^{-2}\,2\sqrt{6}}{r^2} \qquad \text{Eq. (1.1)}$$

Where coefficients (Cnm, ‘M’ defocus, and ‘J’ astigmatism at 0 deg or 45 deg) are expressed in micrometers, and ‘r’ is the pupil radius in mm. Such refractive errors are usually corrected with spectacles or contact lenses. Detailed explanations of the refractive errors and corrections are included in the following sections.

The monochromatic wavefront aberration is usually described as a phase map, W (x,y), representing the distortions of the wavefront as it goes through an optical system. The wavefront surface is orthogonal to the corresponding rays going into the eye (or exiting the eye) at every point. Figure 1.8 depicts a schematic illustration of the effect of ocular aberrations on the quality of the retinal image in (A) an aberration-free eye where all parallel rays are entering the pupil and will intersect the retina at the same point, the wavefronts will be spherical, and the image point will be in the center of the wavefronts; and (B) an aberrated eye where there is no longer a point focus, different rays will intersect the retina at different points, and the wavefront will no longer be spherical.

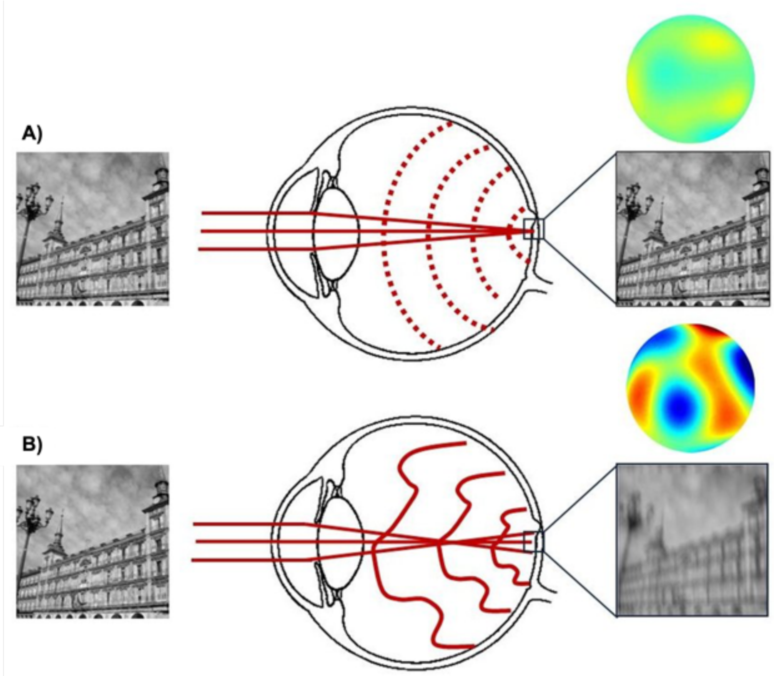

Figure 1.8. Diagram showing the impact of monochromatic wave aberrations on the quality of the retinal image in an A) aberration-free eye and an B) aberrated eye (29).

Wave aberrations can be defined as the separation between each wavefront point and the ideal sphere at the exit pupil allowing the optical aberration to be defined in terms of wave aberration maps(30). Mathematically, a polynomial series can be used to characterize the wave aberration of a general optical system. Because they are orthogonal across the unit circle and ocular aberrations often correspond to circular pupils, Zernike polynomial expansion has become the industry standard for describing ocular wave aberration data(31). The so-called Zernike coefficients, which represent the magnitude of each aberration present, can be used to weigh the sum of Zernike polynomial functions that describe a wave aberration. The spatial frequency of Zernike modes increases with their order.

$$W(x,y)=\sum_{n,m} c_n^m Z_n^m \ (x,y) \qquad \text{Eq. (1.2)}$$

Where W (x,y) is the wave aberration phase in microns as a function of polar coordinates, Cnm are the corresponding Zernike coefficients, and Znm (x,y) is the Zernike polynomial of order ‘n’ and frequency ‘m’. A set of recommendations regarding the sign, normalization , and order were established by The Optical Society of America (OSA, currently OPTICA) and that will be followed throughout this thesis(32).

Apart from the low order aberrations, the eye also suffers high order aberrations (HOAs), which are not usually measured in clinic.

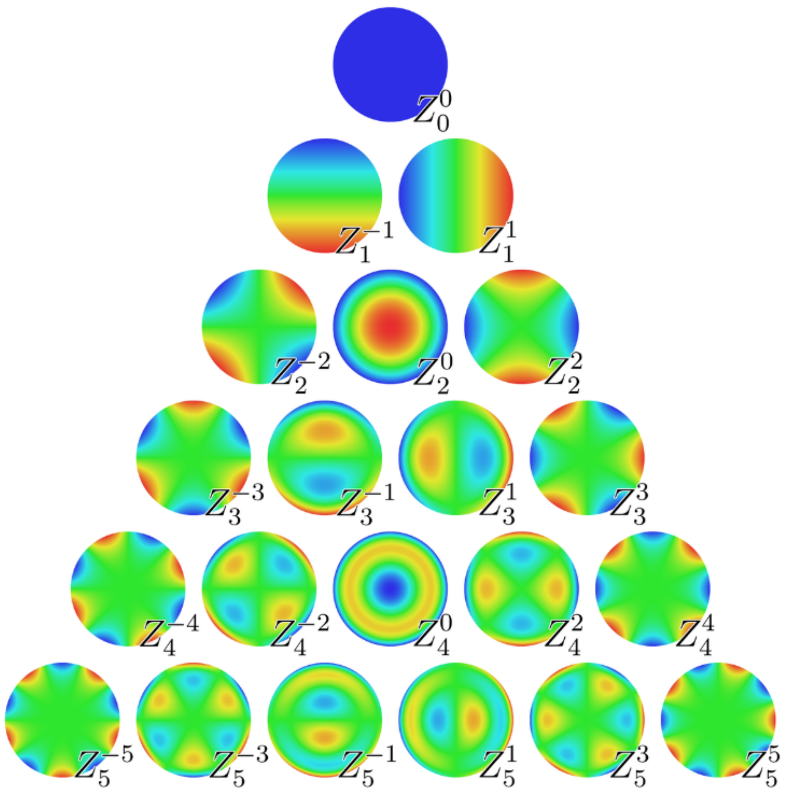

Figure 1.9. Zernike polynomials up to 5th order. Each row in the pyramid corresponds to a radial order of a polynomial, and each column to a meridional frequency.

The ocular spherical aberration was measured for the first time by Ames and Proctor in 1921(33). Smirnov(34) in 1961 measured ocular aberrations using the vernier alignment technique. Other more recent techniques are the spatially resolved refractometer, the ray-tracing , and the Hartmann-Shack wavefront sensor. Most aberrometers operate by measuring the deviation of the emergent wavefront (outgoing aberrometry) or the image of the standard beam at the retina to determine the local derivative (slope) of the wave aberration (ingoing aberrometry). In this thesis, an outgoing aberrometer called a Hartmann-Shack wavefront sensor (HS) that we developed specifically for this purpose was used.

The monochromatic high-order aberrations (HOAs) are measured using monochromatic light, typically near-infrared (NIR). The human eye has reduced sensitivity to NIR light, which makes the measurement more comfortable for the subjects, and also avoids the pupil constriction induced by visible light. However, for evaluating the effect the aberrations would have on visual performance it is necessary to consider them in the visible spectrum. It has been experimentally shown that HOA measurements in NIR and green light are nearly identical(35,36), only differing in the defocus term. The longitudinal chromatic aberration of the eye can be then calculated as the chromatic difference of focus between the red and blue ends of the visible spectrum.

1.3.2 Chromatic aberrations

Chromatic aberrations appear as a consequence of the chromatic dispersion of the ocular media, producing a change in the aberrations as a function of wavelength(37). Chromatic aberration adopts two forms: Longitudinal Chromatic Aberration (LCA) and Transverse Chromatic Aberration (TCA). LCA results in a wavelength-dependent change of refractive power(37,38) while TCA produces a wavelength-dependent change in the magnification of an extended image(38,39). LCA is said to be relatively constant among subjects(38,40), TCA has a high variability preventing its correction using the average values(41).

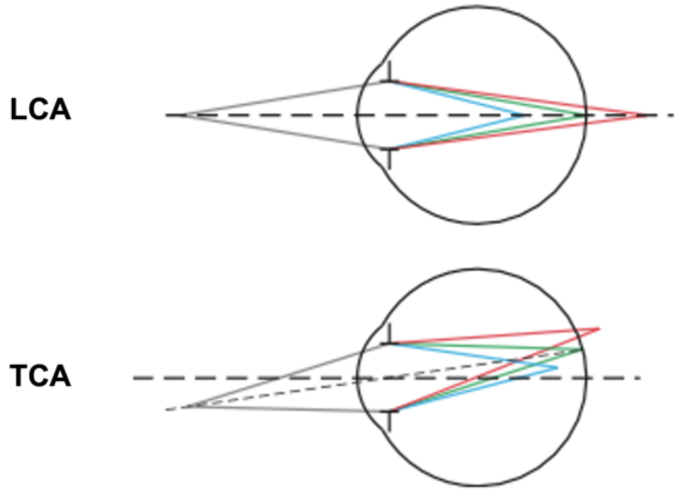

Figure 1.10. Schematic showing the chromatic aberrations of the eye. Top panel shows the LCA and below panel shows the TCA.

The ocular media of the human eye have a lower refractive index for longer wavelengths than for shorter ones. As a result, the eye that is emmetropic for green light is myopic for blue light and hyperopic for a red light. Across the visible spectrum (from 400 to 700 nm), the amplitude of LCA in the eye approaches roughly 2D(2,38,42). In TCA the objects in blue light are less magnified than the red light.

1.3.3 Optical quality metrics

Several optical quality measures have been established, which are typically computed from the measured wave aberrations. Additionally, as optics impose initial limits on vision, there have been several attempts to link optical and visual quality. Typically the largest correspondence between optical and visual quality has been found using retinal image quality metrics for optical quality. However, other metrics are often used for convenience. The following sections describe the optical quality metrics used in this thesis.

A. Root Mean Square wavefront error (RMS)

The Root Mean Square wavefront error is a common global pupil plane metric for assessing optical quality (RMS). The degree of divergence between a perfect wavefront and the actual one is represented by the Root Mean Square (RMS) wavefront error, which is frequently used as a general metric for optical quality from the Zernike coefficients (wave aberration). A lower RMS indicates better optical quality. An ideal concordance between the wavefront and the reference sphere is implied by a theoretical "zero" value. RMS is often used as a quantitative objective indicator of optical quality at the pupil plane level, either including all aberrations, high-order aberrations, or specific terms or orders. In Equation (1.3), the piston (C0) and tilts (C0±1) have been removed, since they only represent a displacement of the image and not degradation.

$$\mathrm{RMS}=\sqrt{\sum_{n,m}(c_n^m)^2} \qquad \text{Eq. (1.3)}$$

Where Cnm is the Zernike coefficient corresponding to the order 'n' and the frequency 'm'. RMS is measured in microns (μm).

B. Retinal image quality metrics

Retinal image quality measures derived from wave aberration incorporate the combined effects of diffraction and aberrations but exclude scattering. Utilizing criteria that are based on retinal image quality, which have been shown to more closely correlate with visual function, the optical quality is characterized. Retinal image quality measurements employed in this thesis include the Point Spread Function (PSF), Modulation Transfer Function (MTF), Strehl Ratio (SR), and Visual Strehl Ratio (VSOTF).

Point Spread Function (PSF)

Light from a point source is scattered throughout the image as indicated by the Point Spread Function (PSF). The size of the pupil, aberrations, blur, and diffraction are all factors that affect it. A perfect optical system has an Airy disk as its point spread function (diffraction is the only restriction) (43). A bigger PSF than the aberration-free PSF for the same pupil size is produced when there are ocular aberrations because they spread out light over a region.

The pupil function, P(x,y) defines how light is transmitted by the eye's optics, where P(x,y) is the pupil function, A(x,y) is an apodization(44,45) function (when the waveguide nature of cones is considered) and W(x,y) is the wave aberration (in Cartesian coordinates). P(x,y) is zero outside the pupil.

$$P(x,y) = A(x,y)\, exp(i\frac{2\pi}{\Lambda}W(x,y)) \qquad \text{Eq. (1.4)}$$

The PSF is calculated as the squared magnitude of the inverse Fourier transform of the pupil function(29,46,47) where FT is the Fourier transform operator, K is the constant and z is the distance from the pupil to the image.

$$PSF(x,y) = K\left|FT\left[A(x,y)\, exp(i\frac{2\pi}{\Lambda}W(x,y))\right]_{f_x=\frac{x}{z},f_y=\frac{y}{z}}\right|^2 = K\left|FT[P(x,y)]_{f_x=\frac{x}{z},f_y=\frac{y}{z}}\right|^2 \qquad \text{Eq. (1.5)}$$

Modulation Transfer Function (MTF)

The Modulation Transfer Function (MTF) is the ratio of the image contrast to the object contrast as a spatial frequency. Mathematically, it is the modulus of the Fourier transform of the PSF which is the Optical Transfer Function (OTF)(48). This function explains how the contrast of sinusoidal waves is altered by the optical system and shows how much the object's frequency content is transferred to the image by the optical system. The transmission of frequencies from object to the image will be worsened by system aberrations as the MTF will decline more quickly. High spatial frequencies, or the minute details in the image, experience a significant contrast decrease.

$$\mathrm{MTF(x,y)=|FT(PSF(x,y))|} \qquad \text{Eq. (1.6)}$$

Aberrations reduce the contrast (MTF) of the retinal image or translate the image sideways to cause a spatial phase shift with spatial frequency (PTF). Good MTF readings and low PTF values suggest a high-quality OTF in the eye.

Strehl ratio (SR)

The Strehl ratio (SR) is a scalar metric calculated as the ratio of the aberrated eye's maximum PSF value to the maximum PSF value in a diffraction-limited eye. The range of the SR can be between 0 and 2, with 1 defining a perfect optical system.

$$SR_{SPATIAL} = \frac{\max(PSF)}{\max(PSF_{DL})} \qquad \text{Eq. (1.7)}$$

In the frequency domain, the SR is computed as the volume under the MTF of an aberrated system normalized by the diffraction-limited MTF, for the same pupil size.

$$SR_{FREQUENCY} = \frac{\int_{-\infty}^{\infty}\int_{-\infty}^{\infty} MTF\,(f_x,f_y)df_x df_y}{\int_{-\infty}^{\infty}\int_{-\infty}^{\infty} MTF_{DL}(f_x,f_y)df_x df_y} \qquad \text{Eq. (1.8)}$$

Where MTF is the MTF of the aberrated wavefront, while the MTFDL is the diffraction-limited MTF(29,47).

Visual Strehl (VS)

Visual Strehl (VS) is an image quality metric that has been reported as an optimum metric for predicting the visual performance of the eye based on its aberrations. The VSOTF is determined in the frequency domain, and the OTF is weighted by the neural contrast sensitivity function (CSFN).

$$VS = \frac{\int_{-\infty}^{\infty}\int_{-\infty}^{\infty} CSF_N\,.OTF(f_x,f_y)df_x df_y}{\int_{-\infty}^{\infty}\int_{-\infty}^{\infty} CSF_N.OTF_{DL}(f_x,f_y)df_x df_y} \qquad \text{Eq. (1.9)}$$

Where CSFN is the neural contrast sensitivity function, OTFDL is the OTF limited by diffraction, OTF is the OTF of the aberrated system, and (fx,fy) are the spatial frequency coordinates.

1.4 REFRACTIVE ERRORS

The formation of a clear image on the retina is a prerequisite for the proper operation of human vision. Emmetropia is defined as a refraction state where, when accommodation is at rest, parallel streams of light from infinity are focused at the retina. Because of this, an emmetropic eye consistently produces a clean image of a faraway object without the need for any internal optics change. Infinity is the distance at which an emmetropic eye may concentrate clearly without exerting too much effort to accommodate. Ametropia is a refraction condition where, with accommodation at rest, parallel beams of light from infinity concentrate in front of the retina (myopia) or behind it (hypermetropia), in one or both meridian (astigmatism), or in both (hypermetropia). The various types of refractive errors will be covered in this section, along with associated epidemiology.

1.4.1 Hyperopia

The name "hypermetropia" comes from the Greek word "ops," which means "eye" and implies "beyond measuring." Farsightedness, or hypermetropia, happens when parallel light beams from infinity concentrate behind the retina while accommodation is at rest. The consequence is a blurry retinal image because the retina is behind the posterior focus point and distant point of the eye (Figure 1.11). Young people with mild to moderate hypermetropia can readily be accommodated by using accommodation techniques.

1.4.2 Astigmatism

The words "astigmatism" and "stigma" are both ancient Greek words that mean "point" (absence). Due to uneven refractive power in various meridians of the refractive surfaces (cornea and/or lens), astigmatism is a refractive mistake that occurs when parallel light rays enter the eye and are unable to focus at a single place. The distance in the retina between two focus locations is known as the Sturm interval. The least distorted field of vision in an untreated astigmatic eye is known as the "circle of least confusion."

After a uniform shift in refraction, regular astigmatism happens when the meridians with the highest and lowest refractive powers are parallel to one another. With-the-rule (WTR) and against-the-rule (ATR) astigmatisms are two types of common astigmatism that depend on whether the meridian is steep or flat. The eye's most curved meridian is perpendicular to the negative astigmatic axis, which is perpendicular to both the WTR and ATR (49).

1.4.3 Myopia

The name "myopia" comes from an ancient Greek word that means "to close" and "ops" is the word for eye. A refractive eye disorder known as myopia, sometimes known as nearsightedness, occurs when light rays entering the pupil are focused in front of the retina, causing distant objects to seem blurry. Due to an imbalance between the eye's optical power and axial length, light rays in myopia fail to focus on the fovea (2). Figure 1.11 illustrates how the emmetropic eye's optical system allows light rays to pass through and focus on the retina for clear distance vision, whereas the myopic eye's light rays fall short and focus in front of the retina.

Myopia can be classified as low (-0.5 to -2.99D), moderate (-3.00 to -5.99D), or high (-6.00D) dioptric levels in terms of power (50). According to the age of onset, myopia was categorized as follows: Myopia that was present at birth and persisted throughout the neonatal years is referred to as congenital myopia. Myopia appears in young people between the ages of 6 and 20. People aged 20 to 40 were impacted by early adult-onset myopia, but those beyond 40 are affected by late adult-onset myopia.

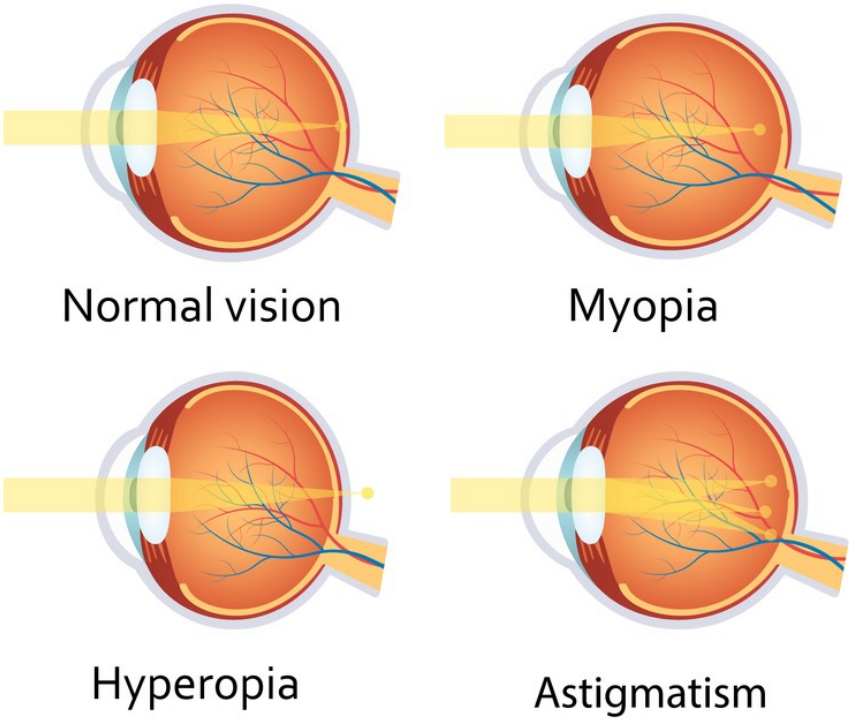

Figure 1.11. Schematic of emmetropic (normal vision), myopic eye, hyperopic eye , and astigmatism.

1.4.4 Prevalence of myopia

Myopia is the leading cause of vision impairment worldwide, as well as the second most common cause of blindness(51). The prevalence of myopia has rapidly grown in recent decades, especially in East Asia, reaching epidemic levels(52) and the Western Pacific region. The incidence of myopia increasing all over the globe, including the United States(53,54) and Europe (53,54). If myopia progression continues at this rate, half of the world's population will become myopia by the year 2050(52). The predictions assume that increased urbanization and development in countries will continue to spread the associated lifestyle changes, such as decreased time outdoors and increased near-work. The so-called high-pressure educational systems in East Asian countries seem also a factor in the growth of myopia prevalence.

The burden of myopia is not only associated with poor sight (which can be compensated with the appropriate correction), but with the increased risk of other sight-threatening pathological changes, such as retinal detachment, myopic macular degeneration , and glaucoma, causing permanent vision loss(55,56). The term "pathological myopia" is used to describe situations where high myopia levels have resulted in irreversible changes. The myopia associated with excessive axial length elongation of the eye leads to structural changes in the posterior segment, such as myopic maculopathy, high myopia-associated optic neuropathy, and retinal detachment. High myopia is the main risk factor to develop pathologic myopia, although it can also occur in low levels of myopia. The development of posterior staphyloma, which is the outward protrusion of all layers of the posterior eye globe with advancing age, as well as the axial length growth are the two main causes of myopic macular degeneration. High myopia patients who have widespread, patchy macular atrophy, CNV, and/or Fuchs' spot are said to have myopic macular degeneration, a disorder that threatens their vision(57). The axial length elongation associated with highly myopic eyes often creates myopia-associated glaucoma-like optic nerve damage, also known as optical neuropathy. This typically occurs in high myopic eyes with a secondary macro disc or peripapillary delta zone at a normal IOP. Optical neuropathy causes irreversible loss of vision(57). Retinal detachment is another common complication of high myopia, this risk increases with increasing refractive error due to the changes in the peripheral retina. The risk of retinal detachment also greatly increases with age.

Globally, 217 million individuals have moderate to severe visual impairment, 188.5 million people have mild vision impairment, and 36 million people are blind (58). There are 826 million people who suffer from near vision impairment, according to statistics. (59). A recent study(52), Myopia is most common among those aged 20 to 39 worldwide, and it is projected that this trend will continue at the current rate of development. Additionally, some research connected increasing myopia progression and education level (60,61). Numerous methods to slow the progression of myopia have been proposed as a result of the rapid increase in this visual impairment; these methods are discussed in the following sections.

1.4.5 Risk factors of Myopia

Myopia is a multi-factorial disorder with genetic, behavioral, and environmental influences that can affect both myopia onset and progression. This section will investigate potential risk factors as well as the forerunner of myopia prediction (62–64).

Genetic influences

Significant evidence suggests that myopia has a hereditary component that cannot be accounted for by a typical environment. Recent research has linked myopia to a variety of factors, including genetics (55,65,66). When one or both parents are myopic, the prevalence of myopia in children is frequently enhanced (67–69). Myopia is a defining characteristic of some diseases, including the heritable connective tissue diseases Marfan syndrome and Stickler syndrome (70). It has been demonstrated that the inheritance of myopia is complicated, with X-linked, autosomal recessive, or autosomal dominant patterns (50,71).

Near work and education

Numerous research (69) have discovered a link between early schooling, myopia, and education level (72,73). Myopia and levels of near employment have been found to have weak relationships (68,69,72). Researchers have looked into the connections between juvenile-onset myopia, near work, academic success, and parental myopia (69). Significant associations with myopia were found for both parental myopia and, to a lesser extent, close labor. There have been connections shown between myopia development and progression and the lag of accommodation during close work (74–76). Children with myopia may accommodate a close target less than emmetropic children (74) and show an insufficient accommodative response(74). The hyperopic foveal retinal blur is what causes myopia to evolve, then minimizing this blur may stop the advancement of myopia.

Outdoor time

Studies have demonstrated that light has a protective effect on the development of refractive abilities. The best indicators of future myopia were found to be fewer sports and outdoor activities combined with myopic parents. Spending time outside may lower the likelihood of developing myopia and guard against it, although the exact mechanism by which this occurs is uncertain. An increase in the retinal transmitter dopamine, which inhibits eye growth, is stimulated by the greater intensity of light that can be found outside, suggesting that it may offer protection. Animal research back up this theory (55,77–79). According to a different study, the greater distances faced outside compared to indoors may encourage dioptric flattening, which would affect how the eye reacts to the subsequent defocus (55). Children in a different study who were exposed to light everyday had much slower axial elongation than children who were exposed to less outside light (80). Another theory around outdoor activity is that because it does not necessitate large levels of accommodation in response to distant stimuli, the lag in accommodation required to respond to nearby targets is lessened, and as a result, axial elongation is not induced (81).

1.4.6 Ocular optic disruption in Myopia: Central and Peripheral optics

Studying HOAs of the myopic eyes can help to understand whether the retinal image quality has an impact on myopia development. Some studies have found a higher amount of HOA in myopes compared to emmetropes(82,83). Spherical aberration in particular has shown a significant correlation with refractive error(82). Some studies have reported a decrease in visual acuity when in myopes , especially high myopes and hypothesized that the decrease was due to retinal stretching but other studies did not find this decrease when the refractive error was corrected with contact lenses(84).

The optical quality of the eye differs across the visual field with the best optical quality achieved close to the fovea, whereas with eccentricity it degrades. Even in the absence of refractive errors in central vision (emmetropia), the eye experiences a large amount of optical errors in the periphery. It has been found that emmetropic and hypermetropic eyes are relatively myopic in the periphery, whereas myopic eyes have a hypermetropic shift off-axis. HOAs also increase with off-axis angles. Astigmatism is more dominant in the periphery and in terms of HOAs, coma is dominant off-axis. Spherical aberration is more uniform across the visual field and it is, on average, the dominant higher-order aberration on the axis(85,86).

1.4.7 Role of Peripheral Retina

At birth, humans tend to be emmetropic. Through the process of emmetropization during childhood, hypermetropia is reduced. Hypermetropia that occurs at birth triggers axial elongation. If the eye continues to elongate after emmetropization myopia occurs(87).

Animal experiments have demonstrated that axial elongation can be halted or initiated depending on the placement of the image relative to the retina. Experiments in chickens and monkeys with defocused vision, either with negative (image behind the retina) or positive (image in front of the retina) spectacle lenses, revealed that their visual system altered their refractive state by accelerating or slowing axial elongation to compensate for the imposed defocus (88,89). This was true in both the fovea and the peripheral retina. It was previously thought that only foveal optical errors could govern eye growth, however, it has now been demonstrated that peripheral image quality, even in the presence of a sharp foveal image, can influence ocular growth. Benavente-Perez et al(90). found that marmosets whose peripheral visual field was defocused positively developed hypermetropia whereas the negatively defocused animals developed myopia. They concluded that eye growth can be manipulated by the peripheral image quality. Figure 1.12 shows the schematic representation of an eye showing peripheral hypermetropic and myopic defocus while the foveal image is in focus, the hypermetropic defocus blurs the peripheral image, a growth signal is sent to the eye and axial elongation occurs while with the myopic defocus there is a peripheral blurred image, and a signal is sent to stop axial growth.

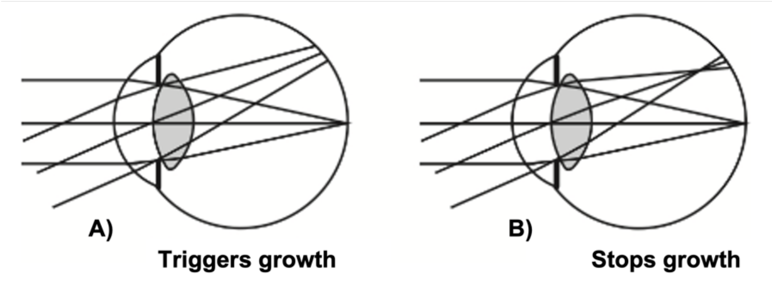

Figure 1.12. is a schematic representation of eyes with A) foveal emmetropia with peripheral hypermetropia and B) foveal emmetropia with peripheral myopia are shown. Peripheral hypermetropic blur triggers axial elongation whereas peripheral myopic blur stops axial growth.

In a foveally, emmetropic eye, relative peripheral hypermetropia occurs when the peripheral image is focused behind the retina, whereas relative peripheral myopia occurs when the peripheral image is focused in front of the retina. In addition, relative peripheral refraction can explain why foveally myopic eyes are less myopic off-axis , and thus their periphery is relatively hypermetropic compared to the fovea (although the peripheral image is still located in front of the retina without correction). Thus, the dioptric correction needed is more negative in the fovea than in the periphery. Similarly, foveally hyperopic eyes tend to be less hyperopic eccentrically, resulting in a relatively myopic periphery compared to the fovea (although the peripheral image is still focused behind the retina without correction) as shown in Figure 1.13. These, do not indicate that relative peripheral refraction is the causing factor of myopia, but are more likely related to the shape of the eye. Therefore, the role of peripheral optics in myopia onset and development is not entirely clear, and relative peripheral refraction is not the only factor that affects peripheral image quality.

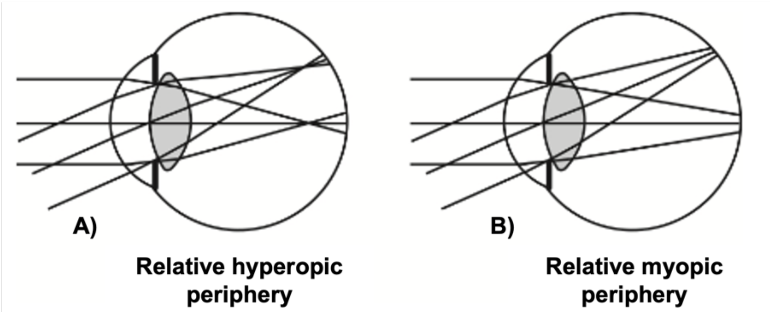

Figure 1.13. Schematic of an eye A) A foveally myopic eye with relative hyperopic periphery B) foveally hyperopic eye with the relative myopic periphery.

1.5 MYOPIA CONTROL INTERVENTIONS

In recent years, a variety of therapies to delay or stop the growth of myopia have been studied. Interventions are proposed based on various theories on why myopia develops, and they include peripheral defocus manipulation and the reduction of near accommodative effort. This section presents different interventions for myopia control and will focus on soft multifocal contact lenses and the active mechanism for myopia control, which is the one studied in this thesis.

1.5.1 Pharmaceutical agents

Atropine, a pharmaceutical cycloplegic agent, a non-selective muscarinic antagonist in low concentration has been found to slow down the increase in axial length and myopia progression, although its action and mechanism are not yet understood. A study by Yam et al(91). investigated the 1-year effect of 0.05%, 0.025% , and 0.01% concentration of atropine in myopic children aged 4 to 12 years, after a year it was found that 1% atropine demonstrated less overall spherical equivalent myopia progression and axial length elongation. On the other hand, in the ATOM1(92,93) study, The 1% atropine had the biggest rebound impact, resulting in the greatest progression of myopia, whereas the 0.01% atropine had the least myopic rebound effect and the most persistent effect of all concentrations. Furthermore, the 0.01% concentration caused the least pupil dilatation and accommodative loss. In comparison to higher doses, 0.01% atropine had the strongest therapy efficacy in delaying the progression of myopia (92).

1.5.2 Orthokeratology

Orthokeratology (ortho-k) lenses remodel the cornea overnight. The center cornea is flattened by the hard gas-permeable lenses, temporarily reducing or eliminating refractive error (93). According to a recent study, axial elongation has been decreasing over time (94–96). Some claim that the peripheral retinal image shell may move to myopic defocuses as a result of orthokeratology lenses' steepening of the peripheral corneal image shell, reducing axial growth (97). Axial length is a more trustworthy comparative metric since ortho-k modifies corneal curvature and refractive error. In another study, the depth of the anterior and posterior chambers as well as lens thickness were examined. When axial changes were compared, related changes in vitreous chamber depth were found. Therapies that slow the progression of myopia and have a long-term effect on the degree of myopia must have a low risk of patient harm. Wearing ortho-k lenses all night could increase the chance of getting infections like microbial keratitis (98).

1.5.3 Scleral cross-linking

It is thought that one underlying issue in the progression of myopia is aberrant scleral re-modeling that leads to weakening, thinning, and expansion of the scleral tissue. Collagen cross-linking naturally occurs in the body with age and UV light exposure. Cross-linking helps to enhance and strengthen the biomechanical properties of the tissue. Given the aberrant changes in the sclera of myopic patients, a similar hope for the stabilization of myopic change via cross-linking of the sclera is held in the research community. There are two forms of scleral cross-linking: physical and chemical. The cross-linking occurs at the level of the outer sclera which is helpful in that it potentially avoids a structural change in the retina/choroid.

The physical method requires opening the conjunctiva to expose the scleral tissue. This is followed by the activation of riboflavin via UVA (370 nm) or blue light. (460 nm) which leads to the excitation of riboflavin to the triplet state and subsequent production of reactive oxygen species. This cross-linking process forms new chemical bonds between collagen and other molecules or between two collagen molecules. The chemical cross-linking enhances scleral stability with reagents such as glutaraldehyde or glyceraldehyde with reactive groups that can cause molecules to form new covalent bonds. Chemical cross-linking has been shown to improve the stiffness of the sclera more effectively than physical cross-linking(99–101).

1.5.4 Optical approaches for myopia intervention

As was said in Section 1.4.5, when a negative lens is placed in front of the eye, the focal point is in the back of the eye, causing a hyperopic retinal defocus that promotes axial elongation and renders the eye relatively myopic. A plus lens, on the other hand, places the focal point in front of the retina, which results in myopia and relative hyperopia. Optic procedures attempt to stop the progression of myopia based on that justification.

1.5.4.1 Monofocal solutions

Under-correction

Initially, it was thought that under-correction might stop the growth of myopia by lowering the accommodative demand for close tasks. Alder et al(102). For a 18 month period, the effects of wearing eyewear with full myopic refractive error correction versus under-correction of myopia by +0.50D in children with myopia were compared. When compared to fully corrected children, the under-corrected participant showed a modest, but non-significant increase in myopia progression of 0.17D. These results were consistent with many other studies(102,103). The risk is that a loss of sharp distance vision caused by under-correction procedures will result in behavioral changes such as reduced outside activities, favoring myopia progression.

Single-vision soft contact lenses

To correct refractive error, contact lenses are widely used as an alternative to or in addition to spectacle lenses. In comparison to single-vision glasses that have very little spherical aberration, most soft lenses with spherical surfaces experience negative spherical aberration in negative powers (104), but this may appear to cause a hyperopic shift in the peripheral refraction, which may promote axial growth of the eye compared to single vision glasses that have very little spherical aberration (105). In contrast to spherically surfaced spectacle lenses, spherical contact lenses generate a greater peripheral myopic shift (2). As a result, if myopic peripheral refraction slows myopia advancement, then single-vision contact lenses may be more protective against myopia progression than single-vision spectacles. To summarize, there is no convincing evidence in the literature that typical soft contact lens usage causes either slower or quicker myopia progression.

1.5.4.2 Multifocal solutions

Spectacle Lenses

One of the theories The idea that hyperopic retinal blur at the fovea generated by a high lag of accommodation during close work drives axial growth of the eye and is crucial to myopia progression. Spectacle-based techniques for myopia control have been shown to reduce myopia progression by lowering accommodative demand. Several studies have been conducted to assess the usage of PALs and bifocal lenses to slow myopia progression by reducing accommodative strain at near (106–111) Given that they are simple to fit, widely recognized and tolerated, affordable, and less invasive, spectacle lenses have several advantages over other types of myopia therapy. All multifocal lens designs, including bifocal lens designs, result in relative myopic shifts in peripheral refractive errors, at least in the superior retinal field (112). There is evidence that certain populations, such as people with significant accommodation lags and people with esophoria at closer viewing distances, may be more affected by treatment with relative plus power for near tasks.

Soft Multifocal contact lenses

Soft multifocal contact lenses traditionally used in the treatment of presbyopia, are now also a proposed solution for myopia progression control. These lenses work under the principle of Simultaneous vision which is an image focused at near vision projected onto the patient's retina overlaid with a degraded image for distance vision, or a focused image for distance vision superimposed on the defocused image of the near scene(113). The asphericity induces a spherical aberration (SA) that causes expanding the depth of focus (DOF). Even though the best image suffers a certain degradation due to induced SA, the expected gain at near is expected to counteract the slight degradation at far, in the majority of patients (114–116). The design of the lenses is originally intended for presbyopes and are used off-label. Different designs of the lenses have been investigated they are discussed as follows:

Center-near design lenses have positive power in the center which abruptly (segmented designs) or gradually decreases towards the periphery. Center-near lenses are a common design for presbyopia correction, and are less frequent in myopia control. To this category belongs the contact lens 1-DAY ACUVUE MOIST MULTIFOCAL (aspheric center-near design, Johnson & Johnson Vision Care, Inc) used in the studies in Chapters 3,4,5 , and 7.

Center-distance designs, with the central region, corrected for far, and an addition in the peripheral region of the lens, are the most common designs for myopia control. As in center-near lenses, the two zones can be segmented with a sharp transition zone, or via an aspheric curve that progressively increases towards the periphery on the anterior surface of the CL to compensate for near vision. The center-distance lenses are said to induce positive spherical aberration(114,117). Traditionally these lenses have been prescribed for myopia control based on their potential effect of decreasing hyperopic defocus in the periphery. However, recent studies report that The effects of center-distance lenses on the periphery are not as significant as expected, as they cause myopic defocus exclusively in one meridian rather than the entire retinal periphery (112).

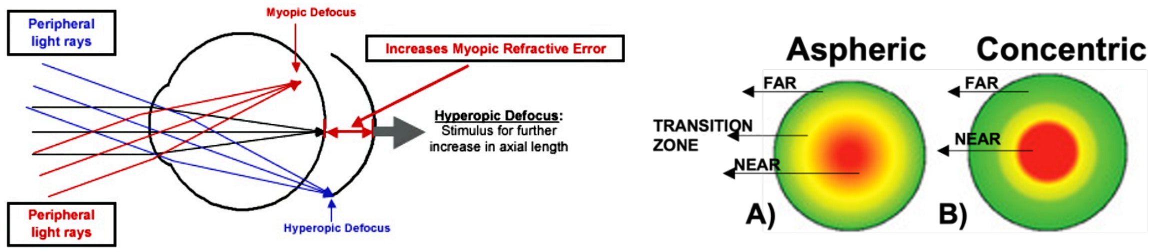

Figure 1.14. (Left) A schematic representation of the principle of the multifocal contact lenses on controlling myopia progression. (Right) different designs of MCLs A) Aspheric design B) Concentric design. Adapted from Charman et al(118).

Multizone-concentric design. The center-near/distance designs described above comprise only two zones or a progressive gradual increase/decrease of power towards the periphery (progressive design) or present in distinct zones (concentric ring design). Other categories of designs involve multiple zones that alternate near-far zones as concentric rings. An example of this design is the Misght contact lens (Cooper Vision, Inc), a multi-zone center-distance design, approved and commercialized for myopia control(119). These contact lenses were created to provide a global retinal picture quality that was enhanced for locations on and anterior to the retina and deteriorated for locations posterior to the retina to prevent axial elongation (i.e. across both the central and peripheral retina). Chapter 7 in this thesis studies the effect of the Misight lens on accommodation, vision foveally , and in the periphery.

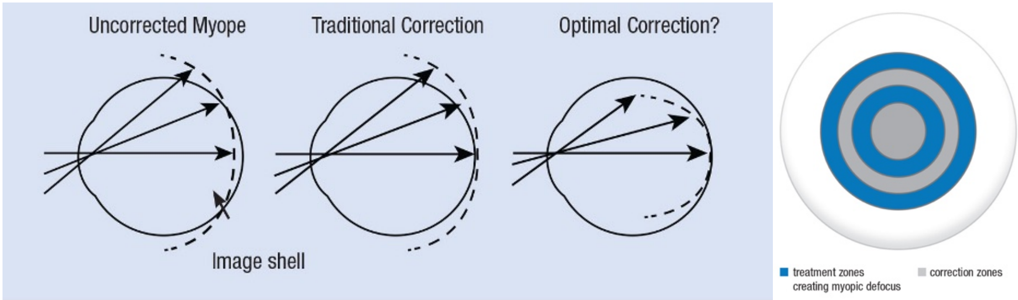

Figure 1.15. A schematic representation illustrating myopic and hyperopic defocus, and the possible target for ideal correction(93). On the right is the Misight lens which has two treatment zones, creating a peripheral myopic defocus that causes the image to focus in front of the retina and slow axial elongation. Myopia is corrected in all gaze positions.

1.5.5 Accommodation and myopia

Three main processes that occur when viewing a near object: accommodation, which changes the curvature of the crystalline lens to focus the eye, and miosis, which increases the depth of focus similar to a pinhole camera. The eyes adduct to converge the visual axes and keep the image on the corresponding areas of the retina (120,121). It is believed that these occurrences are simply related, not connected and that any one of the three may be absent without having an impact on the other two. (121). Most people accommodate less than is necessary to bring the subject into focus when they are either presented with close targets or with minus power lenses in front of their eyes. The lag of accommodation, also known as underaccommodation, is measured as the difference between the observed accommodating response and the accommodative stimulus. Myopia development has often been linked to continuous near work requiring high levels of accommodation(122). Several epidemiologic studies have revealed a link between the volume of near work and the development of myopia(69,123,124) and suggested that the larger amount of accommodative effort needed during near activity is a factor in the development of myopia. More specifically, a large body of work refers to the hyperopic blur produced by the lag of accommodation (i.e the eye not accommodating completely to shift the image plane to the retina) to close targets, which results in the image lying behind the retina, as the trigger or contributor to eye elongation. This is also consistent with studies on experimental models of myopia in many animal species, that show robust responses in eye elongation to hyperopic defocus imposed with negative lenses(81). Several studies have reported larger lags of accommodation in myopes compared with emmetropes(74,125–128), although it is debated whether this is a cause or a consequence of myopic changes (129,130). Differences in accommodative lag have even been related to the higher amounts of high-order aberrations, since myopes have, on average, larger high-order aberrations (HOAs) (82,83,131,132). The potential link between myopia development, reduced accommodation, optical aberrations, and hyperopic defocus (particularly in the peripheral retina) has motivated various non-pharmacological alternatives for myopia control. Among those options, bifocal, and progressive additional spectacle lenses (133–136), orthokeratology (137,138) and soft multifocal contact lenses (MCLs) have shown different levels of success in controlling the progression(133,134).

According to experiments conducted on animals, hyperopic defocus caused by lenses accelerates axial eye growth, which causes myopia (81). As accommodative lags induce hyperopic defocus, high lags are considered a risk factor for myopia(74,111,128,139). Higher accommodating demands are associated with a greater lag of accommodation in myopes, according to human studies (74,129), the myopia of more recent onset(140,141) , and blur-driven accommodation induced by negative lenses(76). Larger lags also are associated with the progression of myopia(76,128). Direct evidence of an association between near work and myopia has been difficult to obtain (as explained in the previous section).

Pupil

Sympathetic and parasympathetic nerves control pupil size, and the dilator and sphincter muscles in the iris act as antagonists to change this. Pupil size is regulated by ambient light and tends to reduce with age(142). Also, generally, pupil size decreases during accommodation(142). Both the baseline pupil diameter and its light and accommodation response vary across the populations. Pupil size is important in refractive multifocal corrections in presbyopes, as the relative area of the contact lens devoted for far and near depends on pupil diameter. When using dual or multifocal contact lenses, which depend on a sufficiently large pupil diameter to provide access to the peripheral retina, pupil size can also be crucial.

1.6 AGING PROCESS IN THE EYE: PRESBYOPIA

Presbyopia

With age, the eye loses its ability to focus near objects. The ability of accommodation declines steadily with age from 14D during infancy to 1.5D at 60 years of age(143). This age-related physiological inadequacy in accommodation is called Presbyopia (Figure 1.16). This decrease in the amplitude of accommodation results primarily from the stiffening of the crystalline lens material. For the majority of the population, the symptoms of presbyopia start at around 40-45 years, when the amplitude of accommodation decreases below functional ranges(143). Several factors influence the perceived onset of presbyopia, including the patient's preferred working distance, the nature of the close work, uncorrected residual myopia, light levels , or the presence of ocular high-order aberrations.

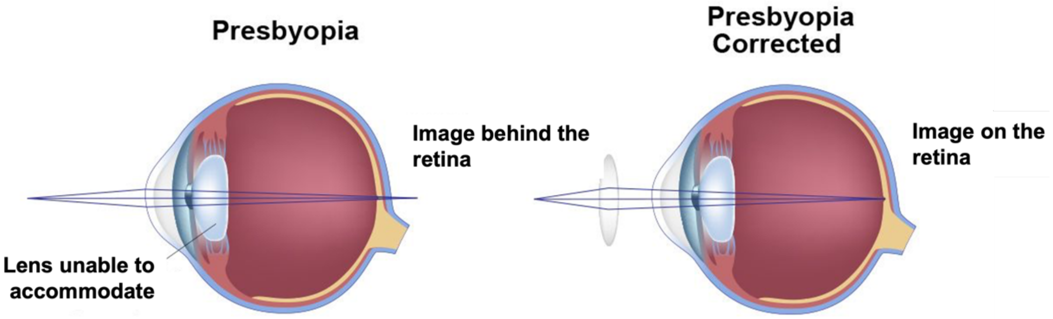

Figure 1.16. Near vision in a presbyopic eye (Left), the crystalline lens is unable to accommodate. Presbyopic eye with correction (Right), focused on the retina.

Other accompanying factors to lens aging include increased thickness and lens diameter, index gradient flattening, surface steepening, and the shift of spherical aberrations to more positive values(144). These changes are due to the continuous growth of the lens, accumulating fibers in the lens nucleus. Chemical modifications also occur, inducing a decrease in the transparency and increased scattering of the lens, resulting in a cataract later in life

1.6.1 Presbyopia solutions

Presbyopia is treated by using a convex lens—properly referred to as the "near addition"—to add additional positive power. The amount of addition given is regulated by the patient's age, working distance, and needs. There are numerous strategies to treat presbyopia, either non-surgical (spectacles or contact lenses) or surgical (modifications in the cornea or IOL implant) treatments(118,143). Most frequent presbyopic solutions are based on: Alternating vision (bifocal and progressive spectacle lenses) where changes in gaze or head position allow the selection of the viewing zone for the desired distance(143,145), Monovision where one eye is corrected for distance and the other for near vision (usually dominant eye for far)(146,147), simultaneous vision It is a growingly common simultaneous vision-based approach where the eye is concurrently developed for near and far vision, typically in the form of contact lenses or intraocular lenses (148).

1.6.1.1 Contact lens designs for presbyopia

Compared to spectacles, contact lenses offer a wider field of vision because they are placed closer to the eye, causing less distortion. Besides, unlike progressive spectacles that require changing gaze, and produce image distortions particularly when looking through the corridor between far and near regions, multifocal contact lenses operate under the principle of simultaneous images and sharp/focus of images for far and near are always present. A drawback to the use of contact lenses at an older age is the increased incidence of dry eye(149,150). Contact lenses for presbyopia correction tend to be refractive (segmented or smooth profiles): two focal points for far and near (bifocal), multifocal contact lenses where the distribution of the near and distant regions can also vary, as the central region can be either devoted to distance or near. Some of the examples of bifocal contact lenses for presbyopia are CooperVision Biofinity Multifocal, Bausch and Lomb Ultra contact lenses for presbyopia, Biotrue One day for presbyopia, Alcon Air Optix Plus HydraGlyde Multifocal.

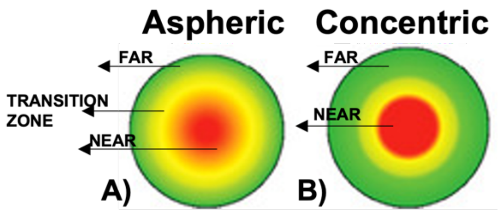

Figure 1.17. Different designs of MCLs for presbyopes A) Aspheric B) Concentric. Adapted from Charman et al.

Aspheric design (Figure 1.17), currently the most widely used designs in the field of CLs are progressive design with aspherical geometry, with a wide variety of designs available in the market. Aspheric CLs designs are rated for a certain viewing distance in the central area and an aspherical curve that produces a progressive variation in power as you approach the periphery. In this thesis, we have used a center-near design contact lens design of low, medium , and high addition (1-DAY ACUVUE MOIST MULTIFOCAL, Aspheric center-near design, Johnson & Johnson Vision Care, Inc) to compare the visual performance (Chapter 3 & 4).

1.6.1.1 Intraocular lenses design for presbyopia

Unlike multifocal contact lenses that are placed on the eye, intraocular lenses are implanted intraocularly. Generally, they are implanted following removal of the intraocular lens material, generally inside the capsular bag that is left intact (except for a window, capsularhexis created to allow surgical maneuvers). IOLs are generally implanted in patients that require cataract removal, although there is an increasing number of procedures performed in younger patients, referred to as clear lens extraction or refractive lens exchange. The first intraocular lenses were made of PMMA (polymethylmethacrylate). Since then, materials, designs , and techniques have continually evolved. The monofocal form of intraocular lens is still the one that is implanted most frequently today. Patients with monofocal intraocular lenses with fixed focal lengths are spectacle free for one distance (generally far), but the quality rapidly deteriorates at other distances, requiring the usage of near spectacles. Relatively frequent management of presbyopia is monovision, where one eye is implanted with a monofocal lens at the far, and the contralateral eye with a monofocal lens at the near. Candidates for monovision with IOLs tend to be those previously fitted with a monovision correction with contact lenses. Increasingly used corrections of presbyopia with intraocular lenses include multifocal, hybrid, or EDOF lenses, and (very limited) accommodative IOLs.

Accommodative IOLs

Accommodative lenses are monofocal lenses with flexible haptics capable of mobilizing their optical zone, thus varying their focus. When the ciliary muscle contracts, the zonular fibers relax and the energy released allows the lens to move forward, thus increasing its dioptric power to focus at close or intermediate distances. In practice, the true accommodative effect achieved with these designs is small and highly variable(151,152).

Multifocal and EDOF IOLs

Multifocal IOLs aim at producing multiple foci or expanding the depth of focus in the eye. We can divide multifocal IOLs according to the optical principle used to create multifocality in refractive or diffractive lenses.

- ⇒ Refractive Lenses: based on the phenomenon of refraction of light, which is the change in direction experienced by a ray of light obliquely passing from one meridian to another with a different refractive index (IOL material)(153–155). An example of refractive, bifocal IOL is the Oculentis MPlus, with a segmented, non-centrosymmetric near/far distribution.
- ⇒ Diffractive Lenses: based on the scattering phenomenon that light experiences when it passes through the edge or step of a transparent surface. Diffractive lenses use the optical principles of diffraction and refraction to form two independent focal points, far and near(156–158). Examples of diffractive trifocal IOLs include the Alcon Panoptix or PhysIOL FineVision IOL.
- ⇒ EDOF IOLs are generally refractive IOLs with the aim of producing an extended range of focus with constant vision quality (generally from far to intermediate). Examples of refractive EDOF IOLs include the Alcon Vivity or the PhysIOL Isopur IOL(159–162).

1.7 CLINICAL REPORTS OF MULTIFOCAL CONTACT LENSES INTERVENTIONS FOR MYOPES

Two theories have been proposed to support the use of MCLs as an intervention in progressive myopia. The first is based on correlations between myopia and greater accommodative lag that have been discovered (74,111,128,130). No matter where on the lens it is, the existence of a near addition that provides a focus at a close distance will lessen the amount of accommodative lag-induced hyperopia defocus, thereby weakening the signal for eye growth. Myopia progression control lenses often have a center-distance design. Clinically, however, MCLs with a center-near configuration has also been beneficial for people who have a significant accommodation lag and are near esophoria (163). The second theory for how MCLs work to correct myopia is based on evidence that the peripheral retina is important for proper emmetropization (93,164,165). In particular, it is believed that the peripheral hyperopic defocus caused by myopic eye globe shape and its correction with typical spherical lenses stimulates the growth of the eye (93). According to this theory, MCLs would halt the progression of myopia by causing myopic peripheral defocus, which would offset naturally occurring hyperopic defocus and function as a stimulus for eye growth. However, other studies either found no correlation between peripheral defocus and foveal axial elongation or discovered statistical variances in the retinal morphology of myopes or emmetropes, raising doubts about the role of the peripheral retina in the development of myopia (166,167).

Walline et al(168) In a two-year prospective research, kids aged 8 to 11 with Proclear D soft multifocal contact lenses with a +2.00D add. Twenty-seven of the 40 children finished the trial and were matched in terms of age and gender to participants from a prior study who were using single-vision soft contact lenses. For the multifocal and single-vision wearers, the adjusted mean axial elongation was 0.29mm ± 0.16mm and 0.41mm ± 0.16mm, respectively. The scientists concluded that using soft multifocal contact lenses over the two-year treatment period reduced axial length elongation by 29%. Sankaridurg et al(169) Recently, the results of a two-year clinical trial with five arms, in which children were randomized to receive soft contact lenses with single vision, two soft lens designs that imposed myopic defocus across the peripheral and central retina, or two extended-depth of focus (EDOF) soft lenses incorporating higher-order aberrations to modulate retinal image quality, were published. The axial elongation was reduced by between 22% and 32%, with the single vision group making the maximum progress (0.58mm), while the other groups made less progress (0.41mm-0.46mm). Paune et al(170). For the experiment, a soft radial refractive gradient (SRRG) contact lens was employed. This lens corrects the central refraction while creating a peripheral myopic defocus that moves progressively from the center of the optical axis outward. After two years, myopia growth was 43% slower in kids who wore SRRG contact lenses. Cheng et al(171) The reduction of relative peripheral hyperopia was achieved by creating a soft contact lens for myopia control with a positive spherical aberration in the optical design to shift retinal hyperopic defocus in the opposite direction. The first six months showed the biggest myopia control impact, which was around 56%; at the end of the year, it had significantly decreased to 20%. These contact lenses performed more effectively overall than similar ophthalmic lenses in the treatment of eye conditions. This might be because soft contact lenses follow the movements of the eye, maintaining the optical correction's center for all viewing gazes.

Chamberlain et al(119) published results of a three-year randomized clinical trial of MiSight 1-day soft contact lenses where the mean change in axial length was 0.32mm. A study by Aller et al(172). reported the most encouraging result of 70% using a different kind of soft contact lenses that are bifocal, although this was only observed for the kids with eso fixation discrepancies at close. A study by Anstice and Philips et al(173), designed a dual focus soft contact lenses to limit the progression of myopia. The lens has a central zone for refractive error correction and concentric treatment zones with +2D addition to impose concurrent peripheral myopia defocus for far- and close-range viewing. Compared to the control eyes, which progressed by -0.69 (-0.38) D during the first period, the dual focus test eyes' myopia rose by -0.44 (-0.33) D. There was an increase in axial length of 0.11 (0.09) mm and 0.22 (0.0.10) mm, respectively. In the second phase, similar figures were discovered. 70% of the participating children had a reduction in myopia progression of 30%, and 50% of the children saw a reduction of 50%. These results suggest that myopia progression can be slowed by continual myopic defocus and concurrent clear images. Lam et al(174), compared the performance of a specially manufactured "Defocus Incorporated Soft Contact" (DISC) lens to single vision contacts. The DISC lens had a concentric ring design with an addition of +2.50 D, which was alternated with the distance correction. This addition was significantly higher than the +2.00 D addition used in the Anstice and Phillips (2011) lens. At the study's conclusion, the DISC group experienced 25% less progression and a corresponding reduction in axial elongation.

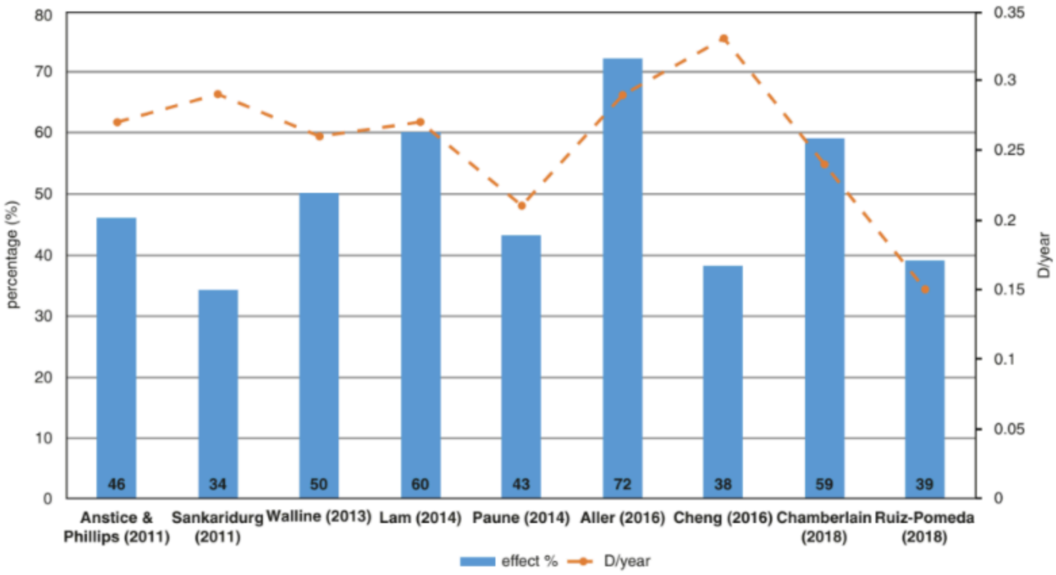

Figure 1.18. Comparison of the effects of soft bifocal and multifocal contact lenses on reducing the progression of myopia. The percentage difference between the treatment and control groups during the study period is represented by the bar. The dotted line shows the annual decrease in myopia progression (D/year). Adapted from Tien Y. Wong(175).

1.8 SIMULATING MULTIFOCAL CONTACT LENSES

1.8.1 Adaptive Optics: The technique

Initially, the techniques were proposed in 1953 by Babcock(176) for astronomical applications, in order to correct distortions introduced by the atmosphere on the astronomical images retrieved by ground-based telescopes. The practical implementation of AO was accomplished in the 1970s(176) using a shearing interferometer to measure the aberrations generated by a turbulent medium and corrected them with a piezoelectric deformable mirror. Since then, the technique has been widely used in the field of astronomy. Normally, an artificial guide star is generated by a laser source from the ground to measure the aberrations induced by the atmosphere at any point in the sky. The correction is then performed by dedicated optics within the telescope. The AO systems can be separated in two groups: open-loop and closed-loop systems. In closed-loop systems, measurements of aberrations and their modulation are done iteratively following a feedback loop, the wavefront system has to be located after the wavefront modulator in the path of light. In open-loop systems, a single measurement of aberrations is done with a single correction , and no feedback is provided by the sensor, the wavefront sensor is typically located before the corrector.

The AO techniques were applied in vision research starting in the 1990s. The aberrations were typically measured with the help of artificial light, which is a point-like spot emitting from the observer's retina. Normally, it is created by using a laser beam passing through the ocular media. AO provides an unprecedented platform to study the optics of the eye and its visual performance. Liang et al.(177) demonstrated the first closed-loop AO system that could deliver "Supernormal Vision and High-Resolution picture" and correct higher-order aberrations in the eye. The first system required 4-5 loops and 15min for each loop of measuring and correcting the wave aberration to complete the correction.

Correction of the wave aberration in real-time was not possible until the development of automated wavefront sensing, which allowed the first real-time measurement of the eye's wave aberration(178). The most significant temporal changes can be captured using an adaptive optics system with a closed-loop bandwidth of just a few hertz(179). The use of the AO system to measure, correct, or produce aberrations paves the way for a greater variety of experiments to investigate the relationship between optics and vision, both in the high-resolution retinal picture and psychophysical testing.

1.8.2 Optics and the Brain: AO-based Visual Simulators

Adaptive optics can be used to manipulate aberrations in addition to correcting them, going beyond the imaging-related uses and possibilities. Through manipulation of the wavefront, we may test the visual system and compare the outcomes under various optical conditions(46,136,180). We have the ideal technology to investigate how optics affects vision and comprehend visual function, perception , and accommodation change when the environment is seen through simulated multifocal contact lenses. Such applications will be the main emphasis of this thesis.

Designing novel ophthalmic optic components and studying the visual system is vital, as was evident in the previous sections. Furthermore, visual testing through modified optics can be carried out utilizing an adaptive optics system to manipulate ocular aberrations, which may ultimately result in improved optical solutions. When innovative phase profile designs are intended to be applied in permanent elements, such as intraocular lenses or multifocal contact lens profiles, using an AOVS for non-invasive preliminary testing has significant advantages. In the process of creating novel ophthalmic optical components, this is one of the most exciting applications for adaptive optics visual simulators. When a non-reversible therapy is planned, it is essential to use the AOVS to demonstrate to a patient the outcomes of a certain correction prior to surgery.

1.8.3 Principal components of an AO system

A schematic of AO shows a basic layout of an AO system for the eye (Figure 1.18). Adaptive optics corrections in the eye are comprised of three steps, represented in the figure.

Wavefront sensing - The wavefront sensor receives light that has been reflected off the retina and quantifies any remaining wavefront distortion.

AO control - In order to determine the proper voltages to apply to the wavefront corrector in order to change its form, the centroid coordinates are extracted from the wavefront sensor data and processed by a calculator.

Wavefront correction - The deformable mirror changes its shape in response to the inputted data and returns the light to the sensor.

An adaptive optics control computer connects the wavefront sensor and the wavefront corrector, which are located in pupil-conjugated planes.

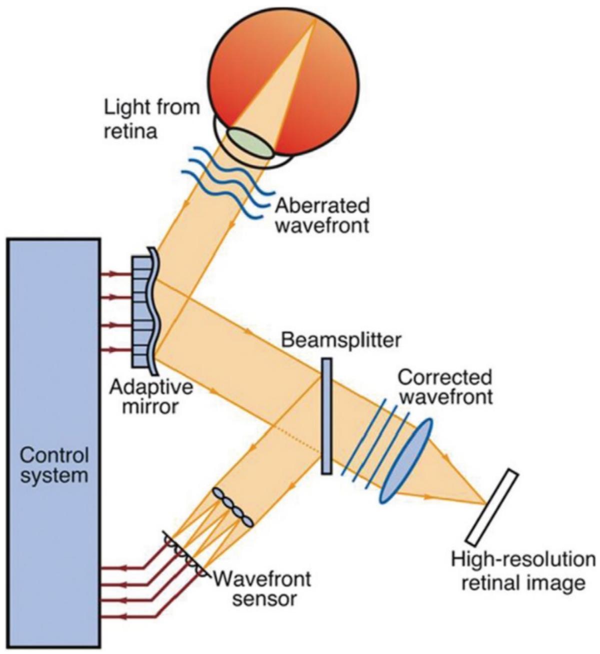

Figure 1.18. The basic design of an AO system with the three parts of the procedure for imaging and vision testing (1) Wavefront sensing (2) AO control, and (3) wavefront correction are all mentioned. Adapted from Roorda 2011.

1.8.4 Wavefront sensing techniques

In order to create cutting-edge vision correction techniques like adaptive optics, tailored contact lenses, and/or laser refractive surgery, it is crucial to have wavefront sensing technologies. The spatially resolved refractometer(181,182), laser ray tracing(183,184), and the Hartmann-Shack wavefront sensor(185)are the three most popular wavefront sensors. Hartmann-Shack wavefront sensors have been used in this thesis.

Hartmann-Shack Wavefront Sensor (HS)

A HS sensor contains a two-dimensional array of a few hundred lenslets, all with the same diameter and the same focal length. A narrow beam of light is sent into the eye through the pupil and focuses on the retina. The focused light acts as a point source that is reflected, and as it passes through the eye it forms an aberrated wavefront due to ocular aberrations. This aberrated wavefront exits the eye and ends up on a microlenses array. The microlens array sub-divides the aberrated wavefront and focuses the sub-divided parts on a corresponding spot on a detector. The displacement of each spot from the reference (flat/aberration-free) wavefront spot, represents the local slope of the aberrated wavefront over the pupil. From these slopes, the wavefront can be reconstructed and described by Zernike polynomials. In an ideal eye, light reflected from the retina leaves the pupil as a collimated beam, and HS spots form along each lenslet's optical axis, forming a grid of spots that are uniformly spaced apart in the focal plane of the lenslet array. (Figure 1.19).

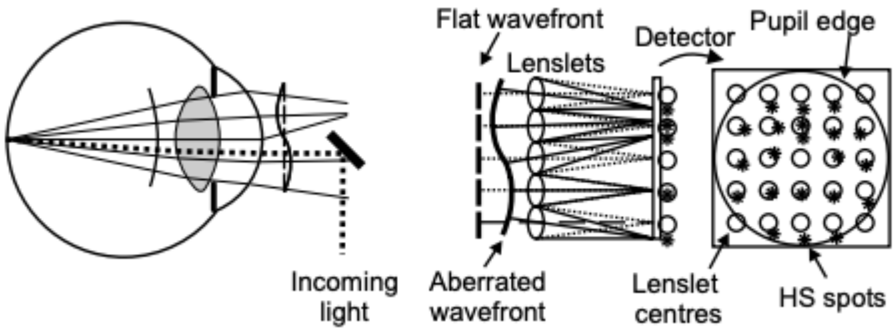

Figure 1.19. A schematic representation of the principle of the Hartmann-Shack wavefront sensor. On the left side, the narrow beam of light that enter the eye (dashed line) and the wavefront that exits the eye are shown. On the right side, the microlens array, the detector , and the spot pattern are shown. The aberrated wavefront and the displacements from the reference wavefront are shown as black spots, whereas the open circles are the reference wavefront and the corresponding ideal image positions(186).

1.8.5 Active optical elements for visual simulation

Wavefront modulators, or simply correctors, are devices that can change the incoming phase of the wavefront in a controlled manner. This action is typically accomplished by altering the optical path of the light. The use of such devices in the AO system is fundamental. There are two main types of wavefront modulators: Deformable mirrors (DMs) and liquid crystal spatial light modulators (LC-SLMs). In this thesis, SLMs were used for simulations.

Deformable Mirror (DM)

DMs are devices that allow fast control of the wavefront, controlled by a series of actuators located at its rear, deforming the mirror in the desired way. The actuators are composed of a magnet located behind the reflective membrane and a coil. Depending on the voltage applied, the surface of the mirror is deformed by the active movement of the actuator to introduce gain/delays in the optical path of the different parts of the wavefront after reflecting the beam on the mirrored surface. DM is not suitable to simulate abrupt phase change patterns.

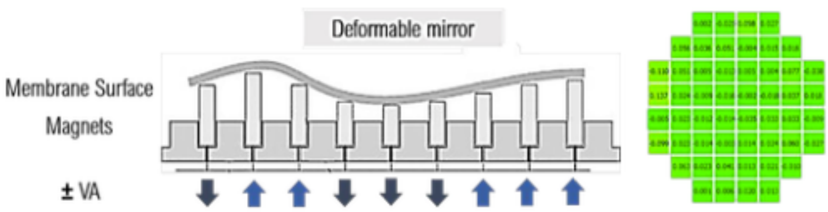

Figure 1.20. Schematic representation of the continuous flexible surface magnetic deformable mirror and the corresponding 52 actuators in the MIRAO52 (Imagine eyes, France)(48).

Spatial Light Modulator (SLM)

The Liquid crystal SLM (Figure 1.21) devices introduce phase retardation by locally changing the refractive index of the liquid crystal (LC) material. An applied voltage to an LC cell changes the orientation of the molecules inside. A typical device contains a large number of cells, or pixels, allowing for precise phase modulation. The LC-SLM operates either in transmission or in reflection, with reflective SLMs exhibiting higher resolution. Although the stroke of a single SLM cell is not large (usually up to 2π, dependent on the wavelength)(187), phase wrapping can be employed in order to extend the working range dramatically. The modulation depth changes the wavelength, negatively affecting their performance in wide-spectrum light.

The SLM(48) has greater versatility than deformable mirrors continuous-membrane since they are not subject to a continuous surface, they can introduce abrupt phase changes, allowing the simulation of more complex multifocal patterns(188). Due to their working principle of changing the refractive index of LC material, LC-SLMs are wavelength sensitive. Using them in white light or polychromatic conditions , in general, requires special considerations. This simulation technology has been used in this thesis to simulate bifocal and multifocal contact lens designs in Chapter 3,6.

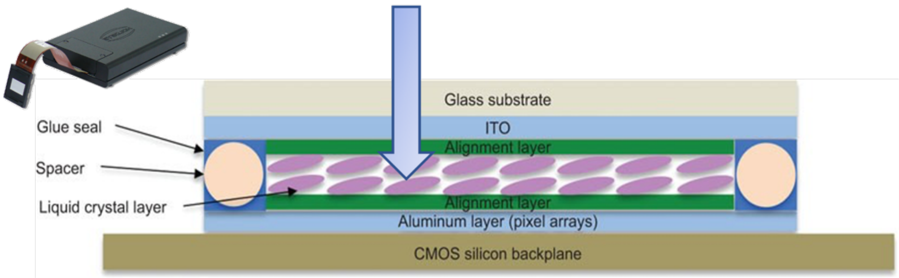

Figure 1.21. Schematic of a typical LCOS-SLM. Adapted from Zhang et al.(189).

1.8.6 Adaptive Optics Visual Simulators

Before the lens fitting on the eye, adaptive optics (AO) visual simulators are used to test patients with MCL designs' eyesight. In some circumstances, it is even possible to accomplish this before manufacturing potential commercial MCLs or specially-made lenses tailored to the patient's demands (136,188,190–193). Through the use of AO simulations, new multifocal corrections can be investigated in terms of how the patient's optics interact with a particular correction, differences between corrections can be compared, and ultimately the correction that best enhances patients' perceptions of visual performance and quality is chosen. Numerous studies in the literature cover the topic of using visual simulators to project a certain multifocal design onto the pupil plane. As a result, the patient has previous experience with a multifocal correction, and the interaction between the multifocal phase profile and the patient's eye aberrations is realistic. In earlier research (188,194) the Polychromatic AO visual simulator from VioBioLab was used to examine generic multifocal (2, 3 , or 4 zones), concentric zonal, and asymmetric refractive multifocal designs that had been mapped in the Spatial Light Modulator (SLM) (CSIC, Madrid, Spain) (136,188,195–197). Surface-modulated segmented phase maps that were SLM-simulated performed consistently and showed variations in perceived visual quality that was dependent on the number of zones and the distribution of the distant, intermediate, and near zones (194). The same AO device (as well as SLM) was used to mimic two multifocal IOLs (bifocal refractive and trifocal diffractive) with comparable TF visual acuity. Phase maps representing the IOL simulated in the SLM and the real IOL (in a cuvette) physically projected in the eye yielded similar TF visual acuity curves (136). Additionally, visual performance with the implanted IOL in the same individuals who underwent simulations of the trifocal IOL prior to cataract surgery was identical (198). Additionally, previous studies using SLMs to simulate bifocal, trifocal, and tetrafocal corrections as well as angular and radially segmented corrections reported perceived visual quality at far, moderate, and close ranges (192). Other studies have also used SLMs to simulate the effect of corneal inlays on visual performance (199) and to map different types of diffractive optics (200).

The eye's optics may be manipulated in a fairly flexible way using AO visual simulators. As an alternative, various smaller visual simulators that aren't reliant on active AO have been created expressly to model multifocal optics. Examples include the systematic investigation of the effects of near addition (191), the near-far pupillary distribution in bifocal corrections (190,191,201), and the effect of rotation of an asymmetric bifocal pattern on perceived visual quality and visual acuity using a two-channel simultaneous vision simulator equipped with a transmission SLM (202). Additionally, testing interactions between the natural aberration pattern of the eye and the spatial distribution of the lens design is possible using both the AO and the 2-channel Simultaneous Vision simulators.

Visual simulators in the clinic

Visual simulators allow the simulation of different patterns (multifocal, bifocal, diffractive)(188,203) following a non-invasive procedure. In addition, visual simulators are useful to identify and test multiple conditions before physically fitting lenses in the eye, and also to choose a pattern specific to that individual. The majority of AO visual simulators are prototype versions (29). However, based on the above-mentioned technology, various clinical visual simulators have been created (Figure 1.22).

Figure 1.22. Commercial visual simulators A) Crx1 by Imagine Eyes B) VAO by Voptica C) SimVis Gekko by 2EyesVision.

The ImagineEyes Crx1 is one of the commercially available DM-based simulators (204,205). DM-based simulators are typically monocular, while there have been reports of lab systems with binocular vision. Voptica sells a gadget called the VAO which is an SLM-based binocular simulator (206,207). SimVis Gekko, produced by 2EyesVision, is a commercial device that uses the technology (208) It functions as a wearable, head-mounted, see-through, completely programmable, and remote-controlled device.

1.8.7 Changes in the ocular structure with MCLs: Optical Coherence Tomography (OCT)

The Optical Coherence Tomography (OCT) procedure is frequently carried out using a Michelson interferometer and is based on the low coherence interferometry premise. Low-coherence interferometry, a traditional optical method, is the foundation of OCT. A broadband light source's interferometric qualities are the foundation of low-coherence interferometry, which was utilized in photonics to measure optical echoes and backscattering in optical fibers. The first biological application of low-coherence interferometry was reported by Fercher et al. in 1988(209) for measuring the eye axial length(210) Soon after its discovery, the optical sectioning capability of the OCT was used to view in vivo microscopic tissue structures at depths beyond the capability of traditional confocal microscopes. The following significant benefits of OCT over alternative imaging methods include: (1) As infrared is the typical laser source, it is safe for human tissue and comfortable for the patient when used at a controlled power; (2) High resolution (1–10 m) can be achieved because the system is based on a low-coherence interferometer and the resolution is constrained by the laser's coherence length. (3) Additionally, the system can be fiber-based, making it simple to create a compact, inexpensive OCT. (4) Real-time imaging can also be accomplished, (5) and it is faster than other imaging techniques. OCT has become a crucial tool in biomedical imaging because of these benefits, particularly in the field of ophthalmology (being now very common in the clinic).

The two primary subgroups of OCT technology are time-domain (TD) and spectral-domain (SD) OCT. In TD-OCT, the depth-scanning signal of the sample correlates to a mechanical axial movement of the reference mirror, which directly measures the autocorrelation of the light field (209,210). In contrast, the autocorrelation in SD-OCT is determined using the Fourier transform of the directly observed power spectral signal. Modern OCT systems are typically not based on time-domain theory, but rather on SD-OCT, which is faster (there is no axial movement of the reference mirror dependent) and significantly more sensitive for the same laser intensity. Setting up a spectrometer (SD) to find the interference signal is one way to use SD-OCT (211) or using a swept source (SS) to scan the frequency of the laser(212). The most recent development in ocular imaging is SS-OCT, which has a deeper depth range (up to 50 mm) and a faster speed (up to 1.68 MHZ) (213,214).

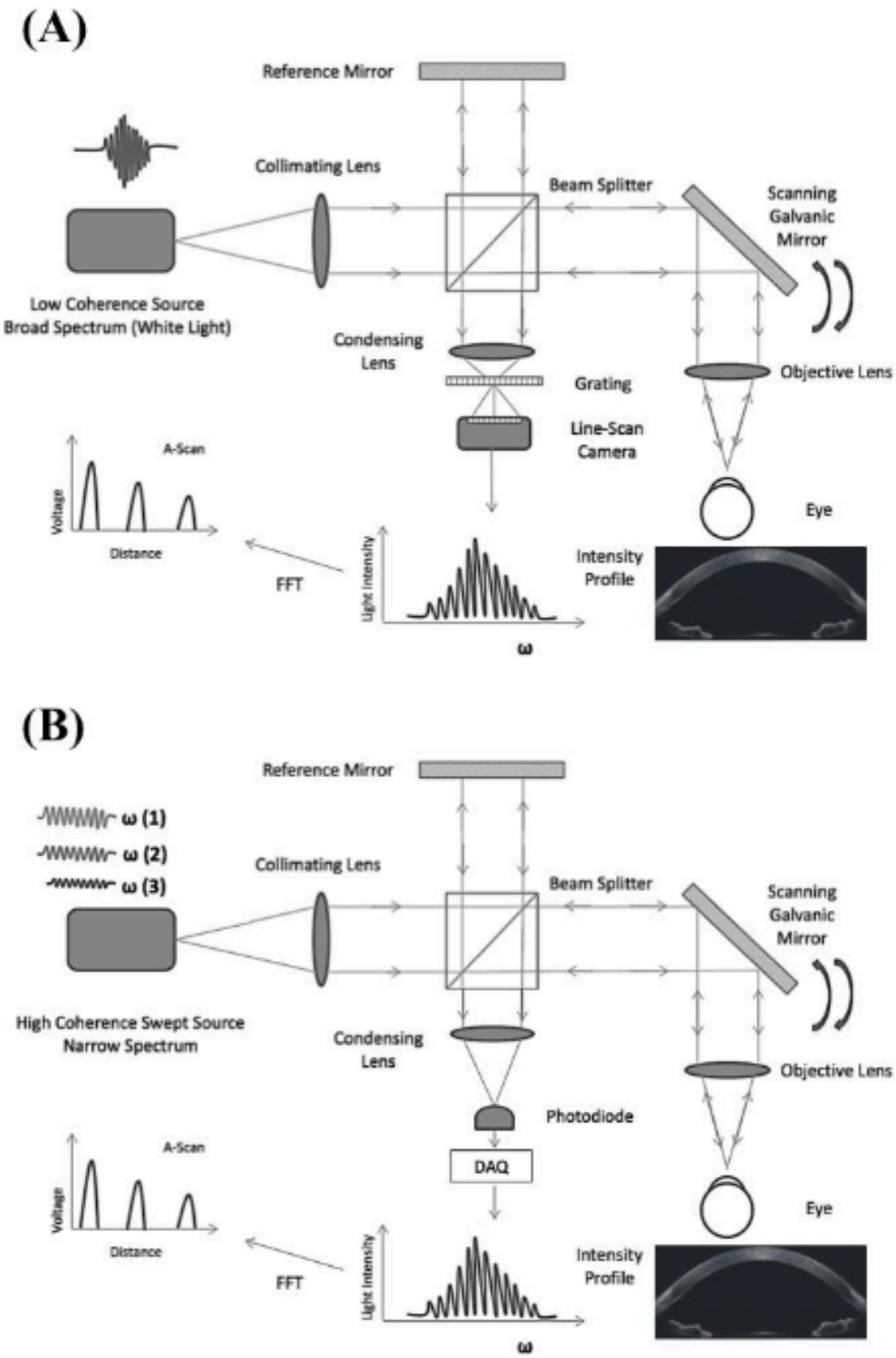

Figure 1.23. (A) Spectral-Domain OCT (B) Swept-Source OCT. Adapted from Pablo Perez's thesis(214).

The anterior portion hasn't been examined with OCT as frequently as the retina. All optical techniques intended for direct imaging of the posterior corneal surface and crystalline lens produce distorted images due to ray refraction at the cornea and lens. Furthermore, the scanning technique results in fan distortion (resulting in a combination of geometric aberrations, including field distortion, astigmatism, and spherical aberration). In the recent past, accurate data regarding the cornea and the entire anterior region were retrieved using correction algorithms.

The method used to measure the geometry and biometry of the anterior segment of the eye in this thesis is a specially created SD-OCT, and the actual laboratory implementation is discussed in Chapter 2.

1.9 OPEN QUESTIONS

In recent years, the use of multifocal contact lenses (MCL), which operate on the simultaneous vision concept and project an image that is simultaneously focused at near and far, has increased. Their use spans from presbyopia, an age-related condition where MCLs are increasingly used for providing functional vision at near, and in young myopes, where MCLs are offered as a solution for myopia progression control. Adaptive optics technology allowed simulations of multifocal patterns, allowing systematic non-invasive studies of visual function and accommodation in subjects. The current thesis addresses the following questions using Adaptive Optics visual simulations of multifocal contact lenses

(1) How is the visual performance with the same Multifocal contact lenses in presbyopia versus a young population? In particular to what extent do multifocal contact lenses improve vision at near and degrade vision at far in comparison with monofocal contact lenses in these two populations?

(2) Are visual simulators capable of replicating the visual performance of contact lenses on the eye?

(3) To what extent does a multifocal contact lens on the eye conforms to the cornea, and is the theoretical contact lens multifocal pattern preserved on the eye?

(4) How do the eye's aberrations interact with the contact lens design? In particular, what is the influence of native eye aberrations in the through-focus optical performance with a contact lens?

(5) To what extent the optical design of the multifocal contact lens (positive/negative spherical aberration; center distance/center near; smooth vs segmented profile modulates the accommodative response (and therefore accommodative) lag in myopic subjects?

(6) Is peripheral image quality used by the eye to detect the sign of defocus? In particular, how is peripheral image quality modified with different multifocal contact lenses?

1.10 GOALS OF THE THESIS

The main purpose of the thesis is to use a custom-made polychromatic Adaptive Optics visual simulator system to understand the impact/interaction of multifocal contact lenses of different additions and designs on the visual function and optics of the eye.

The specific goals are:

- To evaluate the through-focus visual acuity (TFVA) performance with the multifocal contact lenses in the eye, in the presence and absence of accommodation in different age groups

- To compare the through-focus visual acuity in patients wearing multifocal contact lenses in the eye and with corresponding simulated multifocal patterns in the Spatial Light Modulator (SLM) using a multichannel adaptive optics visual simulator

- To evaluate the contact lens profile on the eye, and potential conformity to the cornea using a custom-developed spectral anterior segment OCT (AS-OCT)

- To evaluate the influence of native ocular aberrations on the through-focus optical performance of MCLs and to understand the contribution of eye aberrations in the inter-subject variability of multifocality parameters

- To evaluate the impact of induced spherical aberration and contact lens design in the accommodative response of young myopes

- To evaluate the short-term impact of multifocality foveally and peripherally on accommodative behavior clinically and visual quality over the visual field

1.11 HYPOTHESIS

The thesis addresses the following hypothesis:

- MCLs improve visual performance at near at the expense of some degradation of visual performance at far, both in presbyopes and young myopes. The effects are largely dependent on the specific lens design.

- Visual simulators allow subjects to experience vision with multifocal contact lenses prior to testing them on the eye

- The intended profile of the multifocal lens design is largely preserved when fitted on the cornea

- The interactions between the eye's optics and the lens design are subject dependent, therefore should be considered when prescribing a given lens design.

- The accommodative response of young myopes through multifocal lenses is largely dominated by the lens design. The modulation of accommodative response may be responsible for the success or failure of multifocal contact lenses in myopia control

- The center-distance design, lenses inducing positive spherical aberration reduces the accommodative lag in myopes

- MiSight contact lenses in myopia control have a larger peripheral blur, a more asymmetric point spread function due to the additional astigmatism and coma, and that this leads to the increased accommodative response

1.12 STRUCTURE OF THE THESIS

The body of this thesis is structured as follows:

CHAPTER 1 presents a brief introduction to the studies and concepts and the motivation of the thesis

CHAPTER 2 provides an overview of the psychophysical methods and description of monochromatic and polychromatic Adaptive optics optical setups used throughout this thesis. In particular, it includes how the Adaptive Optics system is used to measure the subject's aberrations, visual acuity , etc including its calibrations, validation ,and developed custom software with their specific characteristics. It also includes a description of the active elements of the Adaptive Optics system, which were used to simulate complex patterns of multifocal contact lenses, IOLs , etc.

CHAPTER 3 presents a study that evaluates the visual quality of multifocal contact lenses in two age groups (Young adults, Presbyopes). The visual acuity was measured using the 8-Alternative forced choice method with a tumbling E letter. Center near aspheric design MCLs of three additions Low (+1.25DS); Medium (+1.75DS); High (+2.50DS) were tested in the presence (Natural accommodation) and absence of accommodation (Paralyzed accommodation). With paralyzed accommodation, the through-focus visual acuity was measured for a 5/4/3mm pupil controlled by the artificial pupil of the system, while with natural accommodation the pupil size was not controlled and it was the natural pupil of the subject.

CHAPTER 4 presents a study that evaluates the quality of visual simulating technologies by comparing through-focus visual acuity with simulated MCLs and real MCLs in the eye in the same subject group. A Spatial Light Modulator (SLM) was used to simulate the MCL (1) Through-focus optical quality of the MCLs on the bench (1-pass correlation metric) (2) Through-focus decimal visual acuity (TFVA) with (a) SLM simulated MCLs and (b) real MCLs was measured on 7 subjects. Monocular in monochromatic light using the 8-Alternative forced choice method.

CHAPTER 5 presents a study that evaluates the contact lens profile on the eye, and potential conformity to the cornea using Optical coherence tomography (AS-sOCT). AS-sOCT images were obtained on 13 subjects with naked eyes and with MCLs on the eye. All eyes were tested with the same MCLs (5 repetitions).

CHAPTER 6 presents a study that evaluates the impact of MCLs design and addition on accommodative behaviour in young myopes (n=6). A Hartmann-Shack wavefront sensor in an Adaptive Optics (AO) visual simulator was used to measure the wavefront aberrations in 6 myopic subjects while viewing a stimulus changing between 0-6D (randomized, 1D steps) through multifocal/bifocal corrections, under natural viewing conditions, measurements were repeated 5times for repeatability. The corrections were simulated in the Spatial Light Modulator, or a deformable mirror, and the accommodative response was calculated from wavefront aberrations. 7 conditions were tested: NoLens and when viewing through aspheric designs of high, medium add (2.50D,1.75D), bifocal (2.5 D) - center distance (CD), center near (CN) and with inducing positive and negative 1μm spherical aberration (PSA, NSA) using deformable mirror was measured.

CHAPTER 7 presents a study that investigates the short-term impact of multifocality on accommodative behavior and visual quality over the visual field. Two multifocal contact lens designs were evaluated and compared to single-vision spectacles: (1) MiSight (center-distance design) (2) 1-Day Acuvue Moist (center-near design). 8 myopic subjects underwent foveal clinical accommodation evaluation (letter visual acuity, near point of accommodation, accommodative facility, and accommodative response) as well as 10% contrast vision evaluation (resolution grating acuity) foveal and at 20° nasal visual field with those contact lenses, and spectacles as a control.

CHAPTER 8 presents a summary of the major findings of this thesis.

CHAPTER-2 METHODS

This chapter describes the experimental setups used in this thesis, especially two different Adaptive Optics (AO) systems developed previously at the Visual Optics and Biophotonics Lab (VIOBIO lab)(29,46), as well as a 3D spectral domain OCT. In this chapter we describe also the objective and psychophysical experiment's measurements that have been carried out during the time of the thesis, and the methodology common to the different studies described in later chapters.

Although both systems include the fundamental components of an adaptive system, they differ in their capabilities. The monochromatic AO system was the first generation of AO and has been used to test the effects of manipulating optical aberrations on visual perception and visual performance. In particular, to test the visual benefits produced by correcting high-order aberrations in visual acuity(215), contrast sensitivity(216), familiar face and facial expression recognition(217), accommodation dynamics(132,218), the ability of the visual system to adapt to the level and orientation of the aberrations(180), and the impact of astigmatism(219–221).

The polychromatic multichannel AO visual simulator system was the second generation of AO and has allowed for the measurements of monochromatic and polychromatic aberrations in the phakic and pseudophakic eye with objective and subjective techniques in a broader spectral range (supercontinuous laser) and has represented a significant advance in visual simulation capabilities, combining for the first time different active element technologies such as the deformable mirror, phase plate, real IOLs in a cuvette, spatial light modulator, and tunable lens working under the principle of temporal multiplexing(136,188,194,222).

The author of the thesis worked in both systems, providing alignment and calibration when needed. In the monochromatic AO system as a user of psychophysical measurements aiming at investigating the visual acuity with different additions of multifocal contact lenses in the eye, Chapter 3. The polychromatic multichannel AO visual simulator system, has been involved in the alignment, calibration of specific channels, and implementation of optical elements in the system. This has allowed the author to have more knowledge of the system and develop projects that are detailed in the following chapters. This was done with the guidance of Dr. Maria Vinas and the help of the other members that make up the AO team, supervised by Prof. Susana Marcos.

2.1. ADAPTIVE OPTICS BASED VISUAL SIMULATORS

Two custom-developed AO systems were used in this thesis. Common components of the systems include a wavefront sensor (HASO) that allows the aberrations of the system and the eye to be measured. Once the aberrations are measured, they are corrected using a Deformable mirror (DM). Both elements, the DM and HASO are in conjugate pupil planes and work in a closed loop to measure and correct aberrations. In combination with the AO elements, a psychophysical channel allows to perform psychophysical measurements under aberration correction and manipulation.

Following four different processes, measurements and closed-loop correction of wave aberrations were carried out: local slope acquisition, interaction matrix acquisition, command matrix construction, and lastly close-loop correction of wave aberrations. An artificial eye with a 50.8mm focal length achromatic doublet lens and a revolving diffuser serving as an artificial retina was put in the pupil plane of the device to perform this process on a bench.

Contact lenses are simulated on the DM (smooth, spherical aberration patterns) or the SLM (segmented and segmented patterns). A series of control studies were performed to ensure equivalency between the simulated pattern and the real contact lens.

2.1.1. General description of the Monochromatic AO system

This was the first AO system (monochromatic AO) in the VIBIO lab which was designed and developed in 2006(132,218). A detailed description of the system has been presented in previous studies. The system is composed of 5 different channels. (1) The main components of the system are a Hartmann-Shack wavefront sensor (HASO 32 OEM, Imagine eyes, France) composed of a matrix of 32 x 32 microlenses with a 3.6mm effective diameter and an electromagnetic deformable mirror (MIRAO, Imagine Eyes, France) with 52 actuators in a 15mm effective diameter. (2) Superluminescent Diode (SLD) coupled to an optical fiber (Superlum, Ireland) emitting 827nm provides illumination. An irradiance of 8µW on the cornea was set according to the ANSI standards, from which the limit of exposure when measuring human eyes was set to 90mA. (3) A motorized Badal system is used to compensate for the refractive error, and also induce defocus in some cases. (4) The stimuli were presented on a CRT monitor (Mitsubishi Diamond Pro 2070, Australia) and were controlled by the psychophysical platform ViSaGe (Cambridge Research System, UK). (5) A CCD camera (TELI, Toshiba, Japan) that monitors the pupil is conjugated to the eye. The camera allowed for continuous pupil viewing, and the line of sight was utilized as a guide to properly center the subject's eye within the system (x-y-z stage).

Custom Matlab and Visual C++ routines were used to control the system from two different computers. One computer was used to control the Badal system and the AO system (DM, Hartmann-Shack wavefront sensor), and the other computer was used to control the ViSaGe psychophysical platform and the Mitsubishi Monitor.

Figure 2.1 shows a schematic of the VIOBIO lab monochromatic AO system that has been used in the study presented in Chapter 3 of this thesis

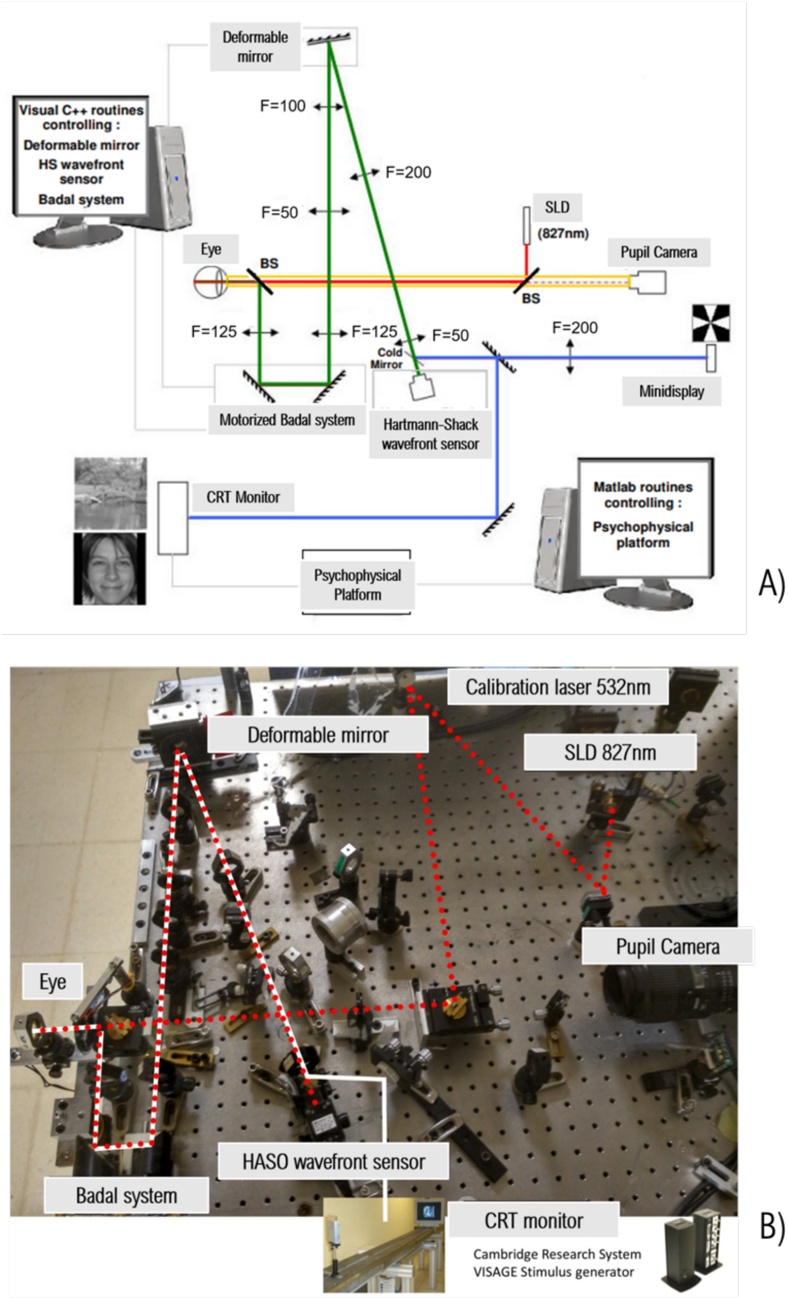

Figure 2.1 A) A diagram showing the system's five channels. AO-control channel with the Hartmann-Shack wavefront sensor and the deformable mirror (green); illumination channel with an 827 nm SLD source (red); Pupil monitoring channel; Psychophysical channels, one with a mini-display and the other with a CRT monitor (blue) (yellow). B) A picture of the key parts of the VioBio lab's monochromatic AO system. Modified from Sawides thesis (46)and Marcos et al(215).

2.1.2. General description of the Polychromatic AO system

The AOII system is a polychromatic multichannel AO visual simulator in the VioBio lab which was designed and developed from 2015(29) to 2019. A detailed description of the system has been presented in previous studies(29,188,195,197,223) where it was used to evaluate the visual benefits of AO correction, vision with simulated multifocal correction, optical aberrations in pseudophakic and phakic eyes, chromatic aberrations and their visual impact, and neural adaptation to ocular aberrations. Figure 2.2 shows a schematic diagram and top view of the polychromatic multichannel

AO visual simulator set-up. The current configuration of the system is formed by 8 different channels. Different chapters of this thesis were performed in this AOII system.

(1) The Illumination- Channel, contains a supercontinuum laser source (SCLS, SC400 femto-power 1060 supercontinuum laser, Fianium Ltd, United Kingdom), in combination with a dual acousto-optic tunable filter (AOTF) module (Gooch & Housego, United Kingdom), operated by radio frequency (RF) drivers, to automatically select the wavelength in the different channels (visible 450-700 nm or near-infrared light 700-1100 nm, in our system configuration). Very recently, in 2020, the dual module was substituted by a single VIS module (Fyla SL, Spain), which allowed higher control of the wavelength selection. The output is a collimated beam coupled to two independent multimode fibers. One for visible light (VIS) and the other for near-infrared (NIR) light, with a spectral bandwidth of approximately 12nm (10-12nm (VIS), 12.15nm (NIR)). The illumination coming from the two independent fiber channels of the SCLS enters the system collinearly through a hot mirror (HM), allowing wavefront sensing and retinal aerial imaging with VIS and NIR light. The 2-mm diameter beam entering the eye is slightly (1mm) decentred with respect to the pupil center to avoid corneal reflections in the Hartmann-Shack images. A variable-size pupil (VS-P) allows modifying the beam size and position entering the eye. The illumination coming from the VIS multimode fibre is also used to monochromatically illuminate the visual stimuli. The laser power measured at the corneal plane ranged between 0.5 and 50μW, which was one order of magnitude below the ANSI standard's safety limits at all tested wavelengths
(2) The AO channel consists of a Hartmann-Shack wavefront sensor (microlens array 40 x 32, 3.6mm effective diameter, centered at 1062 nm, HASO 32 OEM, Imagine Eyes, France) and an electromagnetic deformable mirror (DM) (52 actuators, 15-mm effective diameter, 50- μm stroke, MIRAO, Imagine Eyes, France), to measure and correct subjects and system aberrations respectively. Both devices are placed in conjugated pupil planes of the system through different relay lenses. Thus, an x2 magnification factor is achieved from the subject's pupil plane to the deformable mirror and an x0.5 from the subject's pupil to the microlenses array plane.
(3) The SLM-Channel that consists of a reflective phase-only LCoS-SLM (PLUTO-VIS; VIS resolution: 1920 x 1080; 0.7" diagonal; Pixel pitch: 8.0 μm; image frame rate: 60Hz; max resolution: 62.5 lines/m; 8bits, Holoeye Photonics AG, Germany) is used to generate the multifocal designs. A linear polarizer is placed in the path of the SLM at the calibrated polarization angles, in this case, 232 degrees, to ensure maximum efficiency.
(4) The Testing Channel, placed in a conjugate pupil plane of the system, allows evaluation of alternative simulating technologies. In the current configuration, it allows a) phase plates (i.e. representing angular or radial segmented zonal designs with different powers), and b) real IOLs (in a custom-developed cuvette). There are two possibilities to test real IOL, cuvette 0D IOL and non-0D IOL (around 20D) using a Rassow system. Or other simulating technologies, such as the tunable lens (Lens model; EL-10-30-TC; aperture: 10mm; tuning range +8.3 to +20D; Offset lens: -5.00D, Optotune AG, Switzerland) called SimVis operating by temporal multiplexing
(5) The Retinal imaging Channel allows capturing retinal images and consists of a CCD camera (Retina 1300, CCD Digital Camera, 12-bit, Monochrome, 6.7 x 6.7 μm pixel size, 1024 x 1280 pixels; Imaging, Canada), and a camera lens (Sigma Mini-Tele 1:35, 135-mm focal length multicoated Japan) in the 'double-pass retinal' imaging channel. The laser beam is filtered before entering the eye using a spatial filter.

(6) The Psychophysical Channel, placed in a conjugate retinal plane, consists of a Digital Micro-Mirror Device (DMD) (DLP DiscoveryTM 4100 0.7 XGA, Texas Instruments, USA) and allows displaying visual stimuli with a 1.62 deg angular subtend. The DMD is monochromatically illuminated with light coming from the SCLS (555nm) or with a fiber white light source (Halogen Fibre Light Sources LQ, Output Power 20-250 W, 3.000-3.400K, Linos; Qioptiq, Rhyl, UK). When light is perpendicularly incident on the flat surface of the DMD, light can be deflected towards two possible directions at ±12° (optical angle) by each micromirror, hence projecting high-resolution grayscale stimuli. The brighter pixels are projected onto a common screen using the 'ON-position' while deflecting light away with the 'OFF-position' provides a darker appearance. The amount of time each pixel is ON or OFF is varied to create a gray scale image, with lighter gray pixels corresponding with mirrors being ON more than OFF. A D4100 DVI to DMD (D2D) Interface Board (Digital Light Innovations Incorporated, Texas Instruments Incorporated, USA) was added to the original DLP Discovery 4100 kit in this system's configuration to display a video on the DMD via a DVI interface and control the generations of grayscale images. The DMD was calibrated to offer linear brightness levels and has an effective luminance of 100 cd/m2 (calibrated with a Cambridge Research Systems ColorCal luminance meter/colorimeter). The gamma correction was calibrated using the ViSaGe platform and Cambridge Research System ColorCal colorimeter, with 64 tones, linear fitting, and 64 readings per line. It was then applied to the DMD after being validated using a technique similar to that used in Psychtoolbox's visual gamma demo. A holographic diffuser (HD) placed in the beam path breaks the coherence of the laser, providing uniform illumination of the stimulus.

(7) The Pupil Monitoring Channel allows monitoring of pupil size and subject position during measurements. It consists of a camera (DCC154M, High-Resolution USB2.0 CMOS Camera, Thorlabs GmbH, Germany) conjugated to the eye's pupil. Subjects are stabilized using a dental impression and the eye's pupil is aligned to the optical axis of the system (with an x-y-z stage moving a bite bar) using the line of sight as a reference, while the natural pupil is viewed on the monitor.

(8) The Badal optometer Channel (formed by two lenses of a 125-mm focal distance and two mirrors) allows correction or induces defocus. Mounted on a motorized stage can be controlled by the researcher automatically or by the subject using a keyboard. Three automatized shutters allow simultaneous illumination of the eye and the stimulus for monochromatic light or white light. To ensure constant pupil diameter during measurements, an artificial pupil is placed in the first pupil plane of the system with x1 magnification from the subject's pupil.

All optoelectronic and mechanical elements of the AO set-up were automatically controlled and synchronized using ready-made or custom-built software programmed in Visual C++ and C# (Microsoft, Redmond, WA, USA) and Matlab (MathWorks, Natick, MA, USA)

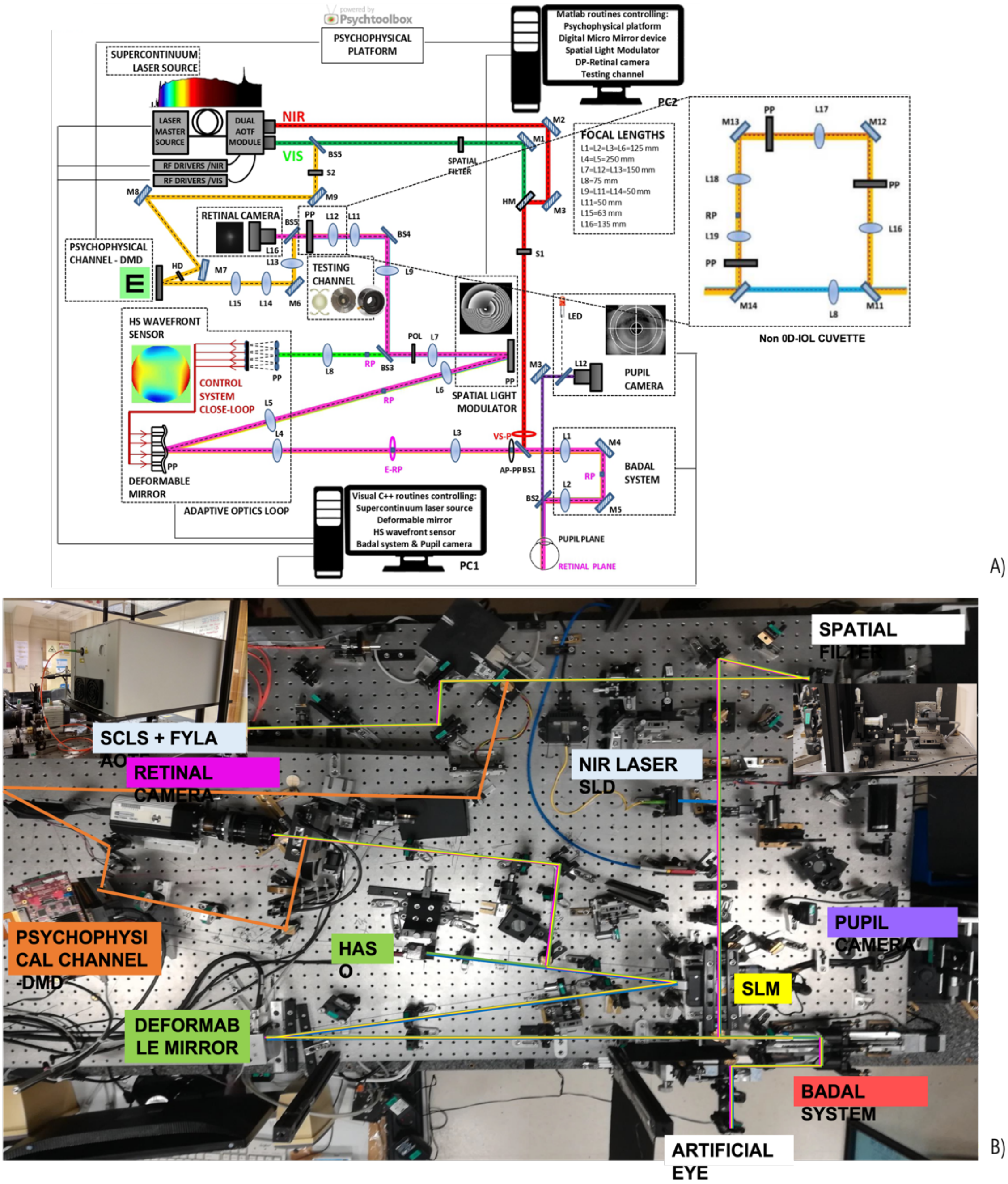

Figure 2.2. The VioBio Lab polychromatic multichannel AO visual simulator system in its ultimate version (2022) is shown in Figure A. Channels for illumination (red line), AO (green line), SLM (yellow line), retinal imaging (pink line), pupil monitoring (purple line), and psychophysical (blue line) are all shown (blue line). Near-infrared light, visible light, the pupil plane (PP), the retinal plane (RP), the lens (L), the mirror (M), the hot mirror (HM), the polarizer (POL), the retinal pinhole (E-RP), the artificial pupil (AP-PP), and the variable size pupil (VS-P) are all used in this sentence. Modified from Vinas et al. and Benedi-Garcia et al.(29,224) B) Top view photo of the VIOBIO Lab system in its 2019 configuration.

2.2 OPERATION AND CALIBRATION OF THE SPATIAL LIGHT MODULATOR

This section briefs about the Spatial Light Modulator (SLM) channel of the AO system. The SLM was used to simulate the multifocal/bifocal designs in many of the chapters of the thesis. An active matrix reflective mode phase-only liquid crystal display made of liquid crystal on silicon (LCoS) is controlled by a spatial light modulator (SLM) (PLUTO-VIS; Holoeye Photonics AG, Germany) (LCD). An LCoS display enables wavefront phase modification by altering the refractive index and consequently the optical path by applying various voltages to the device's various pixels. As a result, there is a phase difference between the various pixels, with each degree of the phase corresponding to a distinct level of gray. To provide the highest level of effectiveness, a linear polarizer is positioned in the path of the SLM (POL) at the calibrated polarization angle. Each of the 256 gray levels utilized for the phase pattern corresponds to a different phase shift that is achieved when various voltages are applied to each LCoS pixel.

2.2.1 Phase pattern generation using the SLM

The LCoS active matrix reflecting mode phase-only LCD driven by the SLM was used to generate complex phase maps after being numerically simulated using Matlab techniques and converted into.jpg files. The Fourier Optics wavefront maps are used to construct phase maps, although SLM can only provide a limited range of phase modulations, generally equivalent to one wave of compensation. Remapping the extra phase to a phase between 0 and 2π is required (47,225). Phase wrapping, a straightforward modular procedure that yields a maximum phase difference of 2π, is employed to accomplish this. To do so, multiplying each wavefront point by the appropriate wave number yields the wavefront's phase ($k=2\pi/\lambda$)(29).

The angles are then wrapped in lambdas, in radians, to the range (0 to 2π), where 0 maps to 0 and 2π maps to π. The wavefront is now confined to the range of 0 and 2π and expressed according to its phase. The resulting pattern is then an image in greyscale, where each shade of grey represents a certain phase difference between 0 and 2π.

2.3 PSYCHOPHYSICAL ROUTINES FOR IN VIVO MEASUREMENTS

This section describes the general protocols followed by the subjects who participated in the studies. A total of 35 subjects participated in the different experiments described in this thesis. The inclusion criteria for the subjects were: good general health, no ocular pathology, no previous ocular surgery, and no binocular vision anomaly. The studies were conducted on young and presbyopic subjects in an age range of 22 to 53 years old. The refractive error ranged from 0 to -5.5D with less than 0.75D of astigmatism.

2.3.1 General protocols with human subjects

Ethics Statement

Prior to enrolment in the study, all participants signed an informed consent form after being fully told about the nature of the studies and the potential outcomes. All protocols had received prior approval from the bioethical council of the Spanish National Research Council (CSIC), and they all adhered to the principles of the Helsinki Declaration.

Refractive error measurements and ophthalmologic evaluation

Before the experiments, the subjects followed a routine optometric evaluation at the School of Optometry Clinic of the University Complutense of Madrid (UCM) which includes sphero-cylindrical refractive errors and tests for adverse effects of mydriasis. Also, in the optometry cabinet corresponding to VioBio Lab (Institute of Optics), a measurement of the refractive error was carried out objectively using an autorefractor (AR 597, Humphery Zeiss Inc., Germany) that allowed an initial adjustment for the measurement of the best subjective approach with the Badal system.

Pharmacological pupil dilation

Tropicamide 1% was administered sub-cycloplegic for all studies. Two drops were administered 10 minutes before the study began, and one drop was administered every hour. Prior clinical evaluations had been performed on each participant to look for any negative mydriasis effects.

Alignment of the eye and pupil monitoring

A tooth impression was made using nontoxic mouldable paste on mountable metal support in order to precisely center and align the subject's eye with the optical system. For alignment, this impression was positioned on an x-y-z stage. The monitor displays the natural pupil while the pupil of the eye was oriented to the optical axis of the system utilizing the line of sight as a reference. The subjects may fixate on a red LED or a Maltase cross that is projected on the DMD.

Best subjective focus correction with the Badal System

A blurred Maltase cross is projected on the DMD, and the subject is instructed to select the best subjective focus (beginning from an artificially generated myopic defocus) while viewing it while using a keyboard to operate the Badal system. In order to prevent wasting any of the DM's capacity, which is needed for correcting HOAs and causing specific aberrations, the defocus of the subject is corrected using the Badal system rather than the DM. The best subjective focus was obtained for the different states of aberrations (AO-correction or natural aberrations) under test. The process of searching for the best subjective focus is repeated several times until the standard deviation between the values is small and the mean of the values is chosen.

2.3.2 Measurements of Aberrations in the AO systems

A calibration of the AO channel is performed before each testing session. Before each experimental session, the four steps—wavefront measurement, interaction matrix acquisition, command matrix building, and closed-loop system aberration correction—were completed each day with the artificial eye. The interaction matrix was generated for the entire pupil diameter, whereas the correction was carried out for a specific pupil diameter (depending on the psychophysical experiment, typically 5 or 6mm pupil diameter was used). Once, the aberrations of the system were corrected called "flat mirror state" is loaded in the DM before the measurements on real subjects. After that, the subjects were aligned to the system and placed in the badal at the best subjective focus (as chosen by the subject), according to the protocol described above the aberrations were measured to obtain the natural aberrations of the subject. This thesis only involves measurements of the subject's aberrations and did not involve correction or induction of the eye aberrations.

2.3.3 Measurements of Accommodative response in the AO system

The accommodative response to a stimulus in the psychophysical channel was obtained from the Hartmann-Shack. The process outlined below was followed in chapter-7 of this thesis.

Once the subject is properly aligned, the best subjective focus for far vision (0D badal position) was initially searched with the Maltese cross illuminated at a wavelength of 555nm, subjects moved the Badal using the keyboard towards the position where the blurred stimulus appeared sharp for the first time, after repeating for at least 5 times that value was set as zero. Natural aberrations were measured with the Hartmann-Shack wavefront sensor at different accommodative demands as induced by the badal system (0-6D), in 1D steps. These aberration measurements were made in 827nm NIR, while the accommodative stimulus was displayed in the DMD of the psychophysical channel illuminated in 555nm.

2.4 EXPERIMENTAL PROCEDURES

Psychophysical studies provide quantification of the link between the qualities of the physical stimulus and the perceptual experience. (226)

2.4.1 Visual stimuli

Different images were used in the experiments depending on the psychophysical tasks, which include high contrast Snellen E-letter for VA tests, Siemens star or Maltese cross for best focus, and specific cross as an accommodative stimulus. All the stimuli were presented in the DMD of the polychromatic multichannel AO system except for the Maltese cross stimuli which we presented in the CRT monitor (monochromatic AO). In the polychromatic multichannel AO visual simulator, the stimuli subtended 1.62 degrees, while in the monochromatic AO, the stimuli subtended 1.98 degrees (Figure 2.3 from A-D).

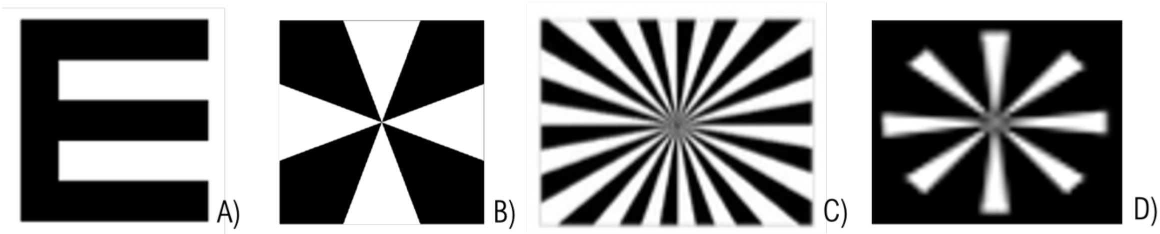

Figure 2.3. Example of stimuli used in the experiments of this thesis. A) Snellen E-letter (used in different sizes and orientations); B) Siemens star; C) Maltese Cross; D) Accommodative stimulus

2.4.2 Psychophysical measurements under Adaptive Optics controlled aberrations

We have used different psychophysical paradigms throughout the thesis. The subject's responses were recorded (using a keyboard in all cases) and analyzed off-line.

Visual Acuity

Visual acuity was measured using a four or eight Alternative Forced Choice procedure (4AFC-4 orientations: up, down, left, right; 8AFC-8 orientations the same as 4AFC which includes oblique positions addition to that) depending on the age of participants. The stimulus was a high contrast tumbling Snellen E-letter displayed on the DMD or CRT monitor. Subjects were asked to identify the orientation of the E-letter, whose size and orientation changes during each trial. Each run had 40 trials that were displayed for 0.5 seconds. With Psychtoolbox, a Matlab algorithm called QUEST (Quick Estimate by Sequential Testing) was created (227–229) to select the size of each stimulus and optimize the estimation of the spatial resolution threshold, following the subject's response. The cut-off point was set at 75%. The average of the ten most recent data was used to estimate the threshold for VA measurement. The measurements were discarded if convergence was not reached. VA was expressed in terms of decimal or logMAR VA (logMAR = -log10/decimal acuity). This has been described in detail with specifications in Chapters 3 and 4.

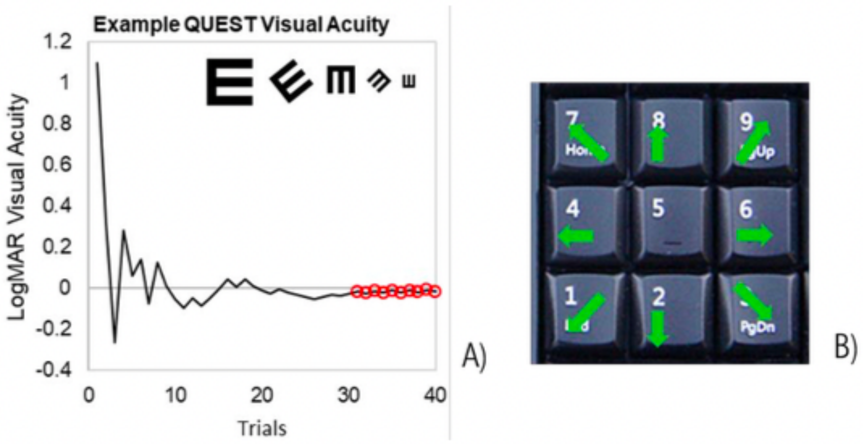

Figure 2.4. A) Example of VA QUEST, 40 trials convergence; B) Keyboard directions to indicate the different stimulus orientations (up-down (8,2), left-right (4-6), oblique (1,3,7 &)).

Subjective Best Focus at different Wavelengths

When observing a particular blurring stimulus that was illuminated with a variety of visible light wavelengths, the Badal system was used to achieve the optimal perceived focus. The subject moves the Badal until the stimulus looks sharp. The search for the sharpest image was repeated several times to have an average measure and a small standard deviation. More detail and specifications are described in Chapter 3.

2.5 OPTICAL QUALITY ANALYSIS

2.5.1 Optical quality metrics

From the wave aberration measurements obtained from the Hartmann-Shack wavefront sensor, we can calculate the image of a point on the retina (PSF), MTF and OTF, are some of the metrics used to evaluate the optical quality of a retinal image, described in detail in chapters 6. These measurements allow us to evaluate the optical quality of the subject's retinal image and compare it to the subject's perceptual perception. The eye is a low-pass filter in humans. Consequently, the drop for high spatial frequencies is larger (fine details in the image). The Strehl ratio (SR), a metric that compares the maximum image of a spot on the retina of an aberrated optical system to the maximum PSF of a system without aberrations, is frequently used to assess the quality of an optical system.

If we weigh the SR and NCSF, as a result, we have Visual Strehl (VS), a metric that describes the optical quality of the subject eye, used in Chapters 6 and 7. The NCSF is the neural contrast sensitivity function of the visual system ignoring optical factors and has been defined as the observer's contrast sensitivity function (CSF) divided by the MTF of their eye(230–232).

$$VS = \frac{\iint_{-\infty}^{\infty} NCSF_{(f_x,f_y)} \cdot OTF_{(f_x,f_y)}\, df_x\, df_y}{\iint_{-\infty}^{\infty} NCSF_{(f_x,f_y)} \cdot OTF_{DL(f_x,f_y)}\, df_x\, df_y}$$

Where NCSF is the Neural Contrast Sensitivity Function, OTF the Optical Transfer Function of an aberrated eye, OTFDL the OTF of a diffraction limit (DL) eye, and (fx,fy) the spatial frequency coordinates. In Marsack et al(233) study, the VS metric has been shown to account for 81% of the variance in high-contrast logMAR VA, making this metric a strong predictor of visual performance in normal eyes.

2.5.2 Correlation metric

The optical quality of images collected in on-bench measurements was analyzed using a 2D-correlation metric(48,136). A series of images were taken (1 pass-images, 1P), and each image was correlated with a reference image. The stimulus used in all cases was a Snellen E-letter (Chapter 4). The correlation coefficient (correlation of the E-letter with a reference monofocal correction and each recorded image in the same conditions: laser power, pupil diameter, exposure duration, Badal location at 0D) of the image series was obtained following the centering of each image.

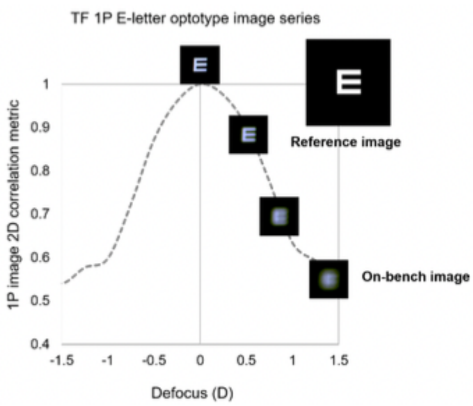

Figure 2.5. TF optical quality. TF image correlation metric (1P) of an E-optotype (side images in each focus), for a monofocal lens and reference image.

2.6 3D – ANTERIOR SEGMENT SPECTRAL DOMAIN OCT

2.6.1 Custom setup

In a spectral domain OCT (SD-OCT) system, a spectrometer with a line scan camera records a spectral fringe pattern (channelled spectrum), and a tomogram line is produced by unevenly sampling the recorded fringe pattern using Fourier analysis. With this method, imaging can be done much more quickly without the need for mechanical depth scanning, and 3D anterior segment data can be collected in a matter of milliseconds with a high degree of lateral and axial resolution to assess ocular anterior segment biometry (from the anterior cornea to the posterior crystalline lens/IOL).

In recent years, various new components and specially created processing algorithms have been added to the customized SD-OCT system in the VIOBIO lab, which was created in partnership with Nicolaus Copernicus University (Torun, Poland). A detailed description of the setup was described in previous thesis and publications(211,213,234,235).

The main components of the SD-OCT system are the light source, reference arm, sample arm (which includes an accommodation/fixation channel, scanning galvanic mirror, objective lens, and subjects), and spectrometer (including condensing lens, grating, and line-scan camera). A superluminescent diode (SLD, ($\lambda 0$ = 840nm) with a near Gaussian emission bandwidth of 50 nm (Superlum, Ireland) serves as the light source. In order to prevent back-reflected light from the reference and sample arms from returning to the SLD, the laser beam is separated into reference and sample arms by a fiber mate to an 80:20 fiber coupler. The reference arm is made up of a collimating lens to create a collimated beam, a neutral density filter to adjust the power of light in the reference arm, a converging lens, and a reference mirror to improve detection performance.

In the sample arm that includes the fixation channel, a second beam splitter is installed for measurement reasons. This channel features the Badal system, which consists of two achromatic doublets with identical 150 mm focal lengths that form an x1 afocal system, two flat mirrors, and a motorized stage (VXM-1, Velmex) that may be rotated to alter the optical path between the lenses. This makes spherical refractive errors compensable. Vergence is adjusted using the Badal technique from -10D to 10D, and trial lenses positioned in the pupil plane are used to make up the difference. The image stays in focus under all circumstances (in 1-D steps). For the fixation channel, a 20/25 white Snellen E-letter presented on a black background using a Digital Light Processing (DLP) pico-projector (854x480 pixels, Picopix PPX2055/F7, Philips NV, Amsterdam, Netherlands; 55 Lumens) subtending a 5-arcmin viewing angle serves as the fixation stimulus. To create an average luminance of about 30cd/m2 in a dark setting, two neutral density filters (ND 16) are added after the picoprojector.

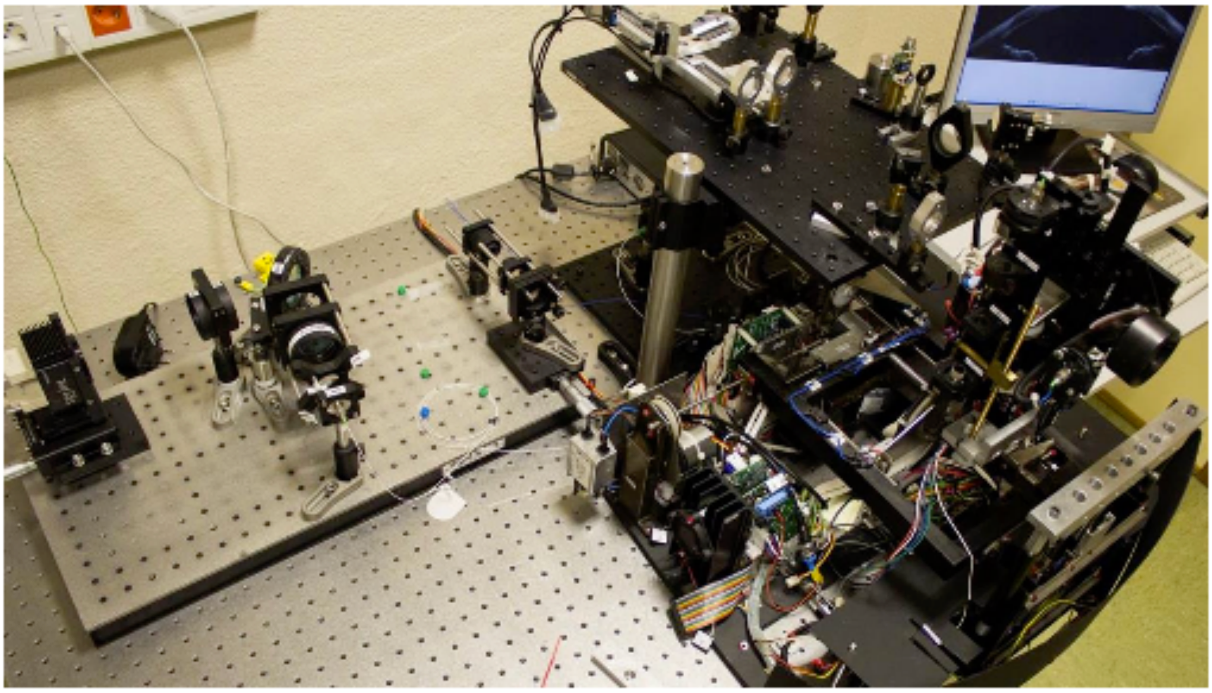

Figure 2.6. Set up of the actual custom developed Spectral-Domain Optical Coherence Tomography device at the VIOBIO lab (Institute of Optics)

2.6.2 Experimental procedure

The visual fixation stimuli are displayed on a screen external to the body via a picoprojector. The fixation stimulus is a picoprojector (854x480 pixels, Philips NV, Amsterdam, Netherlands; 55 lum), which projects a 20/25 white Snellen E-letter against a black background at a viewing angle of 5 arcmins. Following the picoprojector, two ND 16 neutral filters were employed to produce an average brightness of roughly 30cd/m2 in a fully dark environment. We developed a Matlab script that can move the target every 0.5 pixels along the horizontal and vertical axes once it has been first aligned with the OCT axis in order to measure in the line of sight. The collimating lens causes a collimated beam to be created on the cornea. The galvanometer optical scanners, which are made by Cambridge Technology Inc. in Bedford, Massachusetts, are driven by an analog input/output card from National Instruments in Austin, Texas. An objective lens is required to collimate the main beams' rays and focus the irradiance impinging on the sample. Beam splitting is used to combine the light that has been split into its components and transmitted to the spectrometer after being reflected back by the reference and sample arms. The components of a spectrometer include a condensing lens for collimating light, a volume diffraction grating for spatially separating the spectrum, and a magnifier objective comprised of two converging lenses for focusing the signal on the detector. To measure the interference fringes of the spectrum, a 12-bit line-scan CMOS camera with 4096 pixels (Basler sprint spL4096-140k; Basler AG, Germany) is used.

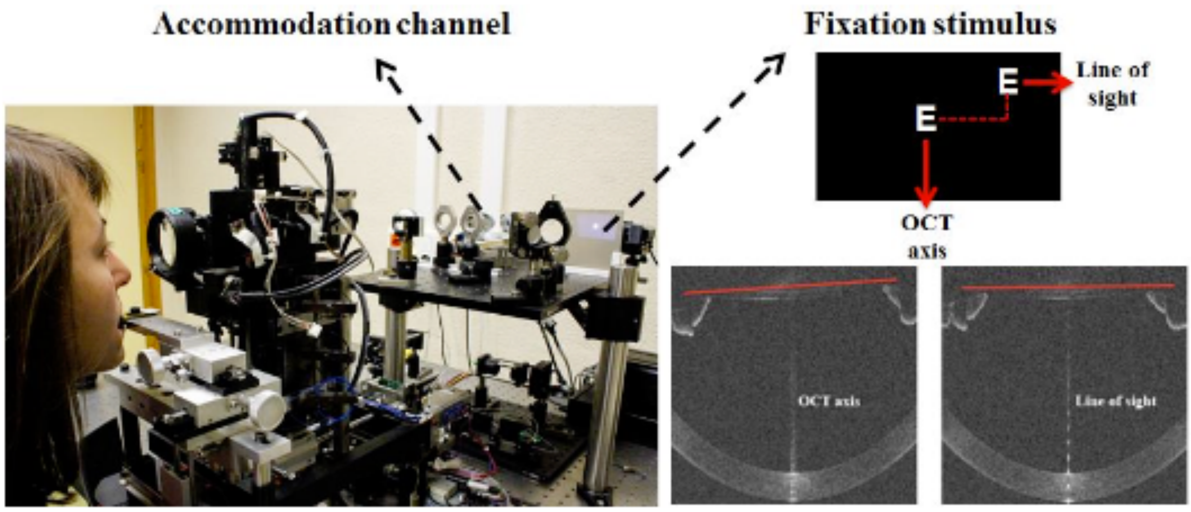

Figure 2.7. On the OCT, a channel for external accommodation and fixing has been implemented. an image of the moving stimulus that will help your eyes align more clearly.

2.6.3 Data Analysis

The algorithm is summarized in three different steps(214):

(1) 3-D image processing:

Volume clustering and multilayer segmentation: Classes of related point volumes were established. Classes with volume sizes below a predetermined cut-off were removed. The threshold was calculated as a certain percentile between 95 and 99% of all connection points. The number of classes was further reduced with the application of volume clustering, and the larger volumes (cornea, iris, crystalline lens, ICRS, and IOL) were automatically categorized. Following the classification of the volumes, an algorithm based on the first derivative boundary region identification identified the locations of each A-peaks scan and ranked them according to their locations and intensities.

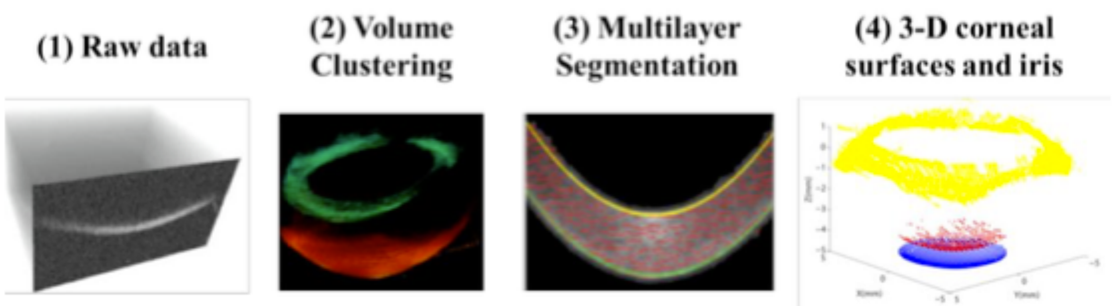

Figure 2.8. Illustration of the segmentation process

CHAPTER-3. VISUAL PERFORMANCE WITH MULTIFOCAL CONTACT LENSES IN YOUNG ADULTS AND PRESBYOPES

To limit the progression of myopia in young eyes, where MCLs may be prescribed, and in presbyopes, where MCLs are increasingly utilized to make up for the lack of accommodation, it is crucial to have a better understanding of visual performance with multifocal contact lenses (MCLs). The through-focus visual acuity (TFVA) with center-near MCLs of various adds was evaluated in the study presented in this chapter, and the effects of accommodation, age, and pupil diameter (in cycloplegic patients) on visual performance were also examined.

This chapter is reproducing the paper by **Vedhakrishnan et al.**(236) “Visual performance with multifocal contact lenses in young adults and presbyopes”, published in Plos One (2021). The co-authors are Maria Vinas, Clara Benedi-Garcia, Pilar Casado, and Susana Marcos.

The work was presented as a poster at ARVO annual meeting in 2020 by **Vedhakrishnan et al**. under the title “Vision with Multifocal contact lenses”. It was also presented as an oral presentation by Vedhakrishnan et al in the PhD day event conducted at Complutense University, Madrid, under the same title.

The author of this thesis designed the experiment, implemented the experimental protocol, performed the experimental measurements on subjects, collected and analyzed the data, and prepared the manuscript in collaboration with Maria Vinas and Susana Marcos.

3.1 Introduction

One of the most frequent eye conditions, myopia is becoming more and more prevalent worldwide and is regarded as a serious global health issue (237). Many different therapies have been suggested to stop the progression of myopia. Based on the theory that retinal blur is the visual signal that promotes the development of refractive error, optical therapies have been preferred to slow down myopia. Multifocal contact lenses (MCLs), which operate on the idea of simultaneous vision, i.e., projecting an image focused simultaneously at far and near, have been utilized more frequently in recent years among these optical techniques (111).

All people over the age of 45 are affected by presbyopia, the age-related decrease in the crystalline lens's capacity to dynamically accommodate from far to near. Presbyopia is increasingly being treated with simultaneous vision, such as MCLs and multifocal intraocular lenses (MIOLs). While still correcting vision at a distance, these multifocal corrections seek to restore the near vision capabilities lost in the presbyopic eye. Different studies(198,223,238,239) Through-focus (TF) visual performance measures in presbyopic individuals treated with MCLs or MIOLs show an improvement at close distance, typically accompanied by a decline at a distance. It's crucial to choose the right correction and optimize patient management if you are aware of the elements that affect MCL performance in presbyopes, including lens design, pupil diameter, and residual accommodation.

Even though it has been noticed that the effect is lessened at close distances, center-distance multifocal lenses are likely to cause peripheral myopic defocus for far distances (112). Since the center-distance lenses predominantly produce myopic defocus in one meridian rather than the entire retinal periphery, their effects on the periphery are not as significant as could be predicted (112). Surprisingly, a study discovered that myopia-related peripheral defocus might still occur in eyes wearing center-near multifocal lenses (240), probably reflecting the wide inter-subject variation in the peripheral retina's shape. Therefore, as the sign of defocus in the peripheral area can vary, the MCLs' process could not entirely depend on doing so. While the majority of the peer-reviewed literature on using MCLs to manage myopia progression mentions the use of center-distance lens designs (115,240), Additionally, there is anecdotal evidence that center-near lens designs have been successful in halting the growth of myopia (163,240).

Studies have investigated the degree to which MCLs interact with accommodation. Petterson et al.(241) found no difference in accommodation in young participants wearing multifocal aspheric contact lenses compared to their lag with single vision lenses when subjects were wearing bifocal center-distance corrections, suggesting that pre-presbyopic adults do not relax their accommodation. Contrary to what was found in a study on accommodation dynamics with induced spherical aberration (using adaptive optics), accommodative lag is modified differently depending on whether there is a positive or negative spherical aberration (corresponding to center-distance add or subtraction) (equivalent to center-near add) (132). According to that study, positive spherical aberration increased accommodative lag whereas negative spherical aberration reduced it, which may support the usage of center-near addition lenses. Interestingly, Theagarayan et al.(138) both positive and negative spherical aberration contact lenses were utilized, and the same result was found: Again, suggesting that center-near MCLs would prefer a more precise accommodative response, adding negative spherical aberration enhances the slope of the accommodation stimulus-response curve and minimizes latency of accommodation. This contrasts with adding positive spherical aberration. Regardless of the mode of action, the existence of a close addition, whether central or peripheral, appears to generate a potent enough inhibitory signal to halt the advancement of myopia. Because there are more center-near lenses available commercially, it is interesting to examine visual performance in young adults wearing center-near addition lenses.

Center-near lenses are more common among presbyopes than center-distance lenses because comparative studies have shown that center-near lenses perform better (242,243). Except for minor adjustments, one might anticipate that the optical design of MCLs will be fairly similar for both target populations (young adults and presbyopes). The fact that accommodation is functional in young adults when MCLs are prescribed, at least to a far greater extent than in presbyopes, indicates a significant fundamental difference between the two groups. Additionally, young people tend to have larger pupils than people with older eyes (119,244). However, in both groups, the unintended visual compromise brought on by simultaneous vision, which has mostly been assessed in investigations on presbyopic subjects, is a potential drawback to the use of MCLs (245). Understandably, the majority of studies seen yet on young adults wearing MCLs assess their effectiveness in slowing myopia progression (133,172,246,247), and only a few studies have thoroughly evaluated visual performance and visual quality with MCLs(238,248,249). In fact, differences in visual performance with MCLs are expected to depend on several lens design factors (i.e., the power profile of the lenses, near add(104,250) , and the patient's optical profile, including pupil size(114,250) and optical aberrations). To the best of our knowledge, no prior study has evaluated the impact of lens design, inherent aberrations, pupil diameter, and the presence or lack of accommodation on TF visual performance with MCLs.

In this work, we assessed TF visual performance with center-near multifocal designs that were commercially available, with additions of three distinct magnitudes (low, medium, and high) at various foci, both with natural and paralyzed accommodation. A group of young adults and a group of presbyopes participated in the study.

3.2 Methods

Through-focus visual acuity (TFVA) was assessed in young adults and presbyopes, two groups of participants with various refractive profiles, under natural lighting, both with natural and paralyzed accommodation, and for various pupil diameters. The measurements were performed both with and without MCLs (NoLens) on the eye.

3.2.1. Subjects

In the study, 15 participants of European descent were split into two groups: (1) 5 presbyopes, average age 53 ±2.0; average spherical equivalent 0.25±0.9D; (2) 10 young adults, average age 26.9±2.2; average spherical equivalent -2.2±0.8D. The profiles of the different subjects are shown in Table 1. All test individuals had experience placing on and taking out contact lenses because they regularly wore soft lenses or occasionally wore them.

The CSIC Institutional Review Boards had given its blessing to the study protocols, which adhered to the principles of the Declaration of Helsinki. Before the experimental session, all participants completed an informed permission form after receiving information about the study and its experimental methods.

Subject	Group	Age (yrs)	Gender	Measured Eye	Spherical error (D)	Astigmatism (D)	Astigmatism axis (deg)	Duration: Habitual (H)/Occasional (O) lens wearer
S1	YOUNG ADULTS	24	F	OD	-1.25	-0.5	70	O (SCL)
S2		24	F	OD	-2.5	-	-	H (SCL)
S3		24	M	OD	-4.5	-	-	O (SCL)
S4		24	F	OD	-4	-	-	O (SCL)
S5		25	F	OD	-0.5	-	-	O (SCL)
S6		26	M	OD	0	-	-	O (SCL)
S7		26	F	OD	-4.5	-	-	H (SCL)
S8		27	F	OD	-1.5	-	-	H (SCL)
S9		31	F	OD	-1.75	-0.5	90	O (SCL)
S10		38	M	OD	0	-0.5	108	O (SCL)
S11	PRESBYOPES	47	F	OD	1.5	-	-	O (MCL)
S12		52	F	OD	2.5	-	-	H (MCL)
S13		53	F	OD	-2.75	-	-	H (MCL)
S14		55	M	OD	0	-	-	O (MCL)
S15		58	M	OD	0	-	-	H (MCL)

Table 3.1: Individual refractive indices of the two groups' participants (young adults and presbyopes). ID, age, gender, measured eye (always the dominant eye), spherical error, astigmatism, astigmatism axis, and period of lens wear: habitual (H) or occasional (O) of the SCL and MCL (for standard soft CLs).

3.2.2. Multifocal Contact lenses (MCLs)

In this trial, 1-Day Acuvue Moist MCLs were used (Johnson and Johnson Vision Care, Jacksonville, FL, USA)(193,251). It has a center-near aspheric profile and is a soft daily disposable lens. With three separate enhancements, Low (+1.25D), Medium (+1.75D), and High (+2.50D), all individuals were fitted with a -2D for far. A prior study using the identical MCLs demonstrated that the depth of focus increased as the number of lenses was added (193). A motorized Badal system was used to correct the subject's remaining refractive error.

3.2.3. Experimental set-up

A custom-built Adaptive Optics (AO) system, which was previously extensively documented, was used for the measurements (217). The system and setup are described in detail in section 2.1.1 of this thesis (Figure 2.1). The visual stimulus channel contained a conjugate pupil plane with a 7-mm artificial pupil, allowing measurements with various pupil diameters (5, 4, and 3 mm).

3.2.4. Experimental procedure

Each subject underwent two separate sessions of measurement. Alcon Cusi, Barcelona, Spain, performed the first session while using 1% Tropicamide to induce cycloplegia (2 drops before the experiment, and repeated every hour). The non-cyclopleged eyes were used for the second session. In both sessions, TFVA measurements were performed under 4 different settings (NoLens, LowAdd, MediumAdd, and HighAdd real MCLs in the eye). TFVA measurements were made in session 1 for pupils with diameters of 5, 4, and 3 mm, with the artificial pupil of the system controlling the pupil size. Measurements were only taken for the normal pupil in session 2 (i.e., not limited by the artificial pupil in the system). Every session took place on a different day (separated by 1-2 days or less). With regular breaks, session 1 lasted for 7-8 hours. The second session lasted for around 4 hours. Prior to the start of the measurements, the subjects were given contact lenses at the beginning of the session, instructed to put them in, and given 10 to 15 minutes to adjust. The addition of the MCLs was kept blinded from the individuals.

In a dimly lit space, all measurements were made monocularly (with the dominant eye). The subjects received information about the purpose of the experiment before the measurements began, and they also went through some practice runs. The position of the Badal system was then adjusted by the subject to provide the finest focus possible under each circumstance (NoLens, LowAdd, MediumAdd, HighAdd). The zero-defocus setting for each situation was calculated by averaging five of the best focus values. The optimal focus with these MCLs did not deviate from the NoLens by more than 0.375/0.50/0.50D across conditions (LowAdd/MediumAdd/HighAdd), which is consistent with the anticipated focus shift generated by these MCLs (193,203) and demonstrating that for distant vision, the far focus (rather than a near focus) was always chosen.

3.2.5. Through-focus visual acuity (TFVA)

The whole dioptric range of 4 D (-3.00D to +1.00D) in 0.5 D steps around the optimum focus was used to test visual acuity (VA) for each condition. A forced choice with eight alternatives was used to measure VA (8AFC) (252) technique using the QUEST (Quick Estimation by Sequential Testing) algorithm and Tumbling E letters (Black E letters on a white backdrop) created with the Psychtoolbox software (228) to determine the order in which the test's provided stimuli—letter size and orientation—will be presented after the subject's response. The orientation of the E-letter had to be determined by the subjects, and depending on their response, the stimulus size in the subsequent presentation changed. Each VA measurement was subjected to 35 trials of the QUEST routine, with a 75% threshold criterion. The average of the 10 most recent stimulus readings was used to estimate the threshold VA measurement. VA was calculated using the formula logMAR = -log10 [decimal acuity](253).

3.2.6. Data Analysis

For each subject and condition, various metrics of analysis (illustrated in Fig. 3.1) were derived from the TF curves, evaluating absolute values of visual performance at various distances (Fig. 3.1 A), relative differences in performance with MCL in comparison to a standard spherical correction (Fig. 3.1 B), and the consistency of vision across distances (Fig 3.1 C).

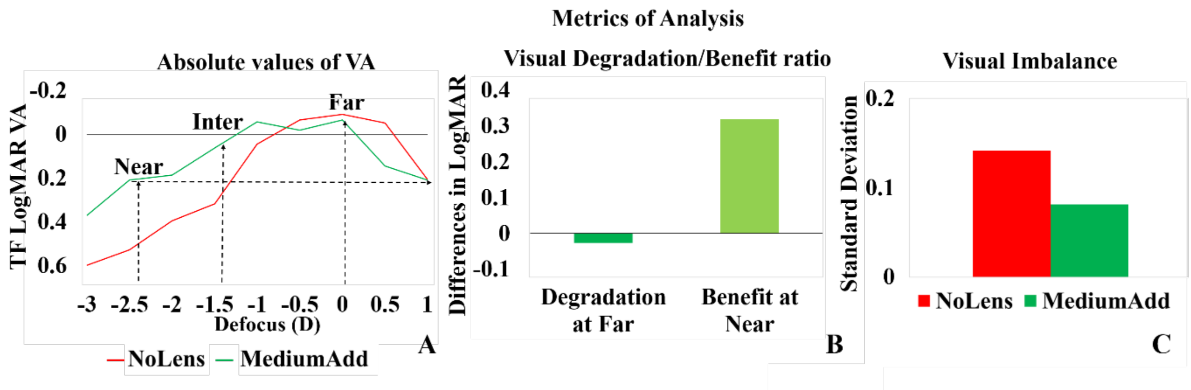

Fig 3.1. Example of several metrics for S#9, a young subject, using NoLens and MediumAdd CL. (A) Depth of Focus (defined as the dioptric range where VA is better than 0.2logMAR) is indicated by a horizontal line, and TF logMAR VA highlights the absolute value of logMAR VA at far (best focus), intermediate (1.5D), and near (2.5D) distances. (B) Visual degradation at a distance (dark green) and near (differences in logMAR VA for NoLens and MCL) (2.5D, Visual benefit at near). (C) Visual Imbalance across Distances for the NoLens (Red bar) and MediumAdd CL, defined as the Standard Deviation of the logMAR VA values over the TF curve (Green Bar).

Absolute VA values for far The TFVA curve's (0D), intermediate (1.5D), and near (2.5D) values were extracted (A). These figures represent the visual performance of the MCLs at various distances.

Depth-of-focus (DOF) is outlined as the defocus range where the VA is at least 0.2 logMAR [43].

Visual Degradation at far & Visual Benefit at near was acquired as the difference between VA with MCLs in comparison to VA with NoLens at far (best focus) and at near (+2.50 D), as shown in Fig 1. (B). The formula for defining visual degradation at far is (logMAR VA @far (NoLens) - logMAR VA @far (MCLs)). The formula for the Visual Benefit at Near is (logMAR VA @near (NoLens) - logMAR VA @near (MCLs)). MCLs are anticipated to improve visual performance at close range and decrease visual performance at a distance (i.e., negative values) (i.e., positive values). The classifications made using ratios in earlier research are identical to those made here because the logarithmic notation of logMAR differences is converted to ratios in other metrics, like decimal visual quality or perceptual scorings. [44].

Visual Imbalance, shown in Fig. 1, is the standard deviation of VA throughout a TF curve and is illustrated in Fig. 1(C). This meter accurately measures the variations in visual performance over a range of distances. For example, it is expected that VA with a bifocal correction or monofocal correction in a patient with paralyzed accommodation will vary more across distances (resulting in a higher standard deviation and therefore a higher visual imbalance) than with extended depth of focus lenses producing a smoother variation of VA across distances (lower standard deviation, and thus lower imbalance). Visual imbalance after normalizing (by a factor of 0.2) is used to assess visual constancy, which is then multiplied by -1.

Overall quality metric the visual degradation/benefit and visual constancy metrics were combined to create this metric. The overall metric is defined by Visual benefit at near – Visual degradation at far + Visual constancy. A high overall visual performance is shown by a positive value, whereas a low visual performance is indicated by a negative value. The differences in visual performance among lenses and age groups were examined, and these metrics were analyzed across all individuals and lenses.

SPSS Statistics 24.0 was used to conduct the statistical analysis (IBM, United States). The Shapiro-Wilk test was used to verify the normality assumption. A power analysis (Post hoc analysis) was performed. All the comparisons within the group for each condition had a power value greater than 0.8, indicating a sufficiently large sample. Some comparisons across the two groups (young adults and presbyopes) had a power value of 0.4-0.6 which still indicate significant results. Specific non-parametric tests were used: (1) the Mann-Whitney U test to analyze differences between two independent samples (young adults, presbyopes) (2) the Wilcoxon test to analyze differences between two related samples (Accommodation, Visual Benefit and Degradation, Visual Imbalance) within each group, and (3) the Kruskal-Wallis test to analyze differences between NoLens and MCLs conditions. The similarity in the shape of the TF curves between the individual's native VA and with the MCLs was done using a cross-correlation analysis, with lag k and rho values representing the largest spike of the series when the elements of both TF curves match exactly and the correlation coefficient, respectively.

3.3. Results

3.3.1. Visual Acuity at far and near

Figure 3.2 (A) displays the VA at a distance (best focus) and (B) the VA at a near distance for all individuals and lenses as a function of age, including both paralyzed (solid symbols) and natural accommodation (open symbols). Different hues correspond to various lens types (LowAdd: Orange; MediumAdd: Green; HighAdd: Purple and NoLens: Red). In terms of quality, only three participants in the group of young adults had logMAR VA that was significantly worse than 0 under various MCL settings. The worst VA values also occurred for Medium and HighAdd MCLs in most cases (except for individuals 1 and 3, all 24 years old). With the MCLs in the group of young people, the best VA was attained at close range. The MCLs' (LowAdd/MediumAdd/HighAdd) performance with natural adaptation varied statistically considerably between the two young adults. (Kruskal-Wallis test, p=0.011) and presbyopes (Kruskal-Wallis test, p=0.033) for far.

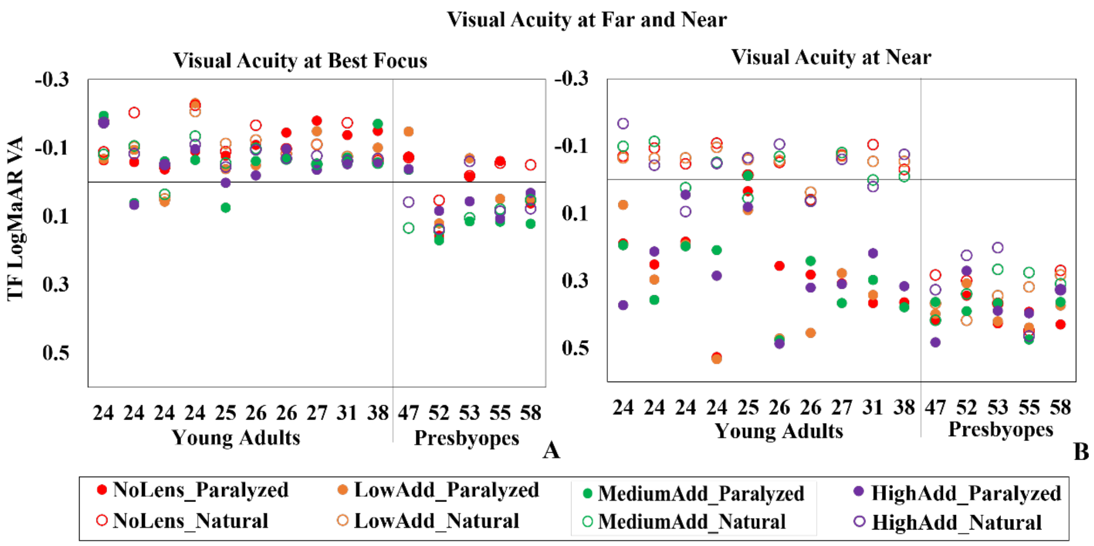

Fig 3.2: Near and far logMAR VA. For all lenses and situations, (A) logMAR VA at far and (B) logMAR VA at close, with age as a function. The color of the lenses can be used to distinguish them. NoLens in red, LowAdd in orange, MediumAdd in green, and HighAdd in purple. Open symbols represent natural accommodation, while solid symbols represent paralytic accommodation. Young adults are the subjects to the left of the separation bar, while presbyopes are the subjects to the right of the separation bar.

In presbyopes, there were statistically significant differences in VA between far and near for the NoLens condition and with all MCLs with both natural and paralyzed accommodation (Wilcoxon signed rank test, NoLens/LowAdd/MediumAdd/HighAdd: p=0.043 for paralyzed and natural accommodation, respectively). This shows that presbyopes have degraded near vision as expected and that MCLs do not improve near vision to the same extent as they do far vision. With all MCLs and the NoLens condition with paralyzed accommodation, VA was statistically significantly different between far and near in young adults (Wilcoxon signed rank test, p=0.005/0.005/0.007/0.005), but only for the NoLens condition (Wilcoxon signed rank test, p=0.007) with natural accommodation.

Young adults and presbyopic groups had significantly different VA under natural accommodation for both far (Mann-Whitney U test, NoLens/LowAdd: p=0.008; MediumAdd: p0.001; HighAdd: p=0.003) and near (Mann-Whitney U test, p0.001). Under paralytic accommodation, statistically significant differences between young adults and presbyopes occurred in nearly all circumstances for far and only with the NoLens (p=0.028) for near (Mann-Whitney U test, NoLens (p=0.013), MediumAdd (p=0.003), and HighAdd conditions).

As anticipated given the lack of accommodation and smaller natural pupil diameters, there were no appreciable differences between VA assessed under paralyzed and natural accommodation in presbyopes. However, owing to operative accommodation, there were statistically significant variations in VA assessed under paralyzed and natural accommodation in young adults across all circumstances (Wilcoxon signed rank test, NoLens/LowAdd p=0.005; MediumAdd/HighAdd p=0.007).

3.3.2. Through-focus VA: Effect of lens design and accommodation

TFVA – Paralyzed Accommodation

Figure 3.3 depicts the TFVA measured with a fixed 5-mm diameter pupil in all young adults (top panels) and presbyopes (bottom panels) for all three lenses (LowAdd: Orange; MediumAdd: Green; HighAdd: Purple) as well as the NoLens condition (NoLens: Red), under-paralyzed accommodation. When comparing the TFVA curves between conditions (NoLens/LowAdd/MediumAdd/HighAdd) within each group, no statistically significant differences were found between the groups. This suggests that the visual performances were similar across the conditions.

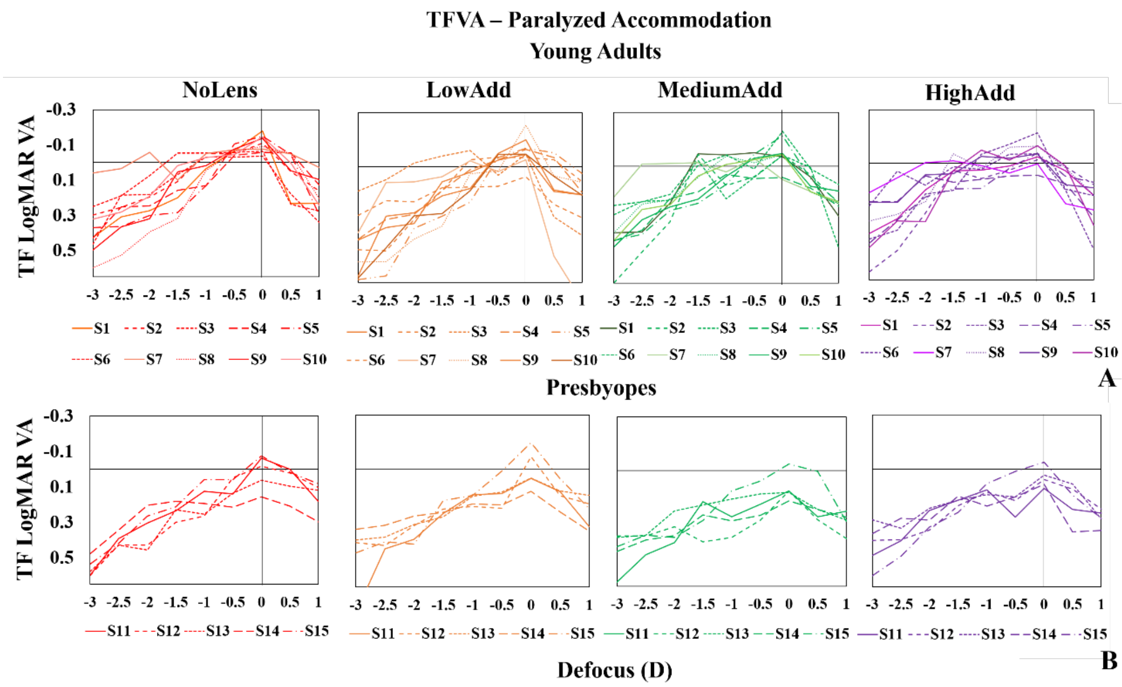

Fig 3.3. Under paralyzed accommodation, TFVA values are displayed for all participants and circumstances with 5 mm pupil diameters. (A) young adults (top panels); (B) presbyopes (bottom panels). Conditions are NoLens,

LowAdd, MediumAdd, and HighAdd, in that order. Lens color indicates condition - NoLens in red, LowAdd in orange, MediumAdd in green, and HighAdd in purple.

TFVA – Natural Accommodation

In the top panels of Fig. 3.4, all young adults and presbyopes with all 3 lenses (LowAdd: Orange; MediumAdd: Green; HighAdd: Purple) and the NoLens condition (NoLens: Red) had their TFVA assessed under natural accommodation (and natural pupil diameter). Young adults and presbyopes have considerably different TFVA curves, showing an obvious influence of accommodation in the younger group and a less distinct qualitative effect of MCLs. Unlike under paralyzed accommodation (where both young adults and presbyopes show similar trends, i.e., narrower TFVA with NoLens, which broadens with MCLs), TFVA curves are notably different between young adults and presbyopes, indicating a clear effect of accommodation in the young group, and the effect of MCLs in this group is not qualitatively as clear.

Overall, no statistically significant differences were identified between the paralyzed (Fig. 3.3) and natural accommodation (Fig. 3.4) within any group for the presbyopic population. However, due to the presence of accommodation in the young adult's group, there were statistically significant differences between paralyzed and natural accommodation for all conditions (Wilcoxon signed rank test, NoLens: p=0.005, LowAdd: p=0.005, MediumAdd: p=0.007; HighAdd: p=0.005).

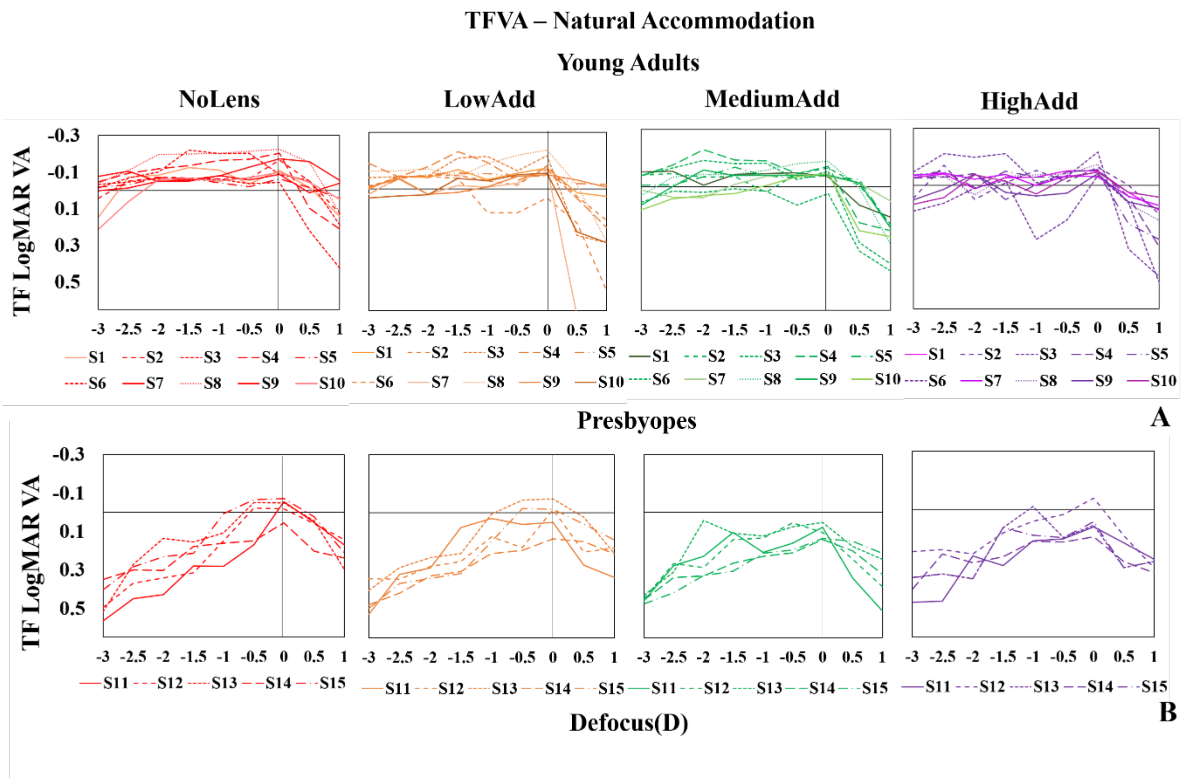

Fig 3.4. TFVA curves under natural accommodation with normal pupil diameters for all subjects and circumstances. (A) young adults (top panels); (B) presbyopes (bottom panels). Conditions are NoLens, LowAdd, MediumAdd, and HighAdd, in that order. Red indicates no lens, orange low addition, green medium, and purple high addition.

3.3.3. Intersubject Variability

Young adults' intersubject variability in VA at best focus rose with MCLs with paralyzed accommodation, while it decreased with NoLens (0.023logMAR). The overall inter-subject variability was higher with paralyzed than with natural accommodation, despite differences in inter-subject variability not reaching statistical significance in either group.

3.3.4. Average Through-focus VA

Figure 3.5 displays the TFVA curves for paralyzed accommodation (left panels) and natural accommodation (right panels) for young adults (A) and presbyopes (B) averaged across participants (right panels). A separate lens type is represented by each line (LowAdd: Orange; MediumAdd: Green; HighAdd: Purple and NoLens: Red). In young adults, there was a statistically significant difference in the TFVA curve shape between the conditions of normal accommodation and paralyzed accommodation (cross-correlation: lag k=0; rho=0.561 NoLens; rho=0.204 LowAdd; rho=0.360 MediumAdd; rho=0.337 HighAdd). As expected, given the much-reduced accommodation, there were no statistically significant variations in the TFVA curves' shapes in presbyopes (cross-correlation: lag k=0; rho=0.965 NoLens; rho=0.979 LowAdd; rho=0.897 MediumAdd; rho=0.950 HighAdd).

Medium and HighAdd MCLs improved performance at the intermediate and near vision in comparison to the NoLens and LowAdd situations when accommodation was paralyzed in both groups and natural in presbyopes. When young adults were housed in a paralyzed position, the average DOF increased from 1.95 D (NoLens) to 2.25 D (HighAdd), but in presbyopes, it increased from 1.4 D (NoLens) to 1.5 D (HighAdd).

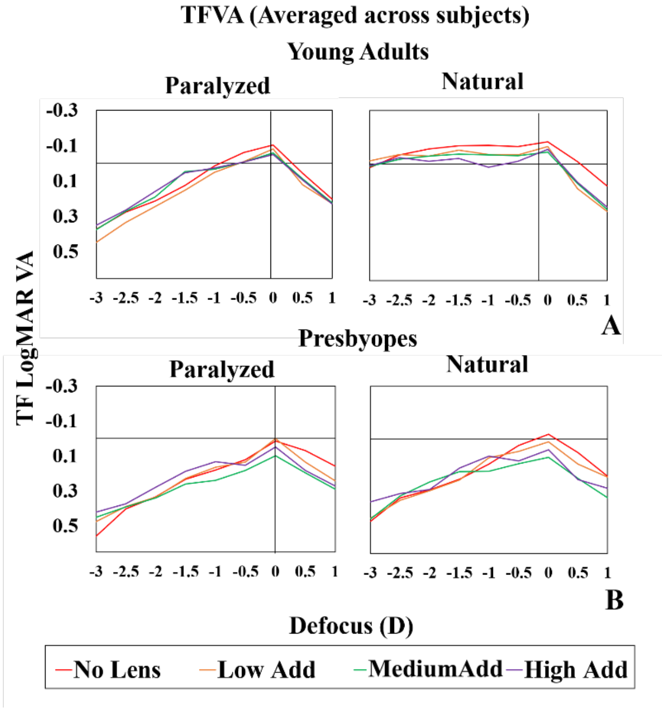

Fig 3.5: Average TF logMAR VA for the paralyzed and natural accommodation groups, across all participants. Average TFVA curves for presbyopes and young adults, respectively. Right plots: natural accommodation; left plots: paralyzed accommodation. Each lens condition is indicated by the color - Purple: HighAdd, Green: MediumAdd, Orange: LowAdd, and Red: NoLens.

3.3.5. Through-focus VA: effect of pupil diameter

Young adults (A-upper panels) and presbyopes (B-lower panels) were subjected to TFVA measurements under paralyzed accommodation and averaged across all participants for three distinct pupil diameters (5, 4, and 3 mm) for the LowAdd, MediumAdd, and HighAdd lenses (Fig. 3.6). For the three pupil sizes with the NoLens, LowAdd, and MediumAdd lens conditions, VA at distance was typically within 93% LogMAR in young adults. With larger pupils, VA for the HighAdd lens significantly enhanced (0.08 logMAR shift from 3-mm to 5-mm pupil). For presbyopes, on the other hand, VA at far was highest with the lowest pupil diameter in the NoLens condition (0.05 logMAR shift), Medium, and HighAdd lenses (0.042 and 0.041 logMAR shifts).

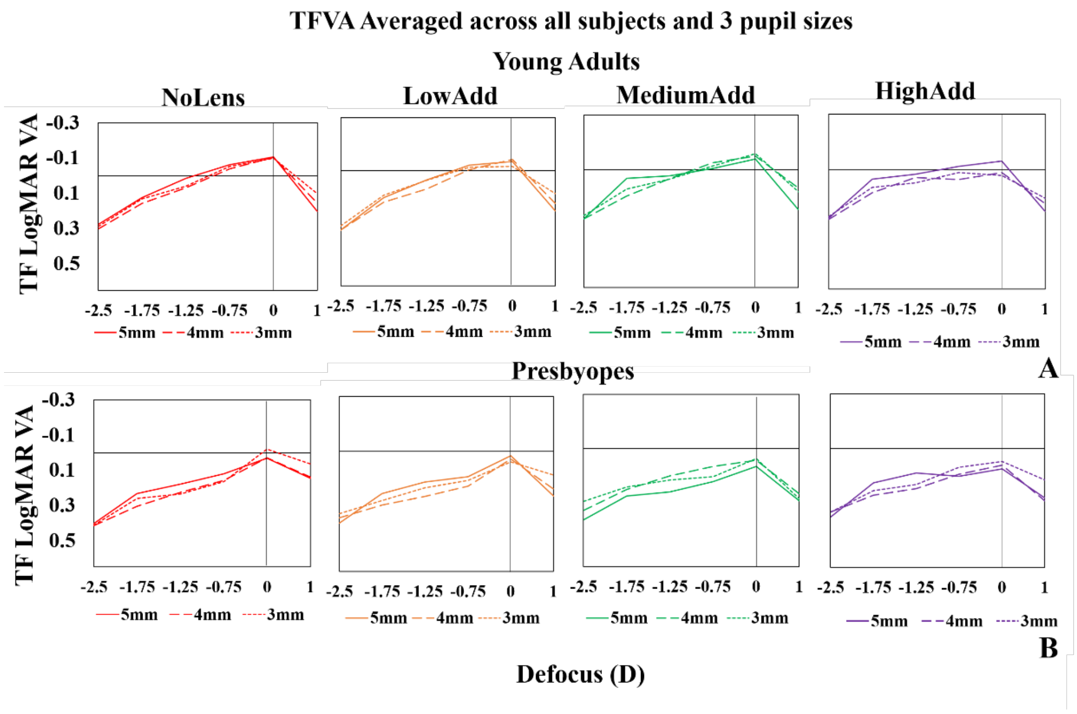

Fig 3.6: Average TF VA for pupils with sizes of 3, 4, and 5 mm while accommodating paralysis. Lens color indicates condition - NoLens in red, LowAdd in orange, MediumAdd in green, and HighAdd in purple. (A) young adults; (B) presbyopes.

In all cases, the partial correlation coefficients between the TFVA curves of the 5-mm pupil and the 3- and 4-mm pupil diameters varied from 0.464 to 0.797 and 0.548 to 0.806, respectively, and were statistically significant (p0.001). In presbyopes, DOF increased from 1D (3mm) to 1.5D (5mm) on average across all lenses in young adults, and from 1.5D (3mm) to 2D (5mm) in young adults (Partial correlation, p<0.001). For all lenses with the largest pupil, the TFVA curves in young adults had a propensity to be wider (by an average of 42.14%). However, in presbyopes, performance at the best focus was better with the 3-mm lens, and the broader curve was discovered with the 5-mm pupils. For the HighAdd lenses, performance at the best focus was better with the 3-mm lens, and the larger curve was found with the 5-mm pupils. Between 0.01 and 0.11 was the standard deviation for all participants.

3.3.6. Visual Acuity at far, intermediate and near

From the TF curve, we calculated the average impact of the multifocal lenses on VA at far (0D), moderate (1.5D), and close (2.5D) distances. The average visual acuity (VA) of young adults (A) and presbyopes (B) at those distances for all lenses (LowAdd: Orange; MediumAdd: Green; HighAdd: Purple; and NoLens: Red), both for paralyzed (solid bars) and natural (open bars) adaptation circumstances, is shown in Fig. 3.7.

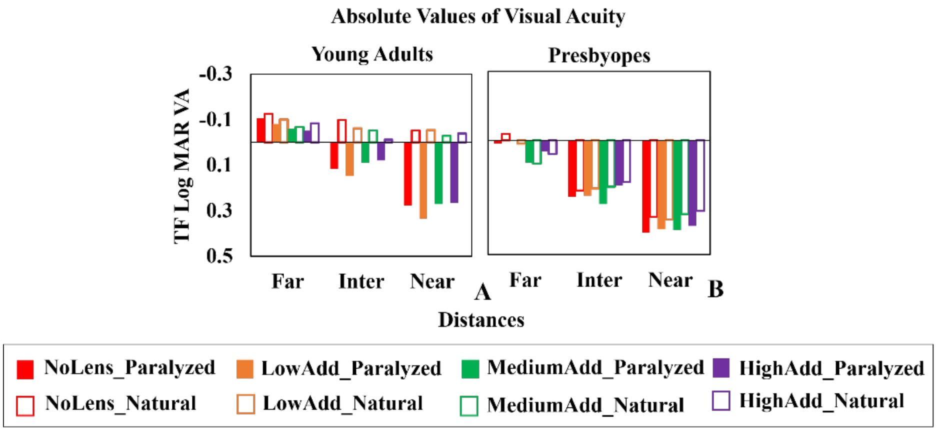

Fig 3.7. Average logMAR VA for far, intermediate, and close ranges for both paralyzed accommodation and natural accommodation (across participants). young adults, i.e. (B). presbyopes. Red indicates no lens, orange low addition, green medium addition, purple high addition, solid bars indicate paralyzed accommodation and open bars indicate natural accommodation.

In all situations at far, intermediate, and close distances for natural accommodation, VA was statistically substantially superior in young adults than in presbyopes (Mann-Whitney U test, NoLens p=0.0008; LowAdd p=0.008; MediumAdd p<0.001; HighAdd p=0.003). In terms of paralyzed accommodation, VA for far (Mann-Whitney U test, NoLens p=0.013; MediumAdd p=0.003 and HighAdd p=0.019); intermediate (Mann-Whitney U test, NoLens p=0.019; MediumAdd/HighAdd p0.001); and near (Mann-Whitney U test, NoLens p=0.028) was statistically better in young adults than in presbyopes.

Young adults, but not presbyopes, demonstrated statistically significant differences in VA values for all circumstances at intermediate (Wilcoxon signed rank test, p<0.013) and near (p<0.007) for paralyzed and natural accommodation. In young adults and presbyopic subjects, VA at intermediate and near was, on average across conditions (lenses and accommodation status), poorer than at far in all cases, with differences of -0.11 and -0.18 logMAR for intermediate and -0.20 and -0.32 logMAR at near respectively. Under natural accommodation, VA was consistently superior to 0 logMAR in young adults.

3.3.7. Visual Benefit at near and Visual Degradation at far

Fig 3.8 shows the visual degradation at far (Left panels, A and C) and the visual benefit at near (Right panels, B and D) for young adults (upper panels) and presbyopes (lower panels) produced by all lenses (LowAdd: Orange; MediumAdd: Green; HighAdd: Purple) relative to the NoLens, as a function of the lens near add. Positive values in the y-axis represent a gain and negative values represent a loss in visual performance produced by the lens. Lines represent linear regression fitting of the data, as a function of near add values (slopes are in logMAR/Diopter of near add; and r stands for correlation coefficients).

On average, the MCLs produced a small but consistent degradation of far vision with increasing add in both groups and conditions (s=-0.013 logMAR/D, r=0.98 in young adults; s=-0.03 logMAR/D, r=0.24 in presbyopes), and a consistent benefit at near in the young adults with paralyzed accommodation (s=0.06 logMAR/D, r=0.75), and in presbyopic subjects with both paralyzed (s=0.013 logMAR/D, r=0.58) and natural accommodation (s=0.029 logMAR/D, r=0.96).

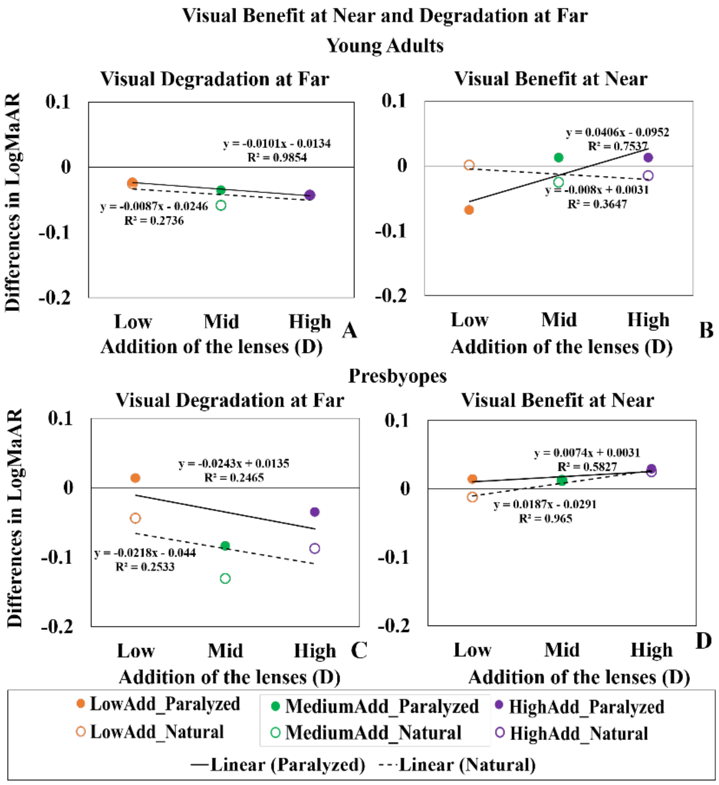

Fig 3.8: Visual Benefit and Visual Degradation at far. In young adults (upper panels) and presbyopes (lower panels), visual degradation at a far (A), and visual benefit at a near (B), are assessed as differences of logMAR VA with the MCLs and NoLens, averaged across participants. Orange indicates a low addition, green a medium addition, and purple a high addition, respectively, for lenses. The fill pattern indicates the accommodation condition (solid symbols: paralyzed accommodation; open symbols: natural accommodation). Regression lines are displayed as dashed lines in the case of natural accommodation and as solid black lines in the case of paralyzed.

3.3.8. Visual Imbalance

As a function of near add, the visual imbalance metric is depicted in Fig. 3.9 for young adults (Fig. 3.9 A) and presbyopes (Fig. 3.9 B), with averaged data for all lenses (NoLens: Red; LowAdd: Orange; MediumAdd: Green; HighAdd: Purple) across subjects and conditions. This metric accounts for variations in VA across the TF curve in all conditions (solid symbols: paralyzed accommodation; open symbols: natural accommodation).

Young adults and presbyopes showed statistically different visual imbalances with natural accommodation in all situations (Mann-Whitney U test, NoLens p=0.001, LowAdd p0.001, MediumAdd p0.001, and HighAdd p=0.003). Additionally, young adults in all situations showed statistically significant variations in the visual imbalance between paralyzed and natural accommodation (Wilcoxon signed rank test, NoLens p=0.005, LowAdd p=0.007, MediumAdd p=0.005 and HighAdd p=0.009), but not presbyopes.

Young adults with paralyzed accommodation (s=-0.06 D-1; r=0.65) and presbyopes with both paralyzed and natural accommodation (s=-0.01 D-1; r=0.88) had a reduction in visual imbalance on average with increasing add. Young individuals with natural accommodation had the lowest imbalance, yet even in this case, the visual imbalance was diminished by 13.33% with MCLs compared to the NoLens condition (averaged across the three near additions).

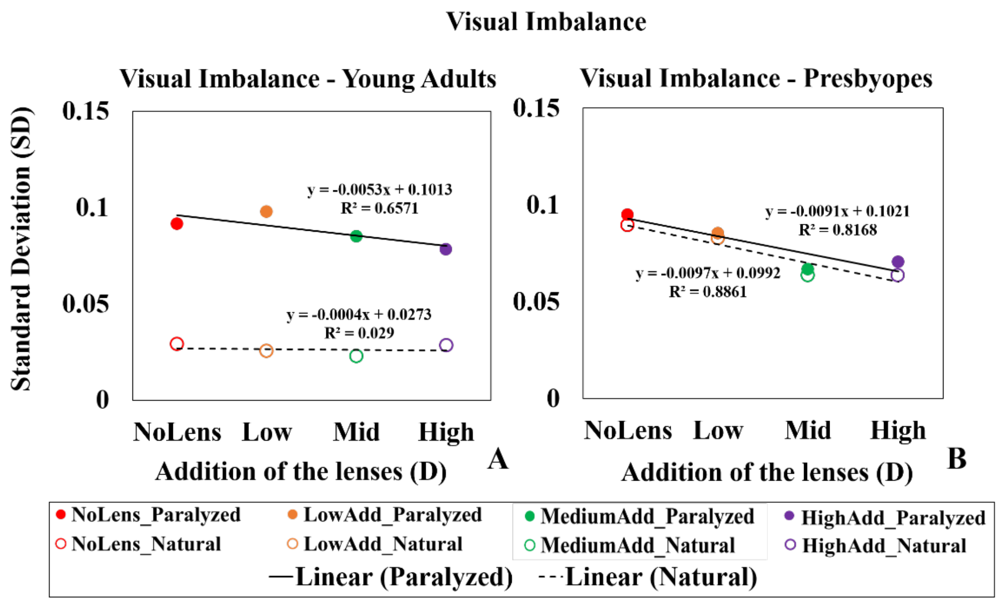

Fig 3.9: Visual imbalance along the VA curve. Young adults (A) and presbyopes (B) using various lenses and paralyzed (solid symbols) and naturally accommodating (open symbols) data are shown (averaged across all subjects). (Lens status is shown by color: Red: NoLens, Orange: LowAdd, Green: MediumAdd, and Purple: HighAdd.) Regression lines are represented by solid black lines for paralysis and dashed lines for natural accommodation.

3.3.9. Overall Visual Performance with MCLs

The visual degradation/benefit and visual imbalance measurements (normalized) from the preceding sections are combined to create this analysis. According to the specified metric, the lens performs better overall when the value is higher. The total visual quality was favorable in each instance, even though the metric might also have negative values. Young folks living in paralyzed accommodations displayed the best overall performance (LowAdd:0.36; MediumAdd:0.37; HighAdd:0.35). With LowAdd lenses, presbyopes' performance (under both natural and paralytic accommodation) was at its best (0.22). With paralyzed accommodation, the overall performance with MCLs was superior to the overall performance with natural accommodation (by 76.2% in young adults and by 17.7% in presbyopes).

3.4. Discussion

MCLs are well-known presbyopia treatments. The use of MCLs as a common method to arrest the progression of myopia makes it crucial to assess the visual performance of these lenses and determine the numerous factors that affect it. Some presbyopia MCL designs may be applicable in myopes, even if the state-of-the-art currently prioritizes center-distance designs to treat myopia, and particular lenses appear to target this market. Therefore, it is important to comprehend the basic variations in MCL function between presbyopic and young adult individuals.

Our study looked at a center-near multifocal lens design and assessed the impact of different near add levels (low, medium, and high) on visual acuity in two age groups (young adults and presbyopes with natural and paralyzed accommodation). All participants in the study wore the identical -2 D distance-corrected contact lens, regardless of their refraction, to decrease the number of variables. The remaining defocus was then corrected with a Badal system. The TF optical performance of the multifocal lenses was calculated in a prior study using the same MCLs (based on their theoretical power profile), and this information was used as the basis for simulations of the lenses in a Simultaneous Vision Simulator (193,194,254) and a Spatial Light Modulator in an Adaptative Optics system(203) The TFVA of subjects who were presbyopic was measured using the MCLs on the eye and the comparable SimVis simulated lenses. In line with a previous study, we discovered that MCLs reduced far visual acuity when compared to a monofocal condition (NoLens). This is to be expected because simultaneous vision corrections split the energy into two foci, where a blurred image is always superimposed atop a sharp component. Overall, we observed a significant intersubject variability with paralyzed accommodation (Fig. 3.3) and intra-subject variances that varied with lens design, paralyzed or normal accommodation (only in young adults), and to a lesser extent, pupil diameter (Fig 3.6). Due to the fact that visual acuity decreases with age, presbyopes had maximum visual acuity (usually far vision with NoLens) than young adults did.

The near add magnitude is a critical factor in multifocal lenses. All subjects were put through three MCL addition tests (Low: +1.25D; Medium: +1.75D; High: +2.50D). Lower additions are prescribed to early presbyopes and higher additions to older presbyopes in clinical practice with presbyopes because the choice of addition is related to the remaining accommodation amplitude. A wide variety of adding capabilities are considered suitable for prescription MCLs to progressive myopes.

Based on earlier research, where we employed simultaneous vision simulators to examine how near addition to pure simultaneous vision visual acuity affected performance (136,164,165,194) in patients with paralyzed accommodation, we found that far vision was not equally degraded with all near add magnitudes. A difference that could be solely explained on optical grounds, additions about +2.50D created a bigger degradation than additions lower and higher. Testing lenses with enhancements greater than +2.50 D was not possible for the current investigation. In any case, the average increase in far visual degradation with near add observed in the current investigation, both in young adults and presbyopes, is consistent with that earlier finding, i.e., with HighAdd the degradation at far was larger than the Low and Medium additions.

Clinical trials conducted in the past on young adults wearing MCLs have revealed varying degrees of visual impairment. Fedtke et al(238) found that bifocal lenses reduced visual acuity when compared to single vision lenses, though the reduction was less noticeable when using MCLs with negative spherical aberration (center-near design). On the other hand, Shah et al(249) found relatively higher high contrast visual acuities with concentric lenses and with center-distance, exceeding the visual acuities reported by Anstice & Philips, Walline et al, and Fedtke et al(173). With center-near MCLs with HighAdd, Fedke et al. recorded a high contrast visual acuity of 0.10 0.12 logMAR, whereas the center-near LowAdd achieved the best overall visual acuity, up to -0.05 0.11 logMAR. Additionally, we found that performance with LowAdd lenses performed more similarly to the NoLens condition than with higher add MCLs. In any event, we did not find that the center-near MCLs significantly worsened single vision, so it does not seem appropriate to not use MCLs based on the possibility that they perform worse than center-distance MCLs, as recommended in previous work (256). Furthermore, while differences in pupil diameter between young and presbyopic subjects have frequently been cited as potential reasons for the different performance of center-near add MCLs in both groups, our results show only minor variations in TF performance with pupil diameter, indicating that pupil diameter only has a minor impact on their performance.

The TF-related young adults and presbyopes (as well as presbyopes with natural accommodation) display identical visual performance with paralyzed accommodation, with consistent performances with increasing near add, suggesting that the lens designs take precedence over other considerations. The curves in the same patients expand with natural accommodation, demonstrating that accommodation affects the MCL performance in young adults in addition to lens design. In order to focus on the near aiming lower accommodating demand, the near peak of accommodation could be adjusted to achieve this. The defocused image of the near focus is always out of focus, suggesting that young adults accommodate the entire range utilizing the far peak (by different amounts). In this situation, a center-near and the spherical aberration's natural change in combination with accommodation may help to reduce accommodative latency and enhance performance at close range. Most of the subjects in our study wearing Medium and HighAdd lenses (Fig. 3.4) seemed to employ the far peak to account for the full tested near vision range. Only two participants (S#3, S#10) seemed unable to handle the entire range.

Our findings demonstrate that MCLs create more consistent vision across distances. The high level of acceptability of MCLs, when prescribed to myopes, may be explained by the hypothesis that a higher visual constancy is a preferred scenario over overall better (but also less uniform) vision, as achieved in young adults with natural vision. The success of multifocal lenses in controlling myopia should be taken into consideration when choosing them for myopes, although great near and distant vision cannot be compromised. The best lens design can be chosen based on performance using the overall visual quality metric, which also considers other factors including visual consistency. The application of new Simultaneous Vision Simulators would permit non-invasive testing of a variety of designs without placing them on the eye (193,194,202). It is advised to give patients (both young and presbyopic) experience with multifocality prior to fitting due to the relatively high intersubject variability.

In conclusion, the current study shows that center-near lenses have some visual benefits at close range in presbyopes and young adults with high contrast visual acuity while retaining far vision. When treating myopia and presbyopia using MCLs and learning more about how these lenses work, factors including visual impairment at a distance, visual benefit up close, and visual consistency (uniformity of vision across distances) should be considered. Future research on the visual quality of MCLs may examine contrast sensitivity and the Multifocal Acceptance Score metric, which employs natural sceneries for far/near and day/night lighting to gauge perceptual quality with non-high contrast images (257,258).

3.5. Conclusions

- For all conditions, VA was generally superior in the young adult group compared to the presbyopic group (NoLens and MCLs)
- In young adults, the shape of the TFVA curve was significantly different between paralyzed and natural accommodation conditions. In contrast, presbyopes did not show significant differences between paralyzed and natural accommodation, as expected due to lack of accommodation in the older group.
- In comparison to the NoLens, the MCLs reduced the visual imbalance (variations of VA consistency from far to near). The result is consistent with an increase in the negative spherical aberration with center-near design, which has a favorable effect in decreasing accommodative lag.
- The MCLs produced a small but consistent degradation at far in all conditions, and a consistent benefit at near in young subjects with paralyzed accommodation and in presbyopic subjects with both paralyzed and natural accommodation. Visual degradation at far increases with more addition in the lenses.

- Under paralyzed accommodation, both in presbyopes and young adults, the depth of focus of the TF curve increased with increasing pupil diameter (3mm to 5mm).

In this chapter, we have studied the visual performance with real multifocal lenses of three different additions in young adults and presbyopes, and compared across the subject groups, with and without accommodation and different addition of the lenses. In the next chapter, we will study the ability of the Spatial Light Modulator to simulate these designs of multifocal contact lenses and compare the visual performance of the simulated vs real contact lenses in the eye.

CHAPTER-4. VISION WITH SPATIAL LIGHT MODULATOR SIMULATING MULTIFOCAL CONTACT LENSES IN AN ADAPTIVE OPTICS SYSTEM

As multifocal contact lenses (MCLs) expand as a solution for myopia though traditionally used in the treatment of presbyopia experiencing multifocal vision before physically fitting them on the eye becomes critical both to systematically test different multifocal designs and to optimize selection specific to each subject in the clinic. In this chapter, we evaluated the ability of a Spatial Light Modulator (SLM) to represent MCLs by comparing through-focus visual acuity with real CLs on the eye and simulated MCLs in the SLM.

This chapter is reproducing the paper by **Vedhakrishnan et al**(203). "Vision with Spatial Light Modulator simulating multifocal contact lenses in an adaptive optics system", published in BOEx (2021). The co-authors are Maria Vinas, Sara Aissati, and Susana Marcos.

The work was presented as an oral presentation by Vedhakrishnan et al in the PhD day event conducted at the Complutense University, Madrid, under the title "Comparison of vision with real and simulated MCLs in Spatial Light Modulator".

The author of this thesis designed the experiment, implemented the experimental protocol, performed the experimental measurements on subjects, collected and analyzed the data, and prepared the manuscript in collaboration with Maria Vinas and Susana Marcos.

4.1. Introduction

Presbyopia, an age-related eye disorder in which the crystalline lens loses its capacity to dynamically focus, can be corrected by multifocal contact lenses (MCLs) (259). In addition, MCLs have shown promising results in controlling myopia progression(133,172,255). MCLs operate on the simultaneous vision theory, which entails the simultaneous projection of both a far- and a near-focused image. For presbyopes, center-near, center-distance, and concentric alternating-zone types of MCLs are available on the market. Presbyopes gain intermediate/near vision at the expense of some optical degradation at far (143,249,259,260). It is unclear how MCLs slow down eye growth in myopes, however, they may do so via lowering peripheral hyperopic defocus or by lowering accommodative lag (93,130). The MCLs that are typically utilized to halt the growth of myopia are center-distance or alternate center-near and distance zones (104).

In a recent study by our group (236), In two age groups (young myopes and presbyopes), we investigated the visual performance with center-near MCLs on the eye in the presence and absence of accommodation. We discovered that accommodating young myopic subjects generally compensate for the multifocal visual performance compromise at far vision (236).

There are more and more commercially available MCL designs, and the main difference among them is their power profile. While some designs have aspheric smooth surfaces that try to increase the eye's depth of focus rather than establishing two distinct foci, others have quite abrupt transitions between near and distance. The locations and quantity of pupillary zones allocated for far and near also vary between designs (143,259). The effectiveness of the MCLs with regard to visual performance in various populations, the impact of added near magnitude, and other design factors have been the focus of some studies (116,261,262) or the effect of the eyes aberrations and pupil diameter (263). Due to the intricate nature of the experimental techniques, which demanded the testing of numerous MCLs on the same patient, the scope of those research was, however, constrained.

The Simultaneous Vision Simulator- Sim + Vis technology, often known as SimVis, is an alternative to spatial visual simulators. SimVis is a small device with a wide field of view that operates on the idea of temporal multiplexing with an optotunable lens driven at high speed (193,254,264,265). Based on that technology, the wearable, binocular, and see-through SimVis Gekko system (2EyesVision, Madrid, Spain) was developed for commercial use. To our knowledge, only the SimVis visual simulator has been reported to accurately imitate MCLs that are now available on the market (193). In that study, a channel in the Polychromatic AO visual simulator from VioBioLab was used to implement the Sim + Vis Technology. High-contrast visual acuity targets were used in the investigation, which was conducted for fixed pupil diameter (4 mm). The average TF visual acuity with the real MCL on the eye was nearly matched by simulations, showing that the SimVis effectively reflects the power profile of the MCL (193). Despite the positive outcomes of that work, additional research is required to fully understand the phase map representation and the possibility of visual simulators representing MCLs. The phase map representation of the MCL, along with additional compensations for dynamic effects in the optotunable lens, serves as the foundation for the temporal patterns that drive the SimVis temporal multiplexing simulators (193,265). The representation of MCLs in terms of phase mapping involves several implicit assumptions, some of which may include potential differences between the theoretical and actual power profiles, conformity of the MCL to the underlying cornea, decentration of the lens, and shift between the corneal and pupil plane.

Using an SLM (PLUTO-VIS; Holoeye Photonics AG, Germany) in an AO visual simulator, we investigated the accuracy of a phase map representation of a commercially available MCL design in this work for the first time to our knowledge. This method retained the natural interactions between the aberrations of the lens designs and the aberrations of the subject. We specifically assessed TF visual performance (TF visual acuity) in the same participants with real MCLs on the eye and the identical designs (center-near aspheric MCLs of three different addition magnitudes (low/medium/high) simulated in an AO visual simulator. The ability of the SLM to imitate the MCLs were evaluated by comparing the real and simulated TF curves. In an earlier study (193) We simulated the multifocal lenses of various additions using the SimVis visual simulator. As the basis for several laboratory-based visual simulators and, to our knowledge, one commercial visual simulator, we are using an SLM in the current investigation. The work thus supports the use of phase map representations of MCLs, which are also utilized as a first step in other types of simulators like SimVis, as well as the usage of SLM-based simulators to mimic MCLs (at least with monochromatic stimuli).

4.2 Methods

The three simulated MCLs' TF optical performance was evaluated on a bench. Under cycloplegia and a fixed pupil diameter of 5 mm, through-focus visual acuity (TFVA) was assessed with both simulated and real MCLs placed in the eye. We chose 5-mm pupils because this size ensures that the retinal image was influenced by both near and far vision. Three MCL additions were used to measure all patients (low, medium , and high).

4.2.1. Subjects

The study included a total of 7 participants, whose ages ranged from 24 to 55, had spherical errors between -4.00D and -1.50D, and had astigmatism less than 0.75D. The profiles of each patient are displayed in Table 4. Except for S6 and S7, every subject regularly wore contact lenses. Prior to beginning the measurements with each MCL, a contact lens settling period of 10 to 15 minutes was given to all subjects to ensure proper fitting and comfort. The study protocols received approval from the CSIC Institutional Review Boards and adhered to the principles of the Declaration of Helsinki. Prior to any study procedures, informed consent waivers were signed by all participants after they received information about the study and its experimental methods. The IRB assigned project reference number is 080/2016.

Subject	Age (yrs)	Measured eye	Spherical error (D)	Astigmatism (D)	Astigmatism axis (deg)
S1	24	OD	-4	-	-
S2	27	OD	0	-	-
S3	27	OD	-4.5	-	-
S4	28	OD	-1.5	-	-
S5	31	OD	-1.75	-0.5	90
S6	48	OD	1.5	-	-
S7	55	OD	0	-	-

Table 4. Shows the individual refractive profile of the two groups of subjects (Young myopes and Presbyopes): ID, age, Eye measured, Spherical error, Astigmatism , and Astigmatism axis

4.2.2. Multifocal contact lenses

The MCLs used in this investigation were soft, daily disposable, with a center-near aspheric profile (higher plus power is in the center and gradually reduces towards the periphery), the base curve of 8.4 mm , and diameter of 14.3 mm, and were made of etafilcon A with a 58% water content (193,266). Three different additions (low, medium, and high) of center-near MCLs were examined in this study.

All patients wore -2 D for far (with the residual refractive error corrected using the Badal Optometer) and with three different additions: Low (+1.25D), Medium (+1.75D), and High (+2.5D). This eliminated any potential differences in MCL performance related to lens base power (i.e., lens thickness and central near zone diameter).

4.2.3. Adaptive optics visual simulator

Measurements were made in the VIOBIO lab's polychromatic multichannel AO visual simulator system, which are thoroughly discussed in prior publications (136,195,198) and section 2.1.2 of this thesis. The Spatial Light Modulator was used to see the visual stimuli for the study's purposes. A 5-mm artificial pupil was positioned in a conjugate pupil plane to ensure the measurements were conducted with the right pupil diameter.

4.2.4. SLM phase map generation

The phase map created for the SLM using the three MCLs is shown in Figure 4.1. In order to numerically simulate the designs, MATLAB procedures were employed. The designs were afterward programmed in a reflective phase-only LCoS-SLM using the same protocols as Vinas et al. (2017)(194). To obtain a maximum phase difference of 2, as specified by the SLM's calibration, a wrapping process (188) was used on the phase patterns. The resultant pattern is a greyscale image, with each shade of grey denoting a specific phase difference between 0 and 2. At the conjugated pupil plane, where the SLM was positioned, images were produced for a 5-mm pupil. The SLM was calibrated for a wavelength of 555 nm using the methods recommended by the manufacturer. The MCL phase maps have a distance power of 0D.

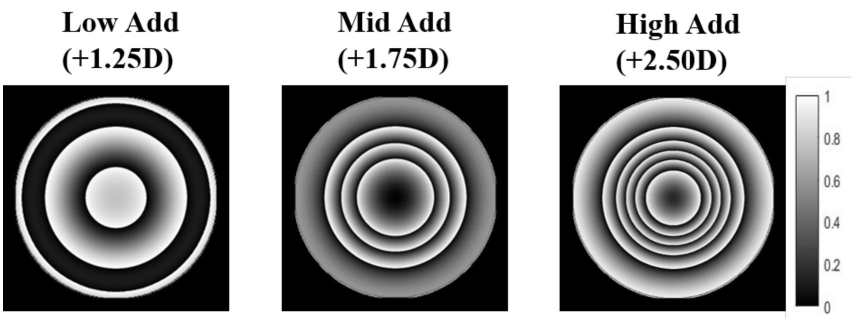

Fig.4.1. Phase maps of the MCLs simulated in the SLM for LowAdd (+1.25DS), MediumAdd (+1.75DS) , and HighAdd (+2.50DS). Pupil diameter = 5mm.

4.2.5. On-bench through-focus optical quality

TF optical quality through the SLM simulated MCLs was tested on a bench using 1-pass TF images of an E-letter (0.86 logMAR, 29arc min) optotype displayed in the DMD imaged on an artificial eye made up of a 50-mm focal length achromat and a CMOS sensor acting as a "retina" (DCC1240C - High-Sensitivity USB 2.0 CMOS Camera, 1280 ×1024, Global Shutter, Color Sensor, Thorlabs GmbH, Germany), as described earlier (194). 555 nm light from the SCLS was used to illuminate the stimuli (similar to the measurements in patients). The Badal optometer was moved from +1D to -4.5D in 0.25 steps for all measurements to achieve focus changes.

4.2.6. Experimental procedure in subjects

Measurements were performed on subjects when they were being cycloplegic with 1% Tropicamide, monocularly (using their dominant eye, as determined by the Miles test), and without correcting for any of their intrinsic aberrations in a dimly lit setting (20 cd/m2) (2 drops prior to the experiment, and repeated every hour). The study started after 20 minutes of cycloplegia. The eye that wasn't being measured was covered with a patch throughout the experiment. To align the patient with the system, the instrument's optical axis was placed in the center of the subject's pupil, which was visible in the pupil monitoring channel. After settling into a centering position, the subject was told to move the Badal system in order to achieve the best focus for far vision by utilizing a Maltese cross. When compared to their projected best focus, the subject was told to start with positive defocus values. After several focus settings were made, the zero-defocus setting was determined to be the average of at least five focus settings. This procedure was applied repeatedly for each of the analyzed conditions (LowAdd/MediumAdd/HighAdd and NoLens) utilizing both real and simulated MCLs.

Seven different conditions were divided over two sessions to test TFVA (see Section 2.7). Session 1: NoLens (control), LowAdd Real MCL, MediumAdd Real MCL, HighAdd Real MCL, and Session 2: NoLens (control), LowAdd SLM simulation, MediumAdd SLM simulation, and HighAdd SLM simulation. Every time an MCL was placed on the eye, a settling period of 10 to 15 minutes was given. At the beginning of each condition, the MCLs' fitment and centration were verified in the slit lamp. Sessions 1 and 2 lasted between 3 and 4.5 hours, respectively. Two separate days were used for each session.

4.2.7. Through-focus visual acuity (TFVA)

Using a Badal optometer, VA was assessed for a fixed defocus range of -3D to +1D in 0.5 steps. VA was calculated using an 8-Alternative Forced Choice (8AFC) (252) technique using Tumbling E letters (Black E-letter on a Green Background at 555 nm shown on the DMD display) and QUEST (Quick Estimation by Sequential Testing) algorithm programmed with the Psych toolbox software (228,229,267) to determine the order in which the test's provided stimuli—letter size and orientation—will be presented after the subject's response. The orientation of the E-letter had to be determined by the subjects, and a quaternion estimate technique was used to adjust the stimulus size in the subsequent presentation by following the subjects' responses. Each VA measurement was subjected to 35 trials of the QUEST routine, with a 75% threshold criterion. The average of the previous 10 stimulus values was used to estimate the threshold VA measurement. VA was calculated using the formula logMAR = -log10 [decimal acuity] (253).

4.2.8. Data analysis

Image quality was measured for the on-bench optical quality experiment (TF E-letter imaged in the artificial eye) as the image correlation coefficient between the E-letter obtained for a particular condition (MCL and all focus points) and the image of the E-letter with NoLens (monofocal at best focus). A comparison of the real and SLM simulated MCLs' TFVA curves for patient measurements was done. (1) The Shapiro-Wilk normality test was conducted between the two groups (real MCLs & simulated MCLs) (2) Non-parametric tests were conducted to compare specific conditions between the actual and simulated MCLs. (3) Intraclass correlation coefficients were calculated to examine the association between SLM and actual MCLs. (4) Shape similarity of the TF curves as determined by the cross-correlation of the SLM and actual MCL TFVA curves. To examine any differences between the outcomes of the SLM simulated and real MCLs, statistical analysis was carried out using SPSS software Statistics 24.0 (IBM, United States). Additionally, two analyses were carried out: (1) RMS difference of the linearly interpolated TF curves (SLM vs real MCLs), in a 4-D range; and (2) Bland-Altman analysis (SLM vs real MCLs).

4.3. Results

4.3.1. Through-focus optical performance (on-bench) of the simulated MCLs

For the three MCLs simulated in the SLM (Low, Medium, and HighAdd), with defocus varying from -4.5 to +1 D, Figure 4.2 A displays TF raw images of an E-letter stimulus projected in the artificial eye for each MCL. Qualitatively, the series of images show that the depth of focus increases with increasing additions. The calculated TF optical quality measure (image correlation) from those photos is displayed in Figure 4.2 B. For LowAdd, MediumAdd, and HighAdd MCLs, respectively, the highest picture quality correlation at the best focus was 0.99, 0.93, and 0.87. For LowAdd, MediumAdd, and HighAdd MCLs, respectively, the image quality decreased by 28.9%, 18.4%, and 6.4% at -0.25 D from the best focus. With increased near addition, the best-focus peak shifts negatively, along with a minor decline in image quality at best focus and curve broadening.

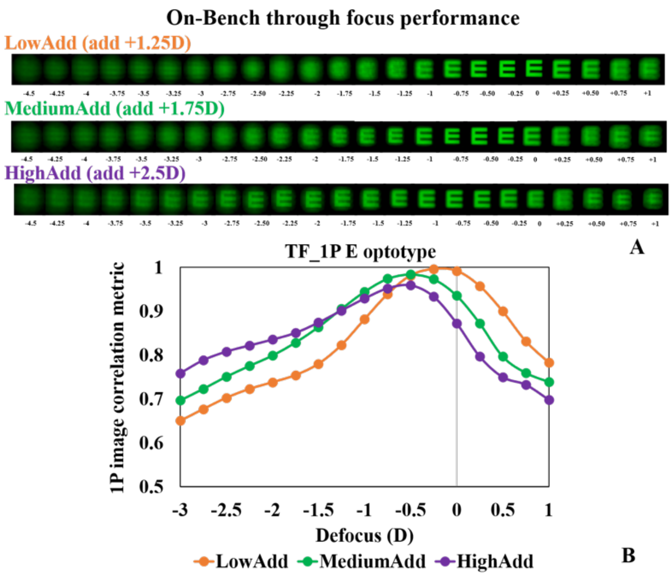

Fig.4.2. TF optical performance on the bench (A) On bench TF one-pass (1P) image series of an E-letter through the SLM simulated MCLs (LowAdd: Upper panel; MediumAdd: Middle panel; HighAdd: Lower panel). (B) TF image correlation metric for the three SLM simulated MCLs (LowAdd: Orange; MediumAdd: Green; HighAdd: Purple).

4.3.2. Through-focus visual performance real and simulated MCLs–individual data

For all three adds (LowAdd, first column, orange; MediumAdd, second column, green; HighAdd, third column, purple), all subjects, and when assessed with a fixed pupil diameter, Figure 4.3 displays the TF logMAR VA with the simulated (dashed lines) and real MCLs (solid lines) (5 mm). Real and simulated MCLs at each focal position are contrasted using black bars.

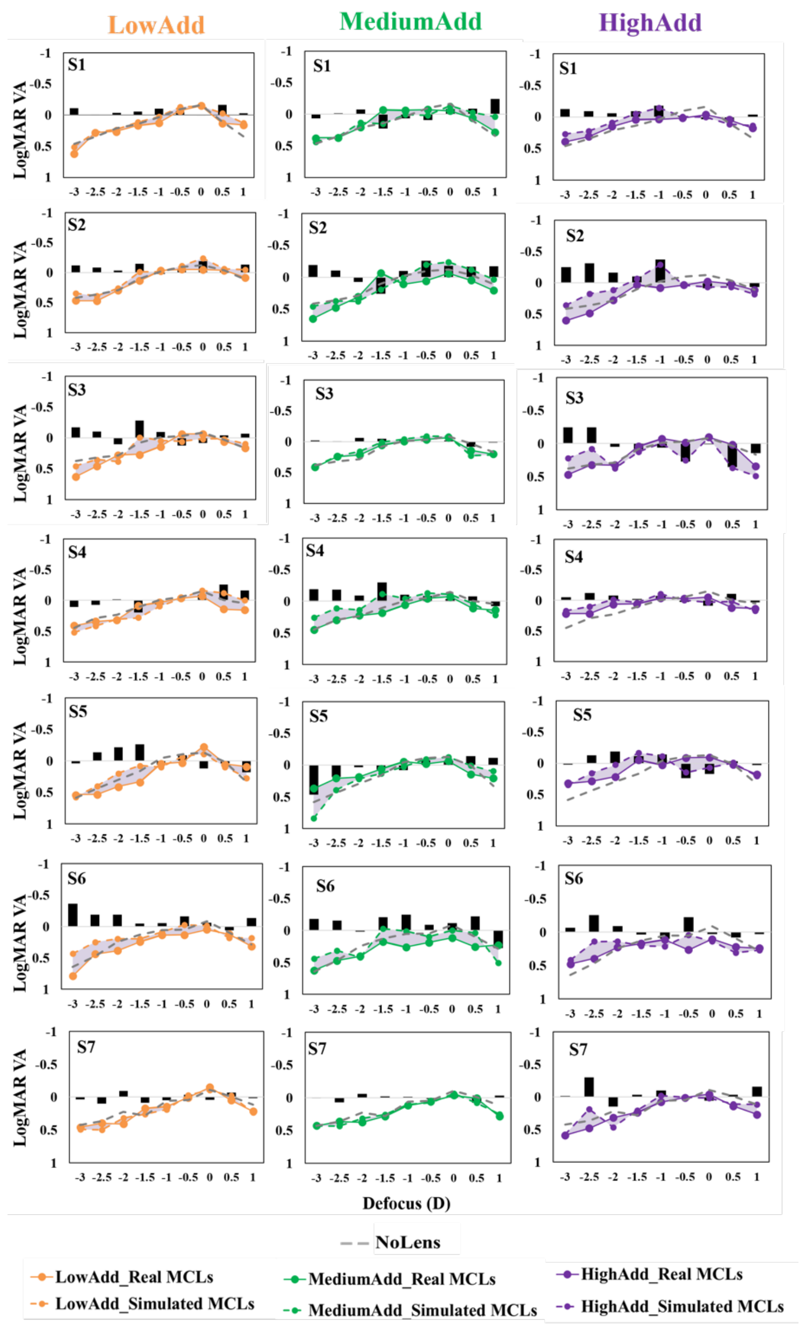

Fig.4.3. TFVA with both simulated (dashed lines) and real MCLs (solid lines). The subjects are displayed in distinct rows. There are a distinct MCLs addition in each column (LowAdd – first column, orange; MediumAdd – second column, green; HighAdd – third column, purple). The control condition with no lens (monofocal) is shown by the grey lines. The difference between the simulated and real curves is shown by the black bars. Data are for paralyzed accommodation and 5-mm pupil diameters.

For LowAdd, MediumAdd, and HighAdd MCLs, respectively, there is an average magnitude difference of -0.01, -0.07, and 0.06 logMAR units between real and simulated MCLs at best focus. In terms of individual MCLs, the median differences between real and simulated MCLs are, for LowAdd, MediumAdd, and HighAdd, respectively, -0.048 with 95% CI [-0.078, -0.017], -0.049 with 95% CI [-0.080, -0.014], and -0.033 with 95% CI [-0.069, 0.000]. The average Simulated-Real difference (with sign) was negative (-0.04 ± 0.01, -0.03 ± 0.01, and -0.03 ± 0.04, for LowAdd, MediumAdd, and HighAdd

MCLs, respectively), showing that the simulated MCLs performed on average a little bit better than the real MCLs.

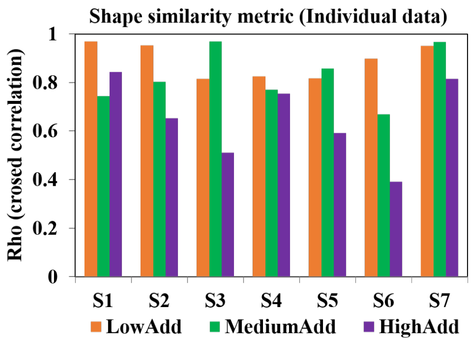

Fig.4.4. Shape similarity metric displaying unique data for each subject for each of the three conditions (cross-correlation of the TFVA curves with real MCLs on eye and simulated MCLs) (LowAdd: orange; MediumAdd: green; HighAdd: purple).

For all subjects, Figure 4.4 displays the shape similarity measure (rho) comparing the actual MCLs on the eye with the simulated MCLs imprinted on the SLM. The average shape similarity metric for LowAdd, MediumAdd, and HighAdd MCLs was k=0, rho = 0.889 0.03, k=0, rho=0.825 0.05, and k=0, rho=0.651 0.08 (average rho across individual subjects), respectively. This shows a high degree of correspondence between real and simulated MCLs, not only in terms of VA magnitudes but also With HighAdd MCLs, only two patients (S3 and S6) displayed rho values below 0.5.

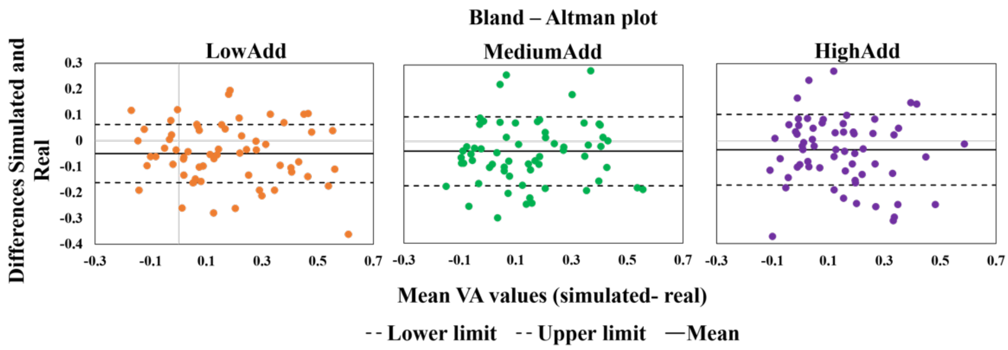

Fig.4.5. Bland-Altman figure for VA comparing real and simulated MCLs, with the three MCLs (LowAdd: orange; MediumAdd: green; and HighAdd: purple) showing data for individual participants throughout the entire focus range (-3D to 1D). Two standard deviations apart from the mean are represented by vertical dashed lines.

Figure 4.5 compares the VA measured with real and simulated MCLs using Bland-Altman plots for all individuals and defocus settings for each MCL (LowAdd: orange; MediumAdd: green; HighAdd: purple). Two standard deviations are represented by dashed lines. As a function of mean VA values, there is no trend for differences between real and simulated MCLs. For LowAdd, MediumAdd, and HighAdd, the average intraclass correlation coefficients were 0.905 with a 95% confidence interval of [0.818,0.947], 0.853 with a 95% confidence interval of [0.754,0.912], and 0.792 with a 95% confidence interval of [0.655, 0.874].

4.3.3 Averaged TFVA

Figure 4.6 displays TFVA curves for all additions averaged across subjects (LowAdd, orange; MediumAdd, green; HighAdd, purple; NoLens, grey). Solid lines represent actual MCLs on the eye, whereas dashed lines represent simulated MCLs. For Low, Medium, and High additions, respectively, the average RMS difference between real and SLM simulated MCLs in the TFVA curves was 0.016 ± 0.004, 0.013 ± 0.004 and 0.025 ± 0.009, respectively.

The Bland-Altman plot of the averaged VA data across subjects for various MCL conditions is shown in Figure 4.7. Given that each letter has a value of 0.02 log units, the confidence intervals for the Low and MediumAdd were ±0.01 logMAR, while those for the HighAdd were ±0.06 logMAR (difference of 3 letters), indicating VA differences of less than one letter. For LowAdd, MediumAdd, and HighAdd, the average bias was -0.049, -0.039, and -0.035 logMAR, respectively. Additionally, for all additions, there was a highly significant shape similarity between the actual MCLs on the eye and the simulated MCLs (Crossed correlation: LowAdd: k=0. Rho=0.995; MediumAdd: k=0; HighAdd: k=0; averaged across all subjects).

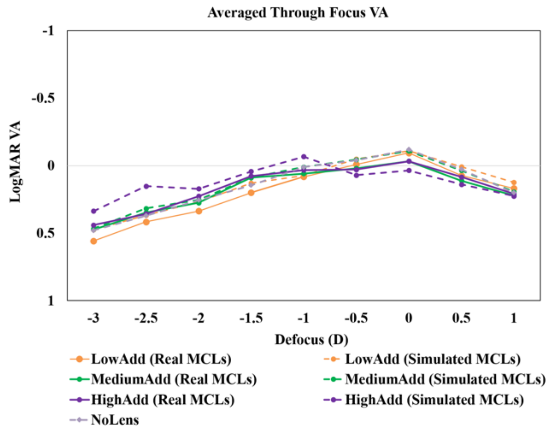

Fig.4.6. By focusing on VA and averaging all subjects (LowAdd, orange; MediumAdd, green; HighAdd, purple). Measurements with real MCLs on the eye correspond to solid lines; measurements with simulated MCLs on the SLM correspond to dashed lines; the grey line denotes the NoLens (monofocal) control condition.

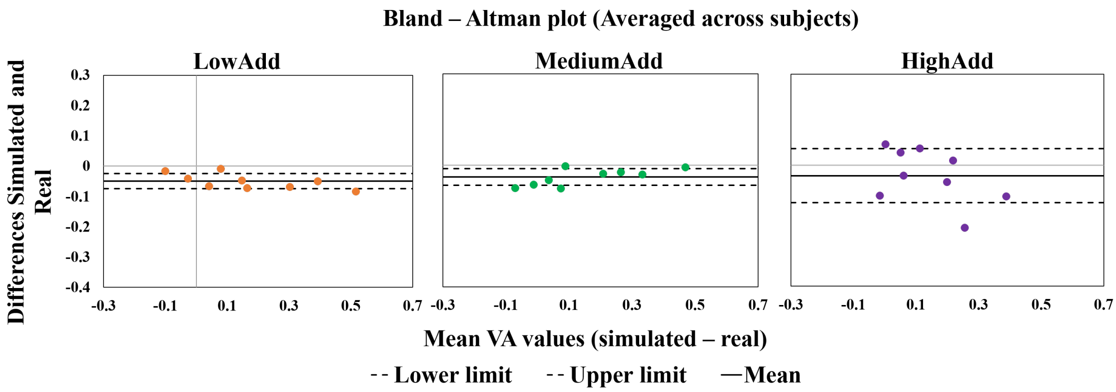

Fig.4.7. Comparing genuine and synthetic MCLs, the Bland-Altman plot of VA for the three MCLs (LowAdd: orange; MediumAdd: green; HighAdd: purple) averaged across individuals. Plotting is done for a standard deviation of ±2 from the mean.

4.4 Discussion

MCLs have shown to be an effective therapeutic option for slowing or stopping the progression of myopia, and they are increasingly being used as a therapy for managing presbyopia. Visual simulation is an effective method for quickly comparing different MCL design parameters on the same patient and isolating features that are only linked to design, as opposed to MCL fitting or wearability. In several papers in the literature, AO visual simulators are used to test both commercial intraocular lenses and experimental lens designs to imitate visual performance with multifocal designs (188,194,201). In a previous study, we looked into the temporal multiplexing principle-based simultaneous vision simulator (SimVisability)'s to represent MCLs. In this work, we compared vision in the same subjects using real MCLs on the eye and a simulation of the MCLs in an SLM of a lab AO device. Since this is a common assumption in all simulators and an intermediary stage in SimVis simulations, it is crucial to compare performance with the real MCL to the spatial phase representation of an MCL (derived from the MCL power map).

Three various additions (low, medium, and high) center-near MCLs were examined in this study. By allowing all patients to wear -2 D for far distance, any potential disparities in MCL performance related to lens base power (i.e., lens thickness and central-near zone width) were avoided. Additionally, measurements were carried out with a fixed pupil diameter and during cycloplegic to prevent the effects of accommodation. For the SLM-simulated MCL on the bench, the effect of the tested MCLs to expand depth-of-focus with increasing near addition was shown with both the real MCLs and the SLM-simulation of the MCLs (TFVA curves, Figs. 4.3 and 4.6). (1-P correlation metric in Fig. 4.2). These findings relate favourably to earlier literature. The average VA values obtained in this investigation are comparable to those discovered in earlier studies that made use of the same MCLs, paralyzed accommodation, and similar pupil diameters (4-5 mm). The VA was reported to be 0.31 logMAR at near, 0.13 logMAR at intermediate, and -0.06 logMAR at far in a prior study using SimVis simulated lenses (193). The VA was 0.37 logMAR at near, 0.12 logMAR at intermediate, and -0.05 logMAR at far, according to a study evaluating the real MCLs' (236) performance on the eye. These values are within the scope of our report, which includes both real and SLM-simulated MCLs. For SLM against real MCL at 40 cm & 67 cm for Near and Intermediate distances, 0.27 vs 0.37 logMAR at Near, 0.09 vs 0.12 logMAR at Intermediate, and -0.06 vs -0.05 logMAR at Far. In general, VA at intermediate and near distances are better in free accommodation (subjects with low and medium additions typically have some residual accommodation). Similar to earlier research, variations in ocular aberration patterns between people (and their interactions with the lens optics) as well as neural factors must be the cause of performance variances with the same MCL across subjects. The differences between the TFVA and the real MCLs and the SLM simulated MCLs are, on average, within -0.04 logMAR. In general, the shape similarity measure (indicating the relative TF performance) between simulated and real MCLs is high. Interestingly, there is a modest bias towards greater performance (17% to 22.2%) with the SLM simulation than with the actual MCL, despite the average TF differences being below statistical significance. Individually, several participants or situations (e.g., S1, all MCLs, S3 MediumAdd lenses, and S5, all MCLs) showed almost complete agreement between simulation and real MCL. At different defocus settings in each subject and addition power, respectively, a great degree of similarity between the real and simulated lenses was found. Other times, the simulated MCL outperforms the real MCL practically everywhere (S4). Most significantly, however, variations above 0.1 logMAR are restricted to a small number of isolated defocus conditions, mostly with HighAdd MCLs. We hypothesize that these inconsistencies may potentially result from MCL degradations or tear film disruption, motion-related effects during blinking that are present with real MCLs on the eye but absent from the simulations in the SLM, and other factors that may be attributable to the tear lenses. Because disparities with HighAdd MCL tend to be higher, the effect of MCL decentration seems to be the most likely cause. Our research shows that the SLM simulator can successfully simulate multifocal vision in rotationally symmetric center-near MCLs, simulating the visual experience at far, intermediate, and near distances offered by real MCLs. The SLM was used with an AO system, a fixed pupil diameter, and monochromatic stimuli for this work, which was carried out in an experimental set up. Even though it has been demonstrated that the SLM accurately depicts the phase maps describing the MCL optics, there are still a number of issues: As the phase map is precisely mapped on the SLM for a single wavelength, there may be (1) possible chromatic artifacts. As we matched the illuminating wavelength to the phase map calculations, these artifacts were not present in the current study, but they may be a problem with polychromatic targets (268) (2) the reflective nature of the SLM limits the ability to create a very compact simulator , and (3) the small field of view (2 deg) is not a problem in visual acuity testing, but it restricts the ability to represent real-world scenes. These limitations do not apply to SimVis simulators based on the temporal multiplexing principle. However, they vitally depend on a phase map that accurately depicts the MCLs.

According to the most recent research, the implicit presumptions used to depict the MCL as a phase map are often true. In a previous study (193) In SimVis, we compared TFVA with actual MCLs and MCL simulations. Unlike the current study, which examined MCLs with different base powers (from -9D to +6D), only one MCL design was fitted to each patient (the one recommended by the fitting guide protocol). Although MCLs were simulated using SLM in the current study, the degree of through-focus performance similarity with the SimVis MCL and the real MCL was comparable to that found there, with a similar shape similarity metric (k=0 & rho = 0.895, 0.944, and 0.915 for the Low, Medium, and HighAdd, respectively). In a previous SimVis study, it was discovered that real MCLs performed better on average than VA measures obtained using SimVis simulations. The slightly higher average VA (16.6%) with real MCLs compared to SimVis simulated MCLs may be due to an inability to account for the eye's optics, specifically a positive spherical aberration in the eye and negative spherical aberration in the MCL, which may occur with real MCLs but is not possible under temporal multiplexing. Additionally, recent advancements in the corrections of dynamic effects in optotunable lenses (264,265) have made SimVis' representations of the TF optical performance more accurate, which may ultimately lead to an even better match between the SimVis-simulated MCLs and real MCLs in accordance with the findings of the current study. High contrast visual acuity targets were employed in the current investigation and the preceding study to measure visual performance. Other measurements, however, might be a better indicator of visual quality in the actual world. In a recent study (258), we provided the multifocal acceptance score metric MAS-2EV, which offers a more thorough assessment of vision in the actual world. Natural images representing day and night situations at a distance and up close were presented. In addition, because it can be completed in around 2 minutes per correction, especially with the SimVis simulator, it is highly suited for evaluating vision with multifocal corrections (actual or simulated) in a clinical setting. In conclusion, our investigation shows that the SLM may be used consistently to simulate multifocal vision in people before actually testing them on the eye, simulating the visual quality at different distances offered by the real center-near MCLs under test. Measurements were made while the accommodation was paralyzed and the pupil diameter was fixed. We did not attempt to completely characterize performance under more natural circumstances because the purpose of the study was to compare the visual performance of the real MCLs on the eye and the SLM-simulated MCLs. Furthermore, only high-contrast visual acuity was compared; other characteristics of perceived visual quality, which may be measured using different psychophysical paradigms that use real-world images, were not included in the comparison (202,258,264,269). Except for situations where tear film breakup or decentration disrupted quality with the real MCL, the subjects nonetheless indicated informally that there was a high degree of agreement between the perceived quality of the E letters between real MCLs and simulation.

4.5 Conclusions

At least in monochromatic light, spatial phase map representations of MCLs, mapped in an SLM, can depict the profile design of the MCLs, separating MCL design elements from those related to lens wearability and physiology. Accurate visual models of MCLs show great promise for contact ophthalmology practice and even before the production of new lenses, allowing patients to try out various MCL designs quickly and completely non-invasively. Future research will take into account mimicking center distance MCLs because these lenses are increasingly utilized to slow the evolution of myopia as well as to correct presbyopia.

In this chapter, visual performance with multifocal contact lenses both real lenses and simulated lenses was evaluated through-focus, demonstrating the spatial light modulator is capable of accurately simulating the performance of the real lenses. In the next chapter, we will study to what extent the profile of the lens fitted on the eye matches the theoretical profile of the lenses

CHAPTER-5. IN VIVO ASSESSMENT OF MULTIFOCAL CONTACT LENS FITTING BY IMAGING THE ANTERIOR SEGMENT OF THE EYE WITH OPTICAL COHERENCE TOMOGRAPHY

Multifocal contact lenses are designed to provide near vision functionality in presbyopia, though they are used recently in myopia progression control. They rely on the proper deployment of the multifocal power profile on the cornea and optical interactions between the MCL and eye. Slit lamp examination is considered an essential part of contact lens practice, however, it provides limited information on the interaction of those aspects. Optical Coherence Tomography (OCT) is a non-invasive, non-contact imaging technology used to obtain high resolution cross-sectional images from within optical scattering media. In this chapter, using custom-developed fully quantitative spectral Anterior Segment Optical Coherence Tomography (AS-SOCT) we evaluated the contact lens profile on the eye and potential conformity to the cornea.

This chapter is reproducing the unpublished manuscript by Gonzalez et al., “In vivo assessment of multifocal contact lens fitting by imaging the anterior segment of the eye with optical coherence tomography”. The co-authors are **Shrilekha Vedhakrishnan**, Susana Marcos, Eduardo Martinez-Enriquez.

The work was presented as an oral contribution in the RNO 2021, Spanish National Meeting on Optics 2021 by Gonzalez et al under the title “In vivo assessment of multifocal contact lens fitting from optical coherence tomography images of the anterior segment of the eye”. This work was also presented in ARVO 2022 by Gonzalez et al under the title “OCT-based quantification of multifocal contact lenses on eye”.

The author of the thesis implemented the experimental procedure, performed the experimental measurements on subjects, and collected the data in collaboration with Ana Maria Gonzalez and Eduardo Martinez.

5.1 INTRODUCTION

Multifocal contact lenses are designed to address the age-related vision changes experienced with presbyopia, a condition that affects near vision, hindering focus on close objects. There are a variety of options available for multifocal contact lenses that can be worn depending on the wearer's preferences and lifestyle. Two main designs of multifocal contact lenses that work in different ways: (1) simultaneous vision, which might use concentric, aspheric , or diffractive designs that have specific zones for close or far vision, with which the eye will look through both prescriptions at the same time, but will use the section of the lens that is needed, depending on what distance the wearer is looking at, and (2) segmented or alternating vision, a design that works in a similar way to bifocal glasses: the middle and top segment of the lens contain the prescription for distance vision, and the lower segment has the prescription for close vision.

Slit lamp examination is considered an essential part of contact lens practice. However, it provides limited information on the interaction between the posterior surface of the contact lens and the anterior surface of the eye. In addition, it requires a lot of time of training to perform a complete successful examination. Therefore, the use of other technologies has emerged to improve clinical evaluation of the cornea and contact lens fitting (270).

Previous studies have confirmed that the primary reason for discontinuing contact lens wear is discomfort (271–274), which accounts for between 43 and 72% of the dropouts(275). Although the discomfort feeling in patients could be due to various causes, in a study carried out for the UK population, a worryingly high percentage (21%) of interruptions had to do with obvious errors in the evaluation of the fit of the contact lens by the practitioner. The most common error was the usage of an inappropriate lens design, for instance, excessively loose-fitting lenses or lenses that failed to provide enough oxygen(275).

Optical Coherence Tomography is a non-invasive, non-contact imaging technology used to obtain high resolution cross-sectional images from within optical scattering media (e.g., biological tissue). It uses low-coherence light to capture micrometer-resolution, two- and three-dimensional images, typically employing near-infrared light. The use of relatively long wavelength light allows it to penetrate the scattering medium. Due to these features, it enables *in vivo* ophthalmologic imaging of retinal and corneal morphology with an axial resolution of 2–3 µm. This resolution allows *in vivo* visualization of intraretinal and intra-corneal architectural morphology that had previously only been possible with histopathology(276). Swept-source optical coherence tomography (SS-OCT) is the latest advancement in anterior segment imaging. The introduction of SS-OCT for ocular imaging provides an even more improved sensitivity and signal-to-noise ratio compared with the previous models of SD-OCT(277,278).

The development of Fourier domain OCT (FdOCT) resulted in better quality images and the possibility of more rapidly obtaining images of the anterior and posterior segments of the eye (279). An improved sensitivity variant of FdOCT has been developed then(212,280,281), spectral domain OCT (SD-OCT), which with its shorter acquisition time, enables very high quality and real-time, three-dimensional imaging(282–284). Motion artifacts are highly reduced due to the high speed of the images(285), thus, SD-OCT tomograms are not affected by distortions caused by the movement of the object, which could be mistakenly interpreted as structural imperfections. Many applications have been described for SSOCT, including tear film evaluation, the in vivo assessment of all corneal layers, and measurements of corneal thickness and refractive corneal power to aid in refractive surgical planning. To determine whether soft contact lenses will fit properly, topographical characteristics of the corneoscleral junction, as well as the central and peripheral corneas, are crucial. Soft contact lenses cover the surface of the cornea and extend beyond the limbus onto the sclera by around 1 mm. Recent research suggests that the contact between the lens edge and the ocular surface at the periphery plays an equal or greater influence on lens fitting than the smooth, gradual transition in topography between the cornea and the sclera, which typically has a tangential profile. In order to properly fit lenses, it is therefore essential to determine the topography of the anterior sclera, corneoscleral junction, and peripheral cornea. High-resolution cross-sectional imaging of the eye with a contact lens is possible with SOCT. Research and optometric practice may benefit from the capacity to conduct a thorough analysis of the fitting relationship between the lens and the ocular surface. The diagnosis, assessment, and documentation of contact lens problems can all be aided by SOCT.

Therefore, the aforementioned characteristics make OCT a valuable tool for obtaining *in vivo* high-resolution images of the anterior segment of the eye and for the evaluation of contact lenses fitted over the cornea. Imaging of eyes fitted with a contact lens has only been reported in a couple of studies.

In 2002, the first low-resolution OCT *in vivo* images in two naked eyes and only one eye fitted with a contact lens was obtained(286). In 2006, nine eyes of six different subjects fitted with various contact lenses were examined with a slit lamp and a prototype SOCT instrument(287). Since then, no further work in this field has been presented nor have previously been obtained tomograms of *in vivo* eyes fitted with multifocal contact lenses with an OCT device. The purpose of this article is to show, for the first time to our knowledge, the application of high-resolution OCT in vivo eyes fitted with multifocal contact lenses.

5.2 MATERIALS AND METHODS

5.2.1 Subjects

Measurements were performed of 13 eyes from 13 healthy volunteers (4 males, 9 females) aged between 24 to 58 years (mean age: 35.69 ± 13.83 yrs), without a history of previous ocular surgery or disease. For each subject, the selected eye is the one with the best visual acuity and with less than 1.00D cylinder.

All participants submitted written informed permission after being told of the study's purpose and potential outcomes. All protocols had received prior approval from the Spanish National Research Council's (CSIC) Bioethical Committee and adhered to the principles of the Declaration of Helsinki.

5.2.2 Contact lenses

The investigational contact lens is the 1-Day Acuvue® Moist Brand Multifocal Contact Lens (Johnson & Johnson® Vision Care, Inc., Jacksonville, USA) with the same parameters for all subjects: -2.00D; base curve: 8.4mm; nominal diameter: 14.3mm, and with three different additions as follows: +1.25D (Low), +1.75D (Mid) and +2.50D (High). From now on, these lenses with these three different additions will be called lens L, lens M, and lens H, respectively.

5.2.3 OCT system

Measurements were performed using a custom-developed spectral domain Optical Coherence Tomography (sdOCT) system described previously (26) consisting of a fiber optic Michelson interferometer setup. It uses a superluminescent diode (λ_0=840nm, $\Delta\lambda$=50nm) as a light source and a spectrometer (4096 pixels) as a detector. The system has an acquisition speed of 25000 A-Scans/s and an axial range of 7mm in depth, resulting in a theoretical pixel size of 3.4µm. The nominal axial resolution, estimated from the bandwidth/coherence length of the source, was 6.9µm in tissue. In addition, a motorized Badal system corrects for defocus allowing the fixation of sharp stimuli consisting of a 20/25 white Snellen E letter presented in a black background on a Digital Light Processing (DLP) picoprojector (854x480 pixels, Philips NV, Amsterdam, Netherlands; 55 lums). Two neutral filters (ND 16) were placed after the picoprojector to produce an average luminance of ~30cd/m^2 in an otherwise dark environment.

5.2.4 Experimental protocols

To correct the spherical error with and without contact lenses, patients adjusted their best subjective focus by performing a psychophysical test in an adaptive optics system. For this purpose, patients were instructed to move a Badal system controlled by a keyboard while viewing a stimulus illuminated with a laser source of 555 nm to find the position where the stimulus appeared sharp. The best focus settings were repeated 3 times.

The lens was inserted in the eye chosen for the study. Lenses were allowed to settle for at least 10 minutes before proceeding.

To ensure stabilization and alignment of the patient with the OCT system, a bite bar was fabricated using the Dental Kerr impression and was mounted in the x-y-z stage in the OCT device. The chosen eye was aligned in the OCT system while the patient stared at a visual stimulus in the picoprojector so that the patient's eye pupillary axis was aligned to the optical axis of the instrument, and the contralateral eye was covered with a patch. The operator aligned the eye moving the x-y-z stage while viewing horizontal and vertical OCT-B scans until the corneal reflex is obtained.

This process was done for four conditions: naked eye, an eye with CL_L, an eye with CL_M, and eye with CL_H. At least, five repeated measurements were collected in each condition. The device configuration for image acquisition consisted of a scanning area of 11x11 mm containing 50 B-scans and 300 A-scans per B-scan.

5.2.5 OCT 3D eye models construction

The construction of accurate 3-D eye models from the OCT images involved three steps as described in [24]: (1) surface detection and segmentation, (2) distortion correction , and (3) centering processes.

Custom-developed segmentation routines were implemented for the detection of the anterior and posterior surfaces of the cornea and contact lens. Fan distortion (due to the scanning system configuration) and optical distortion (due to the refraction of rays in different surfaces) were corrected by using 3-D ray tracing routines on the segmented volumes. The corneal and aqueous humor group refractive indices were taken as 1.385 and 1.345, respectively, and the contact lens refractive index was 1.40.

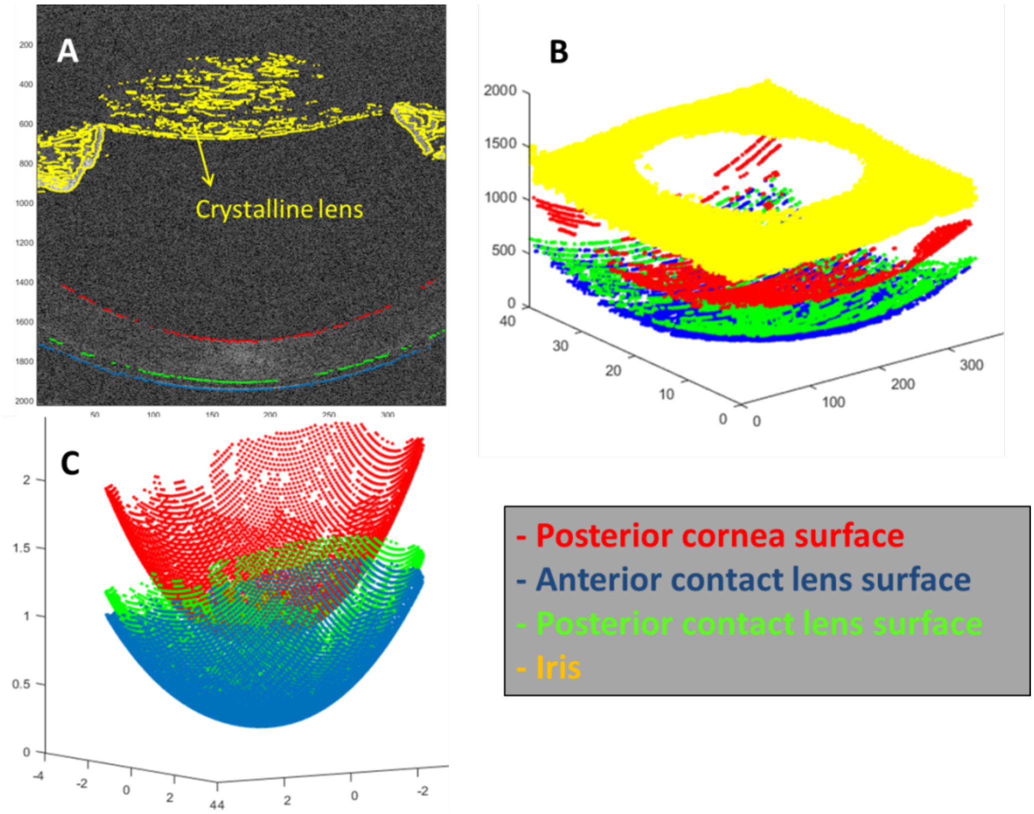

Figure 4.1. Different processes in a measurement of the cornea with contact lens. (A) Segmentation process, (B) 3-D model before distortion correction, (C) 3-D model after distortion correction.

The following biometric parameters were quantified: (1) corneal thickness (ThC), (2) corneal radius of curvature (RAC), (3) contact lens thickness (CLT), (4) contact lens anterior radius of curvature (RCLa), (5) contact lens posterior radius of curvature (RCLp), and (6) corneal thickness (ThC), measured through the lens on-eye. Some of them are shown below in figure 4.2.

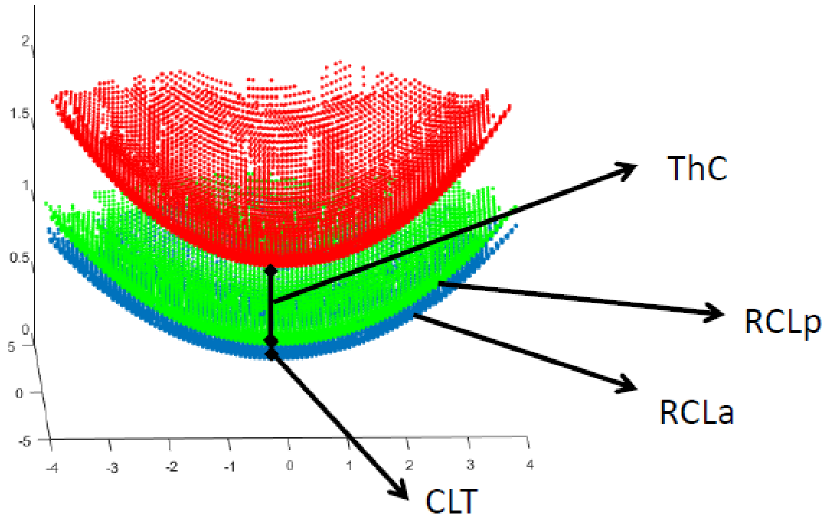

Figure 4.2. Graphical representation of some of the quantified parameters.

Surface radii of curvature (RAC, RCLa, and RCLp) were estimated following 6th order Zernike, best sphere fitting (11 mm optical zone diameter) concerning their apex. As a parameter associated with the conformity of the contact lens to the cornea shape, the RMS of the astigmatism coefficients was calculated for all the surfaces. Furthermore, to estimate the central addition, the power was calculated in two different areas as shown in figure 4.3 central area (3 central mm), and periphery (from 3 to 6 mm).

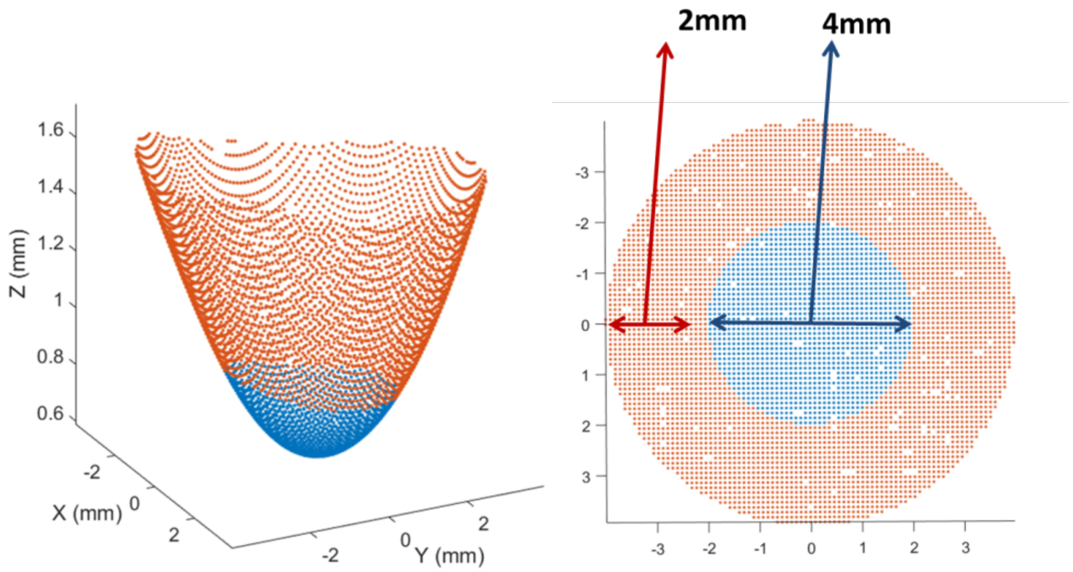

Figure 4.3. The central area (blue) and peripheral area (red) for the estimation of the addition.

The addition was estimated as the central power (P_{center}) referred to as the peripheral power ($P_{periphery}$), i.e., $\Delta P = P_{center} - P_{periphery}$. This can be expressed as a function of the radius of curvature of the center (Rc) and the periphery (Rp) as:

$$\Delta P = \frac{1.4-1}{Rc(m)} - \frac{1.4-1}{Rp(m)} = \frac{400}{Rc(mm)} - \frac{400}{Rp(mm)}$$

Also, to assess the spatial extent of the near add, the diameter of the central area (Dc) was changed from 1 to 6, and the ΔP was estimated as a function of this diameter. The maximum of ΔP should approximately match the boundary of the additional area.

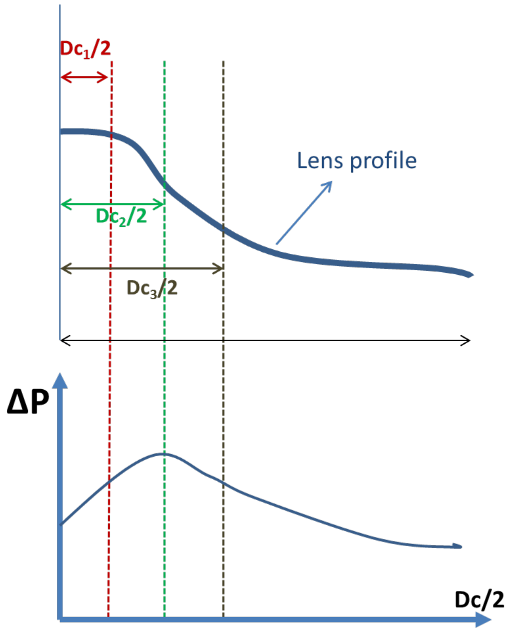

Figure 4.4. $\Delta P = P_{center} - P_{periphery}$ as a function of the diameter of the central area (Dc).

5.2.6 Data analysis

All corneal and contact lens parameters were obtained as the mean of five different measurements. Linear relationships of the parameters and several ratios between parameters with RC and with RCL were analyzed. Slopes, correlation coefficients, and p-values were calculated from linear regressions.

5.3 RESULTS

Figure 4.5 shows the correlation between the RC and the RCL in the periphery for the different additions (Low: RCL_L; Mid: RCL_M; and High: RCL_H; from left to right), with the best-fitted line indicated in purple. Each point corresponds to a different eye, and the error bars are calculated across the 5 different measurements for each eye. The correlation coefficient (ρ) and p-values are also shown. Note that the correlation was high for all the additions, indicating that the MCL changes its shape according to that of the underlying cornea (corneal conformity).

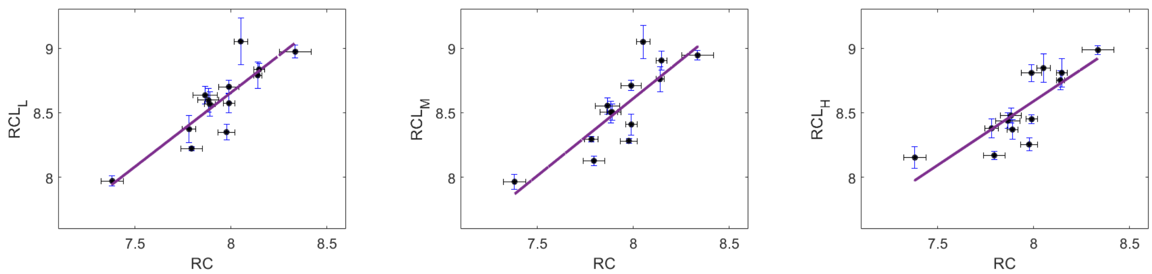

ρ=0.87, p<<0.001 **ρ=0.84, p<<0.001** **ρ=0.82, p<<0.001**

Figure 4.5. Correlation between RC and RCL. (a) Low addition (L); (b) Middle addition (M); (c) High addition (H).

The mean radius of curvature across subjects in the addition area was: RCL_L=8.37±0.31 mm, RCL_M=8.32±0.34 mm, RCL_H=8.30±0.28 mm, and RC=7.82±0.24 mm. As expected, the radius of curvature was lower (higher curvature and power) for the highest addition ($RCL_H<RCL_M<RCL_L$). The radii of curvature in the periphery were: RCL_L=8.59±0.30 mm, RCL_M=8.54±0.33 mm, RCL_H=8.53±0.28 mm, and RC=8.02±0.22 mm. As expected, the radius was lower in the addition area than in the periphery for each type of lens. The difference in power between cornea and periphery, ΔP (an estimation of the correction for far) were: -1.40 D, -1.13 D, and -1.10 D for lenses L, M, and H respectively. Note that these values were estimated from the radius of curvature using an index of refraction of n=1.40 for the MCLs and n=1.38 for the cornea. We did not find the correlation between corneal power and ΔP (p=0.45, 0.40, 0.72), i.e., there is a constant shift in far correction independently of the power of the cornea of the subject. Finally, the RCL was highly correlated with the cornea in the addition area (ρ=0.85, ρ=0.82, ρ=0.78 for lenses L, M, and H respectively). This also indicates a change in the MCL addition area with the underlying cornea.

5.4 DISCUSSION

Our results are in good correspondence with reported isolated MCL shape measurement using a high-resolution power mapping instrument in phosphate-buffered saline(251) In this study, the optical power profiles of commercially available soft multifocal contact lenses were evaluated to compare their optical designs, among which is included the 1-Day Acuvue® Moist Brand Multifocal Contact Lens. With a center-near aspherical design, this lens has a gradual change in power between near and distance zones, although according to the power profiles, a smooth transition between the near central power is distinguished in the radius of 1.5 mm from the center of the lens, so we assume that the near power is in the central area of the lens with a diameter of 3 mm.

As expected, the radius of the MCL was lower (higher curvature and power) in the addition area than in the periphery for each type of lens. Therefore, the radius of curvature was lower (higher curvature and power) for the highest addition.

This, translated into power, means that the power of the contact lens with high addition will be higher in the center area than the contact lenses with medium and low addition, in this order. Furthermore, we can conclude that the power in the central 3 mm of any of the three lenses with the three different additions will be higher than the power in the periphery since it is the area where the addition is in the design of these lenses.

Two previous studies have shown the usefulness of OCT as a very valuable tool in contact lens practice. One of them rates the quality of the images as sufficient to diagnose different conditions of the anterior segment as well as to estimate the quality of contact lens fit and its influence on corneal metabolism(287). A more recent study (286) has provided more detailed images of the cornea with contact lenses of different types of materials (soft contact lenses and rigid gas permeable lenses), which show the different complications associated with the use of contact lenses. In this study, the design, shape, and lens edge position can be visualized, and the thickness of the lens, corneal epithelium, and stroma can be measured. However, these studies have focused more on the visualization of ocular anatomical structures as well as the anterior surface of the contact lens fitted on the cornea and the possible complications derived from the use of contact lenses, while the present study focuses mainly on the calculation of the different parameters of the MCL that will influence the fit of the contact lenses on the eye, such as corneal thickness (ThC), corneal radius of curvature (RAC), contact lens thickness (CLT), contact lens anterior radius of curvature (RCLa), contact lens posterior radius of curvature (RCLp) and corneal thickness (ThC), obtained with our algorithms and providing more quantitative information on contact lens fitting.

In both studies, the evaluated lenses were monofocal, therefore we can conclude that the present study is the first one in which OCT images of MCLs fitted on the eye have been taken in vivo.

The gold standard for assessing the fit of contact lenses with the anterior part of the eye is the slit-lamp test. Although it cannot be determined objectively, it provides information about poor lens fit. The best contact lens for a given eye's topography can therefore sometimes be difficult to determine with a slit-lamp test (286). Other technologies that can be useful to provide more information about contact lens fit. Those are high-frequency ultrasound imaging, Scheimpflug camera, and OCT. The first one can achieve only 20-30 µm axial resolution (288) and Changes in the examination conditions may result from the requirement to use an immersion bath. The second way involves using a Scheimpflug camera, an optical technique. Pentacam is the most advanced instrument based on this technology that is now commercially available (Oculus, Wetzlar, Germany). However, it is unable to visualize a contact lens on the surface of the eye (286). The last technique is OCT, analogous to conventional ultrasonic imaging, with the advantage that OCT does not need direct contact with the investigated tissue. Our SD-OCT prototype system provides images from which we can obtain the 3-D model construction of the eye fitted with the MCL and several parameters that can be helpful in the objective assessment of contact lens fitting.

5.5 Conclusions

Our results are in good correspondence with reported isolated MCL shape measurement using high-resolution power mapping instruments in phosphate buffered saline(251). In conclusion, Optical Coherence Tomography provided with quantification tools allows us to study of the fitting of multifocal contact lenses on the eye *in vivo.* We have shown that, while the soft contact lens overall conforms to the underlying cornea, near adds are provided as expected.

In this chapter, we have studied the fitting of multifocal contact lenses on the eye using the Optical Coherence tomography and confirmed the presence of the central addition consistent with the design of the lenses. In the following chapter, we simulate these lenses in the Spatial Light Modulator and for the first time studied the accommodative response through these simulated lenses.

CHAPTER-6. ACCOMMODATION WITH SIMULATED MULTIFOCAL CONTACT LENSES IN MYOPIC SUBJECTS

There is an association between myopia progression and near work that has led to speculation that the larger accommodative lags reported in myopes may be a factor or an effect in progression. The effectiveness of multifocal contact lenses (MCLs) in slowing myopia progression may highly depend on the patient's accommodative response. In this chapter, we have evaluated the impact of contact lens design and addition on the accommodative behavior in myopes.

This chapter reproduces the paper by Vedhakrishnan et al(289) under the title "Accommodation through Simulated multifocal optics", published in BioMedical Optics Express (2022). The co-authors are Alberto De Castro, Maria Vinas, Sara Aissati and Susana Marcos.

The work was presented as a poster presentation at ARVO annual meeting in 2022 by **Vedhakrishnan et al** under the title "Accommodation with simulated multifocal contact lenses in myopes". It was also presented as an oral contribution by Vedhakrishnan et al. in an invited talk in the Optica Vision and Color Summer data blast 2022, under the same title.

The author of this thesis designed the experiment, implemented the experimental protocol, performed the experimental measurements on subjects, collected and analyzed the data and prepared the manuscript in collaboration with Susana Marcos.

6.1 Introduction

The ability of the human eye to focus on both near and distant objects by adjusting the geometry of its crystalline lens is referred to as accommodation. In reaction to a near stimulus, there are changes in pupil size, convergence, and accommodation(290). Binocular vision, chromatic aberration, and other cues, such as stimulus size have been shown to contribute to accommodation(291), although accommodation can occur in their absence, triggered by blur cues (218).

Although the causes of myopia are likely multiple, there are still some unknowns. The concept of simultaneous vision is the foundation of most bifocal and multifocal contact lenses (CLs), which are sold mostly for the correction of presbyopia with some designs developed for myopia control. In contrast to alternating vision corrections, which require the patient to look through distinct portions of a spectacle lens for near and far, simultaneous vision refers to multifocal corrections that are applied at (or near) the pupil plane. In the case of a pure bifocal correction, the superposition of sharp and blurry pictures reduces contrast and degrades the MTF. Smooth refractive profiles produce broader through-focus curves rather than two separate foci (135,136). The action of bifocal and multifocal contact lenses on the peripheral retina is the most widely accepted theory for how they work to manage myopia. It has been established that spectacle lenses cause hyperopic defocus in the periphery, which is thought to trigger elongation to occur (110) The peripheral retina would experience a relative myopic defocus with bifocal lenses that have a center distance and near addition, which is intended to slow the growth of myopia. According to this idea, lenses that include a zone to correct the central refractive error and a relative plus in the periphery can act as a stop sign for an eye that is developing to become increasingly myopic (173,174). However, the accommodating behavior of the individual eye when these lenses are worn is extremely important for the capacity of multifocal contact lenses to remove hyperopic defocus and introduce myopic defocus in young eyes. In particular, when discussing both peripheral and central defocus, if the eye relaxes its accommodation to use the near acuity for near vision tasks, the anticipated myopic defocus may not occur, leaving the eye exposed to the hyperopic blur of the out-of-focus distant peak and possibly favoring eye elongation (292)

However, the accommodating behavior of the individual eye when these lenses are worn is extremely important for the capacity of multifocal contact lenses to remove hyperopic defocus and introduce myopic defocus in young eyes. In particular, when discussing both peripheral and central defocus, if the eye relaxes its accommodation to use the near acuity for near vision tasks, the anticipated myopic defocus may not occur, leaving the eye exposed to the hyperopic blur of the out-of-focus distant peak and possibly favoring eye elongation (132,137,138), providing generally contradictory results, such as positive spherical aberration reducing the accommodative latency and negative spherical aberration lengthening the accommodative lag.

To examine potential variations in the accommodative response across multifocal lens designs, adaptive optics (AO) visual simulators seem to be the best possible experimental platform. First of all, AO enables non-invasive simulation of lens designs without requiring the contact lens to be placed on the eye. Additionally, because the lens designs are digitally designed, they are not limited to those that are physically or commercially available (193,194). We recently demonstrated the precision of the Spatial Light Modulator (SLM) of a specially created AO Visual Simulator's simulation of commercial center-near multifocal contact lenses (low, medium, and high near add). In the -3D to +1D range, the average difference in through-focus Visual Acuity between the real lens and the simulated lens was less than 0.03 logMAR (203). Clinically, AO visual simulators can be utilized to assess patients with multiple MCL designs' vision before lens insertion. A lens that optimizes perceived visual quality and visual performance can be chosen by using AO visual simulation to investigate interactions between the eye's optics and a specific lens design and to compare variations among lens designs (136,202). Additionally, the Hartmann-Shack (HS) wavefront sensor, a crucial part of the AO system, can be utilized to calculate the focus shift of the best retinal picture to assess low and high order aberration, estimate retinal image quality and quantify the accommodation response (293,294). In general, segmented or diffractive optics make it difficult for an HS wavefront sensor to accurately quantify aberrations. While this obstacle is challenging to overcome in research involving contact lenses placed on the eye, it is possible to get around the SLM since it projects the multifocal phase map onto the pupil of the eye and is located in a conjugate pupil plane (196,215). By evaluating the response of the eye (crystalline lens) alone to an accommodating stimulus, the HS wavefront sensor enables this. By computationally combining the eye's wavefront aberration and the contact lens phase map, the optical quality and accommodative lag of the eye with the multifocal contact lens may be determined.

In this work, we programmed six different multifocal contact lens designs: purely bifocal segmented Center Near and Center Far [30,37]; medium and high add center near commercial multifocal designs (193,203), as well as positive and negative spherical aberration. We measured the changes in the eye's spherical aberration and the accommodative response through each of those designs with those lenses projected onto the eye. We created new techniques for measuring changes related to the eye alone and for quantifying the accommodative latency without accounting for the SLM contribution. We discovered that the design of the lens, as well as, to a lesser extent, individual variations in the eye's aberrations and pupillary dynamics, had a significant impact on the accuracy of accommodation in eyes through the multifocal patterns.

6.2. Methods

Six young myopes participated in the evaluation of the accommodative response (to blur-only stimuli) using six distinct multifocal patterns and a control monofocal pattern. In a specially created AO Visual Simulator, the patterns were reproduced as phase maps in the Spatial Light Modulator (center near and center distance designs) and in the Deformable Mirror (positive and negative spherical aberrations). As a function of accommodative demand, the change in spherical aberration and focus shift from the optimal retinal image quality was assessed.

6.2.1. Subjects

Six young myopic subjects in total, with ages ranging from 23 to 29 years (average, 28$\pm$1.5 years), had spherical errors between 1.75 and 3.25 D (-2.41$\pm$0.3 D) and had astigmatism less than 0.25 D. Apart from their ametropia, the patients were healthy. The CSIC Institutional Review Boards had given its blessing to the study protocols, which adhered to the principles of the Declaration of Helsinki. Prior to any study procedures, informed consent waivers were signed by all participants after they received information about the study and its experimental methods.

6.2.2. Adaptive Optics Visual Simulator

The experiment was conducted at the Visual Optics and Biophotonics Lab (Institute of Optics, Spanish National Research Council, Madrid, Spain), utilizing a specially designed AO system that was extensively documented in other publications (195,198,223) and section 2.1.2 of the thesis.

In this study, an SLM was used to map the MCLs (center near and center distance designs), and a DM was used to induce spherical aberration (positive and negative spherical aberration). In this study, an infrared light source with a wavelength of 827 nm was used to assess aberrations, and a visible light source with a wavelength of 555 nm was used to illuminate the visual stimuli. The subject's refractive error was corrected, and defocus was induced, using a Badal optometer. For this study, the pupil size was the natural pupil of the subjects, and not controlled in the system using artificial pupils.

6.2.3. Multifocal contact lenses

The experiment was performed for 7 conditions: NoLens (NL) (the subjects viewed the target under their natural aberrations through a flat SLM); Center Distance (CD), Center Near (CN), MediumAdd Center Near (MA), High Add Center Near (HA); Positive Spherical Aberration (PSA) and Negative Spherical Aberration (NSA). The MA (+1.75D near add) and HA (+2.50D near add) tested in this study represent commercially available 1-Day Acuvue Moist Multifocal (Johnson and Johnson Vision Care, Jacksonville, FL). The specifications of these lenses are described in previous studies(193,203) The CN, and CD lenses were pure segmented bifocal design lenses with a 4-mm pupil central zone (distance in CD and near in CN). This 4-mm design was selected such that the central zone had a similar diameter to that of the commercial lenses, but instead of a smooth blending zone, to have a segmented, abrupt transition from near too far. The induced PSA and NSA were ±1μm over a 6-mm pupil.

6.2.4. SLM and DM phase map generation

Fig. 1 shows the phase map of the four bifocal/multifocal designs used in this study mapped on the SLM and the two pure 4th-order spherical aberration designs mapped on the DM. MATLAB routines were used to numerically simulate the designs, which were later programmed in the reflective phase-only LCoS-SLM following the same protocols as from previous studies(194). In order, to map the maximum phase difference on the SLM, a 2π wrapping process was applied to the phase pattern generation process (188). The patterns were generated as a grey-scale image over a 6-mm pupil. The SLM was calibrated for a wavelength of 555nm. Measurements of the induced PSA and NSA in the HS using an artificial eye showed deviations of less than 0.01% from the attempted 1μm induction. The magnitude of the induced aberrations changed across the experiment due to pupillary miosis when accommodating.

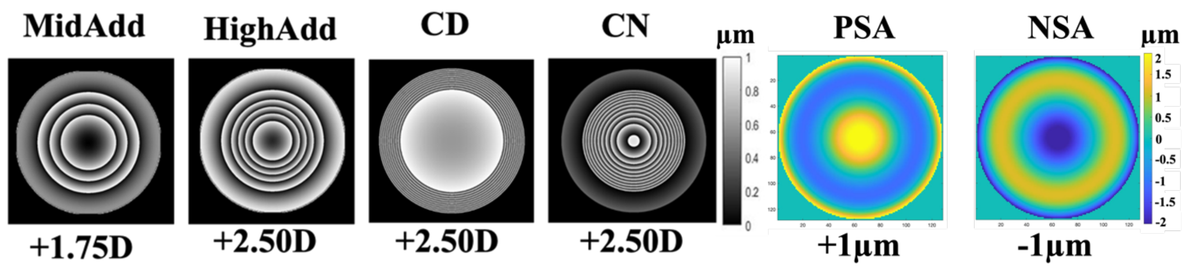

Figure 1. Phase maps of the MCLs simulated in the SLM: MediumAdd (+1.75 D near add), HighAdd (+2.50 D near add), Center Distance (+2.50 D near add), Center Near (+2.50 D near add), right grayscale panels, and 1μm positive and negative SA, left color panels, were induced on the DM. Maps are represented for a pupil diameter of 6 mm.

6.2.5. Experimental procedure in subjects

Measurements in subjects were performed monocularly on the dominant eye (determined with the Miles test) with the natural aberrations of the subject uncorrected, in a darkened room, while fixating at Maltese-Cross (1 deg field) projected on the DMD, illuminated by green light (555 nm, 20 cd/m^2). The non-measured eye was covered with a patch throughout the experiment. The residual aberrations of the system were corrected in all cases using an AO closed-loop correction. Subjects were aligned to the system using the line of sight as reference (i.e., pupil the was imaged with the pupil monitoring channel, and the pupil center aligned to the optical axis of the instrument as the patient was fixating foveally. A commercial auto refractometer (Zeiss/Humphrey) was used to measure objective refraction before the experiment, and this value served as the initial setting for the system's defocus adjustment. The subject was instructed to center the pupil before adjusting the Badal system's location to acquire the optimal focus for distant vision. To avoid adapting while looking for the best focus, positive defocus values were used in relation to the subject's anticipated spherical error correction. The zero-defocus setting was determined by averaging at least five repetitions of the focus setting over several trials. The same procedure was used to find the focus for each simulated pattern, which was selected independently for each of the seven experimental conditions. Ocular aberrations were measured for each condition and accommodative demands from 0 to 6D, in 1-D steps, introduced using the motorized Badal optometer. Each measurement was repeated 5-6 times, which took around 40-50 seconds. The pupil diameter was extracted from the HS images. By carrying out a few preparatory experimental sequences, subjects were introduced to the setup and process. The same session was used to measure each condition sequentially, beginning with the NL condition and concluding with the randomized conditions with multifocal patterns.

6.2.6. Data Analysis

SLM residuals

Fig 2A shows the schematic of the AO system that was used in the experiment. Ocular aberrations were measured in infrared light (880nm), while the subject viewed the accommodative stimulus in green light (555nm). Since the SLM was calibrated for green wavelength and the aberrations of the eye were measured in IR, to compensate for differences in the wavefront induced for the two wavelengths, a baseline measurement was made to remove the residuals of the SLM. The wave aberrations were measured in IR (880nm) for the different phase maps simulated in the SLM for 555 nm, using a diffraction-limited artificial eye. This was considered the residual baseline which was removed from the real-time measurements of the eye. The residual measurements were made for a 6 mm pupil diameter and the residual wavefront was cropped according to the subject’s pupil size in each case. This procedure allowed us to obtain wave aberration for the eye alone, eliminating any artifact from the SLM. Fig. 2B illustrates this process with a real wavefront map captured in a real eye (S4) with the MA design in the SLM. In a second step (Fig. 2C), the corresponding phase maps were computationally added to the measured eye-alone wave aberration, considering the pupil size of the subjects for each accommodation demand as shown in Fig.2C for 0 and 6D.

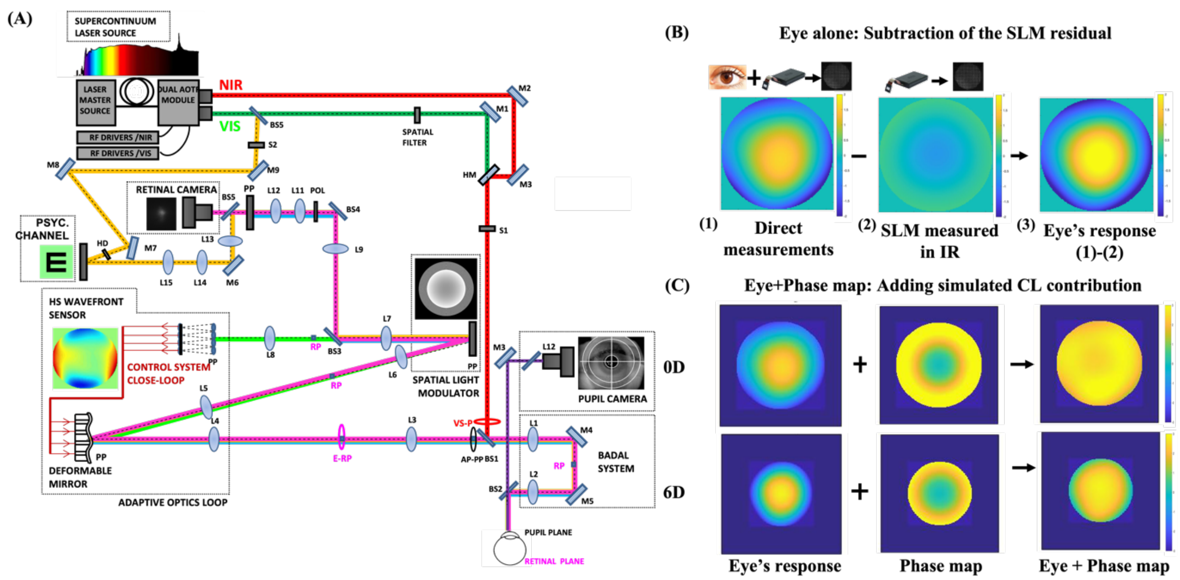

Figure 2. Left panel (A) Schematic of the AO system used in this experiment; Right upper panels (B): Illustration of the removal of SLM residuals on S4 with the HA pattern (1) Wave aberration measured in IR light (eye +SLM

with MA pattern) (2) SLM residual of MA measured with an artificial eye in IR light (3) Wave aberration of the eye alone after removing the SLM residual. Right lower panels (C): Illustration of adding the simulated CL computationally to the eye, shown as an example of subject S4 with HA phase map. The pupil diameter was 4.36mm for 0D and 3.24mm for 6D.

6.2.7. From Aberrations to Accommodative response

Wave aberrations were fitted to seventh-order Zernike polynomials (with nomenclature following the Optica -formerly Optical Society- standard(132)) using a least-mean square procedure. The pupil diameter at each accommodative demand was obtained as an average of individual measurements, whereas each Zernike coefficient was the average of 5-repeated measurements. Wave aberration maps (and 4th order spherical aberration Zernike coefficients) were calculated for the eye alone (i.e., after subtraction of the SLM residuals, as shown in Fig 2, for the SLM-based conditions, and after direct subtraction of the induced spherical aberration for the DM-based conditions), and for the eye + phase map.

Point Spread Functions (PSF) were calculated from the eye+phase map aberration maps, as the magnitude square of the Fourier transform of the pupil function, where the amplitude pupil function was the normative Stiles-Crawford function(295,296). The piston and prismatic terms (the first three Zernike terms) were omitted in the analysis, and the Zernike defocus was set such that retinal image quality was maximized at 0 D. The MTF was estimated from the calculated PSFs. Retinal image quality was estimated using two different metrics: (1) Volume under the MTF in the 3-5 c/deg range (thought to be key for accommodation(218,297) and (2) Visual Strehl, defined as the volume enclosed between the MTF and the inverse of the neural CSF (188). For each accommodative demand a through-focus image quality curve was calculated, including the corresponding defocus term (relative to the Zernike coefficient that maximizes the curve for 0 D demand) in the PSF calculations. The accommodative lag for each accommodative demand was calculated from the defocus shift in the peak of the TF curve from 0 D (assuming the best focus for relaxed accommodation).

6.2.8. Statistical Analysis

Statistical analysis was performed with SPSS software Statistics 24.0 (IBM, United States) to test differences between conditions. The normality assumption was checked using Shapiro-Wilk's test. Specific non-parametric tests were used for different comparisons: (1) For comparing across conditions: Related-Samples Friedman's analysis of variance by ranks and paired tests (2) For comparing across subjects and accommodation demands Independent-Samples Kruskal-Wallis and paired tests.

6.3. Results

6.3.1. Changes in pupil size with accommodation

Fig 3 shows the pupil size change with accommodation from 0-6 D for different conditions for each subject. The color code represented in shades of brown are the lenses inducing positive spherical aberration (CD and PSA) and in shades of green the lenses inducing negative spherical aberration (CN, HA, MA, NSA).

There was a systematic decrease in pupil diameter with accommodative stimulus for all conditions with an average slope of change from 0D to 6D across conditions of -0.17mm/D. Even at 0 D, the pupil diameter varies across conditions in the majority of the subjects. On average, the standard deviation in pupil diameter across all 7 conditions was 0.21mm, while the repeated measurement variability in pupil diameter was 0.041mm. On average across subjects, two conditions showed less response in pupil constriction with accommodative demand (HA and NSA, -0.11mm/D) and one condition showed a higher slope (PSA, -0.2 mm/D), but the maximum slope was found for the NoLens condition (-0.23 mm/D). The rate of change in pupil diameter differed across conditions and subjects significantly (p=0.003, Related-Samples Friedman's analysis of variance across conditions and p=0.000, Independent-Samples Kruskal-Wallis tests across subjects).

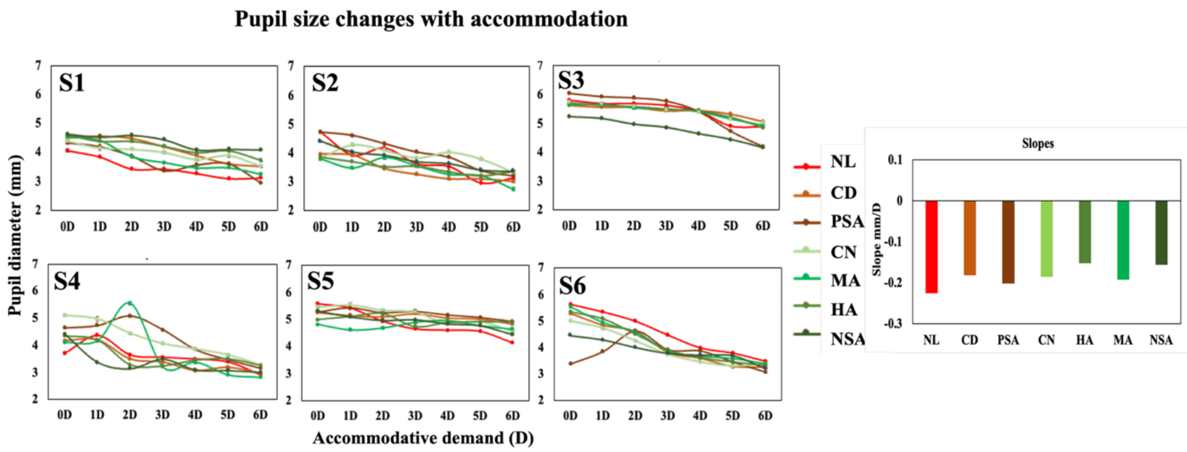

Figure 3. Left panels: Pupil diameter changes with accommodation for all subjects plotted against accommodation demands from 0 to 6D. Right panel: Average slope (across subjects) for each condition. Red lines/bars represent NL; light brown represents CD; dark brown represents PSA; light green represent CN; bright green represents MA; olive green represents HA; darkest green represents NSA.

6.3.2. Spherical aberration of the eye at a uniform pupil diameter

Fig. 4 shows the spherical aberration of the eye alone (relative to value at 0 D) cropped to the smallest pupil across conditions in each subject plotted against the tested accommodative demands. The pupil diameter is indicated in the lower right corner of each panel. Data from different subjects are plotted on a different scale to accommodate larger variations associated with a larger pupil diameter. Error bars of five repetitions of the wavefronts are shown at each point.

Spherical aberration shifted to negative values with accommodative demand, in all subjects except for subject S3 (which happens to be one the subject with the largest pupil diameters). Fig. 4 (right panel) shows the average slopes (spherical aberration/D of accommodative demand) for fixed pupil diameters. The conditions that produced a larger shift of spherical aberration towards more negative values were the center distance type (CD, PSA) while for CN, HA, MA, and NSA the change in spherical aberration was closer to zero.

The spherical aberration change across demands for each condition was statistically significantly different for NL alone (p=0.042, Independent-Samples Kruskal-Wallis tests) while for the other conditions, the change was not statistically significant (p>0.05, Independent-Samples Kruskal-Wallis tests). Among subjects, the largest change was found for PSA in most of the subjects (error bars shown). The slope for 0-2D was flattest for CN in almost all subjects, indicating that the eye may use the add up to about 2D.

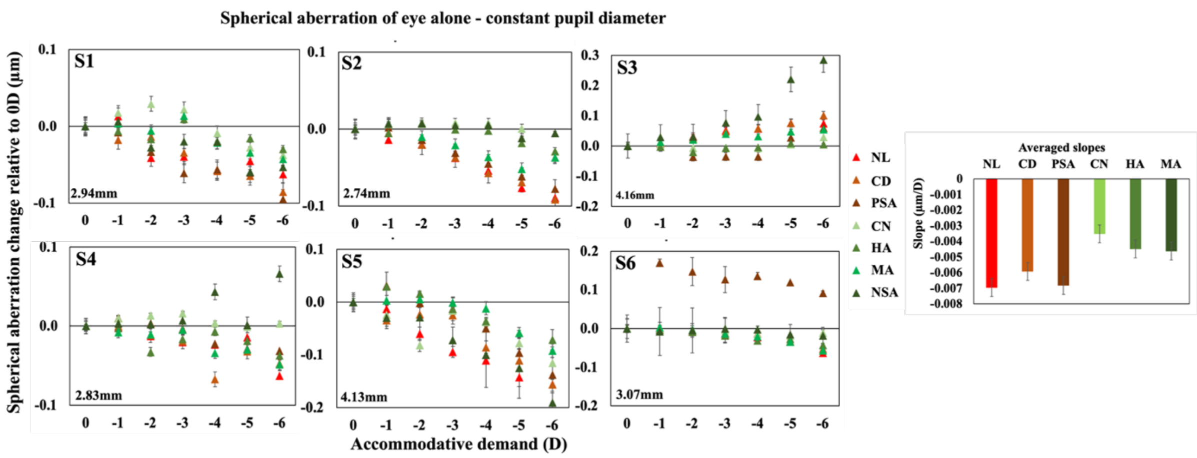

Figure 4. Left panels: Relative change in 4th order spherical aberration of the eye alone for a fixed pupil diameter (shown in the lower left corner of each panel, representing the minimum diameter in the series, to which data have been cropped), for all conditions and subjects. Right panels: Average slope (across subjects) for each condition (spherical aberration/D). Red lines/bars represent NL; light brown represent CD; dark brown represent PSA; light green represent CN; bright green represent MA; olive green represent HA; darkest green represent NSA. Error bars stand for standard deviations across 5 repeated measurements.

6.3.3. Combined eye and CL wave aberration, for natural pupils

Fig. 5 shows the spherical aberration of the eye+phase maps with a natural pupil of each subject across conditions plotted against the tested accommodative demands. As expected, with the lenses inducing positive spherical aberration (CD, PSA in shades of brown) the resulting wavefront has positive spherical aberration, while with the lenses inducing negative spherical aberration to the eye (CN, MA, HA, PSA in shades of green) the resulting wavefront spherical aberration is negative in all subjects. Also, the results show a convergence of spherical aberration towards zero with increasing accommodative demand, triggered mainly the pupil constriction. The superimposed numbers in the bottom left and right corners represent pupil diameter at 0 and 6 D accommodative demand, averaged across conditions The change in spherical aberration across demands was not statistically significant for NL, CN, HA, MA ($p>0.05$, Independent-Samples Kruskal-Wallis tests), while for CD, PSA, NSA the change was significantly different across demands ($p=0.010/0.004/0.003$) respectively.

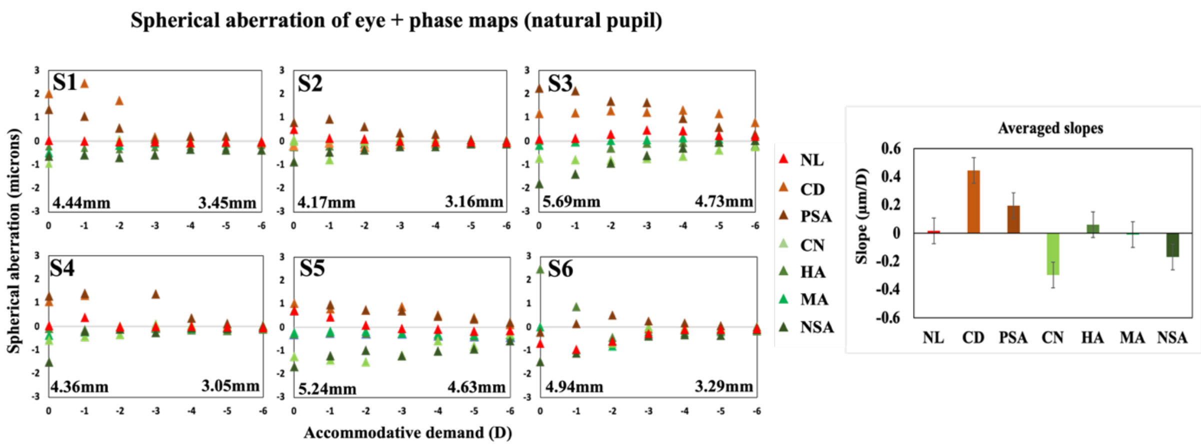

Figure 5. Left panels: Spherical aberration of eye + phase maps for all subjects as a function of accommodative demands (D) for natural pupil diameters. The numbers in the left and right bottom of each panel indicate the pupil diameter (averaged across conditions, for 0 and 6D), for each condition and all subjects. Right panels: Average slope (across subjects) for each condition (spherical aberration/D). Red lines/bars represent NL; light

brown represent CD; dark brown represent PSA; light green represent CN; bright green represent MA; olive green represent HA; darkest green represent NSA. Error bars stand for standard deviations across 5 repeated measurements.

6.3.4. Volume under the MTF

Fig. 6 shows the volume under the through-focus (TF) MTF between spatial frequencies 3 to 5 cycles per degree for subject S4 for example for each accommodative demand and condition). The further the peak appears to the left, the higher the accommodative lag (or signal in the hyperopic defocus). Across subjects (and illustrated in Fig 7 in S1. While we illustrated the TF performance in terms of volume under MTF in a 3-5 c/deg range, the relative shapes of the curves and peak positions were nearly identical to the Visual Strehl TF. On average across subjects, the difference between defocus shifts obtained from volume under MTF (3-5 c/deg) and visual strehl differed by < 0.02D. The volume under MTF was chosen instead of Visual Strehl for illustration purposes, as the change in pupil diameter artificially increased the peak performance (due to normalization in the definition of the Visual Strehl) for the higher accommodative demands.

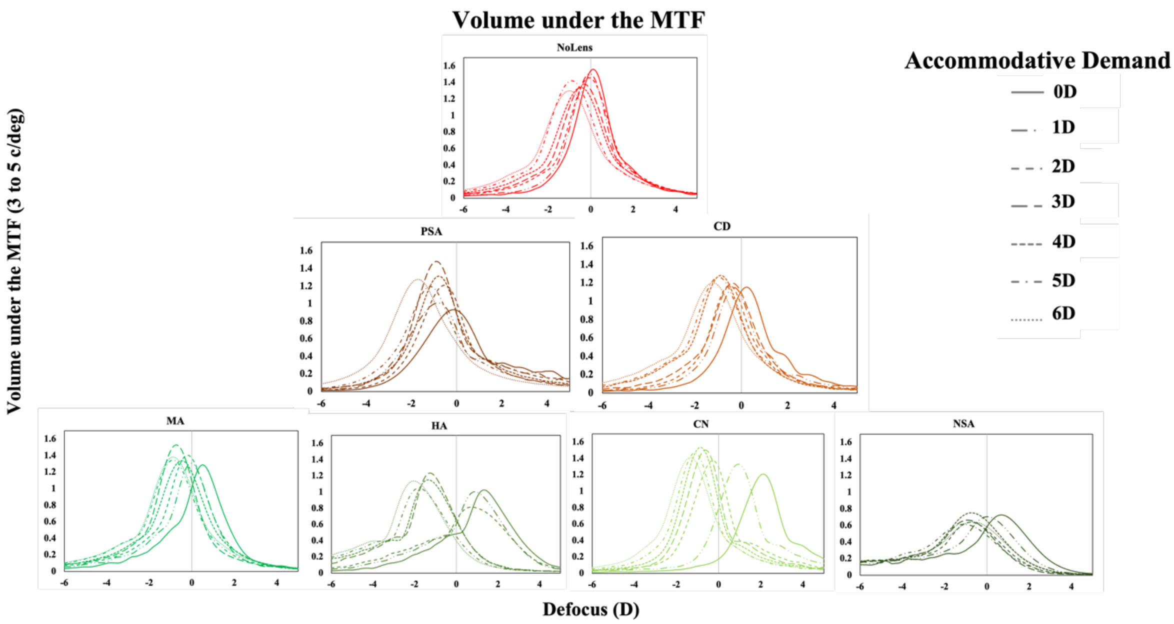

Figure 6. Through-focus Volume under the MTF (3-5 c/deg) curves for subject S1 for each condition and all vergences (0-6 D, indicated by different line styles). The first row shows the NL condition, the second-row center distance conditions (PSA, CD), and the third row the center near conditions (CN, MA, HA, NSA).

6.3.5. Shift in best image quality

Fig. 7 (A panels) shows the accommodative lag calculated as the vergence needed to maximize the visual strehl, i.e., the shift of peak in the through-focus visual strehl curves, for all subjects and conditions. The lag of accommodation was analyzed in terms of slopes of the curves for lower accommodative demands (0-3D) and higher accommodative demands (3-6D), as shown in Figure 7 (B), as well as in terms of area under the curves in Figure 7 (C). The analysis of the slopes shows that the lag in the 0 to the 3D range is larger with CN like conditions and that it is more similar between conditions after 3D. When analyzing all the data from different subjects, the largest lags were consistently obtained for a center near (CN), HighAdd (HA) , and negative spherical aberration (NSA) conditions (p=0.005/0.004/0.011, Independent-Samples Kruskal-Wallis tests) and the smallest lag were found for the positive spherical aberration (PSA) and Center Distance (CD) (p=0.001 & p=0.003, Independent-Samples Kruskal-Wallis tests). In half of the subjects, the accommodative lag was significantly reduced using a correction (ie. MCLs compared to the natural condition). The highest differences were found for the slopes at 0-3 D accommodative demands (B, top panels). The area under the curve metric (C, lower panel) shows significance proving that PSA and CD had the smallest lag.

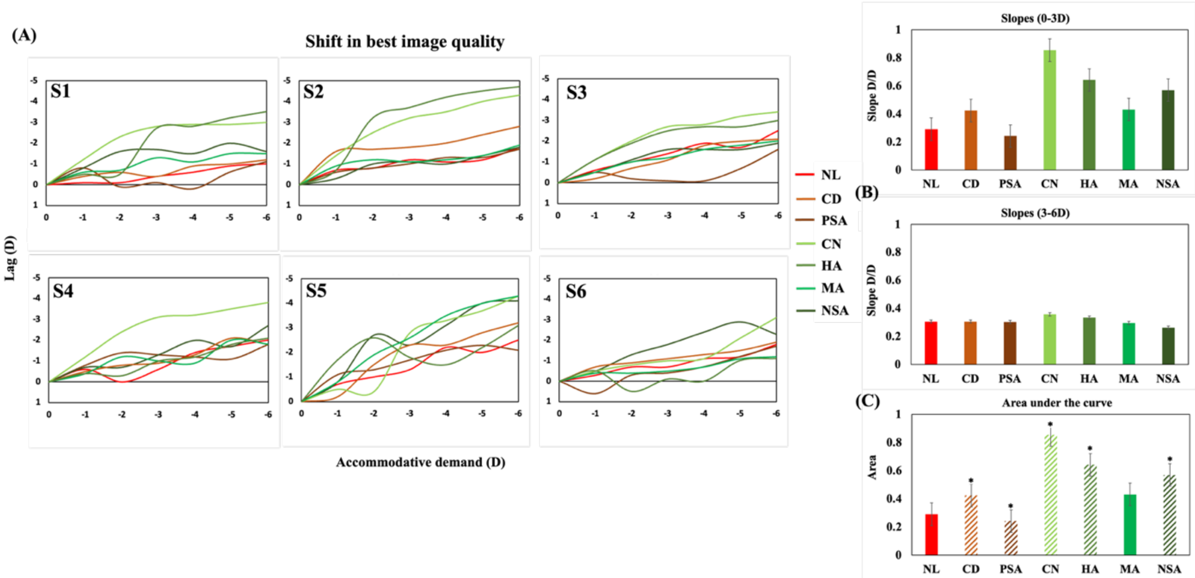

Figure 7. (A) Accommodative lag (defocus shift in best image quality) for all subjects and conditions. (B) Average Slope of Accommodative lag curves (top: 0-3D accommodative demand; bottom: 3-6 D accommodative demand). Red lines/bars represent NL; light brown represent CD; dark brown represent PSA; light green represent CN; bright green represent MA; olive green represent HA; darkest green represent NSA. Error bars stand for standard deviations across 5 repeated measurements.

6.4. Discussion

MCLs are one of the most frequently used strategies for the management of myopia progression. We studied the accommodation behavior in a small group of young myopic adult eyes with different simulated lens designs. We used a custom-developed AO Visual Simulator to (1) simulate various multifocal designs in the active AO elements of the system (SLM and DM); (2) present accommodating visual stimuli (on a DMD) through the simulated optics; (3) induce accommodative demands (using a Badal system) and (4) measure wave aberrations for different accommodative demands, from which the retinal image quality and accommodative lag were calculated. Simulating contact lenses, as opposed to having the subject wearing them on the eye had several advantages: (1) we were not restricted to contact lenses that are commercially available; (2) increased patient comfort and shorter experimental sessions, as the patient did not need to put contact lenses in an out; (3) the eye contribution to aberration measurements could be separated from the CL contribution, also preventing potential artifacts arising from measuring segmented lenses in a Hartmann Shack(265). In previous studies, we had demonstrated the equivalency of real and SLM-simulated lenses (203), in terms of through-focus visual acuity (236). In the current study we measure for the first time the accommodative response with the simulated lenses.

Our control condition (NL) can be compared to the existing literature on accommodation-related changes in spherical aberration and pupil diameter (as a function of accommodative demand). We found that in our subjects, pupil diameter decreased with accommodation at a rate of -0.19mm/D (NL), which agrees with prior studies (for example, -0.18mm/D from Plainis et al (293)). The higher rates reported in other studies (i.e., -0.35 mm/D from Gambra et al(132) or -0.45 mm/D by Alpern et al(298)) may arise from referring to rates as a function of accommodative response (and not demand). We did not find a constant trend across subjects and conditions as for the slope of change of pupil diameter with accommodation, although on average the PSA condition showed a higher slope. Surprisingly, we even found variations in the pupil diameter in the same subject across different lens designs for relaxed accommodation. These findings are consistent with previous literature reports. Gambra et al(132) reported changes in pupil diameter and slope of variation when subjects were accommodated through different patterns (positive or spherical aberration, corrected aberrations, or coma) mapped on a deformable mirror. Tarrant et al(299) observed large changes in pupil diameter following orthokeratology treatment (which induced positive spherical aberration), even in a non-accommodating condition, although in another study those authors did not find significant differences in pupil variation across single vision and multifocal contact lenses (241). On the other hand, Charman et al(300) found that accommodative miosis tended to be greater in subjects with a relatively low lag of accommodation, which according to the author's reasoning appeared counter-intuitive, as poor accommodators would benefit from a smaller pupil diameter to minimize retinal image blur. Differences in the specific definitions of accommodative miosis and accommodative aside between our work and Charman's, our data appear to support those findings. For example, S5 with large pupils and low accommodative miosis exhibits the larger accommodative lag, and conversely S1 and S6 with higher accommodative miosis exhibit lower accommodative lags, for the NL conditions. Therefore, our results appear to support Lowenfeld's (142) point that the pupillary constriction is independent of the accommodative response, and although generally occurring while accommodating, it is not driven by the other actors of the near triad (accommodation and convergence). The average trend in our data that higher pupillary constrictions slopes were found with the PSA condition, and the lowest with the HA and CN, which happen to be the conditions producing lower and higher lags respectively, is consistent with Charman et al(301) conclusion that subjects that were most successful at using blur information to achieve better responses also show most marked miosis.

Under natural conditions (NL), and in agreement with previous studies, SA in natural conditions shifted to more negative values with accommodation, at a rate of -0.006 μm/D on average for a constant pupil diameter, and -0.09 μm/D for natural pupil diameter, which are slightly lower than previous reports likely due to our smaller pupil diameters. When the SA was expressed in diopters to discount the effect of the pupil diameter (-0.174 D/D), the rate of variation was comparable to other studies some of them analyzing the change as a function of accommodative response and others as a function of accommodative demand (−0.153 D/D in Gambra et al(132), −0.184 D/D in Cheng et al(302)., −0.230 D/D in He et al(303)., and −0.170 D/D in Plainis et al(293). The specific experimental configuration using an AO system allowed us to directly assess the changes in SA occurring at the crystalline lens level. By comparing the SA of the eye alone across the different conditions we could assess whether the presence of a multifocal lens pattern produced changes in the physical changes undergone by the crystalline lens, taking the SA as a marker of the accommodative-related changes in lens shape. To make all conditions directly comparable we kept the pupil diameter constant across conditions. Gambra et al(132) in a previous study using AO performed a comparative analysis and concluded that the lens accommodated quite similarly under natural conditions than through induced positive or negative SA, although there were some consistent trends of the induced SA conditions producing more negative SA in the lens at a constant pupil diameter. Our results show a consistently larger shift of SA towards negative values with induced PSA aberration followed by CD, and the lowest shift for the NSA and CN conditions. Only S5 showed a high crystalline lens response (based on the SA negative changes) for NSA. Among all conditions, HA and MA appeared to produce the least activity in the crystalline lens. These results indicate that the accommodative mechanism (understood as the response of the crystalline lens to change its curvature/asphericity) responds differently to different multifocal lens designs, with center distance designs eliciting a larger response, and center near designs inhibiting those changes.

When SA-inducing patterns are added to the aberrations of the eye, the rate of change of SA with accommodation drastically changed (Fig. 5). In total agreement with Gambra et al(132), induction of positive SA (also CD in our study) produced steeper changes in SA towards negative values with accommodation, and conversely, induction of negative SA (and also CN, HA , and MA in our study) made SA shift relatively toward positive values with accommodation, when the combination of the eye's aberration, phase map representing the lenses, and the changes of the natural pupil were considered. The added SA that we report in combination with the eye's measured SA (Fig. 5) is that induced/measured in the DM for the SA-inducing conditions (PSA, NSA), an accurate estimation (-0.3/-0.25μm) for the HA and MA conditions mapped in the SLM, as we showed in previous work(203), and only an approximation for the segmented bifocal corrections (CN, CD), although the trends are consistent. It should be noted that the majority of studies in the literature characterize the optical aberrations of the eye+contact lens on the eye, and therefore intrinsically may suffer from a potential misrepresentation of the aberrations with bifocal/multifocal contact lenses that have sharp transitions between near and far(265). By decoupling the eye and the contact lens in the HS measurements in our AO system, therefore bypassing the multifocal profile, we circumvented this potential problem. Since for calculations of optical quality, we added the measured eye's aberrations and the phase maps (Fig. 1) we did not run into potential artifacts created by a Zernike representation of the bifocal/multifocal patterns.

Estimation of the accommodative lag is controversial, and recent literature suggests that the traditionally believed leads and lags of accommodation may be an artifact of the definition or measurement(304). As proposed by Tarrant et al(241), Plainis et al(293) , and Gambra et al(132) among others, we have used retinal image quality metric (and not Zernike defocus or paraxial defocus) in our estimates of accommodative lag. We used MTF-based metrics (volume under the MTF in a spatial frequency range and Visual Strehl) to estimate the defocus that optimizes the TF image quality for each accommodative demand. Both metrics resulted in similar defocus shifts. VS was used to estimate lag, as this metric has been identified as that showing the largest correspondence with visual acuity and used in refractive error calculations(215). We chose to illustrate the TF optical quality curves using the volume under the MTF metric to avoid normalization by the pupil diameter, which changed across measurements, making the maximum values of the VS noncomparable between accommodative demands. The use of retinal image quality metrics is particularly important in the study of the impact of multifocal lenses, as they introduce relatively large amounts of spherical aberration which interact with defocus, the eye's natural aberrations, and pupil diameter. Our results show that the lens design drastically contributes to the defocus shifts, resulting in large differences in the defocus shifts across lenses. Some studies assume no accommodative residuals at around 2D of accommodative demand, and accommodative leads for lower accommodative demands(132), however, in this study we set 0D of residual defocus (best focus) at infinity. In contrast with other studies, we did not consider leads of accommodation in 0 and lower accommodative demands. In our experimental setting, subjects searched for the best focus in the Badal system starting from a myopic defocus, and they did so individually for each lens design. While the presence of spherical aberration may shift the best focus from the NL condition, the identified best focus represents the refractive error for far (equivalent contact lens distant power of a multifocal lens). The Badal defocus that corrected refractive error at distance is considered the zero defocus, which previous literature (215) has shown to match the peak of the TF Strehl curves.

In this study, we found that CN designs consistently produce the largest accommodative lags, followed by the HA, MA, and NSA, while CD, and to a larger extent PSA produces the lowest lag of accommodation. In two subjects (S1 and S3), PSA drastically reduces accommodative lag with respect to the NL condition. Results from previous literature are inconclusive regarding the effect of multifocal contact lenses or treatments that induce spherical aberration on accommodative response. Some evidence indicates a reduced accommodative response (increased lag) over a range of vergences with multifocal contact lenses. center-near +1.5 D(305); center-near and center-distance with transition zones(167); center-near +2.5 D(306)). However, other studies have shown that children accommodate normally at near with a dual focus lens (173). In addition, several studies have investigated the effect of orthokeratology (a treatment that flattens the central cornea, therefore inducing positive spherical aberration). They consistently show an increase in accommodative amplitude and a decrease in accommodative lag in children and young adults(307), which is in good agreement with the results of our study. In contrast, a contact lens that incorporated negative spherical aberration (-0.1um, i, e, of a much lower magnitude that that of our study) was reported to reduce the lag, but only for a short period(308). In another study, a multifocal contact lens with positive spherical aberration reduced accommodative response at all distances, although surprisingly especially at far(302). Likely, that the variability across studies arises primarily from the definition and measurement protocol of accommodative response (as pointed out above), and from the differences across lens designs. In a recent publication Gifford et al (309)point out that it is the multifocal lens design and not the addition power that drives the accommodative response. In another study, the presence of large transition zones appeared to be the major driver for accommodation to intermediate distances(167) Theoretical modeling based on interactions between lens design and the eye's optics, predicted the accommodative response with dual-focus lenses of different powers and zone distributions and concluded the need to customize the design and correction to increase accommodation accuracy(310). Despite inter-study and inter-subject differences in the accommodative response through multifocal lenses, studies investigating their impact on myopia progression generally conclude that there is a correlation between lag and progression, and more importantly, eyes that accurately accommodated with the contact lens had reduced progression, whereas the myopia control failed in patients or with designs that reduced the accommodative response, likely because the subject used the near add for near vision, leaving the retina exposed to hyperopic defocus. Some authors have proposed the use of biofeedback strategies to train subjects to accommodate with existing multifocal contact lenses(311). Alternatively, one could propose improved lens designs that generally (or even customized to the individual subject) may reduce accommodative lag. Customizable parameters for these lenses could include, but not be limited to, near-far zone distribution, the diameter of the central zone, the extent of transition zones, segmented vs smooth transitions, and incorporation of other high-order aberrations beyond spherical aberration. Adaptive Optics makes an ideal tool for conducting studies to investigate visual performance, and more specifically, the accommodating response with different lens designs, as demonstrated in the current study. If, as suggested by multiple studies, the accommodative behavior with these lenses is, to some extent, a marker of prediction of the success of certain contact lenses to control myopia in a subject, these AO visual simulations could be essential to select the most appropriate treatment for a patient.

Despite the advantages of the visual simulator to simulate multifocal contact lens designs and test accommodation, some aspects of the system may lead to some results bias, likely overcome by the fact that the same patient is tested under identical conditions. To avoid chromatic artifacts associated with the SLM, which is normally only programmed for one wavelength, we used a monochromatic stimulus. Although the role of chromatic defocus to drive the accommodative response may not be as critical as anticipated in some studies(312,313), measurements in polychromatic light would capture performance in the natural world with more fidelity. Also, in our study, the stimuli are presented monocularly and vergence was induced by a Badal system (no change in magnification; no proximity cues), therefore isolating blur cues from other cues to drive accommodation. Binocular measurements (which should involve not only aberration/accommodation measurements but also a binocular simulation of the lens designs)(198,314,315) would again provide a more realistic environment integrating all available cues in a natural world. The success at interpreting proximity from defocus blur is likely inherent to the subject, whereas other subjects may rely habitually upon binocular or proximity cues to drive their accommodation, making a comparison of performance across lens designs direct. However, we cannot rule out that some lens designs interact with a given accommodative trigger mechanism, as suggested by the differences between binocular and monocular measurements with multifocal contact lenses with large transition zones in a recent study(167).

6.5 Conclusions

In summary, the present study shows that positive spherical aberration-inducing conditions (CD, PSA) produced lower accommodative lag in comparison with other conditions in all the subjects. Factors such as pupil size, multifocal lens design, native aberrations of the eye, amount of spherical aberration induced should be considered in the management of myopia with MCLs and to gain insights into the mechanism of operation of these lenses. Future studies may include a larger sample of patients, binocular simulations, and a systematic study of lens designs parameters on the accommodative response. Studies in Adaptive Optics visual simulators are an important step before manufacturing specific contact lenses and fitting them on eyes, to assess additional effects such as tear film, lens-cornea interactions or fitting parameters, or lens decentration among others).

In this chapter, the impact of simulated multifocal contact lenses of different designs on the accommodative response has been studied. In the next chapter, we studied the accommodative responses and visual performance in the fovea and the periphery with multifocal contact lenses in a clinical environment.

CHAPTER-7. FOVEAL AND PERIPHERAL VISUAL QUALITY AND ACCOMMODATION WITH MULTIFOCAL CONTACT LENSES

Accommodation as well as foveal and peripheral vision in young myopic eyes can be affected by multifocality. This chapter presents the short-term effects of multifocal contact lenses on foveal and peripheral vision. The investigated multifocal contact lenses were the MiSight contact lenses designed for myopia control and the Acuvue Moist contact lenses.

This chapter reproduces the paper by Papadogiannis et al. “Foveal and Peripheral visual quality and accommodation with multifocal contact lenses” published in the Journal of the Optical Society of America A (2022). The co-authors are Dmitry Romashchenko, Shrilekha Vedhakrishnan, Britta Persson, Anna Lindskoog Petterson, Susana Marcos , and Linda Lundström from KTH, Stockholm (Sweden).

This work was presented as an oral presentation at the International Myopia Conference, Tokyo in 2019 under the title “Central and Peripheral Visual Quality and Accommodation with Multifocal Contact Lenses”.

The author of this thesis implemented the experimental procedure in collaboration with Petros Papadogiannis and Linda Lundström, performed the experimental measurements on subjects, collected the data in collaboration with Petros Papadogiannis. Prepared the manuscript in collaboration with Petros Papadogiannis, Dmitry Romashchenko, Susana Marcos , and Linda Lundström.

7.1 Introduction

Myopia prevalence has increased significantly over the world in recent years, and the World Health Organization (WHO) predicts that by 2050, 50% of the world's population will be myopic, with 10% being severely myopic (316). Myopes have an increased risk of developing myopic maculopathy(317), retinal detachment(318), cataracts (319) , and glaucoma(320), and thus there is a growing need to decrease myopia progression. A relation between the early onset of myopia and high myopia in adult life has been studied previously(321,322), therefore it is important to control the progression of myopia at an early stage. Although it has not yet been well understood, the two most considered environmental causes for myopia progression are peripheral image quality and lag of accommodation.

However, animal investigations have revealed that the peripheral retina is equally crucial for controlling eye growth. Peripheral image quality can influence ocular growth even in the presence of a clear foveal picture, contrary to the initial belief that only foveal optical defects regulated eye growth(323,324). There are two theories about how peripheral vision affects myopia, both of which are based on extensive animal experiments. The first theory holds that peripheral hypermetropic defocus in the human eye can speed up eye development, and the second holds that optical adjustments that either get rid of peripheral hypermetropic defocus or result in myopic peripheral defocus might reduce the advancement of myopia (325–328). Based on the correlations between underaccommodation and accelerated advancement of myopia, another possible cause of myopia is hypothesized. The eye frequently accommodates less than what is required to focus on the target while viewing distant targets through negative power lenses or when watching close-by targets. The term "lag of accommodation" refers to this underaccommodation (hypermetropic retinal defocus). The onset and progression of myopia have been linked to a larger lag in accommodation during close work (329,330). Additionally, when compared to age-matched emmetropes, myopic children and young adults exhibit greater variability in accommodative response, decreased accommodative facility, and increased accommodative convergence (elevated AC/A ratios) (331).

Many interventions, including pharmaceutical and optical methods, aim to control myopia progression: Atropine in low concentration(332); Orthokeratology rigid contact lenses(333–335); Bifocals and progressive addition spectacles(336–338); and Multifocal soft contact lenses. This study focuses on multifocal contact lenses, a technique for treating myopia that is becoming more and more common. The idea behind this intervention is that by providing two images at once—one focused on the retina and the other in front of it to produce a myopic blur—when gazing at a distant object and relaxing accommodation, a center distance (CD) design limits the progression of myopia. Such multifocal designs, nevertheless, would result in significant irregular optical aberrations in peripheral angles, which may have a greater impact on the depth of focus than peripheral refractive error (339). Furthermore, the effective properties are not yet understood, and the treatment varies across individuals(340). This could be because multifocality can affect both accommodation and the foveal and peripheral image quality(339–342). Numerous earlier research investigated how one commercially available CD contact lens design (MiSight) affected foveal optics, vision, and accommodation, but they did not compare the findings to side effects (343–345). Due to this, it is impossible to determine whether the reduced myopia progression with these multifocal lenses is the result of their impact on accommodation or on the quality of peripheral vision. The short-term impact of MiSight multifocal contact lenses on accommodation as well as foveal and peripheral optical and visual quality will therefore be examined in this study. In addition to combining foveal and peripheral wavefront aberration data obtained during vision exams, the goal is to understand how these lenses compare to conventional glasses in terms of their impact on accommodation and peripheral image quality. The same measurements were made using a common multifocal contact lens with the opposite design, i.e., center near (CN), used for presbyopia, to uncover changes in attributes that are especially associated with myopia control (Acuvue Moist).

7.2. Methods

7.2.1 Subjects and Contact Lenses

Eight myopes, aged 22 to 40 years, with refractive states between -1.50 and -7.00 diopters (D), took part in this investigation (more details in Table 1). Each patient was an experienced contact lens wearer with good eye health. The assessments the individuals underwent were separated into two sections: monocular clinical accommodation assessments and monocular low-contrast vision evaluations, with three different forms of optical correction measured in the order listed below:

a) Spectacles (subject's spectacles were used) (control)

b) MiSight® 1-day (CooperVision)

c) Acuvue® Moist 1-day (Johnson & Johnson)

The MiSight contact lens is a multifocal lens with +2.00 D treatment zones and a center-distance (CD) design. It has been demonstrated to slow down the progression of myopia in children by correcting the myopic refractive defect while displaying a myopically defocused image(343–345). The power profile of a MiSight contact lens with a nominal power of -3.00 D is shown in Figure 1.

The center-near (CN) Acuvue Moist contact lens is a multifocal contact lens intended to treat presbyopia. It provides sharp near vision while correcting myopia or hypermetropia because of the additional power provided by the lens profile. The smooth Acuvue Moist multifocal contact lens has increasingly greater negative power as one move's radially from the center out toward the borders of the lens. It is offered in low, mid, and high adds. The lens utilized in this study has a high add of +2.50 D.

Before beginning the measurements, the contact lens fitting was validated using a slit lamp in accordance with clinical standards to make sure the lens was sitting properly on the subject's eye. The subjects were given some time to become used to the contact lenses before the measurements began when they were at ease. All measurements were conducted with real pupils. The subjects gave their signed, informed consent before the experiment. The study met the requirements of the Declaration of Helsinki and received approval from the Swedish Ethical Review Authority.

Subject	Age	Habitual Spectacle power	MiSight /Acuvue Moist power
S1	26	-7.00/-0.25*160°	-6.00
S2	26	-1.75	-1.75
S3	22	-3.50	-3.50
S4	28	-2.50	-2.50
S5	26	-3.25/-0.50*75°	-3.50
S6	25	-4.50/-0.50*150°	-4.25

S7	40	-1.75/-0.50*140°	-2.00
S8	27	-1.50	-1.50

Table 1. The power of the contact lens that was worn in D, the subjects' age, and their regular eyeglass power in D. As there were no greater powers to purchase, a -6.00 D contact lens was used for subject 1 for both MiSight and Acuvue Moist. Spectacles are used to sort subjects based on how accommodating they are (from minimum to maximum, see Fig 4).

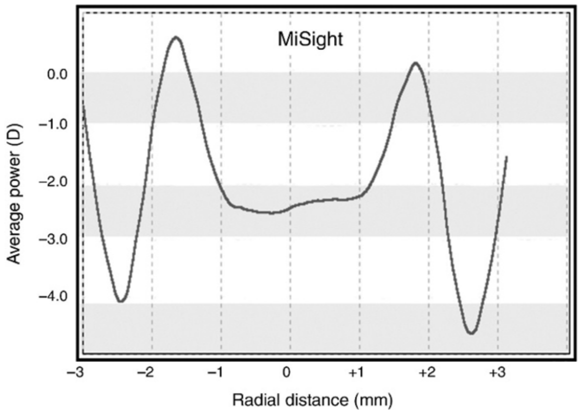

Figure 1. The MiSight contact lens's power profile for controlling myopia. The nominal power of the offered contact lens is -3.00 D. The horizontal bands represent steps of 1.00 D. from Javier Ruiz-Alcocer adopted (346)

Clinical visual function and accommodation evaluation

For the clinical visual function and accommodation evaluation, each of the three optical adjustments was applied to the examined eye one at a time, and the following measurements were taken monocularly: (the other eye was covered with an occluder) Distant and near high-contrast letter visual acuity (VA); Near point of accommodation (NPA); Accommodative facility (AF); Accommodative response (AR)

Most of the tests (near VA, NPA, AF, and AR) were carried out in normal room illumination (700 lux), except for the far VA test, which was carried out in significantly lower light (300 lux). Monocular foveal distant (4m) visual acuity of the individuals was evaluated using a high-contrast EDTRS visual acuity chart with letter sizes ranging from 1.0 to -0.3 logMAR. To test monocular foveal near vision, a high-contrast EDTRS chart with near visual acuity was used at a distance of 0.4 m. The subjects were instructed to read the chart's letters line by line until they became unable to distinguish between them. The Donder's Push-up and Pull-away tests were carried out, and a Royal Air Force (RAF) ruler was employed for monocular foveal NPA measurement. The 2.00 D flipper was used to measure the monocular foveal accommodative capability. The subjects had to concentrate on a row that was a little larger than their best vision for 30 seconds while holding a near vision acuity EDTRS chart at 0.4 m away under typical room lighting.

Monocular foveal AR measurements were performed using the Shin Nippon Natural Vision Auto Refractometer NVISION-K 5001. The participants were measured for refraction first when staring at a non-accommodative target at a distance of 4 m, and then again while gazing at a target that was 0.4 m away from the eye. The spherical equivalent at 4 meters minus the spherical equivalent at 0.4

meters was used to calculate the AR. Additionally, by utilizing the equations developed by Thibos et al (347)., astigmatism was transformed into power vectors. The clinical accommodation examination lasted roughly 1.5 hours. All measures were performed three times to prevent tiredness, and the average data were used for analysis.

7.2.1 Evaluation of image quality and low-contrast vision

A deformable mirror, a Hartmann-Shack (HS) wavefront sensor, and a monitor for stimulus presentation were employed in a lab adaptive optics (AO) setup for the second half of the experiment. The HS wavefront sensor live-captured the foveal and peripheral wavefront data during the experiment to do additional image quality assessments. The AO system functions in near-infrared light even though it is calibrated to measure in visible light. The Mirao 52 D deformable mirror (52 actuators, ±50 µm stroke, corrects up to sixth Zernike order, www.imagine-eyes.com) and the HASO wavefront sensor make up the AO system. This mirror was configured to exclusively provide static compensation for the AO system's internal aberrations (i.e., the AO part of the system was not running in a closed loop during the experiment). The system's specifics have already been disclosed by Rosén et al.(348).

All three conditions (a, b, and c; the beginning of the Methods section) were measured foveally and at the 20° nasal visual field for monocular low-contrast (10%) resolution acuity. The volunteers were asked to fixate on a Maltese cross mounted 2.6 meters distant while wavefront aberrations and peripheral acuity thresholds were assessed in either their right or left eye. The chin-forehead rest, an infrared camera for alignment, and an infrared camera were all used to track the subject's fixation during the experiment. To obtain a complete and precise pupil image, the subjects were changed as necessary.

The same approach as previously described was used to implement the psychophysical procedure in MATLAB and Psychophysics Toolbox to achieve the low-contrast resolution thresholds (349). It was decided to utilize the low-contrast resolution acuity task since it is not limited by neuronal sampling in the periphery but rather by optical features (350,351). Low-contrast (10%), oblique (-45° and 45°), Gabor gratings in a window with a Gaussian distribution and a standard deviation of 1.6° made up the stimulus pattern. To prevent any neuronal preferences brought on by the meridional effect, the gratings' oblique orientation was chosen(352). The size of the gratings on display was altered to take into consideration the spectacle magnification. With the help of Bayesian psychophysical methods, the gratings' spatial frequency was changed, and the acuity thresholds were determined. The participant was presented with the stimuli for 500 milliseconds on a calibrated CRT monitor at a distance of 2.6 meters before being required to pick between two possible orientations for the gratings. To make sure the subject was aware of the stimulus presentation, a sound cue was played at the start of each trial. After that, the participant had to press the correct key on a keypad in accordance with where the gratings were located. The guess rate and lapse rate were set to 50% and 5%, respectively when the stimulus was unclear. The subject was instructed to guess. It took 40 trials to evaluate the acuity, and the subjects were not given feedback on whether or not their answers were right or wrong. After each assessment was performed three times, the average acuity values were chosen for further examination. The participants would rest after every third set to prevent getting too tired (or more frequently if necessary). Before the actual experiment, a trial round was conducted to ensure that the subject understood the process. The second stage of the trial, which assessed low-contrast vision, took each participant about 1.5 hours.

7.2.2 Data analysis

Wilcoxon paired-samples two-tailed signed-rank tests were used to compare multifocal contacts with spectacles (control). Bar plots were used to represent the individual data, and box-and-whiskers plots were used to show how the data was distributed. Box-and-whiskers plots have a central black line that represents the median, outside margins represent the interquartile range, whiskers represent the data outside the middle 50%, and dots represent outliers.

7.3 RESULTS

Assessments were made of the short-term effects on the foveal and peripheral vision of the MiSight and the Acuvue Moist multifocal contact lenses. It should be noted that some test subjects willingly reported that MiSight was substantially less comfortable than Acuvue Moist throughout the testing, both in terms of fitting and visual quality. The following bar graphs group the subjects according to how accommodating they are when wearing glasses (from minimum accommodative response to maximum accommodative response).

7.3.1 Clinical visual function and accommodation evaluation

Distant and near letter visual acuity

For near (0.4 m) and far (4 m), Figure 2 shows the monocular foveal letter-VA values. For distant VA, there was no statistically significant difference between the MiSight lenses and the control case ($p>0.05$), whereas the difference between Acuvue Moist lenses and the control case was statistically significant ($p<0.05$) as expected. Acuvue Moist lenses are used for presbyopia correction and the positive addition (+2.50D) degraded the distant vision of the subjects by 0.20 logMAR on average. For near vision there was no statistically significant difference ($p>0.05$) neither for MiSight versus control nor for Acuvue Moist versus control.

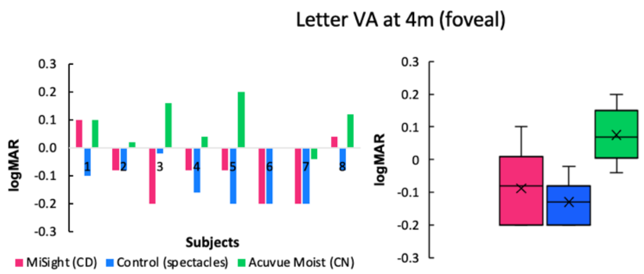

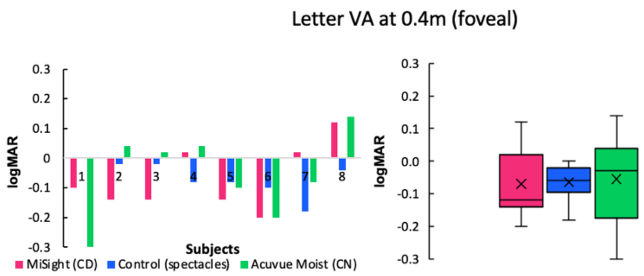

Figure 2. Foveal monocular near (0.4 m, bottom) and far (4 m, top) letter visual acuity in logMAR. Due to the fact that the subject 6 top left graph and the subject 1 bottom left graph to correlate to 0 logMAR, the bars are not visible in these graphs.

Near point of accommodation and accommodative facility

Fig. 3, the monocular NPA (in cm from the eye) and the accommodative facility (in cycles/minute) are presented. The subjects wearing their glasses and the subjects wearing contact lenses did not differ statistically significantly in terms of NPA (p>0.05). The MiSight design and the control for accommodating facilities did not differ statistically significantly (p>0.05). But a statistically significant difference was found between the Acuvue Moist multifocal and the control condition (p<0.05).

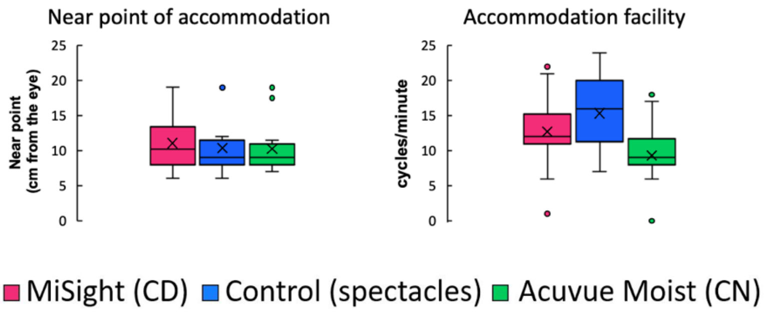

Figure 3. The Donder's Push-up test was used to estimate the monocular near point of accommodation in cm, and the 2.00 D flipper was used to measure the monocular accommodation facility in cycles/minute (right).

Accommodative response

Fig. 4 displays the change in accommodative response as determined by an open-field autorefractor. The accommodative response is calculated as the difference between the spherical equivalent at 4 m and the spherical equivalent at 0.4 m. Six out of the eight subjects experienced an accommodating response increase from the MiSight design compared to the control, but not considerably. When compared to the control, the Acuvue Moist design decreased the accommodative response by 1.00 D on average (statistically significant difference, p0.05).

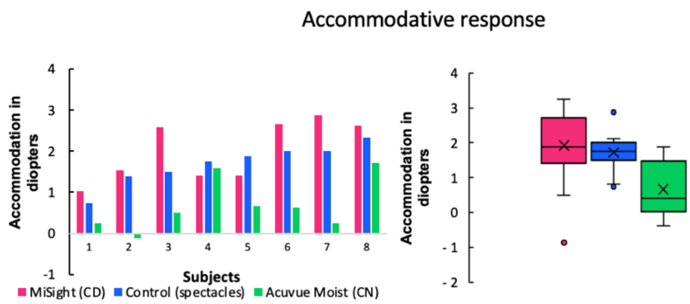

Figure 4. Using an open-field autorefractor, measure the diopter-based monocular accommodative response. The accommodative response is calculated as the difference between the sphere equivalent at 4 meters and the sphere equivalent at 0.4 meters.

Both multifocal designs induced astigmatism when measured in an autorefractor. The MiSight lenses increased the cylinder in all subjects, whereas Acuvue Moist lenses increased the cylinder in five out of eight subjects when compared with the control at 4m, with an average increase of 0.75D and 0.25D, respectively. There was also a change in cylinder with accommodation, as shown in Fig 5. The change is determined as the difference between the cylinder at 4m minus the cylinder at 0.4m, ignoring any change in the axis of the cylinder, a positive sign means an increase in cylinder with accommodation, whereas a negative sign indicates a decrease. For six of the eight subjects, the cylinder increased with accommodation up to approximately 1.50D with MiSight lenses, whereas the Acuvue Moist lenses showed smaller cylinders for most of the subjects.

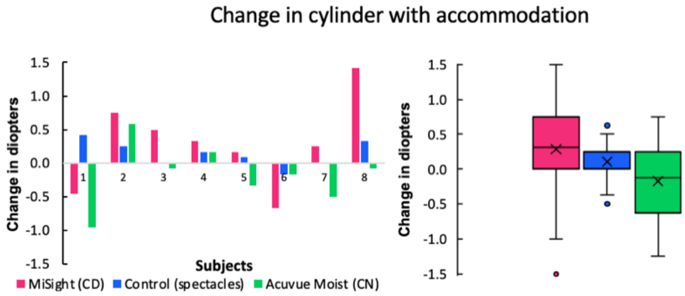

Figure 5. Using an open field autorefractor, the cylinder's monocular shift with accommodation is measured in diopters. By subtracting the cylinder at 0.4 m from the cylinder at 4 m, one may calculate the change in a cylinder with accommodation. Positive signs suggest growth while negative signs denote shrinkage in the cylinder. For subjects 3 and 7, the invisible bars are numbered 0 D.

The autorefractor's measured astigmatism was transformed to power vectors for statistical analysis, and Wilcoxon paired-samples two-tailed signed rank tests were used to compare astigmatism between groups. Table 2 lists the differences that were examined as well as the outcomes of the statistical analysis. On 3 out of 4 occasions, the MiSight lens displayed noticeably more negative values than the control.

J0 at 4 m	**p-value**
Control-MiSight (max diff = 0.62 D)	**p<0.05**
Control-Acuvue Moist	p>0.05
J45 at 4 m	
Control-MiSight (max diff = 0.48 D)	**p<0.05**
Control-Acuvue Moist	p>0.05
J0 at 0.4 m	
Control-MiSight	p>0.05
Control-Acuvue Moist	p>0.05
J45 at 0.4 m	
Control-MiSight (max diff = 0.64 D)	**p<0.05**
Control-Acuvue Moist	p>0.05

Table 2. Wilcoxon paired-samples two-tailed signed rank tests in astigmatism (power vectors)

The outcomes of the Wilcoxon signed rank tests with paired samples and two tails. The rows display the distinctions on which the statistical test was run. Statistically, significant differences are indicated by bold p-values. The maximum difference corresponds to the subject with the greatest difference in value.

7.3.2 Low-contrast vision evaluation

The thresholds for foveal and peripheral (20° nasal visual field) far vision is shown in Fig. 6 for low-contrast (10%) resolution gratings. The foveal resolution acuity decreased by 0.05 logMAR with the MiSight contact lenses when compared to the control, however, this difference was not statistically significant (p>0.05). With the Acuvue Moist, there was a significant (p<0.05) decline in foveal vision, with a mean difference of 0.13 logMAR on average from the control.

When compared to spectacle correction, the peripheral thresholds with MiSight lenses were reduced by 0.10 logMAR, whereas the thresholds with Acuvue Moist were similar to the control case.

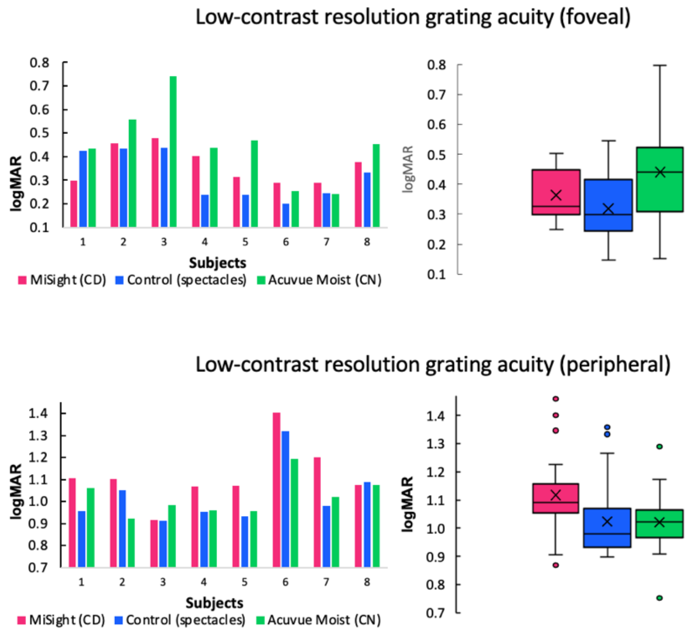

Figure 6. Foveal and peripheral (20° nasal visual field) monocular low-contrast (10%) resolution grating acuity thresholds in logMAR.

7.3.3 Wavefront analysis

For the three optical correction scenarios, Fig. 7 displays the largest foveal and peripheral Zernike coefficients (except for defocus) for a 4 mm pupil diameter. The signs of the coefficients for horizontal coma and oblique astigmatism were modified for the patients whose left eye was measured because the right and left eyes are mirror symmetric for on- and off-axis aberrations (353). Wilcoxon tests on the differences between the conditions (control-MiSight, control-Acuvue Moist) revealed that peripheral vertical astigmatism decreased for both MiSight and Acuvue Moist ($T+ \leq T0.10(2),8$, $p< 0.10$), while foveal horizontal coma showed a statistically significant increase for MiSight lenses ($T- \leq T0.10(2),8$, $p<0.10$).

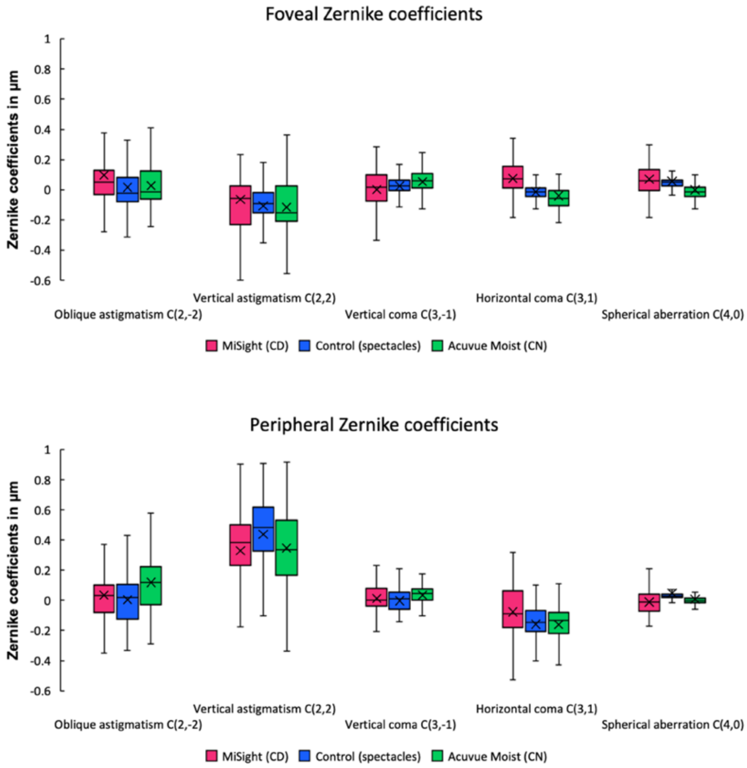

Figure 7. Foveal and peripheral (20° nasal visual field) changes in Zernike coefficients.

For each of the three circumstances, Table 3 shows the individuals' averaged relative peripheral refraction (RPR) over time. The RPR is defined as the difference between the peripheral refractive error minus the foveal refractive error. The refractive error was calculated from the wavefront using second (defocus), fourth (spherical aberration) and sixth (secondary spherical aberration) order Zernike coefficients with natural pupil size. Positive numbers imply a more hypermetropic peripheral in relation to the fovea, whereas negative values denote a more myopic periphery. The Acuvue Moist lenses and the spectacles had a statistically significant difference (p0.05), while there was no statistically significant difference between the MiSight lenses and the control (p>0.05).

Subject	MiSight	Spectacles	Acuvue Moist
S1	-0.60 D	0.37 D	0.87 D
S2	-1.75 D	0.00 D	1.20 D
S3	0.36 D	-0.19 D	0.25 D
S4	-0.48 D	-0.52 D	-0.51 D
S5	-2.81 D	0.33 D	0.88 D
S6	-1.09 D	-0.95 D	-1.01 D
S7	-0.01 D	-0.19 D	-0.05 D
S8	-0.13 D	0.02 D	0.28 D

Table 3. Relative Peripheral Refraction (RPR)

7.3.4 Foveal and peripheral image quality

The foveal and peripheral (20deg nasal visual field) modulation transfer functions (MTFs) were calculated for all subjects and conditions from the wavefront data gathered during the low-contrast vision evaluation. At = 550 nm, the MTFs for natural pupil size was measured. The elliptical pupil shape was taken into account for peripheral measurements using a cosine function (354). The median vs. maximum MTF values for subject 5 is displayed in Fig. 8. Generally, for all subjects except subject 4, the control case showed the best foveal MTF, followed by Acuvue Moist, MiSight which produced the worst foveal MTF. This trend was less clear in the periphery.

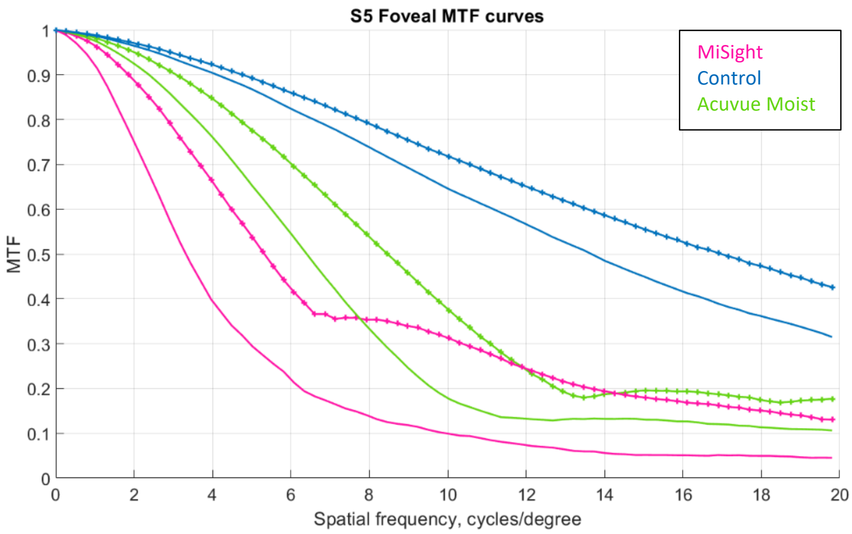

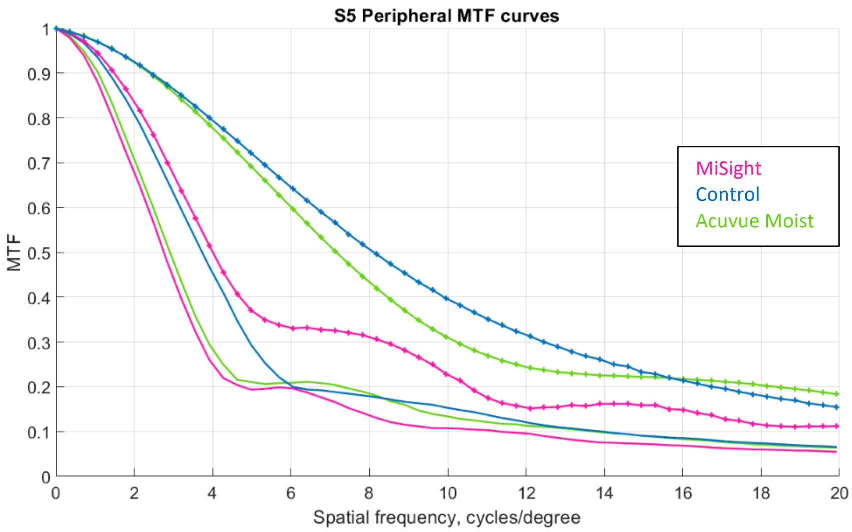

Figure 8. Monochromatic Modulation Transfer Function (MTF) curves for subject 5's natural pupil size at the fovea and peripheral (20° nasal viewing field). The depicted curves show the MTF values' maximum (dotted line) and median (solid line) values.

7.4 DISCUSSION

In this study, the short-term effects of two multifocal contact lenses on foveal and peripheral vision are investigated. The goal is to document changes in accommodation as well as the quality of the fovea and the peripheral vision, as these elements are regarded to be connected to the progression of myopia. The outcomes were compared to those of wearing spectacles, which is the most common method of myopia correction for children.

When compared to spectacles, MiSight contact lenses produced equivalent foveal vision quality for far and near, despite the significant reduction in peripheral low-contrast resolution acuity. While accommodating facility and NPA tended to drop in subjects who wore MiSight lenses, accommodating response increased in six out of eight of the subjects. The level of astigmatism and foveal coma was increased for all individuals. The peripheral low-contrast resolution acuity and foveal VA at 0.4 m of the Acuvue Moist multifocal significantly deteriorated the foveal visual quality as compared to spectacles, whereas these results were essentially the opposite. The astigmatism was equivalent to control from a distance as well as up close, even though the facility and accommodating response were considerably reduced. Notably, despite any potential learning effects, Acuvue Moist, the last lens tested, showed decreased foveal letter VA at 4 m.

In a recent study, Ruiz-Pomeda et al. showed no statistically significant difference between the MiSight group and the single-vision spectacles in terms of accommodation amplitude (MiSight: 13.88 3.58 D, spectacles: 12.40 2.55 D). The accommodative response for MiSight at 0.33 m (1.08 0.61 D) in the same research was comparable to that of single-vision glasses (1.24 0.75 D) (343). Gifford et al. young myopes wearing single vision contact lenses and four different types of multifocal contact lenses for myopia correction were compared for accommodative responses at five distances (including MiSight lenses). They discovered that single vision and MiSight contact lenses had comparable accommodative responses (slopes: 1.01 0.06 and 0.96 0.15, respectively), whereas the slopes for the other multifocal designs were roughly 0.84 0.15 (355). The current study's findings concur with those of Ruiz-Pomeda et al. and Gifford et al.; MiSight lenses did not significantly vary from control lenses in either the NPA or the accommodative response. Additionally, similar distant and near foveal VA was created by the MiSight contact lenses when compared to the control, supporting the earlier findings from Ruiz-Pomeda et al. and Chamberlain et al(345).

Sha et al. examined the visual effectiveness of four various contact lens models, including MiSight, for controlling myopia. When compared to two of the other designs, they discovered that participants wearing MiSight lenses had much inferior monocular adaptation facility (Prototype 1 and Prototype 2). While not statistically significant in the current study, the accommodation facility's MiSight performance was worse than that of its spectacle performance (MiSight 12.8 5 cycles/minute vs. spectacles 15.3 5 cycles/minute), but it was still better than the result of Sha et al. (MiSight 11.7 4.8 cycles/minute) (344). In the same study, the participants evaluated the four distinct designs and found that Prototypes 1 and 2 provided superior visual performance and ocular comfort than MiSight. Similar to the previous study, in the present one all subjects noticed visual problems when using MiSight lenses, whereas this was not the case when wearing Acuvue Moist lenses. The individuals specifically described feeling uneasy, decreased contrast, and mildly hampered near eyesight with ghost pictures. This might, however, be because the subjects did not have enough time to get used to the optics of the MiSight lenses. Despite the pain, when compared to wearing glasses, the subjects' foveal vision quality was not affected by the MiSight lenses. A possible reason for this is that the measurements of the foveal low-contrast resolution acuity were unaffected because the MiSight lenses diminish contrast for such low spatial frequencies.

Bakaraju et al. when the Shin-Nippon autorefractor and the COAS-HD aberrometer (HS sensor concept) for multifocal contact lenses measurements were compared, variations in J0 and J45 were discovered. For J0, they discovered that the autorefractor measurements were more favorable with the CD design while the COAS-HD readings were more favorable with the CN designs. Within both instruments, they discovered that mean deviations for J45 ranged from 0.10 D to 1.50 D (356).

During the examination of low-contrast vision in the current investigation, wavefront aberrations and MTF curves were continuously evaluated. The average changes in the MTFs for various situations should therefore match the observed pattern in low-contrast vision in the absence of long-term vision adaptation. Although this was true on a qualitative level, neither the fovea nor the periphery showed a direct quantitative correlation between the MTF and the logMAR values derived from the psychophysical methods. Although research from the past suggests that multifocal contact lenses can accurately quantify lower and higher order aberrations using Hartmann-Shack wavefront sensors (357), The research is complicated by artifacts like spots that double on the edge of the zones for multifocal contact lenses (358). To verify the correctness of the wavefront reconstruction, further foveal and peripheral wavefront measurements on patients S4 and S7 were performed in a lab-based dual-angle system. This made it possible to manually check the precision of the MTF curves (359). These verification measurements revealed no artifacts and the variations in the MTF curves for the various optical conditions matched those seen in the adaptive optics system. As a result, we concluded that the wavefront measurements were accurate and that the lack of a direct quantitative correlation could have been caused by the wavefront being measured constantly over time rather than just while the Gabor gratings were visible.

7.4.1 Possible properties for myopia control

Myopia-related peripheral blur has been shown in animal research to inhibit eye growth, and it is thought that myopia-related peripheral image quality also exists in humans (323,324,326,328). Children's myopia can be controlled with MiSight contact lenses, according to earlier studies (343,345) Even though the current study only included a small sample of adults, its findings demonstrate that this contact lens alters three aspects of the image quality that may be connected to myopia control.

The MiSight lenses' initial and most likely feature is a decrease in contrast in the periphery vision area. Despite the significant impact on peripheral vision, the wavefront measurements between the MiSight and the glasses did not clearly distinguish any difference in RPR (see Table 3). With this in mind, it may be concluded that the observed contrast loss in the visual field's periphery was not largely caused by defocus but rather a more complex pattern of higher-order aberrations. However, these higher-order aberrations lessen the contrast in the peripheral image while also bringing the depth of focus closer to the center. Therefore, we believe that it could be more efficient with a myopia control intervention that takes into account the peripheral optical errors of the individual eye. This may result in a smaller depth of focus and substantial contrast losses, even at lower RPR magnitudes. The MiSight lenses' increased astigmatism may be the second factor in myopia correction; greater astigmatism and coma result in a more asymmetric Point Spread Function, which the eye may use to more easily determine where an image is in relation to the retina. The third potential characteristic would be the stronger accommodative response displayed by some research participants (see Fig. 4); however, it is unclear whether this is due to the MiSight lenses decreased accommodative lag for a close or larger accommodative lead for far. The accommodating response would have resembled that of the Acuvue Moist lenses if the zones with extra power in the MiSight lens had been utilized by the eye as "reading glasses" during close vision.

It's vital to keep in mind that the same multifocal contact lens can have varied therapeutic effects on various people when it comes to controlling myopia. For example, the MiSight lens' treatment zones won't have the same impact on people with small pupils or in bright lighting compared to those with larger pupils or in darker lighting conditions. Figure 9 provides an illustration of this using the peripheral (20° nasal visual field) Hartmann-Shack spot diagrams of Subject 4 wearing the MiSight and Acuvue Moist contact lenses. While Acuvue Moist has a more homogenous appearance, MiSight's lens zones are more visible (the nonuniformity at the right edge of the picture is because of the optical-zone edge of the lens). The reason for this is that the MiSight lens has a more pronounced profile with alternate distant and near zones, whilst the Acuvue Moist lens has a more gradual change in power between near and distance zones (360).

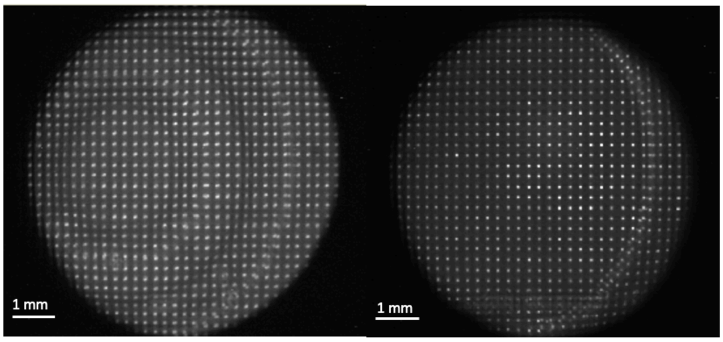

Figure 9. Spot diagrams were taken from Subject 3's Hartmann-Shack sensor at a 20° nasal visual field during the experiment. With 7.5 mm and 6.7 mm average pupil sizes, respectively, the MiSight lens is on the left side and the Acuvue Moist lens is on the right side.

7.5 Conclusion

Two multifocal contact lenses—the MiSight® 1-day center-distance (CD) contact lens (treatment zones +2.00 D, CooperVision) and the Acuvue® Moist 1-day center-near (CN) contact lens (high add +2.50 D, Johnson & Johnson)—were evaluated for their short-term effects on foveal and peripheral vision. In conclusion, MiSight lenses differed from spectacles with more astigmatism and coma, worsened peripheral low-contrast resolution acuity, and increased accommodative response. These variations could be a result of the MiSight lens's myopia management capabilities. It is noteworthy that the reduced peripheral low-contrast vision with the MiSight lenses was not because of a more myopic RPR, which is the common belief about the effect of these lenses. The Acuvue Moist lenses did not show the same astigmatism and peripheral vision that the glasses did, but they did produce greater hypermetropic RPR and less foveal and accommodative response. In spite of this, subjects reported Acuvue Moist as being more comfortable than MiSight. The most likely treatment property for myopia control by the MiSight lenses is the contrast reduction in the peripheral visual field and the changed accommodation. It is interesting to note that the magnitude of the induced peripheral blur is not caused by pure defocus but is still large enough to reduce peripheral visual function even more compared with the already quite poor peripheral image quality produced by the off-axis angle through the spectacles and the natural optics of the eye (361). Daily activities requiring peripheral vision, like detection, orientation, and movement, may be hampered by a decrease in peripheral image quality on this scale. The findings may be crucial in the effort to comprehend and enhance myopia control strategies.

CHAPTER-8. CONCLUSIONS

Achievements

The main accomplishments of this thesis are:

⇒ The calibration and implementation of the studies on existing AO visual simulators, adapting the setting and experimental protocols to the study of multifocal contact lenses

⇒ The development of methods to analyze and evaluate the through-focus visual acuity responses with the multifocal design in comparison with the control condition in presbyopes and young myopes

⇒ The development of methods to evaluate the contact lens profile on the eye and its potential conformity to the cornea using an Anterior Segment Optical Coherence Tomography (AS-OCT)

⇒ Successful reproduction of multifocal contact lenses of different additions (Low, Medium, High) in a Spatial Light Modulator (SLM), and spherical aberration-induced profiles in a Deformable Mirror (DM)

⇒ The implementation of a protocol for objective measurements of the accommodative response of the eye (bypassing the simulated contact lens) and of the eye+simulated contact lens, using retinal image quality-based metrics.

⇒ The study of the effect of myopia control (MiSight) contact lenses on accommodation and on foveal and peripheral image quality and compared them to spectacles

⇒ Ability to handle different optical systems with different complexity and different approaches to developing the projects described in this thesis.

Specific conclusions

(1) The overall visual performance was better in the young adult group than the presbyopic group with the same multifocal design (center-near) for all additions. In comparison with NoLens, there was an improvement in near vision in the young adult group with paralyzed accommodation while in the presbyopic group, there was a benefit for near with both paralyzed and natural accommodation with a consistent degradation at far for all conditions in both groups

(2) Visual simulators are useful tools to predict visual performance with multifocal lenses. The spatial light modulator was able to capture the through-focus visual performance of the MCLs in all subjects. It allowed the testing of multiple designs and additions of lenses at the same time

(3) We found that, overall, soft MCLs conform to the underlying cornea, both in the central addition area and in the periphery. However, the near central add is provided as expected

(4) The optical aberrations of the eye interact with the contact lens design, and therefore intrinsically may suffer a potential misrepresentation of the aberrations with bifocal/multifocal contact lenses that have sharp transitions between near and far.

(5) Positive spherical aberration inducing conditions (center-distance pure bifocal design and smooth positive spherical aberration design) produced a lower accommodative lag in comparison with other designs in all subjects

(6) Myopia-controlling MiSight lenses produced a foveal response very similar to spectacle lenses while producing a reduced contrast in the peripheral visual field as a likely treatment property for myopia control and changed accommodative response

Scientific Activities during this thesis

Scientific Publications

1. **Vedhakrishnan S**, Vinas M, Benedi-Garcia C, Casado P, Marcos S. Visual performance with multifocal lenses in young adults and presbyopes. PLoS One. 2022;17(3 March).

2. **Vedhakrishnan S**, Vinas M, Aissati S, Marcos S. Vision with spatial light modulator simulating multifocal contact lenses in an adaptive optics system. Biomed Opt Express. 2021;12(5).

3. **Vedhakrishnan S**, Castro A, Vinas M, Aissati S, Marcos S. Accommodation through simulated multifocal optics. Biomed Opt Express, 2022

4. S. Marcos, C. Benedí-García, S. Aissati, A. M. Gonzalez-Ramos, C. M. Lago, A. Radhkrishnan, M. Romero, **S. Vedhakrishnan**, L. Sawides, and M. Vinas, "VioBio lab adaptive optics: technology and applications by women vision scientists," Ophthalmic Physiol Opt 40, 75-87 (2020).

5. P Papadogiannis, D Romashchenko, **S Vedhakrishnan**, B Persson, A Lindskoog Pettersson, S Marcos, and L Lundström, "Foveal and peripheral visual quality and accommodation with multifocal contact lenses," J. Opt. Soc. Am. A 39, B39-B49 (2022)

Scientific Publications in conference abstracts and proceedings

1. **Vedhakrishnan S**, Vinas M, Aissati S, Benedi Garcia C, Romero M, Gonzalez-Ramos A, Dorronsoro C, Marcos S; Adaptive-optics vision simulation of multifocal lenses for myopia progression. Invest. Ophthalmol. Vis. Sci. 2019;60(9):605

2. María González Ramos A, **Vedhakrishnan S**, Marcos S, Martinez-Enriquez E; OCT-based quantification of multifocal contact lenses on eye. Invest. Ophthalmol. Vis. Sci. 2022;63(7):1817 – F0433.

3. Marcos S, **Vedhakrishnan S**, Benedi-Garcia C, Sawides L, Dorronsoro C, De Castro A, Vinas M; Optical performance with multifocal contact lenses. Invest. Ophthalmol. Vis. Sci. 2020;61(7):845.

4. **Vedhakrishnan S**, Vinas M, Casado Moreno P, Benedi-Garcia C, Dorronsoro C, Marcos S; Vision with Multifocal contact lenses in Myopes and Presbyopes. Invest. Ophthalmol. Vis. Sci. 2020;61(7):551.

5. **Vedhakrishnan S**, De Castro A, Vinas M, Aissati S, Marcos S; Accommodation with simulated contact lenses in Myopes. Invest. Ophthalmol. Vis. Sci. 2022;63(7):3063 – F0535.

Conferences

Personally presented

(authors are indicated by signature order, p=poster, t=talk)

2022-p	**Vedhakrishnan S**, De Castro A, Vinas M, Aissati S, Marcos S; Accommodation with simulated contact lenses in Myopes. ARVO 2022, Denver, CO, USA
2022-t	**Vedhakrishnan S**, De Castro A, Vinas M, Marcos S; AO Visual Simulators to test multifocal contact lenses for Myopia control. OPTICA Vision and Color Summer Blast!, Applications of AO visual simulators
2020-t	**Vedhakrishnan S**, Vinas M, Casado Moreno P, Benedi-Garcia C, Dorronsoro C, Marcos S; Vision with Multifocal contact lenses in Myopes and Presbyopes. ARVO 2020 (virtual), Baltimore, USA
2019-t	**Vedhakrishnan S**, Vinas M, Aissati S, Marcos S; Optical and Visual quality with multifocal contact lenses, PhDay-FOO, PhD in optics, optometry and vision, School of Optics and Optometry, Complutense University of Madrid.
2019-p	**Vedhakrishnan S**, Vinas M, Aissati S, Benedi Garcia C, Romero M, Gonzalez-Ramos A, Dorronsoro C, Marcos S; Adaptive-optics vision simulation of multifocal lenses for myopia progression, ARVO 2019, Vancuover, Canada
2018-t	**Vedhakrishnan S**, Vinas M, M Romero, Marcos S; Visual Simulations of Bifocal contact lens patterns in young myopic adults for myopia progression control, VPO 2018, Athens, Greece
2018-t	**Vedhakrishnan S**, Vinas M, Aissati S, Benedi Garcia C, Romero M, Gonzalez-Ramos A, Dorronsoro C, Marcos S; Adaptive-optics vision simulation of multifocal lenses for myopia progression control, PhDay-FOO, PhD in optics, optometry and vision, School of Optics and Optometry, Complutense University of Madrid.

Presented by Colloborators

(authors are indicated by signature order, p=poster, t=talk)

2022-p	María González Ramos A, **Vedhakrishnan S**, Marcos S, Martinez-Enriquez E; OCT-based quantification of multifocal contact lenses on eye, ARVO 2022, New Orleans, USA
2021-t	María González Ramos A, **Vedhakrishnan S**, Marcos S, Martinez-Enriquez E; In vivo assessment of multifocal contact lens fitting from optical coherence tomography images of the anterior segment of the eye, RNO 2021, Madrid, Spain
2020-t	Marcos S, **Vedhakrishnan S**, Benedi-Garcia C, Sawides L, Dorronsoro C, De Castro A, Vinas M; Optical performance with multifocal contact lenses, ARVO 2020 , (virtual), Baltimore, USA
2019-t	Lundstorm L, Papadogiannis P, **Vedhakrishnan S**, Romashchenko, Persson B, Lindskoog Petterson A, Marcos S, Central and Peripheral visual quality and accommodation with multifocal contact lenses, 17th International Myopia Conference, Tokyo

Invited talks

2022	**Vedhakrishnan S**, De Castro A, Vinas M, Marcos S; AO Visual Simulators to test multifocal contact lenses for Myopia control. OPTICA Vision and Color Summer Blast!, Applications of AO visual simulators

Visits and stays in research institutions

2018	Laboratory de Optica, Universisty of Murcia (LOUM), Murcia, Spain. Advisor: Prof. Pablo Artal; founding director of the Center for Research in Optics and Nanophysics at Murcia University. Short stay funded as part of the Marie-Curie, MYFUN program
2019	University of KTH, Department of Biomedical and X-ray Physics. Advisor: Prof. Linda Lundström; Professor in Applied physics. Short stay funded as part of the Mari-Curie, MYFUN program
2022	Publication in collaboration with University of KTH short stay – P Papadogiannis, D Romashchenko, **S Vedhakrishnan**, B Persson, A Lindskoog Pettersson, S Marcos, and L Lundström, "Foveal and peripheral visual quality and accommodation with multifocal contact lenses," J. Opt. Soc. Am. A 39, B39-B49 (2022)

Other Scientific activities

2018- today	Member of the IO-CSIC Student Chapter of the Optical Society of America (IOSA, https://sites.google.com/view/iosa-student-chapter-csic/) Member in developing a website including all the scientific chapter We organize scientific seminars as part of the IOSA student chapter, We organize workshops for local community and in educational centers. Have participated in the events of "Week of Science" or the "International Day of Women and Girls in Science 11F". Funded by OSA recently known as OPTICA
2019-2022	Member of the network of PhD students of the CSIC.RED de Doctorand@s
2019,2021	Member of the Organizing committee of the editions of IOSA scientific seminars Organized by IOSA at the Institute of Optics of the Spanish National Research Council (CSIC) Madrid, Spain
2018-2019	Clinical Practice training, Communication and presentation skills development, career development programs, organized by the MYFUN Marie-Curie program, Tubingen, Germany

References

REFERENCES

1. Quinn PMJ, Wijnholds J. Retinogenesis of the human fetal retina: An apical polarity perspective. Vol. 10, Genes. 2019.
2. Atchison DA. Optics of the human eye. In: Encyclopedia of Modern Optics. 2018.
3. Land MF. The human eye: Structure and function. Nat Med. 1999;5(11).
4. Kandel ER, Schwartz JH, Jessell TM. Principles of Neural Science, fourth addition. McGraw-Hill Companies. 2000;4.
5. Curcio CA, Allen KA. Topography of ganglion cells in human retina. Journal of Comparative Neurology. 1990;300(1).
6. Curcio CA, Sloan KR, Kalina RE, Hendrickson AE. Human photoreceptor topography. Journal of Comparative Neurology. 1990;292(4).
7. Dartnall HJA, Bowmaker JK, Mollon JD. Human visual pigments: Microspectrophotometric results from the eyes of seven persons. Vol. 220, Proceedings of the Royal Society of London - Biological Sciences. 1983.
8. The directional sensitivity of the retina and the spectral sensitivities of the rods and cones. Proc R Soc Lond B Biol Sci. 1939;127(846).
9. Stiles WS, Crawford BH. Luminous efficiency of rays entering the eye pupil at different points [4]. Vol. 139, Nature. 1937.
10. Hansen G. Zur Kenntnis des physiologischen Apertur-Farbeffektes Stiles-Crawford-Effekt II. Art. Naturwissenschaften. 1943;31(35–36).
11. Lin FC, Zao JK, Tu KC, Wang Y, Huang YP, Chuang CW, et al. SNR analysis of high-frequency steady-state visual evoked potentials from the foveal and extrafoveal regions of Human Retina. In: Proceedings of the Annual International Conference of the IEEE Engineering in Medicine and Biology Society, EMBS. 2012.
12. HUBEL DH. THE VISUAL CORTEX OF THE BRAIN. Sci Am. 1963;209.
13. Khonsary S. Guyton and Hall: Textbook of Medical Physiology. Surg Neurol Int. 2017;8(1).
14. Hart RW, Farrell RA. Light scattering in the cornea. J Opt Soc Am. 1969;59(6).
15. Morgan MJ, Watt RJ. Mechanisms of interpolation in human spatial vision. Nature. 1982;299(5883).
16. Amano S, Amano Y, Yamagami S, Miyai T, Miyata K, Samejima T, et al. Age-related changes in corneal and ocular higher-order wavefront aberrations. Am J Ophthalmol. 2004;137(6).

17. Guirao A, González C, Redondo M, Geraghty E, Norrby S, Artal P. Average optical performance of the human eye as a function of age in a normal population. Invest Ophthalmol Vis Sci. 1999;40(1).

18. Liang J, Williams DR. Aberrations and retinal image quality of the normal human eye. Journal of the Optical Society of America A. 1997;14(11).

19. Thibos LN, Hong X, Bradley A, Cheng X. Statistical variation of aberration structure and image quality in a normal population of healthy eyes. Journal of the Optical Society of America A. 2002;19(12).

20. Howland HC. High order wave aberration of eyes. Ophthalmic and Physiological Optics. 2002;22(5).

21. Llorente L, Barbero S, Cano D, Dorronsoro C, Marcos S. Myopic versus hyperopic eyes: Axial length, corneal shape and optical aberrations. J Vis. 2004;4(4).

22. Guirao A, Williams DR, MacRae SM. Effect of beam size on the expected benefit of customized laser refractive surgery. Journal of Refractive Surgery. 2003;19(1).

23. Cheng X, Bradley A, Hong X, Thibos LN. Relationship between refractive error and monochromatic aberrations of the eye. Optometry and Vision Science. 2003;80(1).

24. Burns SA. The spatially resolved refractometer. In: Journal of Refractive Surgery. 2000.

25. Atchison DA, Collins MJ, Wildsoet CF, Christensen J, Waterworth MD. Measurement of monochromatic ocular aberrations of human eyes as a function of accommodation by the howland aberroscope technique. Vision Res. 1995;35(3).

26. Navarro R, Williams DR, Artal P. Modulation transfer of the human eye as a function of retinal eccentricity. Journal of the Optical Society of America A. 1993;10(2).

27. Escudero-Sanz I, Navarro R. Off-axis aberrations of a wide-angle schematic eye model. Journal of the Optical Society of America A. 1999;16(8).

28. Guirao A, Artal P. Off-axis monochromatic aberrations estimated from double pass measurements in the human eye. Vision Res. 1999;39(2).

29. Peña MV. Polychromatic adaptive optics to evaluate the impact of manipulated optics on vision. In 2015.

30. CHARMAN WN. Wave-Front Aberration of the Eye - a Review. Vol. 68, Optometry and Vision Science. 1991.

31. Born M, Wolf E, Bhatia AB, Clemmow PC, Gabor D, Stokes AR, et al. Principles of Optics. Principles of Optics. 1999.

32. Thibos LN, Applegate RA, Schwiegerling JT, Webb R. Standards for reporting the optical aberrations of eyes. In: Journal of Refractive Surgery. 2002.

33. Lamont A, Millodot M, Leibowitz HW, Johnson CA. Dioptrics of the periphery of the eye. Science (1979). 1973;182(4107).

34. Smirnov MS. Measurement of the wave aberration of the human eye. Biophysics (Oxf). 1961;6(5–6).

35. Llorente L, Diaz-Santana L, Lara-Saucedo D, Marcos S. Aberrations of the human eye in visible and near infrared illumination. Optometry and Vision Science. 2003;80(1).

36. Marcos S, Moreno E, Navarro R. The depth-of-field of the human eye from objective and subjective measurements. Vision Res. 1999;39(12).

37. Howarth PA, Bradley A. The longitudinal chromatic aberration of the human eye, and its correction. Vision Res. 1986;26(2).

38. Thibos LN, Ye M, Zhang X, Bradley A. The chromatic eye: a new reduced-eye model of ocular chromatic aberration in humans. Appl Opt. 1992;31(19).

39. Howarth PA. THE LATERAL CHROMATIC ABERRATION OF THE EYE. Ophthalmic and Physiological Optics. 1984;4(3).

40. Millodot M. Effect of ametropia on peripheral refraction. Am J Optom Physiol Opt. 1981;58(9).

41. Rynders M, Lidkea B, Chisholm W, Thibos LN. Statistical distribution of foveal transverse chromatic aberration, pupil centration, and angle ψ in a population of young adult eyes. Journal of the Optical Society of America A. 1995;12(10).

42. Campbell FW, Gubisch RW. The effect of chromatic aberration on visual acuity. J Physiol. 1967;192(2).

43. Goodman JW. Introduction to Fourier Optics, Second Edition Problem Soltuions. Optical Engineering. 1996;35(5).

44. Enoch JM. Retinal receptor orientation and the role of fiber optics in vision. Optometry and Vision Science. 1972;49(6).

45. Thibos LN, Xin H, Bradley A, Applegate RA. Accuracy and precision of objective refraction from wavefront aberrations. J Vis. 2004;4(4).

46. Sawides L. Correction and control of ocular aberrations with adaptive optics : effects on human vision [Internet]. Universidad de Valladolid; 2013 [cited 2022 Aug 30]. Available from: http://uvadoc.uva.es/handle/10324/3555

47. Porter J, Queener HM, Lin JE, Thorn K, Awwal A. Adaptive Optics for Vision Science: Principles, Practices, Design, and Applications. Adaptive Optics for Vision Science: Principles, Practices, Design, and Applications. 2005.

48. Sara El Aissati. Simulation and Characterisation optical corrections: impact of design, monochromatic and polychromatic aberrations. 2022.

49. Rosenfield M. Refractive Status of the Eye. In: Borish's Clinical Refraction. 2006.

50. Baird PN, Schäche M, Dirani M. The GEnes in Myopia (GEM) study in understanding the aetiology of refractive errors. Vol. 29, Progress in Retinal and Eye Research. 2010.

References

51. Bourne RRA, Stevens GA, White RA, Smith JL, Flaxman SR, Price H, et al. Causes of vision loss worldwide, 1990-2010: A systematic analysis. Lancet Glob Health. 2013;1(6).

52. Holden BA, Fricke TR, Wilson DA, Jong M, Naidoo KS, Sankaridurg P, et al. Global Prevalence of Myopia and High Myopia and Temporal Trends from 2000 through 2050. Ophthalmology. 2016;123(5).

53. Vitale S, Sperduto RD, Ferris FL. Increased prevalence of myopia in the United States between 1971-1972 and 1999-2004. Archives of Ophthalmology. 2009;127(12).

54. Willis JR, Vitale S, Morse L, Parke DW, Rich WL, Lum F, et al. The Prevalence of Myopic Choroidal Neovascularization in the United States. Ophthalmology. 2016;123(8).

55. Flitcroft DI. The complex interactions of retinal, optical and environmental factors in myopia aetiology. Vol. 31, Progress in Retinal and Eye Research. 2012.

56. Saw SM, Gazzard G, Shin-Yen EC, Chua WH. Myopia and associated pathological complications. Vol. 25, Ophthalmic and Physiological Optics. 2005.

57. Flitcroft DI, He M, Jonas JB, Jong M, Naidoo K, Ohno-Matsui K, et al. IMI – Defining and classifying myopia: A proposed set of standards for clinical and epidemiologic studies. Invest Ophthalmol Vis Sci. 2019;60(3).

58. Bourne RRA, Flaxman SR, Braithwaite T, Cicinelli M v., Das A, Jonas JB, et al. Magnitude, temporal trends, and projections of the global prevalence of blindness and distance and near vision impairment: a systematic review and meta-analysis. Lancet Glob Health. 2017;5(9).

59. Fricke TR, Tahhan N, Resnikoff S, Papas E, Burnett A, Ho SM, et al. Global Prevalence of Presbyopia and Vision Impairment from Uncorrected Presbyopia: Systematic Review, Meta-analysis, and Modelling. Ophthalmology. 2018;125(10).

60. Wong TY, Foster PJ, Johnson GJ, Seah SKL. Education, socioeconomic status, and ocular dimensions in Chinese adults: The Tanjong Pagar Survey. Vol. 86, British Journal of Ophthalmology. 2002.

61. Mountjoy E, Davies NM, Plotnikov D, Smith GD, Rodriguez S, Williams CE, et al. Education and myopia: Assessing the direction of causality by mendelian randomisation. BMJ (Online). 2018;361.

62. Cai XB, Shen SR, Chen DF, Zhang Q, Jin ZB. An overview of myopia genetics. Vol. 188, Experimental Eye Research. 2019.

63. Schaeffel F, Simon P, Feldkaemper M, Ohngemach S, Williams RW. Molecular biology of myopia. Vol. 86, Clinical & experimental optometry : journal of the Australian Optometrical Association. 2003.

64. Mutti DO, Zadnik K, Adams AJ. Myopia: The nature versus nurture debate goes on. Vol. 37, Investigative Ophthalmology and Visual Science. 1996.

65. Morgan I, Rose K. How genetic is school myopia? Vol. 24, Progress in Retinal and Eye Research. 2005.

66. Edwards MH. Effect of parental myopia on the development of myopia in Hong Kong Chinese. Ophthalmic and Physiological Optics. 1998;18(6).

67. Jones LA, Sinnott LT, Mutti DO, Mitchell GL, Moeschberger ML, Zadnik K. Parental history of myopia, sports and outdoor activities, and future myopia. Invest Ophthalmol Vis Sci. 2007;48(8).

68. Saw SM, Chua WH, Hong CY, Wu HM, Chan WY, Chia KS, et al. Nearwork in early-onset myopia. Invest Ophthalmol Vis Sci. 2002;43(2).

69. Mutti DO, Mitchell GL, Moeschberger ML, Jones LA, Zadnik K. Parental myopia, near work, school achievement, and children's refractive error. Invest Ophthalmol Vis Sci. 2002;43(12).

70. Wojciechowski R. Nature and nurture: The complex genetics of myopia and refractive error. Vol. 79, Clinical Genetics. 2011.

71. Hammond CJ, Snieder H, Gilbert CE, Spector TD. Genes and environment in refractive error: The twin eye study. Invest Ophthalmol Vis Sci. 2001;42(6).

72. Rose KA, Morgan IG, Smith W, Burlutsky G, Mitchell P, Saw SM. Myopia, lifestyle, and schooling in students of Chinese ethnicity in Singapore and Sydney. Archives of Ophthalmology. 2008;126(4).

73. Williams SM, Sanderson GF, Share DL, Silva PA. REFRACTIVE ERROR, IQ AND READING ABILITY: A LOIUGITUDINAL STUDY FROM AGE SEVEN TO 11. Dev Med Child Neurol. 1988;30(6).

74. Gwiazda J, Thorn F, Bauer J, Held R. Myopic children show insufficient accommodative response to blur. Invest Ophthalmol Vis Sci. 1993;34(3).

75. Gwiazda J, Grice K, Thorn F. Response AC/A ratios are elevated in myopic children. Ophthalmic and Physiological Optics. 1999;19(2).

76. Gwiazda J, Bauer J, Thorn F, Held R. A dynamic relationship between myopia and blur-driven accommodation in school-aged children. Vision Res. 1995;35(9).

77. Wu PC, Tsai CL, Wu HL, Yang YH, Kuo HK. Outdoor activity during class recess reduces myopia onset and progression in school children. Ophthalmology. 2013;120(5).

78. Smith EL, Hung LF, Huang J. Protective effects of high ambient lighting on the development of form-deprivation myopia in rhesus monkeys. Invest Ophthalmol Vis Sci. 2012;53(1).

79. Pan CW, Ramamurthy D, Saw SM. Worldwide prevalence and risk factors for myopia. Ophthalmic and Physiological Optics. 2012;32(1).

80. Read SA, Collins MJ, Vincent SJ. Light exposure and eye growth in childhood. Invest Ophthalmol Vis Sci. 2015;56(11).

81. Wallman J, Winawer J. Homeostasis of eye growth and the question of myopia. Vol. 43, Neuron. 2004.

82. Collins MJ, Wildsoet CF, Atchison DA. Monochromatic aberrations and myopia. Vision Res. 1995;35(9).

83. Paquin MP, Hamam H, Simonet P. Objective measurement of optical aberrations in myopic eyes. Optometry and Vision Science. 2002;79(5).

84. Collins JW, Carney LG. Visual performance in high myopia. Curr Eye Res. 1990;9(3).

85. Gustafsson J, Terenius E, Buchheister J, Unsbo P. Peripheral astigmatism in emmetropic eyes. Ophthalmic and Physiological Optics. 2001;21(5).

86. Lundström L, Gustafsson J, Unsbo P. Population distribution of wavefront aberrations in the peripheral human eye. Journal of the Optical Society of America A. 2009;26(10).

87. Siegwart JT, Norton TT. Perspective: How might emmetropization and genetic factors produce myopia in normal eyes? In: Optometry and Vision Science. 2011.

88. Hung LF, Crawford MLJ, Smith EL. Spectacle lenses alter eye growth and the refractive status of young monkeys. Nat Med. 1995;1(8).

89. Schaeffel F, Glasser A, Howland HC. Accommodation, refractive error and eye growth in chickens. Vol. 28, Vision Research. 1988.

90. Benavente-Pérez A, Nour A, Troilo D. Axial eye growth and refractive error development can be modified by exposing the peripheral retina to relative myopic or hyperopic defocus. Invest Ophthalmol Vis Sci. 2014;55(10).

91. Yen MY, Liu JH, Kao SC, Shiao CH. Comparison of the effect of atropine and cyclopentolate on myopia. Ann Ophthalmol. 1989;21(5).

92. Chia A, Lu QS, Tan D. Five-Year Clinical Trial on Atropine for the Treatment of Myopia 2 Myopia Control with Atropine 0.01% Eyedrops. Ophthalmology. 2016;123(2).

93. Smith EL. Optical treatment strategies to slow myopia progression: Effects of the visual extent of the optical treatment zone. Exp Eye Res. 2013;114.

94. Cho P, Cheung SW. Retardation of myopia in orthokeratology (ROMIO) study: A 2-year randomized clinical trial. Invest Ophthalmol Vis Sci. 2012;53(11).

95. Cho P, Cheung SW, Edwards M. The longitudinal orthokeratology research in children (LORIC) in Hong Kong: A pilot study on refractive changes and myopic control. Curr Eye Res. 2005;30(1).

96. Hiraoka T, Kakita T, Okamoto F, Takahashi H, Oshika T. Long-term effect of overnight orthokeratology on axial length elongation in childhood myopia: A 5-year follow-up study. Invest Ophthalmol Vis Sci. 2012;53(7).

97. Kang P, Swarbrick H. Peripheral refraction in myopic children wearing orthokeratology and gas-permeable lenses. Optometry and Vision Science. 2011;88(4).

98. Arance-Gil Á, Gutiérrez-Ortega ÁR, Villa-Collar C, Nieto-Bona A, Lopes-Ferreira D, González-Méijome JM. Corneal cross-linking for Acanthamoeba keratitis in an orthokeratology patient after swimming in contaminated water. Contact Lens and Anterior Eye. 2014;37(3).

99. Dotan A, Kremer I, Livnat T, Zigler A, Weinberger D, Bourla D. Scleral cross-linking using riboflavin and ultraviolet-A radiation for prevention of progressive myopia in a rabbit model. Exp Eye Res. 2014;127.

100. Gwiazda J. Treatment options for myopia. Vol. 86, Optometry and Vision Science. 2009.

101. Wollensak G, Spoerl E. Collagen crosslinking of human and porcine sclera. J Cataract Refract Surg. 2004;30(3).

102. Adler D, Millodot M. The possible effect of undercorrection on myopic progression in children. Clin Exp Optom. 2006;89(5).

103. Chung K, Mohidin N, O'Leary DJ. Undercorrection of myopia enhances rather than inhibits myopia progression. Vision Res. 2002;42(22).

104. Wagner S, Conrad F, Bakaraju RC, Fedtke C, Ehrmann K, Holden BA. Power profiles of single vision and multifocal soft contact lenses. Contact Lens and Anterior Eye. 2015;38(1).

105. Jonas JB, Xu L. Histological changes of high axial myopia. Eye (Basingstoke). 2014;28(2).

106. Goss DA, Grosvenor T. Rates of childhood myopia progression with bifocals as a function of nearpoint phoria: Consistency of three studies. Optometry and Vision Science. 1990;67(8).

107. Edwards MH, Li RW hong, Lam CS yin, Lew JK fai, Yu BS ying. The Hong Kong progressive lens myopia control study: Study design and main findings. Invest Ophthalmol Vis Sci. 2002;43(9).

108. Gwiazda J, Hyman L, Hussein M, Everett D, Norton TT, Kurtz D, et al. A randomized clinical trial of progressive addition lenses versus single vision lenses on the progression of myopia in children. Invest Ophthalmol Vis Sci. 2003;44(4).

109. Leung JTM, Brown B. Progression of myopia in Hong Kong Chinese schoolchildren is slowed by wearing progressive lenses. Optometry and Vision Science. 1999;76(6).

110. Lin Z, Martinez A, Chen X, Li L, Sankaridurg P, Holden BA, et al. Peripheral defocus with single-vision spectacle lenses in myopic children. Optometry and Vision Science. 2010;87(1).

111. Gwiazda JE, Hyman L, Norton TT, Hussein MEM, Marsh-Tootle W, Manny R, et al. Accommodation and related risk factors associated with myopia progression and their interaction with treatment in COMET children. Invest Ophthalmol Vis Sci. 2004;45(7).

112. Berntsen DA, Kramer CE. Peripheral defocus with spherical and multifocal soft contact lenses. Optometry and Vision Science. 2013;90(11).

113. Radhakrishnan A, Dorronsoro C, Sawides L, Marcos S. Short-term neural adaptation to simultaneous bifocal images. PLoS One. 2014;9(3).

114. Bakaraju RC, Ehrmann K, Ho A, Papas E. Inherent ocular spherical aberration and multifocal contact lens optical performance. In: Optometry and Vision Science. 2010.

115. Legras R, Benard Y, Rouger H. Through-focus visual performance measurements and predictions with multifocal contact lenses. Vision Res. 2010;50(12).

116. Rajagopalan AS, Bennett ES, Lakshminarayanan V. Visual performance of subjects wearing presbyopic contact lenses. Optometry and Vision Science. 2006;83(8).

117. Montés-Micó R, Madrid-Costa D, Radhakrishnan H, Charman WN, Ferrer-Blasco T. Accommodative functions with multifocal contact lenses: A pilot study. Optometry and Vision Science. 2011;88(8).

118. Charman WN. Developments in the correction of presbyopia II: Surgical approaches. Ophthalmic and Physiological Optics. 2014;34(4).

119. Chamberlain P, Peixoto-De-Matos SC, Logan NS, Ngo C, Jones D, Young G. A 3-year Randomized Clinical Trial of MiSight Lenses for Myopia Control. Optometry and Vision Science. 2019;96(8).

120. Collins MJ, Goode AS, Atchison DA. Accommodation and spherical aberration. Invest Ophthalmol Vis Sci. 1997;38(4).

121. Lowenstein O, Feinberg R, Loewenfeld IIE. Pupillary Movements During Acute and Chronic Fatigue A New Test for the Objective Evaluation of Tiredness. Investigative Ophthalmology & …. 1963;2(1).

122. Lipschutz H. MYOPIA AND NEARWORK. British Journal of Ophthalmology. 1935;19(11).

123. Ip JM, Saw SM, Rose KA, Morgan IG, Kifley A, Wang JJ, et al. Role of near work in myopia: Findings in a sample of Australian school children. Invest Ophthalmol Vis Sci. 2008;49(7).

124. Saw SM, Tong L, Chua WH, Chia KS, Koh D, Tan DTH, et al. Incidence and progression of myopia in Singaporean school children. Invest Ophthalmol Vis Sci. 2005;46(1).

125. Nakatsuka C, Hasebe S, Nonaka F, Ohtsuki H. Accommodative lag under habitual seeing conditions: Comparison between myopic and emmetropic children. Jpn J Ophthalmol. 2005;49(3).

126. Vera-Díaz FA, Strang NC, Winn B. Nearwork induced transient myopia during myopia progression. Curr Eye Res. 2002;24(4).

127. Millodot M. The effect of refractive error on the accommodative response gradient: A summary and update. Ophthalmic and Physiological Optics. 2015;35(6).

128. Schmid KL, Strang NC. Differences in the accommodation stimulus response curves of adult myopes and emmetropes: A summary and update. Ophthalmic and Physiological Optics. 2015;35(6).

129. Rosenfield M, Desai R, Portello JK. Do progressing myopes show reduced accommodative responses? Optometry and Vision Science. 2002;79(4).

130. Mutti DO, Mitchell GL, Hayes JR, Jones LA, Moeschberger ML, Cotter SA, et al. Accommodative lag before and after the onset of myopia. Invest Ophthalmol Vis Sci. 2006;47(3).

131. He JC, Sun P, Held R, Thorn F, Sun X, Gwiazda JE. Wavefront aberrations in eyes of emmetropic and moderately myopic school children and young adults. Vision Res. 2002;42(8).

132. Gambra E, Sawides L, Dorronsoro C, Marcos S. Accommodative lag and fluctuations when optical aberrations are manipulated. J Vis. 2009;9(6).

133. Walline JJ, Greiner KL, McVey ME, Jones-Jordan LA. Multifocal contact lens myopia control. Optometry and Vision Science. 2013;90(11).

134. Remón L, Pérez-Merino P, MacEdo-De-Araújo RJ, Amorim-De-Sousa AI, González-Meíjome JM. Bifocal and Multifocal Contact Lenses for Presbyopia and Myopia Control. Vol. 2020, Journal of Ophthalmology. 2020.

135. Wolffsohn JS, Davies LN. Presbyopia: Effectiveness of correction strategies. Vol. 68, Progress in Retinal and Eye Research. 2019.

136. Vinas M, Benedi-Garcia C, Aissati S, Pascual D, Akondi V, Dorronsoro C, et al. Visual simulators replicate vision with multifocal lenses. Sci Rep. 2019;9(1).

137. Ozkan J, Fedtke C, Chung J, Thomas V, Chandra Bakaraju R. Short-term adaptation of accommodative responses in myopes fitted with multifocal contact lenses. Eye Contact Lens. 2018;44.

138. Theagarayan B, Radhakrishnan H, Allen PM, Calver RI, Rae SM, O'Leary DJ. The effect of altering spherical aberration on the static accommodative response. Ophthalmic and Physiological Optics. 2009;29(1).

139. López-Gil N, Martin J, Liu T, Bradley A, Díaz-Muñoz D, Thibos LN. Retinal image quality during accommodation. Ophthalmic and Physiological Optics. 2013;33(4).

140. Rosenfield M, Gilmartin B. Disparity-induced accommodation in late-onset myopia. Ophthalmic and Physiological Optics. 1988;8(3).

141. Bullimore MA, Gilmartin B, Royston JM. Steady-state accommodation and ocular biometry in late-onset myopia. Documenta Ophthalmologica. 1992;80(2).

142. Lowenstein O, Feinberg R, Loewenfeld I. Pupillary Movements During Acute and Chronic Fatigue. Vol. 2, Investigative Ophthalmology & Visual Science. 1963.

143. Charman WN. Developments in the correction of presbyopia I: Spectacle and contact lenses. Vol. 34, Ophthalmic and Physiological Optics. 2014.

144. Aishwarya Radhakrishnan. Presbyopia Corrections: Optical, Perceptual and Adaptational Implications. Institute of Optics, CSIC, Madrid ; 2016.

145. Han SC, Graham AD, Lin MC. Clinical assessment of a customized free-form progressive add lens spectacle. Optometry and Vision Science. 2011;88(2).

146. Zheleznyak L, Alarcon A, Dieter KC, Tadin D, Yoon G. The role of sensory ocular dominance on through-focus visual performance in monovision presbyopia corrections. J Vis. 2015;15(6).

147. Evans BJW. Monovision: A review. Vol. 27, Ophthalmic and Physiological Optics. 2007.

148. Moshirfar M, Thomson AC, Thomson RJ, Martheswaran T, McCabe SE. Use of presbyopia-correcting intraocular lenses in patients with prior corneal refractive surgery. Vol. 32, Current Opinion in Ophthalmology. 2021.

149. Hutchins B, Huntjens B. Patient attitudes to presbyopia and its correction. Contact Lens and Anterior Eye. 2019;42(6).

150. Balgos MD, Vargas V, Alió J. Correction of presbyopia: An integrated update for the practical surgeon. Taiwan J Ophthalmol. 2018;8(3).

151. Menapace R, Findl O, Kriechbaum K, Leydolt-Koeppl C. Accommodating intraocular lenses: A critical review of present and future concepts. Vol. 245, Graefe's Archive for Clinical and Experimental Ophthalmology. 2007.

152. Marcos S, Ortiz S, Pérez-Merino P, Birkenfeld J, Durán S, Jiménez-Alfaro I. Three-dimensional evaluation of accommodating intraocular lens shift and alignment in vivo. Ophthalmology. 2014;121(1).

153. Brydon KW, Tokarewicz AC, Nichols BD. Amo array multifocal lens versus monofocal correction in cataract surgery. J Cataract Refract Surg. 2000;26(1).

154. Alio JL, Plaza-Puche AB, Javaloy J, Ayala MJ, Moreno LJ, Piero DP. Comparison of a new refractive multifocal intraocular lens with an inferior segmental near add and a diffractive multifocal intraocular lens. Ophthalmology. 2012;119(3).

155. Hashim HT, Al-Hamdani AH, Rashid HG. Design and Evaluation of Refractive Multifocal Intraocular Lenses Implanted within the Human Eye. In: IOP Conference Series: Materials Science and Engineering. 2020.

156. Gatinel D, Pagnoulle C, Houbrechts Y, Gobin L. Design and qualification of a diffractive trifocal optical profile for intraocular lenses. J Cataract Refract Surg. 2011;37(11).

157. Davison JA, Simpson MJ. History and development of the apodized diffractive intraocular lens. J Cataract Refract Surg. 2006;32(5).

158. Weeber HA, Meijer ST, Piers PA. Extending the range of vision using diffractive intraocular lens technology. J Cataract Refract Surg. 2015;41(12).

159. Kohnen T, Suryakumar R. Extended depth-of-focus technology in intraocular lenses. Vol. 46, Journal of Cataract and Refractive Surgery. 2020.

160. Kanclerz P, Toto F, Grzybowski A, Alio JL. Extended depth-of-field intraocular lenses: An update. Vol. 9, Asia-Pacific Journal of Ophthalmology. 2020.

161. Breyer DRH, Beckers L, Ax T, Kaymak H, Klabe K, Kretz FTA. Current Review: Multifocal Intraocular Lenses and Extended Depth of Focus Intraocular Lenses. Vol. 237, Klinische Monatsblatter fur Augenheilkunde. 2020.

162. Breyer DRH, Kaymak H, Ax T, Kretz FTA, Auffarth GU, Hagen PR. Multifocal intraocular lenses and extended depth of focus intraocular lenses. Vol. 6, Asia-Pacific Journal of Ophthalmology. 2017.

163. Gwiazda J, Marsh-Tootle WL, Hyman L, Hussein M, Norton TT, Grice K, et al. Baseline refractive and ocular component measures of children enrolled in the Correction of Myopia Evaluation Trial (COMET). Invest Ophthalmol Vis Sci. 2002;43(2).

164. Fedtke C, Ehrmann K, Thomas V, Bakaraju RC. Peripheral Refraction and Aberration Profiles with Multifocal Lenses. Optometry and Vision Science. 2017;94(9).

165. Rosén R, Jaeken B, Lindskoog Petterson A, Artal P, Unsbo P, Lundström L. Evaluating the peripheral optical effect of multifocal contact lenses. Ophthalmic and Physiological Optics. 2012;32(6).

166. Seidemann A, Schaeffel F, Guirao A, Lopez-Gil N, Artal P. Peripheral refractive errors in myopic, emmetropic, and hyperopic young subjects. Journal of the Optical Society of America A. 2002;19(12).

167. Altoaimi BH, Almutairi MS, Kollbaum PS, Bradley A. Accommodative behavior of young eyes wearing multifocal contact lenses. Optometry and Vision Science. 2018;95(5).

168. Walline JJ, Gaume Giannoni A, Sinnott LT, Chandler MA, Huang J, Mutti DO, et al. A Randomized Trial of Soft Multifocal Contact Lenses for Myopia Control: Baseline Data and Methods. Optometry and Vision Science. 2017;94(9).

169. Sankaridurg P, Bakaraju RC, Naduvilath T, Chen X, Weng R, Tilia D, et al. Myopia control with novel central and peripheral plus contact lenses and extended depth of focus contact lenses: 2 year results from a randomised clinical trial. Ophthalmic and Physiological Optics. 2019;39(4).

170. Pauné J, Queiros A, Quevedo L, Neves H, Lopes-Ferreira D, González-Méijome JM. Peripheral myopization and visual performance with experimental rigid gas permeable and soft contact lens design. Contact Lens and Anterior Eye. 2014;37(6).

171. Cheng X, Xu J, Chehab K, Exford J, Brennan N. Soft contact lenses with positive spherical aberration for myopia control. In: Optometry and Vision Science. 2016.

172. Aller TA, Liu M, Wildsoet CF. Myopia control with bifocal contact lenses: A randomized clinical trial. Optometry and Vision Science. 2016;93(4).

173. Anstice NS, Phillips JR. Effect of dual-focus soft contact lens wear on axial myopia progression in children. Ophthalmology. 2011;118(6).

174. Lam CSY, Tang WC, Tse DYY, Tang YY, To CH. Defocus Incorporated Soft Contact (DISC) lens slows myopia progression in Hong Kong Chinese schoolchildren: A 2-year randomised clinical trial. British Journal of Ophthalmology. 2014;98(1).

175. Ang M, Wong TY. Updates on myopia: A clinical perspective. Updates on Myopia: A Clinical Perspective. 2019.

176. Hardy JW, Lefebvre JE, Koliopoulos CL. Real-time atmospheric compensation. J Opt Soc Am. 1977;67(3).

177. Liang J, Williams DR, Miller DT. Supernormal vision and high-resolution retinal imaging through adaptive optics. Journal of the Optical Society of America A. 1997;14(11).

178. Fernández EJ, Iglesias I, Artal P. Closed-loop adaptive optics in the human eye. Opt Lett. 2001;26(10).

179. Diaz-Santana L, Torti C, Munro I, Gasson P, Dainty C. Benefit of higher closed�??loop bandwidths in ocular adaptive optics. Opt Express. 2003;11(20).

180. Sawides L, de Gracia P, Dorronsoro C, Webster MA, Marcos S. Vision is adapted to the natural level of blur present in the retinal image. PLoS One. 2011;6(11).

181. He JC, Marcos S, Webb RH, Burns SA. Measurement of the wave-front aberration of the eye by a fast psychophysical procedure. Journal of the Optical Society of America A. 1998;15(9).

182. Webb RH, Penney CM, Thompson KP. Measurement of ocular local wavefront distortion with a spatially resolved refractometer. Appl Opt. 1992;31(19).

183. Navarro R, Losada MA. Aberrations and relative efficiency of light pencils in the living human eye. Optometry and Vision Science. 1997;74(7).

184. Navarro R, Moreno E, Dorronsoro C. Monochromatic aberrations and point-spread functions of the human eye across the visual field. Journal of the Optical Society of America A. 1998;15(9).

185. Liang J, Grimm B, Goelz S, Bille JF. Objective measurement of wave aberrations of the human eye with the use of a Hartmann–Shack wave-front sensor. Journal of the Optical Society of America A. 1994;11(7).

186. Linda Lundström. Wavefront Aberrations and Peripheral Vision. [Stockholm]: KTH; 2007.

187. Vargas-Martín F, Prieto PM, Artal P. Correction of the aberrations in the human eye with a liquid-crystal spatial light modulator: limits to performance. Journal of the Optical Society of America A. 1998;15(9).

188. Vinas M, Dorronsoro C, Gonzalez V, Cortes D, Radhakrishnan A, Marcos S. Testing vision with angular and radial multifocal designs using Adaptive Optics. Vision Res. 2017;132.

189. Zhang Z, You Z, Chu D. Fundamentals of phase-only liquid crystal on silicon (LCOS) devices. Vol. 3, Light: Science and Applications. 2014.

190. C. D, A. R, P. DG, L. S, J.R. AS, D. C. Visual testing of segmented bifocal corrections with a compact simultaneous vision simulator. Invest Ophthalmol Vis Sci. 2014;55(13).

191. de Gracia P, Dorronsoro C, Sánchez-González Á, Sawides L, Marcos S. Experimental simulation of simultaneous vision. Invest Ophthalmol Vis Sci. 2013;54(1).

192. Manzanera S, Prieto PM, Ayala DB, Lindacher JM, Artal P. Liquid crystal Adaptive Optics Visual Simulator: Application to testing and design of ophthalmic optical elements. Opt Express. 2007;15(24).

193. Vinas M, Aissati S, Gonzalez-Ramos AM, Romero M, Sawides L, Akondi V, et al. Optical and visual quality with physical and visually simulated presbyopic multifocal contact lenses. Transl Vis Sci Technol. 2020;9(10).

194. Vinas M, Dorronsoro C, Radhakrishnan A, Benedi-Garcia C, LaVilla EA, Schwiegerling J, et al. Comparison of vision through surface modulated and spatial light modulated multifocal optics. Biomed Opt Express. 2017;8(4).

195. Vinas M, Dorronsoro C, Cortes D, Pascual D, Marcos S. Longitudinal chromatic aberration of the human eye in the visible and near infrared from wavefront sensing, double-pass and psychophysics. Biomed Opt Express. 2015;6(3).

196. Marcos S, Werner JS, Burns SA, Merigan WH, Artal P, Atchison DA, et al. Vision science and adaptive optics, the state of the field. Vision Res. 2017;132.

197. Marcos S, Benedí-García C, Aissati S, Gonzalez-Ramos AM, Lago CM, Radhkrishnan A, et al. VioBio lab adaptive optics: technology and applications by women vision scientists. Ophthalmic and Physiological Optics. 2020;40(2).

198. Vinas M, Aissati S, Romero M, Benedi-Garcia C, Garzon N, Poyales F, et al. Pre-operative simulation of post-operative multifocal vision. Biomed Opt Express. 2019;10(11).

199. Tabernero J, Schwarz C, Fernández EJ, Artal P. Binocular visual simulation of a corneal inlay to increase depth of focus. Invest Ophthalmol Vis Sci. 2011;52(8).

200. Zhao L, Bai N, Li X, Ong LS, Fang ZP, Asundi AK. Efficient implementation of a spatial light modulator as a diffractive optical microlens array in a digital Shack-Hartmann wavefront sensor. Appl Opt. 2006;45(1).

201. Dorronsoro C, Radhakrishnan A, de Gracia P, Sawides L, Marcos S. Perceived image quality with simulated segmented bifocal corrections. Biomed Opt Express. 2016;7(11).

202. Radhakrishnan A, Dorronsoro C, Marcos S. Differences in visual quality with orientation of a rotationally asymmetric bifocal intraocular lens design. J Cataract Refract Surg. 2016;42(9).

203. Vedhakrishnan S, Vinas M, Aissati S, Marcos S. Vision with spatial light modulator simulating multifocal contact lenses in an adaptive optics system. Biomed Opt Express. 2021;12(5).

204. Rocha KM, Vabre L, Chateau N, Krueger RR. Enhanced visual acuity and image perception following correction of highly aberrated eyes using an adaptive optics visual simulator. In: Journal of Refractive Surgery. 2010.

205. Ruiz-Alcocer J, Madrid-Costa D, García-Lázaro S, Albarrán-Diego C, Ferrer-Blasco T. Visual simulation through an aspheric aberration-correcting intraocular lens in subjects with different corneal profiles using adaptive optics. Clin Exp Optom. 2013;96(4).

206. Tabernero J, Otero C, Pardhan S. A comparison between refraction from an adaptive optics visual simulator and clinical refractions. Transl Vis Sci Technol. 2020;9(7).

207. Hervella L, Villegas EA, Prieto PM, Artal P. Assessment of subjective refraction with a clinical adaptive optics visual simulator. J Cataract Refract Surg. 2019;45(1).

208. Xoana Barcala Gosende. Binocular simultaneous vision simulator. Universidad Complutense de Madrid; 2021.

209. Drexler W, Morgner U, Kärtner FX, Pitris C, Boppart SA, Li XD, et al. In vivo ultrahigh-resolution optical coherence tomography. Opt Lett. 1999;24(17).

210. Huang D, Swanson EA, Lin CP, Schuman JS, Stinson WG, Chang W, et al. Optical coherence tomography. Science (1979). 1991;254(5035).

211. Grulkowski I, Gora M, Szkulmowski M, Gorczynska I, Szlag D, Marcos S, et al. Anterior segment imaging with Spectral OCT system using a high-speed CMOS camera. Opt Express. 2009;17(6).

212. Choma M, Sarunic M, Yang C, Izatt J. Sensitivity advantage of swept source and Fourier domain optical coherence tomography. Opt Express. 2003;11(18).

213. Ortiz S, Siedlecki D, Grulkowski I, Remon L, Pascual D, Wojtkowski M, et al. Optical distortion correction in Optical Coherence Tomography for quantitative ocular anterior segment by three-dimensional imaging. Opt Express. 2010;18(3).

214. Pablo Perez Merino. Anterior Segment Topography and Aberrations for Clinical Applications. University of Valladolid ;

215. Marcos S, Sawides L, Gambra E, Dorronsoro C. Influence of adaptive-optics ocular aberration correction on visual acuity at different luminances and contrast polarities. J Vis. 2008;8(13).

216. de Gracia P, Marcos S, Mathur A, Atchison DA. Contrast sensitivity benefit of adaptive optics correction of ocular aberrations. J Vis. 2011;11(12).

217. Sawides L, Gambra E, Pascual D, Dorronsoro C, Marcos S. Visual performance with real-life tasks under Adaptive-Optics ocular aberration correction. J Vis. 2010;10(5).

218. Gambra E, Wang Y, Yuan J, Kruger PB, Marcos S. Dynamic accommodation with simulated targets blurred with high order aberrations. Vision Res. 2010;50(19).

219. Benedi-Garcia C, Velasco-Ocana M, Dorronsoro C, Pascual D, Hernandez M, Marin G, et al. Perceptual impact of astigmatism induction in presbyopes. Vision Res. 2019;165.

220. Vinas M, de Gracia P, Dorronsoro C, Sawides L, Marin G, Hernández M, et al. Astigmatism impact on visual performance: Meridional and adaptational effects. Optometry and Vision Science. 2013;90(12).

221. Vinas M, Sawides L, de Gracia P, Marcos S. Perceptual Adaptation to the Correction of Natural Astigmatism. PLoS One. 2012;7(9).

222. Vinas M, Dorronsoro C, Garzón N, Poyales F, Marcos S. In vivo subjective and objective longitudinal chromatic aberration after bilateral implantation of the same design of hydrophobic and hydrophilic intraocular lenses. J Cataract Refract Surg. 2015;41(10).

223. Vinas M, Benedi-Garcia C, Aissati S, Pascual D, Akondi V, Dorronsoro C, et al. Visual simulators replicate vision with multifocal lenses. Sci Rep. 2019;9(1).

224. Benedi-Garcia C, Vinas M, Lago CM, Aissati S, de Castro A, Dorronsoro C, et al. Optical and visual quality of real intraocular lenses physically projected on the patient's eye. Biomed Opt Express. 2021;12(10).

225. Prieto PM, Fernández EJ, Manzanera S, Artal P. Adaptive optics with a programmable phase modulator: applications in the human eye. Opt Express. 2004;12(17).

226. Gabbiani F, Cox SJ. Mathematics for Neuroscientists: Second Edition. Mathematics for Neuroscientists: Second Edition. 2017.

227. Kleiner M, Brainard DH, Pelli DG, Broussard C, Wolf T, Niehorster D. What's new in Psychtoolbox-3? Perception. 2007;36.

228. Brainard DH. The Psychophysics Toolbox. Spat Vis. 1997;10(4).

229. Pelli DG. The VideoToolbox software for visual psychophysics: Transforming numbers into movies. Spat Vis. 1997;10(4).

230. Young LK, Love GD, Smithson HE. Accounting for the phase, spatial frequency and orientation demands of the task improves metrics based on the visual Strehl ratio. Vision Res. 2013;90.

231. Campbell FW, Green DG. Optical and retinal factors affecting visual resolution. J Physiol. 1965;181(3).

232. Iskander DR. Computational aspects of the visual Strehl ratio. Optometry and Vision Science. 2006;83(1).

233. Marsack JD, Thibos LN, Applegate RA. Metrics of optical quality derived from wave aberrations predict visual performance. J Vis. 2004;4(4).

234. Mengchan Sun. Biometric measurements in the crystalline lense: applications in cataract surgery". 2017.

235. Gambra E, Ortiz S, Perez-Merino P, Gora M, Wojtkowski M, Marcos S. Static and dynamic crystalline lens accommodation evaluated using quantitative 3-D OCT. Biomed Opt Express. 2013;4(9).

236. Vedhakrishnan S, Vinas M, Benedi-Garcia C, Casado P, Marcos S. Visual performance with multifocal lenses in young adults and presbyopes. PLoS One. 2022;17(3 March).

237. Dayan YB, Levin A, Morad Y, Grotto I, Ben-David R, Goldberg A, et al. The changing prevalence of myopia in young adults: A 13-year series of population-based prevalence surveys. Invest Ophthalmol Vis Sci. 2005;46(8).

238. Fedtke C, Eehrmann K, Thomas V, Bakaraju RC. Visual performance with multifocal soft contact lenses in non-presbyopic myopic eyes during an adaptation period. Clin Optom (Auckl). 2016;8.

239. Back A, Grant T, Hine N. Comparative visual performance of three presbyopic contact lens corrections. Optometry and Vision Science. 1992;69(6).

240. Pérez-Prados R, Piñero DP, Pérez-Cambrodí RJ, Madrid-Costa D. Soft multifocal simultaneous image contact lenses: a review. Vol. 100, Clinical and Experimental Optometry. 2017.

241. Tarrant J, Severson H, Wildsoet CF. Accommodation in emmetropic and myopic young adults wearing bifocal soft contact lenses. Ophthalmic and Physiological Optics. 2008;28(1).

242. Lopes-Ferreira D, Fernandes P, Queirós A, González-Meijome JM. Combined effect of ocular and multifocal contact lens induced aberrations on visual performance: Center-distance versus center-near design. Eye Contact Lens. 2018;44.

243. Chateau N, Baude D. Simulated in situ optical performance of bifocal contact lenses. Optometry and Vision Science. 1997;74(7).

244. Ruiz-Pomeda A, Villa-Collar C. Slowing the Progression of Myopia in Children with the MiSight Contact Lens: A Narrative Review of the Evidence. Vol. 9, Ophthalmology and Therapy. 2020.

245. Erickson P, Schor C. Visual function with presbyopic contact lens correction. Optometry and Vision Science. 1990;67(1).

246. Kang P, Wildsoet CF. Acute and short-term changes in visual function with multifocal soft contact lens wear in young adults. Contact Lens and Anterior Eye. 2016;39(2).

247. Walline J, Smith M. Controlling myopia progression in children and adolescents. Adolesc Health Med Ther. 2015;

248. Sha J, Tilia D, Diec J, Fedtke C, Yeotikar N, Jong M, et al. Visual performance of myopia control soft contact lenses in non-presbyopic myopes. Clin Optom (Auckl). 2018;10.

249. Sha J, Bakaraju RC, Tilia D, Chung J, Delaney S, Munro A, et al. Short-term visual performance of soft multifocal contact lenses for presbyopia. Arq Bras Oftalmol. 2015;79(2).

250. Plainis S, Atchison DA, Charman WN. Power profiles of multifocal contact lenses and their interpretation. Optometry and Vision Science. 2013;90(10).

251. Kim E, Bakaraju RC, Ehrmann K. Power Profiles of Commercial Multifocal Soft Contact Lenses. Optometry and Vision Science. 2017;94(2).

252. Modern Techniques in Neuroscience Research. Modern Techniques in Neuroscience Research. 1999.

253. Holladay JT. Proper method for calculating average visual acuity. Journal of Refractive Surgery. 1997;13(4).

254. Dorronsoro C, Barcala X, Gambra E, Akondi V, Sawides L, Marrakchi Y, et al. Tunable lenses: dynamic characterization and fine-tuned control for high-speed applications. Opt Express. 2019;27(3).

255. Sha J, Tilia D, Kho D, Diec J, Yeotikar N, Jong M, et al. Visual performance of daily disposable multifocal soft contact lenses. Invest Ophthalmol Vis Sci. 2018;59(9).

256. Korsan JM. Soft Multifocal Contact Lenses for Myopia Control in Children. The Ohio State University; 2015.

257. Xoana Barcala; Maria Vinas; Fernando Hidalgo; Sofia Ruiz; Derek Nankivil; Thomas Karkkainen; Khaled Chehab; Carlos Dorronsoro; Susana Marcos. Comparison of vision with multifocal contact lenses and SimVis Gekko simulations in a clinical site. Investigative Ophthalmology & Visual Science. 2020 Jun; 61:579.

258. Barcala X, Vinas M, Romero M, Gambra E, Mendez-Gonzalez JL, Marcos S, et al. Multifocal acceptance score to evaluate vision: MAS-2EV. Sci Rep. 2021;11(1).

259. Morgan PB, Efron N. Contact lens correction of presbyopia. Contact Lens and Anterior Eye. 2009;32(4).

260. Kollbaum PS, Bradley A. Correction of presbyopia: old problems with old (and new) solutions. Vol. 103, Clinical and Experimental Optometry. 2020.

261. Fedtke C, Bakaraju RC, Ehrmann K, Chung J, Thomas V, Holden BA. Visual performance of single vision and multifocal contact lenses in non-presbyopic myopic eyes. Contact Lens and Anterior Eye. 2016;39(1).

262. Madrid-Costa D, García-Lázaro S, Albarrán-Diego C, Ferrer-Blasco T, Montés-Micó R. Visual performance of two simultaneous vision multifocal contact lenses. Ophthalmic and Physiological Optics. 2013;33(1).

263. Plainis S, Ntzilepis G, Atchison DA, Charman WN. Through-focus performance with multifocal contact lenses: Effect of binocularity, pupil diameter and inherent ocular aberrations. Ophthalmic and Physiological Optics. 2013;33(1).

264. Dorronsoro C, Radhakrishnan A, Alonso-Sanz JR, Pascual D, Velasco-Ocana M, Perez-Merino P, et al. Portable simultaneous vision device to simulate multifocal corrections. Optica. 2016;3(8).

265. Akondi V, Dorronsoro C, Gambra E, Marcos S. Temporal multiplexing to simulate multifocal intraocular lenses: theoretical considerations. Biomedical Optics Express. 2017;8(7).

266. Cheng X, Brennan NA, Toubouti Y, Greenaway NL. Safety of soft contact lenses in children: retrospective review of six randomized controlled trials of myopia control. Acta Ophthalmol. 2020;98(3).

267. Kleiner M, Brainard D, Pelli D, Ingling A, Murray R, Broussard C. What's new in Psychtoolbox-3? Perception. 36(ECVP Abstract Supplement):14. Whats New. 2007;36.

268. Martinez JL, Fernandez EJ, Prieto PM, Artal P. Chromatic aberration control with liquid crystal spatial phase modulators. Opt Express. 2017;25(9).

269. Benedi-Garcia C, Vinas M, Dorronsoro C, Burns SA, Peli E, Marcos S. Vision is protected against blue defocus. Sci Rep. 2021;11(1).

270. Kaluzy BJ, Kałuzny JJ, Szkulmowska A, Gorczyńska I, Szkulmowski M, Bajraszewski T, et al. Spectral optical coherence tomography: A novel technique for cornea imaging. Cornea. 2006;25(8).

271. Pritchard N, Fonn D, Brazeau D. Discontinuation of contact lens wear: A survey. International Contact Lens Clinic. 1999;26(6).

272. Schlanger JL. A study of contact lens failures. J Am Optom Assoc. 1993;64(3).

273. Briggs ST. Profile of contact lens failures in Saudi Arabia. Clin Exp Optom. 1996;79(6).

274. Young G, Veys J, Pritchard N, Coleman S. A multi-centre study of lapsed contact lens wearers. Ophthalmic and Physiological Optics. 2002;22(6).

275. Young G. Why one million contact lens wearers dropped out. Contact Lens and Anterior Eye. 2004;27(2).

276. Drexler W, Morgner U, Ghanta RK, Kärtner FX, Schuman JS, Fujimoto JG. Ultrahigh-resolution ophthalmic optical coherence tomography. Nat Med. 2001;7(4).

277. Maeda N. Optical coherence tomography for corneal diseases. Vol. 36, Eye and Contact Lens. 2010.

278. Karnowski K, Kaluzny BJ, Szkulmowski M, Gora M, Wojtkowski M. Corneal topography with high-speed swept source OCT in clinical examination. Biomed Opt Express. 2011;2(9).

279. Stachura J, Seredyka-Burduk M, Piotrowiak-Słupska I, Kaszuba-Modrzejewska M, Rzeszewska-Zamiara J, Kałuzny BJ. Developments in contact lens imaging: New applications of optical coherence tomography. Vol. 9, Applied Sciences (Switzerland). 2019.

280. de Boer JF, Cense B, Park BH, Pierce MC, Tearney GJ, Bouma BE. Improved signal-to-noise ratio in spectral-domain compared with time-domain optical coherence tomography. Opt Lett. 2003;28(21).

281. Leitgeb R, Hitzenberger C, Fercher A. Performance of fourier domain vs time domain optical coherence tomography. Opt Express. 2003;11(8).

282. Nassif N, Cense B, Hyle Park B, Yun SH, Chen TC, Bouma BE, et al. In vivo human retinal imaging by ultrahigh-speed spectral domain optical coherence tomography. Opt Lett. 2004;29(5).

283. Wojtkowski M, Bajraszewski T, Gorczyńska I, Targowski P, Kowalczyk A, Wasilewski W, et al. Ophthalmic imaging by spectral optical coherence tomography. Am J Ophthalmol. 2004;138(3).

284. Jiao S, Knighton R, Huang X, Gregori G, Puliafito CA. Simultaneous acquisition of sectional and fundus ophthalmic images with spectral-domain optical coherence tomography. Opt Express. 2005;13(2).

285. Yun SH, Tearney GJ, de Boer JF, Bouma BE. Motion artifacts in optical coherence tomography with frequency-domain ranging. Opt Express. 2004;12(13).

286. Kałuzny BJ, Kaluzny JJ, Szkulmowska A, Gorczyńska I, Szkulmowski M, Bajraszewski T, et al. Spectral optical coherence tomography: A new imaging technique in contact lens practice. Ophthalmic and Physiological Optics. 2006;26(2).

287. Kałuzny JJ, Wojtkowski M, Kowalczyk A. Imaging of the anterior segment of the eye by spectral optical coherence tomography. Optica Applicata. 2003;32(4).

288. Reinstein DZ, Silverman RH, Rondeau MJ, Coleman DJ. Epithelial and Corneal Thickness Measurements by High-frequency Ultrasound Digital Signal Processing. Ophthalmology. 1994;101(1).

289. Vedhakrishnan S, de Castro A, Vinas M, Aissati S, Marcos S. Accommodation through simulated multifocal optics. Biomed Opt Express [Internet]. 2022 Dec;13(12):6695–710. Available from: https://opg.optica.org/boe/abstract.cfm?URI=boe-13-12-6695

290. Golnik K. Walsh and Hoyt's Clinical Neuro-Ophthalmology: The Essentials, 2nd Edition. Journal of Neuro-Ophthalmology. 2008;28(4).

291. Atchison DA. Accommodation and presbyopia. Ophthalmic and Physiological Optics. 1995;15(4).

292. Altoaimi BH, Kollbaum P, Meyer D, Bradley A. Experimental investigation of accommodation in eyes fit with multifocal contact lenses using a clinical auto-refractor. Ophthalmic and Physiological Optics. 2018;38(2).

293. Plainis S, Ginis HS, Pallikaris A. The effect of ocular aberrations on steady-state errors of accommodative response. J Vis. 2005;5(5).

294. Tarrant JM. Spherical Aberration, Accommodation and Myopia. ProQuest Dissertations and Theses. 2010.

295. Collins MJ, Buehren T, Iskander DR. Retinal image quality, reading and myopia. Vision Res. 2006;46(1–2).

296. Applegate RA, Lakshminarayanan V. Parametric representation of Stiles–Crawford functions: normal variation of peak location and directionality. Journal of the Optical Society of America A. 1993;10(7).

297. Mathews S, Kruger PB. Spatiotemporal transfer function of human accommodation. Vision Res. 1994;34(15).

298. Alpern M, Mason GL, Jardinico RE. Vergence and accommodation. V. Pupil size changes associated with changes in accommodative vergence. Am J Ophthalmol. 1961;52(5 PART 2).

299. Tarrant J, Liu Y, Wildsoet CF. Orthokeratology Can Decrease the Accommodative Lag in Myopes. Invest Ophthalmol Vis Sci. 2009;50(13).

300. Charman WN, Radhakrishnan H. Accommodation, pupil diameter and myopia. Ophthalmic and Physiological Optics. 2009;29(1).

301. Charman WN. Near vision, lags of accommodation and myopia. Ophthalmic and Physiological Optics. 1999;19(2).

302. Cheng X, Xu J, Brennan NA. Accommodation and its role in myopia progression and control with soft contact lenses. Ophthalmic and Physiological Optics. 2019;39(3).

303. He JC, Gwiazda J, Thorn F, Held R, Vera-Diaz FA. The association of wavefront aberration and accommodative lag in myopes. Vision Res. 2005;45(3).

304. Labhishetty V, Cholewiak SA, Roorda A, Banks MS. Lags and leads of accommodation in humans: Fact or fiction? J Vis. 2018;21(3).

305. Kang P, McAlinden C, Wildsoet CF. Effects of multifocal soft contact lenses used to slow myopia progression on quality of vision in young adults. Acta Ophthalmol. 2017;95(1).

306. Gong CR, Troilo D, Richdale K. Accommodation and phoria in children wearing multifocal contact lenses. In: Optometry and Vision Science. 2017.

307. Yang Y, Wang L, Li P, Li J. Accommodation function comparison following use of contact lens for orthokeratology and spectacle use in myopic children: A prospective controlled trial. Int J Ophthalmol. 2018;11(7).

308. Price H, Allen PM, Radhakrishnan H, Calver R, Rae S, Theagarayan B, et al. The Cambridge anti-myopia study: Variables associated with myopia progression. Optometry and Vision Science. 2013;90(11).

309. Gifford KL, Schmid KL, Collins JM, Maher CB, Makan R, Nguyen E, et al. Multifocal contact lens design, not addition power, affects accommodation responses in young adult myopes. Ophthalmic and Physiological Optics. 2021;41(6).

310. Faria-Ribeiro M, Amorim-de-Sousa A, González-Méijome JM. Predicted accommodative response from image quality in young eyes fitted with different dual-focus designs. Ophthalmic and Physiological Optics. 2018;38(3).

311. Wagner S, Schaeffel F, Troilo D. Changing accommodation behaviour during multifocal soft contact lens wear using auditory biofeedback training. Sci Rep. 2020;10(1).

312. Stark LR, Lee RS, Kruger PB, Rucker FJ, Ying Fan H. Accommodation to simulations of defocus and chromatic aberration in the presence of chromatic misalignment. Vision Res. 2002;42(12).

313. Bobier WR, Campbell MCW, Hinch M. The influence of chromatic aberration on the static accommodative response. Vision Res. 1992;32(5).

314. Sabesan R, Zheleznyak L, Yoon G. Binocular visual performance and summation after correcting higher order aberrations. Biomed Opt Express. 2012;3(12).

315. Fernández EJ, Prieto PM, Artal P. Binocular adaptive optics visual simulator. Opt Lett. 2009;34(17).

316. World Health Organization. The Impact of Myopia and High Myopia. World Health Organization–Brien Holden Vision Institute. 2015.

317. Vongphanit J, Mitchell P, Wang JJ. Prevalence and progression of myopic retinopathy in an older population. Ophthalmology. 2002;109(4).

318. Ogawa A, Tanaka M. The relationship between refractive errors and retinal detachment--analysis of 1,166 retinal detachment cases. Jpn J Ophthalmol. 1988;32(3):310—315.

319. Chang MA, Congdon NG, Bykhovskaya I, Munoz B, West SK. The association between myopia and various subtypes of lens opacity: SEE (Salisbury Eye Evaluation) project. Ophthalmology. 2005;

320. Marcus MW, De Vries MM, Junoy Montolio FG, Jansonius NM. Myopia as a risk factor for open-angle glaucoma: A systematic review and meta-analysis. Ophthalmology. 2011;118(10):1989-1994.e2.

321. Gwiazda J, Hyman L, Dong LM, Everett D, Norton T, Kurtz D, et al. Factors associated with high myopia after 7 years of follow-up in the Correction of Myopia Evaluation Trial (COMET) cohort. Ophthalmic Epidemiol. 2007;14(4):230–7.

322. Braun CI, Freidlin V, Sperduto RD, Milton RC, Strahlman ER. The progression of myopia in school age children: Data from the Columbia Medical Plan. Ophthalmic Epidemiol. 1996;3(1):13–21.

323. Smith EL, Kee CS, Ramamirtham R, Qiao-Grider Y, Hung LF. Peripheral vision can influence eye growth and refractive development in infant monkeys. Invest Ophthalmol Vis Sci. 2005;46(11):3965–72.

324. Benavente-Pérez A, Nour A, Troilo D. Axial eye growth and refractive error development can be modified by exposing the peripheral retina to relative myopic or hyperopic defocus. Invest Ophthalmol Vis Sci. 2014;55(10):6765–73.

325. Smith EL. Prentice award lecture 2010: A case for peripheral optical treatment strategies for myopia. Optometry and Vision Science. 2011;88(9):1029–44.

326. Smith EL, Hung LF, Arumugam B. Visual regulation of refractive development: Insights from animal studies. Eye (Basingstoke). 2014;28(2):180–8.

327. Troilo D, Wallman J. The regulation of eye growth and refractive state: An experimental study of emmetropization. Vision Res. 1991;31(7–8):1237–50.

328. Jaeken B, Artal P. Optical quality of emmetropic and myopic eyes in the periphery measured with high-angular resolution. Invest Ophthalmol Vis Sci. 2012;53(7):3405–13.

329. Gwiazda JE, Hyman L, Norton TT, Hussein MEM, Marsh-Tootle W, Manny R, et al. Accommodation and related risk factors associated with myopia progression and their interaction with treatment in COMET children. Invest Ophthalmol Vis Sci. 2004;45(7):2143–51.

330. Lundström L, Mira-Agudelo A, Artal P. Peripheral optical errors and their change with accommodation differ between emmetropic and myopic eyes. J Vis. 2009;9(6):1–11.

331. Gwiazda J, Thorn F HR. Accommodation, accommodative convergence, and response AC/A ratios before and at the onset of myopia in children. Optom Vis Sci. 2005;82(4):273–8.

332. Yam JC, Jiang Y, Tang SM, Law AKP, Chan JJ, Wong E, et al. Low-Concentration Atropine for Myopia Progression (LAMP) Study: A Randomized, Double-Blinded, Placebo-Controlled Trial of 0.05%, 0.025%, and 0.01% Atropine Eye Drops in Myopia Control. Ophthalmology. 2019;126(1):113–24.

333. Santodomingo-Rubido J, Villa-Collar C, Gilmartin B, Gutiérrez-Ortega R. Myopia control with orthokeratology contact lenses in Spain: Refractive and biometric changes. Invest Ophthalmol Vis Sci. 2012;53(8):5060–5.

334. Hiraoka T, Kakita T, Okamoto F, Takahashi H, Oshika T. Long-term effect of overnight orthokeratology on axial length elongation in childhood myopia: A 5-year follow-up study. Invest Ophthalmol Vis Sci. 2012;53(7):3913–9.

335. Lin Z, Duarte-Toledo R, Manzanera S, Lan W, Artal P, Yang Z. Two-dimensional peripheral refraction and retinal image quality in orthokeratology lens wearers. Biomed Opt Express. 2020 Jul 1;11(7):3523.

336. Hasebe S, Jun J, Varnas SR. Myopia control with positively aspherized progressive addition lenses: A 2-year, multicenter, randomized, controlled trial. Invest Ophthalmol Vis Sci. 2014;55(11):7177–88.

337. Cheng D, Woo GC, Drobe B, Schmid KL. Effect of bifocal and prismatic bifocal spectacles on myopia progression in children: Three-year results of a randomized clinical trial. JAMA Ophthalmol. 2014;132(3):258–64.

338. Cho P, Cheung SW. Retardation of myopia in orthokeratology (ROMIO) study: A 2-year randomized clinical trial. Invest Ophthalmol Vis Sci. 2012;53(11):7077–85.

339. Rosén R, Jaeken B, Lindskoog Petterson A, Artal P, Unsbo P, Lundström L. Evaluating the peripheral optical effect of multifocal contact lenses. Ophthalmic and Physiological Optics. 2012;32(6):527–34.

340. Wildsoet CF, Chia A, Cho P, Guggenheim JA, Roelof J, Read S, et al. IMI-Interventions for Controling Myopia Onset and Progression Report. Invest Ophthalmol Vis Sci. 2019;60(Imi):M106-131.

341. Ji Q, Yoo YS, Alam H, Yoon G. Through-focus optical characteristics of monofocal and bifocal soft contact lenses across the peripheral visual field. Ophthalmic and Physiological Optics. 2018;38(3):326–36.

342. García M, Wahl S, Pusti D, Artal P, Ohlendorf A. 2-D Peripheral image quality metrics with different types of multifocal contact lenses. Sci Rep. 2019;9(1):1–10.

343. Ruiz-Pomeda A, Pérez-Sánchez B, Cañadas P, Prieto-Garrido FL, Gutiérrez-Ortega R, Villa-Collar C. Binocular and accommodative function in the controlled randomized clinical trial MiSight Assessment Study Spain (MASS). Clin Exp Ophthalmol. 2019;257:207–15.

344. Sha J, Tilia D, Diec J, Fedtke C, Yeotikar N, Jong M, et al. Visual performance of myopia control soft contact lenses in non-presbyopic myopes. Clin Optom (Auckl). 2018;10:75–86.

345. Chamberlain P, Peixoto-De-Matos SC, Logan NS, Ngo C, Jones D, Young G. A 3-year Randomized Clinical Trial of MiSight Lenses for Myopia Control. Optometry and Vision Science. 2019;96(8):556–67.

346. Ruiz-Alcocer J. Análisis del perfil de potencia de las nuevas lentes de contacto blandas para miopía progresiva. J Optom. 2017;10(4):266–8.

347. Thibos LN, Wheeler W, Horner D. Power Vectors: An Application of Fourier Analysis to the Description and Statistical Analysis of Refractive Error. Optometry and Vision Science; 1997. p. Vol. 74.

348. Rosén R, Lundstrm L, Unsbo P. Adaptive optics for peripheral vision. J Mod Opt. 2012;59(12):1064–70.

349. Papadogiannis P, Romashchenko D, Unsbo P, Lundström L. Lower sensitivity to peripheral hypermetropic defocus due to higher order ocular aberrations. Ophthalmic and Physiological Optics. 2020;40(3):300–7.

350. Wang YZ, Thibos LN, Bradley A. Effects of refractive error on detection acuity and resolution acuity in peripheral vision. Invest Ophthalmol Vis Sci. 1997;38(10):2134–43.

351. Rosén R, Lundström L, Unsbo P. Influence of optical defocus on peripheral vision. Invest Ophthalmol Vis Sci. 2011;52(1):318–23.

352. Venkataraman AP, Winter S, Rosén R, Lundström L. Choice of Grating Orientation for Evaluation of Peripheral Vision. Optometry and Vision Science. 2016;93(6):567–74.

353. Lundström L, Rosén R, Baskaran K, Jaeken B, Gustafsson J, Artal P, et al. Symmetries in peripheral ocular aberrations. J Mod Opt. 2011;58(19–20):1690–5.

354. Mathur A, Gehrmann J, Atchison DA. Pupil shape as viewed along the horizontal visual field Ankit Mathur. J Vis. 2013;13(6):1–8.

355. Gifford KL, Schmid KL, Collins JM, Maher CB, Makan R, Nguyen E, et al. Multifocal contact lens design, not addition power, affects accommodation responses in young adult myopes. Ophthalmic and Physiological Optics. 2021;41(6):1346–54.

356. Bakaraju RC, Fedtke C, Ehrmann K, Ho A. Comparing the relative peripheral refraction effect of single vision and multifocal contact lenses measured using an autorefractor and an aberrometer: A pilot study. J Optom. 2015;8(3):206–18.

357. Jeong TM, Menon M, Yoon G. Measurement of wave-front aberration in soft contact lenses by use of a Shack-Hartmann wave-front sensor. Appl Opt. 2005;44(21):4523–7.

358. Gutman AS, Shchesyuk I V., Korolkov VP. Optical testing of bifocal diffractive-refractive intraocular lenses using Shack-Hartmann wavefront sensor. Optical Micro- and Nanometrology III. 2010;7718(April):77181P.

359. Romashchenko D, Lundström L. Dual-angle open field wavefront sensor for simultaneous measurements of the central and peripheral human eye. Biomed Opt Express. 2020;11(6):3125.

360. Kim E, Bakaraju RC, Ehrmann K. Power Profiles of Commercial Multifocal Soft Contact Lenses. Optometry and Vision Science. 2017;94(2):183–96.

361. Lundström L, Rosén R. Peripheral Aberrations. In: Artal P, editor. Handbook of Visual Optics, Volume One: Fundamentals and Eye Optics. New York: Taylor & Francis Group, LLC; 2017. p. 313–35.

IO

CSIC

Consejo Superior de Investigaciones Científicas

VIOBIO

VISUAL OPTICS & BIOPHOTONICS LAB

UNIVERSIDAD COMPLUTENSE MADRID